





Iron Catalysts for the Epoxidation of Olefins and C-C Cross-  
coupling

By  
Kamrul Hasan

A thesis submitted to the School of Graduate Studies of  
the Memorial University of Newfoundland  
in partial fulfillment of the requirements of the degree of  
Doctor of Philosophy

Department of Chemistry  
Memorial University of Newfoundland  
St. John's, Newfoundland, A1B 3X7, Canada

Copyright © December 2011 by Kamrul Hasan

## Abstract

This thesis describes the synthesis, structure and catalytic activity of amine-bis(phenolate)Fe(III) complexes. Fe(III) halide complexes were synthesized supported by tetradentate amine-bis(phenolate) ligands. The general formulae of these ligands are abbreviated as  $[\text{O}_2\text{N}_2]^{RR'}$  and  $[\text{O}_2\text{NO}]^{RR'R''}$ , where  $[\text{O}_2\text{N}_2]$  and  $[\text{O}_2\text{NO}]$  to describe the four donor atoms of the ligands, R and R' (Bu or Me) represent the substituents at the 2- and 4- positions on the phenolate rings and R'' defines the pendant donor functionality such as methoxyethyl (Meth) or tetrahydrofurfuryl (Furf). These paramagnetic complexes were characterized by a variety of methods including elemental analysis, MALDI-TOF mass spectrometry, UV-vis spectroscopy, and magnetic moment measurements. Three iron complexes,  $\text{FeCl}[\text{O}_2\text{N}_2]^{BuBu}$  (1),  $\text{FeBr}[\text{O}_2\text{N}_2]^{BuBu}$  (2) and  $\text{FeBr}[\text{O}_2\text{NO}]^{BuMeMeth}$  (3) were structurally characterized by single crystal X-ray diffraction. Magnetic moment measurements of these complexes show high-spin  $d^5$  Fe(III) centers. Also, variable temperature magnetic susceptibility measurements of the three structurally characterized complexes were conducted using a SQUID magnetometer.

For epoxidation of olefins,  $\text{H}_2\text{O}_2$  was chosen as terminal oxidant because it is convenient and produces water as a by-product. The catalytic activity of these amine-bis(phenolate)Fe(III) halide complexes were investigated for the epoxidation of *trans*-stilbene. The complex  $\text{FeCl}[\text{O}_2\text{N}_2]^{BuBu}$  (1) gave modest yield (36%) of *trans*-stilbene oxide after 19 h stirring of the reaction mixture at 25 °C. However, a practical method for the epoxidation of olefins was discovered by the combination of  $\text{FeCl}_3 \cdot 6\text{H}_2\text{O}$  and 1-methylimidazole in acetone. Heating the reaction mixture to 62 °C for 19-21 h

significantly improved the product yields. The optimized catalytic conditions were applicable for both aromatic and aliphatic internal and terminal olefins. Also, *in-situ* generated Fe(III) complexes, made by adding  $\text{FeCl}_3 \cdot 6\text{H}_2\text{O}$  to solutions of selected amine-bis(phenol) ligands, were investigated for the epoxidation of *trans*-stilbene to see whether any enhancement of reactivity could be obtained. Tridentate amine-bis(phenol) ligands (abbreviated  $\text{H}_2[\text{O}_2\text{N}]^{\text{RR}'}$ ) improved the product yields up to 64% but these yields were less than the epoxidation activity (93%) while using  $\text{FeCl}_3 \cdot 6\text{H}_2\text{O}$  and 1-methylimidazole alone.

Finally, six amine-bis(phenolate)Fe(III)(acac) (acac = acetylacetonate) complexes were synthesized by employing previously reported tetradentate amine-bis(phenolate) ligands including  $[\text{O}_2\text{NN}]^{\text{RR}'}$ , where  $\text{R}'$  is the pendant donor functionality such as *N,N*-dimethylaminoethyl (NMe<sub>2</sub>). These paramagnetic complexes were also characterized by a variety of methods including elemental analysis, MALDI-TOF mass spectrometry, UV-vis and IR spectroscopy, cyclic voltammetry, and magnetic moment measurements. Four of these complexes,  $\text{Fe}(\text{acac})[\text{O}_2\text{N}_2]^{\text{BuBu}}$  (**9**),  $\text{Fe}(\text{acac})[\text{O}_2\text{NN}]^{\text{BuBuNMe}_2}$  (**10**),  $\text{Fe}(\text{acac})[\text{O}_2\text{NN}]^{\text{BuMeNMe}_2}$  (**11**), and  $\text{Fe}(\text{acac})[\text{O}_2\text{NO}]^{\text{BuMeMeth}}$  (**13**) were structurally characterized by single crystal X-ray diffraction. Magnetic moment measurements of these complexes indicate high-spin  $d^5$  Fe(III) centers. Cyclic voltammetry of these complexes show ligand-centered reversible redox processes. Preliminary catalytic activity of these complexes was investigated for the C-C cross-coupling of aryl Grignard reagents with alkyl halides. Secondary cyclic halides such as cyclohexyl chloride and

bromides gave high yields, however, benzyl chloride and bromide gave moderate and acyclic 2-chloro- and 2-bromobutanes gave poor yields of cross-coupled product.



## Acknowledgements

I am heartily grateful to my supervisor, Dr. Christopher M. Kozak, for giving me the opportunity to pursue this research, and his continuous guidance and supervision throughout the program. It would not have been possible for me to write this thesis without his help. He shared his vast knowledge with me in a very friendly manner and always encouraged me to think critically. I also extend my deepest gratitude to Dr. Francesca M. Kerton for her valuable suggestions and the use of her instruments throughout the program.

I would like to thank my supervisory committee members, Dr. Paris E. Georghiou and Dr. Francesca M. Kerton for their advice, support and criticism throughout the program. I would like to thank Dr. Louise N. Dawe and Ms. Julie L. Collins for solving my crystal structure. Thanks to C-CART for instrument training, with special thanks to Lidian Tao for running MALDI-TOF mass spectrometry. Thanks also to Dr. Peter G. Pickup for the use of his electrochemistry equipment.

I give thanks to Dr. Kozak, to the School of Graduate studies, and the Department of Chemistry of Memorial University for their financial support.

I would like to thank the past and present Green Chemistry and Catalysis Group members. Finally, I want to express my gratitude to my family members, my parents, my wife Manira Parvin, and especially my son (Nawaf) who came to this world during my PhD and brings joy in my life. Last, but not least, thanks to Allah (God), without his mercy it was not possible for me to achieve all that I have.

## Dedication

This thesis is dedicated to my adorable son **Nawaf Abeer Hasan**

&

my beloved wife **Manira Parvin**

## Table of Contents

Abstract.....	i
Acknowledgements.....	iv
Dedication.....	v
Table of Contents.....	vi
List of Tables.....	x
List of Figures.....	xii
List of Schemes.....	xvii
List of Abbreviations and Symbols .....	xix
Chapter 1. Introduction and overview.....	1
1.1 Scope of this thesis.....	1
1.2 General properties of iron.....	2
1.3 Coordination chemistry of iron.....	4
1.3.1 Iron complexes containing phenolate ligands.....	4
1.3.2 Iron-oxo complexes.....	12
1.4 Introductory magnetochemistry of iron.....	17
1.5 Iron catalysis.....	20
1.5.1 Iron-catalyzed alkane oxidation.....	20
1.5.2 Iron-catalyzed olefin epoxidation.....	27
1.5.3 Fe-TAML complexes in green oxidation reactions.....	39

1.5.4	Iron-catalyzed C-C cross-coupling reactions.....	43
1.6	History and prospects of amine-bis(phenol) ligands.....	57
1.7	References.....	59
	Co-authorship statement.....	76
	Chapter 2. Synthesis and structure of amine-bis(phenolate)Fe(III) halide complexes.....	79
2.1	Introduction.....	79
2.2	Results and Discussion.....	81
2.2.1	Ligand synthesis.....	81
2.2.2	Synthesis of Fe(III) complexes.....	83
2.2.3	Characterization of Fe(III) complexes.....	87
2.3	Conclusion.....	108
2.4	Experimental Section.....	108
2.4.1	Materials and methods.....	108
2.4.2	Instrumentation.....	109
2.4.3	X-ray crystallography.....	110
2.4.4	Synthesis of ligands.....	113
2.4.5	Synthesis of metal complexes.....	115
2.5	References.....	120
	Chapter 3. Iron-catalyzed epoxidation of olefins using hydrogen peroxide.....	130
3.1	Introduction.....	130
3.2	Results and Discussion.....	133
3.3	Conclusions.....	155

3.4	Experimental.....	156
3.4.1	General experimental conditions.....	156
3.4.2	Instrumentation.....	156
3.4.3	General method for epoxidation catalysis reactions.....	156
3.4.4	Method for determination of H <sub>2</sub> O <sub>2</sub> concentration.....	157
3.5	Notes and references.....	157
Chapter 4. Synthesis, structure, and C-C cross-coupling activity of amine-bis(phenolate)iron(acac) complexes.....		163
4.1	Introduction.....	163
4.2	Results and Discussion.....	165
4.2.1	Ligand synthesis.....	165
4.2.2	Synthesis of Fe(III)(acac) complexes.....	166
4.2.3	Structural characterization.....	168
4.2.4	Cross-coupling catalysis studies.....	190
4.3	Conclusion.....	195
4.4	Experimental Section.....	195
4.4.1	General considerations.....	195
4.4.2	Instrumentation.....	196
4.4.3	X-Ray crystallography.....	197
4.4.4	Synthesis of ligands.....	200
4.4.5	Synthesis of metal complexes.....	202
4.4.6	General method for cross-coupling catalysis.....	206

4.4.7	$^1\text{H}$ and $^{13}\text{C}\{^1\text{H}\}$ NMR spectral data of cross-coupled products.....	207
4.5	References.....	208
Chapter 5. Conclusion and prospects for future studies.....		217
5.1	Conclusion.....	217
5.2	Prospects for future studies.....	221
5.3	References.....	225
Appendix.....		available on CD

## List of Tables

Table 1.1 Oxidants used in the metal-catalyzed epoxidations and thier active oxygen content_.....	29
Table 2.1 Selected bond lengths (Å) and angles (°) for the complex 1, 2 and 3.....	95
Table 2.2 Comparison of molar absorption coefficients of the two LMCT bands of FeBr[O <sub>2</sub> NO] <sup>BuMeMeth</sup> (3) and FeBr[O <sub>2</sub> NO] <sup>BuBuMeth</sup> (4) complexes.....	103
Table 2.3 Room temperature magnetic moments determined by Faraday balance or Johnson-Matthey magnetic susceptibility balance.....	105
Table 2.4 Crystallographic and structural refinement data for compounds 1, 2 and 3...112	112
Table 3.1 Epoxidation of <i>trans</i> -stilbene in different solvents. <sup>a</sup> .....	135
Table 3.2 Epoxidation of <i>trans</i> -stilbene in the presence of different iron sources. <sup>a</sup> .....	137
Table 3.3 Epoxidation of <i>trans</i> -stilbene in the presence of different additives. <sup>a</sup> .....	140
Table 3.4 Olefinic substrates screened for epoxidation. <sup>a</sup> .....	145
Table 3.5 Screening of Fe(III) complexes with tetradentate amine-bis(phenol) ligands. <sup>a</sup> .....	148
Table 3.6 Epoxidation of <i>trans</i> -stilbene using tridentate amine-bis(phenol) ligands with FeCl <sub>3</sub> ·6H <sub>2</sub> O. <sup>a</sup> .....	150
Table 4.1 Selected bond lengths [Å] and angles [°] for the complex 9, 10, 11 and 13.....	176
Table 4.2 Selected bond lengths [Å] and angles [°] for H <sub>2</sub> [O <sub>2</sub> NO] <sup>MeMeMe</sup> .....	179
Table 4.3 Effective magnetic moments for complexes 9-13 in the solid state.....	187
Table 4.4 Electrode peak potentials for oxidation and reduction of complexes 9 to 14.....	188

Table 4.5 Cross coupling of aryl Grignard reagents with alkyl halides catalyzed by amine-bis(phenolate)Fe(acac) complexes. <sup>a</sup> .....	193
Table 4.6 Crystallographic and structural refinement data for compounds 9, 10, 11, 13 and H <sub>2</sub> [O <sub>2</sub> NO] <sup>MeMeMeib</sup> .....	199



## List of Figures

Figure 1.1 Active sites of methane monooxygenase (1) and catechol dioxygenase (3,4-PCD) (2).....	4
Figure 1.2 Tripodal tetradentate ligands used by Que <i>et al.</i> .....	5
Figure 1.3 Structure of the complex anion in $\text{HNEt}_3[\text{Fe}(\text{L})(\text{tbc})]$ . Redrawn from reference [23].....	6
Figure 1.4 Structure of $\text{LFe}^{\text{III}}(\text{DBSQ})$ vs. $[\text{LFe}^{\text{III}}(\text{DBC})]^-$ .....	7
Figure 1.5 Amine-bis(phenol) ligands and their Fe(III) model complexes.....	8
Figure 1.6 Tripodal monophenol ligands used by Palaniandavar's group.....	9
Figure 1.7 Fe(III)(acac) amine-bis(phenolate) complexes having THF and pyridine pendant arms. Redrawn from reference [27 and 28].....	10
Figure 1.8 Crystal structure of the $[\text{Fe}^{\text{IV}}\text{O}(\text{TMC})(\text{NCCH}_3)]^{2+}$ cation. Redrawn from reference [45].....	15
Figure 1.9 The d-orbital splitting diagrams for $d^5$ (a) high-spin octahedral $S = 5/2$ ; (b) low-spin octahedral $S = 1/2$ ; (c) high-spin tetrahedral $S = 5/2$ systems; where $n$ is the number of unpaired electrons, $\Delta_o$ and $\Delta_t$ are the octahedral and tetrahedral crystal field splitting parameters.....	19
Figure 1.10 The d-orbital splitting diagrams for $d^5$ (a) low-spin square pyramidal $S = 1/2$ ; (b) high-spin square pyramidal $S = 5/2$ ; (c) low-spin trigonal bipyramidal $S = 5/2$ and (e) intermediate spin $S = 3/2$ systems; where $n$ is the number of unpaired electrons.....	20
Figure 1.11 Iron(II) phosphinoxazoline complexes.....	23

Figure 1.12 Changing the backbone of BPMEN ligands.....	24
Figure 1.13 Fe( <i>S,S</i> -PDP) complex and its catalytic activity.....	25
Figure 1.14 Fe( <sup>RR</sup> PyTACN) (12) and Fe( <i>S,S,R</i> -mcpp) (13) complexes and their catalytic activities.....	27
Figure 1.15 Manganese porphyrin Mn(TPP)Cl complex (14) and Jacobsen's Mn(salen) complex (15) for the epoxidation of olefins.....	30
Figure 1.16 Iron porphyrin Fe(TPP)Cl (16) and Fe(TMP)Cl (17) complexes and their activities towards epoxidation of olefins.....	31
Figure 1.17 Jacobsen's Fe(MEP) catalyst (18) and its activity towards epoxidation of olefins.....	33
Figure 1.18 Stack's Fe(phen) catalyst (19) and its activity towards epoxidation of olefins.....	34
Figure 1.19 Iron TPA and BPMEN complexes with different substituents on pyridine rings.....	35
Figure 1.20 Optically active ligands and their corresponding iron complexes.....	37
Figure 1.21 Biomimetic iron complex containing a pyridine macrocycle ligand bearing a pendant arm.....	38
Figure 1.22 High-valent Fe <sup>V</sup> oxo intermediate of Fe-TAML complex.....	40
Figure 1.23 Fe-TAML activators for degradation of PC.....	41
Figure 1.24 Generation 1 (36) and Generation 2 (37) Fe-TAML activators.....	42
Figure 2.1 Library of amine-bis(phenol) ligands studied in this chapter.....	83
Figure 2.2 Library of synthesized amine-bis(phenolate)Fe(III) halide complexes.....	86

Figure 2.3 MALDI-TOF mass spectrum of $\text{FeCl}[\text{O}_2\text{N}_2]^{\text{BuBu}}$ (1).....	87
Figure 2.4 MALDI-TOF mass spectrum of $\text{FeBr}[\text{O}_2\text{N}_2]^{\text{BuBu}}$ (2).....	88
Figure 2.5 MALDI-TOF mass spectrum of $\text{FeBr}[\text{O}_2\text{NO}]^{\text{BuMeMeth}}$ (3).....	89
Figure 2.6 MALDI-TOF mass spectrum of $\text{FeBr}[\text{O}_2\text{NO}]^{\text{BuBuMeth}}$ (4).....	90
Figure 2.7 ORTEP diagram and atom labeling scheme for $\text{FeCl}[\text{O}_2\text{N}_2]^{\text{BuBu}}$ (1) (thermal ellipsoids shown at 50% probability). Hydrogen atoms removed for clarity.....	92
Figure 2.8 ORTEP diagram and atom labeling scheme for $\text{FeBr}[\text{O}_2\text{N}_2]^{\text{BuBu}}$ (2) (thermal ellipsoids shown at 50% probability). Hydrogen atoms removed for clarity.....	92
Figure 2.9 ORTEP diagram and atom labeling scheme for $\text{FeBr}[\text{O}_2\text{NO}]^{\text{BuMeMeth}}$ (3) (thermal ellipsoids shown at 50% probability). Hydrogen atoms removed for clarity.....	97
Figure 2.10 Electronic absorption spectra of $\text{FeCl}[\text{O}_2\text{N}_2]^{\text{BuBu}}$ (1) and $\text{FeBr}[\text{O}_2\text{N}_2]^{\text{BuBu}}$ (2) in methanol.....	100
Figure 2.11 Electronic absorption spectra of $\text{FeBr}[\text{O}_2\text{NO}]^{\text{BuMeMeth}}$ (3) in methanol, THF, toluene and acetonitrile solutions.....	101
Figure 2.12 Electronic absorption spectra of $\text{FeBr}[\text{O}_2\text{NO}]^{\text{BuBuMeth}}$ (4) in methanol, THF, toluene and acetonitrile solutions.....	102
Figure 2.13 Electronic absorption spectra of $\text{FeCl}[\text{O}_2\text{NO}]^{\text{MeMeFwef}}$ (5), $\text{FeBr}[\text{O}_2\text{NO}]^{\text{MeMeFwef}}$ (6), $\text{FeCl}[\text{O}_2\text{NO}]^{\text{MeMeMeth}}$ (7) and $\text{FeBr}[\text{O}_2\text{NO}]^{\text{MeMeMeth}}$ (8) in methanol.....	104
Figure 2.14 Magnetic moment vs. Temperature plots of $\text{FeCl}[\text{O}_2\text{N}_2]^{\text{BuBu}}$ (1) and $\text{FeBr}[\text{O}_2\text{N}_2]^{\text{BuBu}}$ (2).....	106
Figure 2.15 Magnetic moment vs. temperature plots of $\text{FeBr}[\text{O}_2\text{NO}]^{\text{BuMeMeth}}$ (3).....	107

Figure 3.1 Iron complex 1 and tetradentate amine-bis(phenol) proligands used in this study.....	147
Figure 3.2 Tridentate amine-bis(phenol) ligands used in this study.....	149
Figure 3.3 Yield of <i>trans</i> -stilbene oxide obtained by epoxidation of <i>trans</i> -stilbene vs. equivalents of 1-methylimidazole added.....	151
Figure 3.4 Monitoring the progress of epoxidation of <i>trans</i> -stilbene in presence of (A) and absence of amine-bis(phenol) ligand $H_2[O_2N]^{BuBuBenz}$ (B).....	152
Figure 3.5 Proposed catalytic cycle <i>via</i> an iron-oxo intermediate.....	155
Figure 4.1 Library of amine-bis(phenol) ligands.....	166
Figure 4.2 MALDI-TOF mass spectrum of the complex $Fe(acac)[O_2N_2]^{BuBu}$ (9).....	169
Figure 4.3 MALDI-TOF mass spectrum of the complex $Fe(acac)[O_2NO]^{BuMeMeth}$ (13).....	170
Figure 4.4 ORTEP diagram and atom labeling scheme for the complex 9 (thermal ellipsoids shown at 50% probability). Hydrogen atoms removed for clarity.....	172
Figure 4.5 ORTEP and atom labeling scheme for complex 10 (thermal ellipsoids shown at 50% probability). Hydrogen atoms removed for clarity.....	173
Figure 4.6 ORTEP diagram and atom labeling scheme for complex 11 (thermal ellipsoids shown at 50% probability). Hydrogen atoms removed for clarity.....	174
Figure 4.7 ORTEP diagram and atom labeling scheme for complex 13 (thermal ellipsoids shown at 50% probability). Hydrogen atoms are removed for clarity.....	177

Figure 4.8 ORTEP diagram and atom labeling scheme for ligand $\text{H}_2[\text{O}_2\text{NO}]^{\text{MeMeMeth}}$ (thermal ellipsoids shown at 50% probability). Only O-H bonded hydrogens atoms are shown.....	179
Figure 4.9 Electronic absorption spectra of complexes 9-14 in methanol.....	181
Figure 4.10 Electronic absorption spectra of 9 in methanol, THF, toluene and acetonitrile solutions.....	183
Figure 4.11 Electronic absorption spectra of <b>11</b> in methanol, THF, toluene and acetonitrile solutions.....	183
Figure 4.12 IR spectrum of $\text{Fe}(\text{acac})[\text{O}_2\text{NN}]^{\text{BuMeNMe}_2}$ ( <b>11</b> ).....	185
Figure 4.13 IR spectrum of ligand $\text{H}_2[\text{O}_2\text{NN}]^{\text{BuMeNMe}_2}$ .....	185
Figure 4.14 IR spectrum of the complex $\text{Fe}(\text{acac})[\text{O}_2\text{NO}]^{\text{MeMeMeth}}$ ( <b>14</b> ).....	186
Figure 4.15 Cyclic voltammogram of 9 in $\text{CH}_2\text{Cl}_2$ (0.1M $[(n\text{-Bu})_4\text{N}]\text{PF}_6$ ) at 25 °C and a scan rate of $100 \text{ mV s}^{-1}$ .....	188
Figure 4.16 Cyclic voltammogram of 12 in $\text{CH}_2\text{Cl}_2$ (0.1M $[(n\text{-Bu})_4\text{N}]\text{PF}_6$ ) at 25 °C and a scan rate of $100 \text{ mV s}^{-1}$ .....	189

## List of Schemes

Scheme 1.1 Salan and BAPEN ligands and their Fe(II) complexes.....	12
Scheme 1.2 Intermediates observed in heme and non-heme iron model complexes.....	13
Scheme 1.3 Generation of iron hydroperoxo and iron-oxo intermediates from non-heme iron complexes. ● indicates an isotopically labeled $^{18}\text{O}$ .....	16
Scheme 1.4 Oxidation of adamantane to adamantanol and adamantanone.....	21
Scheme 1.5 Oxidation of 9,10-dihydroanthracene.....	22
Scheme 1.6 Mechanism of iron $^{\text{RR}}\text{PyTACN}$ complexes for epoxidation/hydroxylation of olefins. ● indicates an an isotopically labeled $^{18}\text{O}$ .....	36
Scheme 1.7 Olefin epoxidation by Beller and co-workers.....	39
Scheme 1.8 Cross-coupling reaction between Grignard reagents and vinyl halides.....	44
Scheme 1.9 Stereospecific nature of cross-coupling reaction reported by Kochi <i>et al.</i> .....	45
Scheme 1.10 Kochi's proposed mechanism.....	46
Scheme 1.11 Cross-coupling of vinyl halides with Grignard reagents by Molander <i>et al.</i> .....	47
Scheme 1.12 Effect of NMP in the cross-coupling reactions.....	47
Scheme 1.13 Cross-coupling reaction between functional Grignard reagents with alkenyl halide.....	48
Scheme 1.14 Formation of Bogdanovic's inorganic Grignard reagent.....	49
Scheme 1.15 Fürstner's proposed mechanism <i>via</i> low-valent intermediates vs. organoferrate manifold.....	50

Scheme 1.16 Fe(-2) complex for the cross-coupling of alkyl halides with different functional groups.....	51
Scheme 1.17 Organoferrate complex for the cross-coupling of acid chloride and triflates.....	52
Scheme 1.18 Cross-coupling of alkyl halides with aryl Grignard reagents reported by Nakamura <i>et al.</i> .....	53
Scheme 1.19 Cross-coupling of alkyl halides with aryl Grignard reagents reported by Hayashi <i>et al.</i> .....	53
Scheme 1.20 Fe(III) salen catalyzed cross-coupling by Bedford <i>et al.</i> .....	54
Scheme 1.21 FeCl <sub>3</sub> /amine catalyzed cross-coupling by Bedford <i>et al.</i> .....	55
Scheme 1.22 Novel iron based catalyst systems by Cahiez <i>et al.</i> .....	56
Scheme 2.1 Synthesis of amine-bis(phenol) ligands.....	82
Scheme 2.2 Synthesis of amine-bis(phenolate)Fe(III) halide complexes.....	84
Scheme 2.3 Synthesis of amine-bis(phenolate)Fe(III) halide complexes <i>via</i> salt metathesis.....	85
Scheme 3.1 Nucleophilic addition to the epoxide.....	133
Scheme 3.2 Intra (A and B) and intermolecular (C) hydrogen bonding between H-2 in imidazole and ferric hydroperoxo (FeOOH) species.....	142
Scheme 4.1 Synthesis of amine-bis(phenol) ligands.....	165
Scheme 4.2 Synthesis of amine-bis(phenolate)iron(III)acac complexes.....	167

## List of Abbreviations and Symbols

### *Technical terms:*

MMO: methane monooxygenase

equiv.: equivalent

LMCT: ligand to metal charge-transfer

CF: crystal field

TAML: tetraamido macrocyclic ligand

BAPEN: methylated bis(aminophenolate)-ethylenediamine

TPA: tris(2-methylpyridyl)amine

m-CPBA: *meta*-chloroperoxybenzoic acid

TMP: *meso*-tetramesitylporphinato

TMC: 1,4,8,11-tetramethyl-1,4,8,11-tetraazacyclotetradecane

salan: *N,N'*-bis(4-methyl-6-*tert*-butyl-2-methyl-phenolato)-*N,N'*-bismethyl-1,2-diaminoethane

DBSQ: 3,5-di-*tert*-butyl-*o*-benzosemiquinone monoanion

DBC: 3,5-di-*tert*-butylcatecholate

TACN: triazacyclononane

OTf: perfluorobutane sulfonate

TMEDA: tetramethylethylenediamine

NMP: *N*-methylpyrrolidine

HMTA: hexamethylenetetramine



DME: dimethoxyethane  
Fe(acac)<sub>3</sub>: Fe(III) acetylacetonate  
H<sub>2</sub>O<sub>2</sub>: hydrogen peroxide  
*t*-BuOOH: *tert*-butyl hydroperoxide  
<sup>t</sup>Bu: *tert*-butyl  
<sup>i</sup>Pr: isopropyl  
*J*: coupling constant  
*m/z*: mass-to-charge ratio  
[M]<sup>+</sup>: molecular ion  
MW: molecular weight  
*S*: electron spin  
SCE: standard calomel electrode

***Techniques:***

MALDI: matrix assisted laser desorption/ionization  
MS: mass spectrometry  
IR: infrared spectroscopy  
UV-vis: ultraviolet-visible spectroscopy  
CV: cyclic voltammetry  
NMR: nuclear magnetic resonance  
GC-MS: gas chromatography-mass spectrometry  
SQUID: superconducting quantum interference device

**Units:**

Å: angstrom ( $10^{-10}$  m)

(°): degree

amu: atomic mass unit

emu: electromagnetic unit

cm: centimeter

nm: nanometer

mL: milliliter ( $10^{-3}$  L)

μL: microliter ( $10^{-6}$  L)

wt.: weight

g: gram

M: molar

h: hour

min: minute

s: second

K: Kelvin

T: telsa

$\mu_B$ : bohr magnetron

mV: millivolt

**Latin expressions:**

*et al.*: and co-workers

ca.: around

*e.g.*: for example

*i.e.*: namely

*tert.*: tertiary

vs.: versus

**Symbols:**

$\lambda$ : wavelength (nm)

$\chi$ : magnetic susceptibility

$\epsilon$ : excitation coefficient ( $M^{-1} \text{ cm}^{-1}$ )

$\mu_{\text{eff}}$ : magnetic moment

$\tau$ : trigonality index

**Ligands used in this work:**

$H_2[O_2N_2]^{BuBu}$ : *N,N'*-bis(4,6-*tert*-butyl-2-methylphenol)-*N,N'*-bismethyl-1,2  
diaminoethane

$H_2[O_2NO]^{BuMeMeth}$ : 2-methoxyethaneamino-*N,N'*-bis(2-methylene-4-methyl-6-*tert*-  
butylphenol)

$H_2[O_2NO]^{BuMeMeth}$ : 2-methoxyethaneamino-*N,N'*-bis(2-methylene-4,6-*tert*-butylphenol)

$H_2[O_2NO]^{MeMeFurf}$ : 2-tetrahydrofurfurylamino-*N,N'*-bis(2-methylene-4,6-methylphenol)

$H_2[O_2NO]^{MeMeMeth}$ : 2-methoxyethaneamino-*N, N'*-bis(2-methylene-4,6-methylphenol)

$H_2[O_2N_2]^{BuBuNMe2}$ : *N, N*-dimethyl-*N, N'*-bis(2-methylene-4,6-*tert*

butylphenol)ethylenediamine

$H_2[O_2N_2]^{BuMeNMe2}$ : *N, N*-dimethyl-*N, N'*-bis(2-methylene-4-methyl-6-*tert*-butylphenol)ethylenediamine

$H_2[O_2NO]^{BuBuFurf}$ : 2-tetrahydrofurfurylamino-*N, N'*-bis(2-methylene-4,6-*tert*-butylphenol)

$H_2[O_2NO]^{AmAmFurf}$ : 2-tetrahydrofurfurylamino-*N, N'*-bis(2-methylene-4,6-*tert*-amylphenol)

$H_2[O_2N]^{BuBuPropyl}$ : *n*-propylamino-*N, N'*-bis(2-methylene-4,6-*tert*-butylphenol)

$H_2[O_2N]^{BuBuIsoPropyl}$ : *iso*-propylamino-*N, N'*-bis(2-methylene-4,6-*tert*-butylphenol)

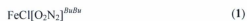
$H_2[O_2N]^{FFPropyl}$ : *n*-propylamino-*N, N'*-bis(2-methylene-4,6-fluorophenol)

$H_2[O_2N]^{BuBuBenc}$ : benzylamino-*N, N'*-bis(2-methylene-4,6-*tert*-butylphenol)

$H_2[O_2N]^{BuMeBenc}$ : benzylamino-*N, N'*-bis(2-methylene-4-methyl-6-*tert*-butylphenol)

$H_2[O_2N]^{AmAmBenc}$ : benzylamino-*N, N'*-bis(2-methylene-4,6-*tert*-amylphenol)

#### **Numbering of the synthesized complexes:**



- $\text{FeBr}[\text{O}_2\text{NO}]^{\text{MeMeFurf}}$  (6)  
 $\text{FeCl}[\text{O}_2\text{NO}]^{\text{MeMeMeth}}$  (7)  
 $\text{FeBr}[\text{O}_2\text{NO}]^{\text{MeMeMeth}}$  (8)  
 $\text{Fe}(\text{acac})[\text{O}_2\text{N}_2]^{\text{BuBu}}$  (9)  
 $\text{Fe}(\text{acac})[\text{O}_2\text{NN}]^{\text{BuBuNMe}_2}$  (10)  
 $\text{Fe}(\text{acac})[\text{O}_2\text{NN}]^{\text{BuMeNMe}_2}$  (11)  
 $\text{Fe}(\text{acac})[\text{O}_2\text{NO}]^{\text{BuBuMeth}}$  (12)  
 $\text{Fe}(\text{acac})[\text{O}_2\text{NO}]^{\text{BuMeMeth}}$  (13)  
 $\text{Fe}(\text{acac})[\text{O}_2\text{NO}]^{\text{MeMeMeth}}$  (14)

## Chapter 1. Introduction and overview

### 1.1 Scope of this thesis

This thesis represents work that was directed at the synthesis and characterization of iron complexes containing amine-bis(phenolate) ligands and halides or acetylacetonate co-ligands and their application towards epoxidation of olefins and carbon-carbon cross-coupling reactions. Chapter 1 presents a brief review of iron complexes and their use as catalysts for alkane oxidation, olefin epoxidation, green oxidation of pollutants and carbon-carbon cross-coupling reactions. Chapter 2 describes the synthesis and characterization of amine-bis(phenolate)Fe(III) halide complexes using MALDI-TOF mass spectrometry, UV-vis spectroscopy and single-crystal X-ray diffraction. Variable temperature magnetic moments of these complexes exhibit Curie-Weiss paramagnetism. Chapter 3 presents the Fe-catalyzed epoxidation of olefins using hydrogen peroxide as the terminal oxidant. *In-situ* generated Fe(III) complexes using tridentate amine-bis(phenol) ligands showed modest yield of *trans*-stilbene oxide in acetone. However, the combination of FeCl<sub>3</sub>·6H<sub>2</sub>O and 1-methylimidazole gave excellent yields of epoxide for both terminal and internal aromatic and aliphatic olefins. Chapter 4 presents the synthesis and characterization of amine-bis(phenolate)Fe(III)(acac) complexes using MALDI-TOF mass spectrometry, UV-vis, IR spectroscopy and single crystal X-ray diffraction and their

catalytic activity towards carbon-carbon cross-coupling reactions. Electrochemical studies showed that the redox potentials of these complexes are mainly ligand-centered. Also, these complexes showed some catalytic activity for carbon-carbon cross-coupling between Grignard reagents and secondary alkyl halides.

## 1.2 General properties of iron

Iron is the fourth most abundant element and the second most abundant metal after aluminium in the earth's crust.<sup>1,2</sup> Usually, iron is extracted from its ores. These include magnetite ( $\text{Fe}_3\text{O}_4$ ), hematite ( $\text{Fe}_2\text{O}_3$ ), goethite ( $\text{FeO}(\text{OH})$ ), limonite ( $\text{FeO}(\text{OH}) \cdot n(\text{H}_2\text{O})$ ) and siderite ( $\text{FeCO}_3$ ). The symbol for iron is Fe, originating from the latin name *ferrum*. Its atomic weight is  $55.847 \text{ g mol}^{-1}$ , specific gravity is  $7.874 \text{ g cm}^{-3}$ , melting point is  $1535 \text{ }^\circ\text{C}$  and boiling point is  $2750 \text{ }^\circ\text{C}$ . Fe is available in nature as four different isotopes:  $^{54}\text{Fe}$  (5.82% abundance),  $^{56}\text{Fe}$  (91.66% abundance),  $^{57}\text{Fe}$  (2.19% abundance) and  $^{58}\text{Fe}$  (0.335% abundance).<sup>3</sup> It can occur in several oxidation states with the two most common being +2 and +3. In air, Fe(II) complexes are easily oxidized to Fe(III) which is therefore its most widespread oxidation state. Rarer oxidation states of Fe are +1, +4, +5, +6, 0, -1 and -2. Among them, Fe(IV) is stabilized by macrocyclic ligands such as the tetraanionic tetraamido macrocycle ligand (TAML, details discussed in section 1.5.3), and forms the complex  $[\text{FeCl}(\text{TAML})][\text{Et}_4\text{N}]$  which is stable in both solution and solid state.<sup>4</sup> Similarly, Fe(V) species have been obtained using an octafluoroporphyrin ligand and  $\text{F}^-$  and  $\text{O}^{2-}$  co-ligands which are coordinated to the metal.<sup>5</sup> The high-valent iron complex  $[(\text{Me}_3\text{cy-ac})\text{FeN}](\text{PF}_6)_2$  ( $\text{Me}_3\text{cy-ac}$  = trimethyl-1,4,8,11-

tetraazacyclotetradecane-1-acetate) bearing a terminal nitrido ligand was synthesized photochemically at low temperature (77 K).<sup>6</sup> The low (-2 or 0) oxidation states of iron are important in organometallic chemistry, especially in catalysis, because they are more reactive than their Fe(II) and Fe(III) counterparts.

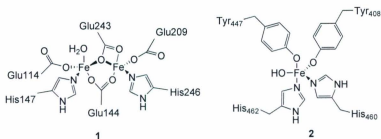
Iron is one of the most important metals for the proper function of nearly all biological systems.<sup>7</sup> It is an essential element for all living organisms except at high concentrations,<sup>8</sup> and is commonly found in a variety of enzymes that catalyze a wide-range of transformations.<sup>9</sup> It plays an important role in biological systems for transporting oxygen within heme-containing proteins such as hemoglobin and myoglobin. Usually in hemoglobin and myoglobin, iron is in a square pyramidal complex where the axial position is occupied by histidine from a protein chain and the four square-planar coordination sites are taken up by a porphyrin ring.<sup>10</sup> Therefore, oxygen can bind with the available coordination site of the iron center and can be transported in blood. Alternatively, non-heme proteins such as hemerythrin possess binuclear iron sites which transport and fix oxygen by forming peroxides.<sup>10</sup> It is also the metal used at the active sites of many important enzymes, such as methane monooxygenases (MMOs) and Rieske dioxygenases. Iron is generally regarded as non-toxic, cheap and environmentally friendly. Therefore, a sustainable metal such as iron is desirable in synthetic chemistry from the economical and ecological point of view.



### 1.3 Coordination chemistry of iron

#### 1.3.1 Iron complexes containing phenolate ligands

Iron is an important metal for naturally occurring non-heme enzymes such as methane monooxygenases (MMOs) and catechol dioxygenases. The active sites of methane monooxygenases (Figure 1.1, **1**) possess two iron atoms bridged by the carboxylate of a glutamate and a  $\mu$ -O bridge of another glutamate, and the other coordination sites are filled by three glutamate residues, two histidine residues and a water molecule.<sup>11</sup> The active sites of catechol dioxygenases, such as protocatechuate 3,4-dioxygenase (3,4-PCD) (**2**), consist of an iron(III) center which is bound to four amino acid residue ligands and a hydroxide. These comprise a  $N_2O_2$  donor set derived from two tyrosine and two histidine residues (Figure 1.1, **2**)<sup>12,13</sup> and exhibit an approximately trigonal bipyramidal geometry.



**Figure 1.1** Active sites of methane monooxygenase (**1**) and catechol dioxygenase (3,4-PCD) (**2**).

These non-heme enzymes have received much attention because of their ability to carry out oxygen transfer reactions and oxidation processes in many biological systems.<sup>14, 15</sup> During the last few decades, several studies have been made to mimic the non-heme iron coordination environment and the structural relationship of these naturally occurring metalloenzymes. In the late 1980s, Que *et al.* reported a series of Fe(III) model complexes comprised of nitrogen-, carboxylate- and phenolate-containing tripodal tetradentate ligands (Figure 1.2).<sup>16-19</sup> The coordination environment of these tripodal ligands influenced the Lewis acidity at the Fe(III) center which played an important role for binding of catechol. These complexes form Fe(DBC)L adducts (DBC = 3,5-di-*tert*-butylcatecholate) and react with oxygen to give intradiol cleavage products, thus showing a good functional mimic of dioxygenase-catalyzed oxidative cleavage.

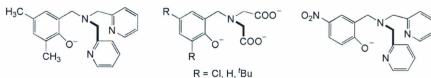
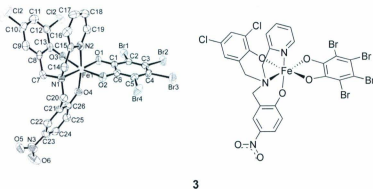


Figure 1.2 Tripodal tetradentate ligands used by Que *et al.*

Krebs *et al.* reported a series of mononuclear Fe(III) complexes as functional and structural model compounds containing tripodal ligands with heterocyclic (benz)imidazolyl/pyridyl/quinolyl nitrogen arms for the cleaving of catechol.<sup>20-22</sup> In all these model complexes, Fe(III) centers exhibit distorted octahedral geometries in the presence of catechol. From their structural analysis, a correlation has been found between the steric demand of ligands and the reactivity of these complexes. When the (O)-Fe-(N)

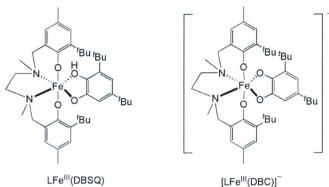
angle between one oxygen of catechol and the nitrogen of the arm is large, the complexes showed low reaction rates towards oxidative cleavage of catechol. Therefore, a ligand consisting of small coordinating groups induces a high Lewis acidity at the Fe(III) center *via* less steric shielding and increases the reactivity of the complex. Furthermore, they synthesized Fe(III) complexes with phenolate-containing tripodal ligands, which are excellent structural models because two oxygen donors of the substituted phenolates mimic the tyrosine groups of the enzyme.<sup>23</sup> The Fe(III) centers have a distorted octahedral coordination sphere with two *cis*-labile ligands such as acetonitrile. These labile ligands are displaced by the catecholate ligand (tetrabromo catecholate = tbc) as shown in complex **3** (Figure 1.3), which is an excellent model compound for the catechol-coordinated intermediate of 3,4-PCD.



**Figure 1.3** Structure of the complex anion in  $\text{HNEt}_3[\text{Fe}(\text{L})(\text{tbc})]$ . Redrawn from reference [23].

Girerd and Münck reported an Fe(III) chloride complex of the tetradentate ligand *N,N'*-bis(4-methyl-6-*tert*-butyl-2-methyl-phenolato)-*N,N'*-bismethyl-1,2-diaminoethane

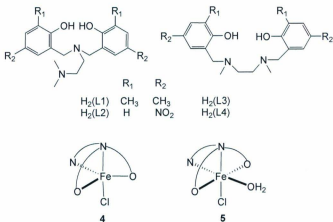
(a so called salan ligand), in which the Fe(III) center resides in a square pyramidal geometry.<sup>24</sup> The crystallographic data reveal that the unit cell of this complex contains two different molecules in the asymmetric unit. In one molecule, two methyl groups in the ethylene fragment are *cis* to each other, whereas in the other they are *trans* to each other. The complex  $\text{LFe}^{\text{III}}\text{Cl}$  reacts with 3,5-di-*tert*-butylcatechol to form the air-stable Fe(III) semiquinato complex,  $\text{LFe}^{\text{III}}(\text{DBSQ})$ , where DBSQ stands for 3,5-di-*tert*-butyl-*o*-benzosemiquinone monoanion. The  $\text{LFe}^{\text{III}}(\text{DBSQ})$  complex is reduced to  $[\text{LFe}^{\text{III}}(\text{DBC})]^-$  (Figure 1.4), which is stable in the presence of  $\text{O}_2$ .



**Figure 1.4** Structure of  $\text{LFe}^{\text{III}}(\text{DBSQ})$  vs.  $[\text{LFe}^{\text{III}}(\text{DBC})]^-$ .

Palaniandavar *et al.* designed a series of Fe(III) model complexes by modifying the substituents of the ligand previously reported by Girerd and Münck. They introduced less sterically bulky H, Me or  $\text{NO}_2$  substituents on the tetradentate linear ligand, or incorporated an *N,N*-dimethylamine pendant arm on tripodal bis(phenol) ligands

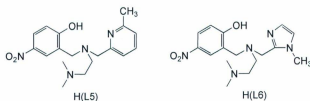
(Figure 1.5).<sup>25</sup> These substituents on the bis(phenol) ligands tune the Lewis acidity of the Fe(III) center, which controls the catechol cleavage activity of the complexes. For example, electron-donating 2,4-dimethyl groups on the bis(phenolate) moieties generated the mononuclear trigonal bipyramidal [LFe(III)Cl] (**4**) complex (Figure 1.5). However, electron-withdrawing NO<sub>2</sub> or less donating H on the bis(phenolate) moieties of the ligands generated octahedral [LFeCl(H<sub>2</sub>O)] (**5**) (Figure 1.5). Room temperature magnetic moment measurements of these complexes are in the range 5.6 to 5.8  $\mu_B$  indicating high-spin d<sup>5</sup> iron centers.



**Figure 1.5** Amine-bis(phenol) ligands and their Fe(III) model complexes.

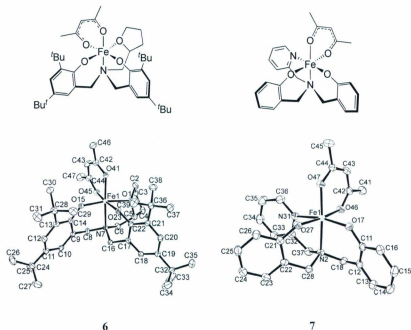
Palaniandavar's group then prepared Fe(III) complexes with tripodal monophenol ligands containing NMe<sub>2</sub> and 6-methylpyridine or *N*-methylimidazole pendant arms (Figure 1.6, H(L5) and H(L6)).<sup>26</sup> The pyridine or imidazole functionality was introduced

to tune the Lewis acidity, coordination environment and the resulting electronic properties of these complexes. For example, in the complex  $[\text{FeLCl}_2]$  (where  $L = \text{L5}$  or  $\text{L6}$ ) two *cis* labile chlorides can be replaced for catechol binding.



**Figure 1.6** Tripodal monophenol ligands used by Palaniandavar's group.

$\text{Fe(III)(acac)}$  ( $\text{acac} = \text{acetylacetonate}$ ) complexes of amine-bis(phenolate) tripodal tetradentate ligands having pendant  $\text{THF}^{27}$  (**6**) or  $\text{pyridine}^{28}$  (**7**) arms have been synthesized and characterized by the Chaudhuri and Bouwman groups, respectively. They were characterized using different techniques such as UV-vis spectroscopy, cyclic voltammetry, elemental analysis and single crystal X-ray diffraction. These complexes exhibit distorted octahedral  $\text{Fe(III)}$  centers where an  $\text{acac}$  co-ligand is coordinated in the usual *cis*-fashion (Figure 1.7). Electrochemical studies showed that redox potentials of these complexes are mainly ligand centered.



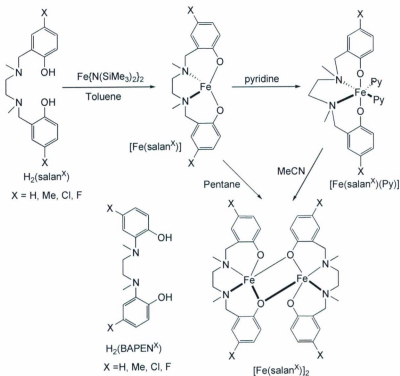
**Figure 1.7** Fe(III)(acac) amine-bis(phenolate) complexes having THF and pyridine pendant arms. Redrawn from reference [27 and 28].

The  $\mu$ -oxo-bridged diiron(III) complexes are of significant interest because of their structural similarity to the active sites of MMOs (methane monooxygenases) and related enzymes.<sup>29,30</sup> Dinuclear Fe(III) complexes containing bis(phenolate) salen ligands such as  $[\text{Fe}_2(\mu\text{-O})(\text{L})_2]^{31}$  ( $\text{H}_2\text{L} = N,N'$ -dimethyl- $N,N'$ -bis(3,5-di-*tert*-butyl-2-hydroxybenzyl)-1,2-diaminoethane) and  $[\text{Fe}_2(\mu\text{-O})(\text{L})_2]\cdot 2\text{H}_2\text{O}^{32}$  ( $\text{H}_2\text{L} = N,N'$ -*o*-phenylenebis(3,5-di-*tert*-butylsalicylidene)diimine) have been synthesized and characterized. The Fe(III) centers are five-coordinate square pyramidal, with  $\text{N}_2\text{O}_2$  donors

occupying the basal plane and an oxo-bridge occupying the axial position. The latter complex was employed for the hydroxylation of alkanes using *m*-CPBA (*meta*-chloroperoxybenzoic acid). Recently, Britovsek *et al.* reported a series of Fe(II) salan complexes containing different substituents, such as Me, Cl and F in the *ortho* and *para* position of the bis(phenolate) moieties.<sup>33</sup> Also, they prepared Fe(II) complexes containing methylated bis(aminophenolate)-ethylenediamine (BAPEN) ligands. These BAPEN ligands generated three five-membered chelating rings around the Fe(II) center, which may increase stability towards oxidation of alkane compared to salan ligands where one five and two six-membered rings are generated. The synthetic route to these Fe(II) complexes involved the reaction of  $H_2(\text{salan}^X)$  or  $H_2(\text{BAPEN}^X)$  with  $[Fe\{N(\text{SiMe}_3)_2\}_2]$  to form dinuclear  $[Fe(\text{salan}^X)_2]$  and  $[Fe(\text{BAPEN}^X)_2]$  possessing phenoxide bridges (Scheme 1.1). Interestingly, in the presence of coordinating solvents such as pyridine (L), mononuclear  $[Fe(\text{salan}^X)L_2]$  and  $[Fe(\text{BAPEN}^X)L_2]$  complexes were formed. Sterically-bulky *tert*-butyl substituents in the *ortho* and *para* positions of the phenolate moieties enhanced the formation of mononuclear complexes. However, in the presence of acetonitrile, phenoxide-bridged dinuclear complexes were formed. These complexes were inert towards the oxidation of alkane, and formed oxo-bridged complexes in the presence of air. Indeed, oxo-bridged Fe(III) complexes were isolated and characterized by single crystal X-ray diffraction.

More coordination chemistry examples of relevance to the work in this thesis will be presented in the introductions to Chapters 2 and 4.



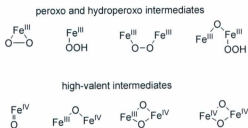


**Scheme 1.1** Salan and BAPEN ligands and their Fe(II) complexes.

### 1.3.2 Iron-oxo complexes

Iron-catalyzed epoxidation of olefins using hydrogen peroxide will be presented in Chapter 3 of this thesis. We speculate that iron-oxo intermediates might form in our catalytic cycle; therefore, a brief literature review on iron-oxo complexes is presented in this section.

Oxygen-transfer reactions *via* metal-oxo species are ubiquitous in biological systems.<sup>34,35</sup> Common examples of metal-oxo species are heme and non-heme iron enzyme model complexes. These model complexes containing Fe(II) or Fe(III) precursors, form mono- or diiron oxo, peroxy, or hydroperoxy intermediates in the presence of oxidizing agents (Scheme 1.2). In 1981, Groves and co-workers reported an Fe<sup>IV</sup>-oxo porphyrin  $\pi$ -cation radical intermediate [(TMP)Fe<sup>IV</sup>=O]<sup>+</sup> (TMP = *meso*-tetramesitylporphyrin) from the reaction of Fe(TMP)Cl and *m*-CPBA in CH<sub>2</sub>Cl<sub>2</sub> and CH<sub>3</sub>OH at -78 °C.<sup>36</sup>



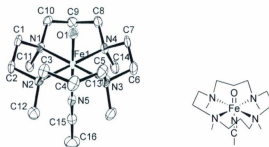
**Scheme 1.2** Intermediates observed in heme and non-heme iron model complexes.

In the late 1990s, the research groups of Ingold,<sup>37</sup> Que<sup>38,39</sup> and Wieghardt<sup>40</sup> speculated about the formation of high-valent Fe<sup>IV</sup>=O as an intermediate species during epoxidation reactions catalyzed by non-heme iron complexes. Evidence was obtained for the formation of Fe<sup>IV</sup>=O from the metastable Fe<sup>III</sup>-OOH species, which was supported by neutral tetra- and pentadentate ligands.<sup>41,42</sup> The metastable Fe<sup>III</sup>-OOH species is short-lived and identified by optical spectra with intense transitions 500-550 nm ( $\epsilon = 1000 \text{ M}^{-1} \text{ cm}^{-1}$ ).<sup>43,44</sup> Fe<sup>IV</sup>-oxo was supported by the formation of [Fe<sub>2</sub>( $\mu$ -O)<sub>2</sub>(5-Et<sub>3</sub>-TPA)<sub>2</sub>](ClO<sub>4</sub>)<sub>3</sub>

(TPA = (tris(2-methylpyridyl)amine) where the formal charges of the irons were III and IV.<sup>39</sup>

In 2003, Münck, Nam, Que and their co-workers isolated a mononuclear non-heme Fe<sup>IV</sup>=O complex (**8**) (Figure 1.8) supported by the macrocyclic ligand TMC (TMC = 1,4,8,11-tetramethyl-1,4,8,11-tetraazacyclotetradecane).<sup>45</sup> Treatment of [Fe<sup>II</sup>(TMC)(OTf)<sub>2</sub>] with iodossyl benzene (PhIO) or hydrogen peroxide gave the pale green complex [Fe<sup>IV</sup>O(TMC)(NCCH<sub>3</sub>)<sub>2</sub>]<sup>2+</sup>, which was stable for at least one month in CH<sub>3</sub>CN at -40 °C. An absorption maximum observed at 820 nm ( $\epsilon = 400 \text{ M}^{-1} \text{ cm}^{-1}$ ), which was too weak for an oxo-to-Fe<sup>IV</sup> charge-transfer transition, was assigned to a d-d transition. Mössbauer studies of this complex showed  $S = 1$ , indicating a low-spin d<sup>4</sup> octahedral iron center. The electrospray mass spectrum of complex **8** exhibited two characteristic peaks at  $m/z$  184.4 (for the dication, corresponding to an exact mass of 368.8) and 476.9 which correspond to [Fe<sup>IV</sup>O(TMC)(NCCH<sub>3</sub>)<sub>2</sub>]<sup>2+</sup> and [Fe<sup>IV</sup>O(TMC)(OTf)]<sup>+</sup> species. A single crystal X-ray structure confirmed the identity of [Fe<sup>IV</sup>O(TMC)(NCCH<sub>3</sub>)<sub>2</sub>]<sup>2+</sup>, which was grown from CH<sub>3</sub>CN/diethyl ether at -40 °C (Figure 1.8). The Fe-O distance in **8** is 1.6446(3) Å, which is close to the deduced distance from the extended X-ray absorption fine structure (EXAFS) spectrum of an Fe<sup>IV</sup>=O porphyrin complex<sup>46,47</sup> but shorter than the Fe-O distance of 1.813(3) Å and 1.79 Å for [Fe<sup>III</sup>(O)(L)]<sup>2+</sup> {L = tris([N'-tert-butylureaylato)-N-ethyl]amine trianion}<sup>48</sup> and di-oxo-bridged [Fe<sup>IV</sup>( $\mu$ -O)<sub>2</sub>(BPMCNCN)<sub>2</sub>]<sup>4+</sup> (BPMCNCN = N,N'-bis(2-pyridylmethyl)-N,N'-dimethyl-*trans*-1,2-diaminocyclohexane),<sup>49</sup> respectively. This distance reflects the Fe-O double bond character. From the crystal structure, it has been observed that the four nitrogen-

containing coordination sites of the ligand are perpendicular to the Fe-O axis and the sixth ligand CH<sub>3</sub>CN, is approximately co-linear with Fe=O.



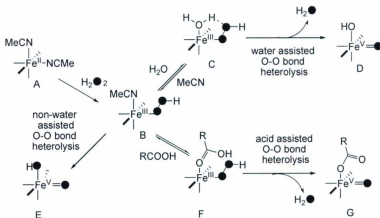
8

**Figure 1.8** Crystal structure of the  $[\text{Fe}^{\text{IV}}\text{O}(\text{TMC})(\text{NCCH}_3)]^{2+}$  cation. Redrawn from reference [45].

Since then, several examples of non-heme  $\text{Fe}^{\text{IV}}=\text{O}$  units<sup>40,45,50-61</sup> were obtained from the reaction of an iron(II) precursor with oxygen transfer agents such as hydrogen peroxide, peroxyacid or PhIO. Also,  $\text{Fe}^{\text{IV}}=\text{O}$  can be formed by the decomposition of  $\text{FeOOR}$  ( $\text{R} = \text{tBu}, \text{H}$ ) species *via* O-O homolysis.<sup>54,62</sup> In these complexes, the  $\text{Fe}^{\text{IV}}=\text{O}$  units are stabilized by ligands containing four neutral amine/pyridine nitrogen donors in a planar or nonplanar arrangement.

High-valent  $\text{Fe}^{\text{V}}=\text{O}$  species have also been proposed as intermediates for oxygen transfer reactions involving enzyme model complexes of iron.<sup>63</sup> Que *et al.* proposed that  $\text{Fe}^{\text{V}}=\text{O}$  might be generated from the low spin  $[\text{Fe}^{\text{III}}(\text{TPA})(\text{OOH})]^{2+}$  species where the Fe(III) center has an available coordination site *cis* to the  $\eta^1\text{-OOH}$  for binding a water molecule.<sup>64</sup> An intramolecular hydrogen bond between water and the terminal oxygen of

Fe-OOH generates a five-membered ring (C). Raman studies and DFT calculations<sup>65,66</sup> were consistent with the coordination of hydroperoxide to Fe strengthens the Fe-O bond and enhances the O-O heterolysis resulting in the formation of HO-Fe<sup>V</sup>=O species (D) (Scheme 1.3).



**Scheme 1.3** Generation of iron hydroperoxo and iron-oxo intermediates from non-heme iron complexes. ● indicates an isotopically labeled <sup>18</sup>O.

Later, the Que group reported a series of non-heme iron complexes that generated an Fe<sup>V</sup>=O intermediate species for the hydroxylation of alkane and olefin epoxidation.<sup>51,67-70</sup> Collins *et al.* have also reported a complex containing an Fe<sup>V</sup>=O unit. It was supported by a TAML ligand and was characterized by mass spectrometry, Mössbauer, electron paramagnetic resonance and X-ray absorption spectroscopy.<sup>71</sup> Recently, the Que<sup>72</sup> group also reported further evidence for the formation of Fe<sup>V</sup>=O

intermediates (G) of non-heme iron complexes with  $\text{H}_2\text{O}_2$  in the presence of acid (Scheme 1.3).

#### 1.4 Introductory magnetochemistry of iron<sup>73-76</sup>

The amine-bis(phenolate) complexes of iron described in this thesis are in the +3 oxidation state, hence possess unpaired electrons in d-orbitals. The examination of the magnetic behavior of these complexes provides important information related to the oxidation and spin states of the iron center. This section will focus briefly on the theory of magnetism in transition metal complexes, in particular iron complexes.

Magnetic susceptibility ( $\chi$ ) is a fundamental term for the study of the magnetism of a material. It is a quantitative measure of response of a material to an external magnetic field. Fundamentally, all materials exhibit two types of magnetic behavior: diamagnetism and paramagnetism. Diamagnetism is generated by paired electrons which oppose the applied field, whereas paramagnetism is generated by unpaired electrons and reinforces the applied field. Diamagnetic susceptibility is negative and rather small, being of the order of  $-1$  to  $-100 \times 10^{-6} \text{ emu mol}^{-1}$ . The value of diamagnetic susceptibility is used for the correction of total susceptibility by adding it to the paramagnetic susceptibility. Paramagnetism is a significantly stronger effect and is characterized by large, positive  $\chi$  values.

Paramagnetic susceptibility is temperature dependant. The magnetic susceptibility varies inversely with temperature, which is known as the Curie law,  $\chi = C/T$ ; where C is

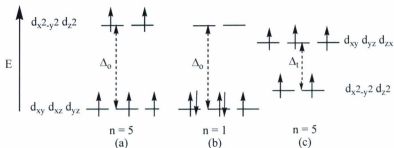
the Curie constant. Deviations from the Curie law are found when the magnetic ions begin to interact with one another. This is described in a high temperature approximation by the Curie-Weiss law,  $\chi = C/(T-\theta)$ ; where a non-zero Weiss constant  $\theta$ , suggests the presence of an interaction. For example, iron(III) has no low lying energy levels whose population changes with temperature, and thus obeys the Curie law (also the Curie-Weiss law) over a wide range of temperatures.

Since the magnitude of the magnetic susceptibility ( $\chi$ ) is an inconvenient number at room temperature, it can be represented by a term called the effective magnetic moment ( $\mu_{\text{eff}}$ ) in units of Bohr magnetons ( $\mu_B$ ), which is defined as:

$$\mu_{\text{eff}} = \left( \frac{3k}{N_A \beta^2} \right)^{1/2} (\chi_m T)^{1/2} = 2.828 (\chi_m T)^{1/2} \mu_B$$

where  $k$  is the Boltzmann constant,  $N_A$  is Avogadro's number,  $\beta$  is the Bohr magneton of the electron,  $\chi_m$  is molar susceptibility and  $T$  is absolute temperature.

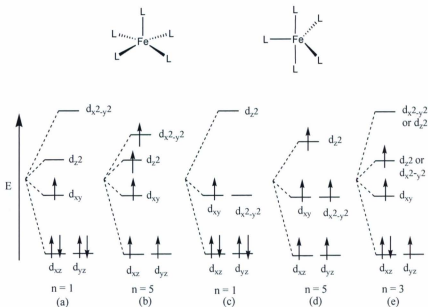
The spin-state of a transition metal complex depends on the splitting of the d-orbitals, as predicted by crystal field (CF) theory. For example, five degenerate d-orbitals of an octahedral iron complex can split into two energy levels, with triply degenerate low-lying  $t_{2g}$  ( $d_{xy}$ ,  $d_{yz}$ ,  $d_{zx}$ ) and doubly degenerate high-energy  $e_g$  ( $d_{x^2-y^2}$ ,  $d_{z^2}$ ) orbital sets. When the complex is in the Fe(III) state, two possibilities exist for the population of  $d^5$  electrons. A high-spin system is achieved when the maximum number of unpaired electrons occupies the available orbitals when the ligands are weak field (Figure 1.9 (a)).



**Figure 1.9** The d-orbital splitting diagrams for  $d^5$  (a) high-spin octahedral  $S = 5/2$ ; (b) low-spin octahedral  $S = 1/2$ ; (c) high-spin tetrahedral  $S = 5/2$  systems; where  $n$  is the number of unpaired electrons,  $\Delta_0$  and  $\Delta_t$  are the octahedral and tetrahedral crystal field splitting parameters.

For strong field ligands, a low-spin system is obtained giving the maximum number of paired electrons in the available orbitals (Figure 1.9 (b)). However, for a tetrahedral Fe(III) complex,  $d^5$ -electrons occupy both the lower energy doubly degenerate  $e$  and higher energy triply degenerate  $t_2$  sets (Figure 1.9 (c)). In the case of square pyramidal or trigonal bipyramidal Fe(III) complexes, low-spin  $S = 1/2$  cases become possible for strong field ligands (Figure 1.10 (a) and (c)). This happens due to one of the d-orbitals shifting to such a high energy that it may not become populated by electrons. However, for weak field ligands, a high-spin  $S = 5/2$  state may occur. (Figure 1.10 (b) and (d)). Sometimes an intermediate  $S = 3/2$  spin state can occur (Figure 1.10 (e)).





**Figure 1.10** The d-orbital splitting diagrams for  $d^5$  (a) low-spin square pyramidal  $S = 1/2$  (considering  $\sigma$  and  $\pi$  bonding interaction); (b) high-spin square pyramidal  $S = 5/2$  (considering  $\sigma$  and  $\pi$  bonding interaction); (c) low-spin trigonal bipyramidal  $S = 5/2$  and (e) intermediate spin  $S = 3/2$  systems; where  $n$  is the number of unpaired electrons.

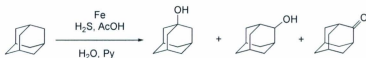
## 1.5 Iron catalysis

### 1.5.1 Iron-catalyzed alkane oxidation

In modern synthetic chemistry, iron has become an alternative choice to traditional precious metal catalysts as it is non-toxic, inexpensive and abundant. Usually, precious transition metals such as Pd, Ir, Rh, and Pt are used for catalytic transformations, such as synthetically important C-H bond activations.<sup>9</sup> A rapid development in iron

catalysts has been observed in the last few years by combining the advantages of Fe chemistry with C-H activation, for example, in the catalytic oxidation of hydrocarbons.

The catalytic oxidation of hydrocarbons especially alkane oxidation, is a particularly challenging task in synthetic chemistry.<sup>7</sup> The C-H bond in an alkane is very strong and stable, therefore, its activation is not very straightforward and requires highly reactive reagents, high temperature and/or pressure. In nature, cytochrome P-450 or the non-heme iron-containing  $\omega$ -hydroxylase enzyme are capable of selective hydroxylation of unactivated C-H bonds in hydrocarbons. Scientists are interested in mimicking these model systems in the laboratory.

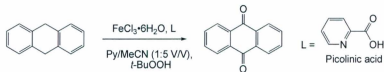


**Scheme 1.4** Oxidation of adamantane to adamantanol and adamantanone.

In 1983, Barton and co-workers discovered an iron-catalyzed oxidation reaction of an alkane.<sup>77</sup> Adamantane was oxidized to 1-adamantanol, 2-adamantanol and 2-adamantanone using molecular oxygen and a system comprised of hydrogen sulfide, and iron powder in pyridine containing acetic acid and water (Scheme 1.4). Also, they found that adamantane could be selectively oxidized to adamantanol and adamantanone in the presence of zinc and iron powder in pyridine containing aqueous acetic acid giving a total yield of oxidized products up to 13.8%.<sup>78</sup> A crystalline black material was isolated from the catalyst mixtures which was found to be a tri-iron cluster compound of the formula

$\text{Fe}^{\text{II}}\text{Fe}^{\text{III}}_2\text{O}(\text{OAc})_6(\text{Py})_3$ . The substrate scope was extended to cyclohexane, methylcyclohexane, cyclooctane and 2-methylbutane,<sup>79</sup> and in all cases the oxidized product mixtures were the corresponding alcohols and ketones.

In addition to molecular oxygen, other oxidants such as  $\text{H}_2\text{O}_2$  and *t*-BuOOH have been used in different alkane oxidation systems. In 2002, Kim and co-workers reported the iron-catalyzed oxidation of an activated methylene unit, such as in 9,10-dihydroanthracene, 1-ethylbenzene, and diphenylmethane, to the corresponding ketones with high yields (up to 100%).<sup>80</sup> The catalyst was a combination of  $\text{FeCl}_3 \cdot 6\text{H}_2\text{O}$  and 2-picolinic acid in a mixture of pyridine (1 mL) and  $\text{CH}_3\text{CN}$  (5 mL), and *t*-BuOOH was used as the oxidizing agent in the presence of air (Scheme 1.5). Picolinic acid possibly acted as the ligand.



**Scheme 1.5** Oxidation of 9,10-dihydroanthracene.

In 2007, Bolm and co-workers improved Kim's system by oxidizing the activated methylene unit in benzylic moieties without using any acid or added ligand, besides the coordinating Lewis basic solvents, pyridine and acetonitrile.<sup>81</sup> The optimized conditions were the use of a 2 mol% loading of  $\text{FeCl}_3 \cdot 6\text{H}_2\text{O}$  and 3 equiv. of *t*-BuOOH in pyridine at 82 °C under air, leading to the formation of the corresponding ketones. Different substrates such as diarylmethylene derivatives and acyclic systems bearing one hetero-

aryl group were oxidized under the optimized conditions. Excellent yields (up to 99%) of ketone products were obtained from most diarylmethylene derivatives. However, *p*-methoxytoluene was converted to the corresponding carboxylic acid in moderate yield (53%).

Bauer and co-workers introduced iron phosphinooxazoline complexes for the oxidation of benzylic CH<sub>2</sub> groups to the corresponding ketones.<sup>82</sup> Two possible structures (9 and 10) of these complexes are shown in (Figure 1.11). The complexes were not structurally characterized. However, IR spectra showed two different ν<sub>C=N</sub> stretching frequencies indicating two non-equivalent nitrogen donor atoms in the coordination sphere. Although paramagnetic, reasonable NMR spectra were obtained with some line broadening. The <sup>1</sup>H NMR chemical shifts of the two oxazoline rings were different. Therefore, the complex was proposed to be the *cis*-isomer. Employing 2 mol% of this complex, 38-93% oxidized products were obtained from dihydroanthracene, diphenylmethane and fluorene using *t*-BuOOH as oxidizing agent.

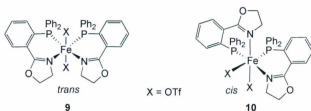
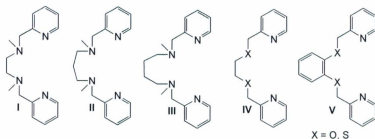


Figure 1.11 Iron(II) phosphinooxazoline complexes.

Selective oxidation of unactivated isolated and aliphatic (sp<sup>3</sup>) C-H bonds is a major challenge in modern chemistry.<sup>83,84</sup> A large number of different catalytic systems

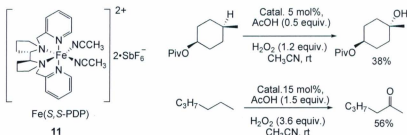
have been developed during the last few decades. Among them, non-heme iron catalysts play a vital role in the aliphatic C-H oxidation process. Iron catalysts containing nitrogen-based ligands, namely the tripodal tetradentate ligands TPA,<sup>50,85</sup> (tris(2-methylpyridyl)amine), linear tetradentate ligands BPMEN<sup>86</sup> (*N,N'*-dimethyl-*N,N'*-bis(2-pyridylmethyl)-1,2-diaminoethane) and BQEN<sup>87</sup> (*N,N'*-dimethyl-*N,N'*-bis(8-quinolyl)-1,2-diaminoethane) have been used for the oxidation of alkanes using H<sub>2</sub>O<sub>2</sub> as oxidant. Common features of these non-heme iron catalysts were the use of tetradentate ligands, which contain at least two pyridine type donors and two *cis* labile coordinating co-ligands such as triflates or acetonitrile. In solution, these labile coordinating ligands easily dissociate and form active iron-oxo species with the addition of H<sub>2</sub>O<sub>2</sub>. Recently, high valent iron-oxo species have been spectroscopically identified and characterized.<sup>72,88</sup> Also, steric and electronic effects of different substituents on these ligands significantly influence the stability of the catalysts under the harsh oxidation conditions. Britovsek and co-workers tried to increase the catalyst stability by modifying the ligand backbone by varying the number and hybridization of carbon atoms (I-V) (Figure 1.12).<sup>89</sup>



**Figure 1.12** Changing the backbone of BPMEN ligands.

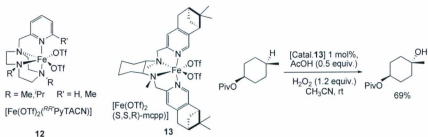
Also, different donor atoms were introduced such as oxygen and sulfur in the ligand backbone.<sup>90</sup> Britovsek found that ligand rigidity and strong ligand field effects increased the catalyst's stability towards alkane oxidation, which is critically important for catalytic activity under harsh oxidation conditions. Oxidation of cyclohexane was carried out using iron complexes of these ligands in acetonitrile at room temperature. A 65% yield of oxygenated products was obtained with a 9:1 ratio of CyOH to CyO using 10 equiv. of H<sub>2</sub>O<sub>2</sub>.

There are few examples of non-heme iron catalysts for the stereospecific hydroxylation of simple alkane substrates.<sup>86,91,92</sup> White and co-workers reported selective aliphatic C-H bond oxidation for a broad range of substrates using electrophilic Fe(*S,S*-PDP) (PDP = 2-((*S*)-2-[(*S*)-1-(pyridin-2-ylmethyl)pyrrolidin-2-yl]pyrrolidin-1-yl)methylpyridine) catalyst (**11**) using inexpensive H<sub>2</sub>O<sub>2</sub> as oxidant (Figure 1.13).<sup>93-95</sup> Selectivity was obtained on the basis of electronic and steric properties of the substrate. In all cases, the most electron-rich tertiary (3°) C-H bonds oxidized to alcohols and methylene C-H bonds oxidized to ketones (Figure 1.13).



**Figure 1.13** Fe(*S,S*-PDP) complex and its catalytic activity.

Costas and co-workers reported a series of novel non-heme iron complexes (**12**) containing methylpyridine derivatized triazacyclononane (TACN) ligands which showed an unprecedented efficiency in the stereospecific oxidation of alkanes (Figure 1.14).<sup>51</sup> The ratio of alcohol (A) and ketone (K) products depend on the substitution pattern of the pyridine ring. When the substituted groups are less bulky, such as H or Me, compared to <sup>t</sup>Pr, then the A/K ratio is increased. Under the conditions (1000 equiv. of substrate, cyclohexane vs. catalyst), 76% of oxidized products were obtained with a remarkably high cyclohexanol to cyclohexanone ratio (12.3:1). These catalysts were also used for the epoxidation of olefins to *cis*-diols. Again, Costas and co-workers reported a very active iron catalyst (**13**) for the stereospecific hydroxylation of alkanes.<sup>96</sup> In that case, they modified the MEP ligand (MEP = *N,N'*-dimethyl-*N,N'*-bis(2-pyridylmethyl)ethane-1,2-diamine) by introducing a bulky hydrocarbon group such as pinene at the 4 and 5 positions of pyridine (Figure 1.14). This steric bulk group prevents the formation of noncatalytic oxo-dimers and oligomeric species. As a result the iron site is embedded in an oxidatively robust cavity. Using 1 mol% catalyst loading, 35-69% of hydroxylated products were obtained from tertiary alkanes such as *cis*-1,2-dimethylcyclohexane, 1-methyl,4-pivaloyl cyclohexane, acetoxy-*p*-menthane and 2,6-dimethyloctane. The preferences for tertiary C-H bond oxidation over secondary C-H bonds indicate site selectivity and strength of C-H bonds. This is the best non-heme iron hydroxylation catalyst reported so far.



**Figure 1.14**  $\text{Fe}^{\text{R}^{\text{R}'}}\text{PyTACN}$  (**12**) and  $\text{Fe}(\text{S,S,R}-\text{mcpp})$  (**13**) complexes and their catalytic activities.

In conclusion, the iron-catalyzed oxidation of alkanes is still in its early stage and much work is needed to further develop the field.

### 1.5.2 Iron-catalyzed olefin epoxidation

Metal-catalyzed oxidation of olefins represents the most elegant and environmentally friendly route for the synthesis of epoxide products.<sup>97,98</sup> Olefins are one of the most important starting materials for organic synthesis and their oxidation leads to various value-added products such as epoxides, alcohols, aldehydes, ketones, and carboxylic acids. These in turn are important building blocks for the production of bulk and fine chemicals.<sup>99</sup>

Different oxidizing agents may be used for the metal-catalyzed epoxidation of olefins. Typical oxidizing agents used are alkyl hydroperoxide, hypochlorite salts (e.g. NaOCl) or iodosylbenzene. Problems associated with these oxidizing agents are the low active oxygen content and waste by-products which lower the atom economy



of the reaction (Table 1.1).<sup>100</sup> One of the current industrial processes for the production of simple epoxides (e.g. propylene oxide) is the chlorohydrin process. This process involves chlorine in the presence of NaOH producing 2.01 tons of NaCl and 0.102 ton of 1,2-chloropropane by-product per ton of propylene oxide.<sup>101</sup> Considering this, molecular oxygen would be the most preferred oxidizing agent because its high content of active oxygen and low cost. However, poor selectivity towards epoxides has been observed to date when using molecular oxygen as terminal oxidant,<sup>102</sup> whereas hydrogen peroxide is suggested to be easier to handle, and more selective.<sup>103</sup>

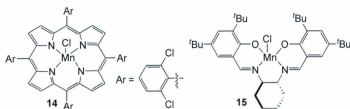
Many catalysts comprised of different metals have been used in the presence of H<sub>2</sub>O<sub>2</sub> for the epoxidation of olefins.<sup>103</sup> Some of these catalysts, which have been developed in combination with H<sub>2</sub>O<sub>2</sub> are polyoxometals<sup>104</sup> (W or Mo), ruthenium<sup>105-109</sup> and rhenium<sup>110</sup> but these metals are expensive and toxic. Therefore, hydrogen peroxide develops an ideal system by combining with a non-toxic and inexpensive metal catalyst for epoxidation reactions, especially in liquid-phase processes in industry.<sup>111-118</sup> Hence, the use of H<sub>2</sub>O<sub>2</sub> in combination with catalytic amounts of first-row late-transition metals such as Fe or Mn, is desirable.

**Table 1.1** Oxidants used in the metal-catalyzed epoxidations and their active oxygen content.

Oxidant	Active oxygen content (wt.%)	Waste by-product*
Oxygen (O <sub>2</sub> )	100	Nothing or H <sub>2</sub> O
Oxygen (O <sub>2</sub> )/ reductor	50	H <sub>2</sub> O
H <sub>2</sub> O <sub>2</sub>	47	H <sub>2</sub> O
NaOCl	21.6	NaCl
CH <sub>3</sub> CO <sub>3</sub> H	21.1	CH <sub>3</sub> COOH
<i>t</i> -BuOOH (TBHP)	17.8	<i>t</i> -BuOH
KHSO <sub>5</sub>	10.5	KHSO <sub>4</sub>
Me <sub>3</sub> SiOOSiMe <sub>3</sub>	9	Me <sub>3</sub> SiOSiMe <sub>3</sub>
PhIO	7.3	PhI

\*Other by-products can be produced depending on substrates.

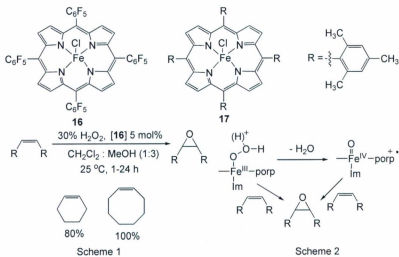
There is an interest in the use of manganese complexes for the epoxidation of olefins. Using H<sub>2</sub>O<sub>2</sub> as a terminal oxidant with this metal can result in decomposition of the catalyst due to the potency of this oxidant. However, Mansuy and co-workers introduced a chlorinated manganese porphyrin complex (**14**) Mn(TPP)Cl (TPP = tetraphenylporphyrin) in the presence of an imidazole or imidazolium carboxylate additive, which efficiently catalyzed the oxidation of alkenes to epoxides (Figure 1.15).<sup>119</sup> The epoxide product in 45% yield was obtained from styrene after 1h stirring using 2.5 mol% Mn(TPP)Cl and 0.5 equiv. of imidazole. An important breakthrough came in the 1990s when Jacobsen and Katsuki simultaneously explored a chiral Mn(salen) complex (**15**) for the enantioselective epoxidation of alkenes (Figure 1.15).<sup>120-122</sup>



**Figure 1.15** Manganese porphyrin Mn(TPP)Cl complex (**14**) and Jacobsen's Mn(salen) complex (**15**) for the epoxidation of olefins.

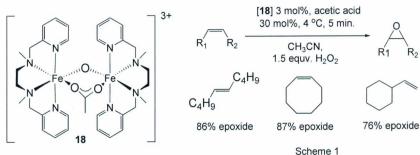
Similar to manganese complexes, iron salts and complexes can also be used as catalysts for the epoxidation of alkenes.<sup>100</sup> For example, iron porphyrin complexes have been used for the epoxidation of an alkene in the presence of hydrogen peroxide as a terminal oxidant. Often, inferior conversion and selectivity were observed due to the rapid decomposition of hydrogen peroxide in the presence of iron. However, Traylor and co-workers reported a polyfluorinated [Fe(TPP)Cl] complex (**16**) (TPP = tetraphenylporphyrin) for the epoxidation of cyclooctene to the corresponding epoxide in high yield (Figure 1.16).<sup>123</sup> The optimal requirements for this process were 5 mol% catalyst loading and slow addition of the oxidant (30% H<sub>2</sub>O<sub>2</sub>) (Figure 1.16, Scheme 1). Also, Nam and co-workers reported an electron-rich Fe(III) porphyrin complex (**17**) (*meso*-tetramesitylporphinato)iron(III) chloride [Fe(TMP)Cl], which catalyzed the epoxidation of olefins with 30% H<sub>2</sub>O<sub>2</sub> in the presence of 5-Cl-1-methylimidazole in an aprotic solvent (Figure 1.16).<sup>124</sup> This electron-poor 5-Cl-1-methylimidazole was shown to have an important role in the catalyst activity of Fe(TMP)Cl. It bonded with the Fe(TMP)Cl complex,

decelerating the O-O bond cleavage of the intermediate [(TMP)Fe-OOH] or (TMP)Fe-H<sub>2</sub>O<sub>2</sub> adduct. As a result, the life-times of the intermediates became longer, and directly transferred oxygen to the olefinic substrates to form epoxides. Also, the intermediate formed a high-valent iron-oxo radical cation (TMP)<sup>+</sup>Fe=O complex by losing water and transferring oxygen to the olefins to form epoxides (Figure 1.16, Scheme 2).



**Figure 1.16** Iron porphyrin Fe(TPP)Cl (**16**) and Fe(TMP)Cl (**17**) complexes and their activities towards epoxidation of olefins.

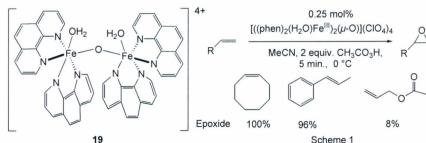
Various research groups<sup>51,68,125-127</sup> reported iron complexes containing multidentate, non-macrocyclic, *N*-donor ligands. These complexes activate the oxidant, H<sub>2</sub>O<sub>2</sub>, without formation of free radicals. In 2001, Jacobsen and co-workers presented an efficient epoxidation catalyst for terminal olefins which are normally a challenging class of substrates.<sup>125</sup> By employing easily-prepared iron complexes in the presence of H<sub>2</sub>O<sub>2</sub> (aqueous 50 wt.%), a wide variety of aliphatic olefins gave the corresponding epoxides within 5 min in 60-90% isolated yields. For example, 1-dodecene was converted to 90% epoxide product using 3 mol% catalyst after 5 min of stirring. This system was also applicable for non-terminal olefins such as cyclooctene, *trans*-5-decene (Figure 1.17, Scheme 1). They explored a catalyst system consisting of the tetradentate MEP ligand (MEP = *N,N'*-dimethyl-*N,N'*-bis(2-pyridylmethyl)ethane-1,2-diamine) and an iron(II) precursor in acetonitrile. The mononuclear [Fe<sup>II</sup>(MEP)(CH<sub>3</sub>CN)<sub>2</sub>](ClO<sub>4</sub>)<sub>2</sub> complex gave a relatively lower yield of epoxide (40% for 1-decene) with 4 equiv. of H<sub>2</sub>O<sub>2</sub>. However, *in-situ* generated [Fe<sup>II</sup>(MEP)(CH<sub>3</sub>CN)<sub>2</sub>](SbF<sub>6</sub>)<sub>2</sub> in the presence of acetic acid increased the product yield up to 90%. They isolated a  $\mu$ -oxo, carboxylate bridged diiron(III) complex (**18**) (Figure 1.17) which is reminiscent of the active site of the oxidized methane monooxygenase (MMO).<sup>29</sup>



**Figure 1.17** Jacobsen's Fe(MEP) catalyst (**18**) and its activity towards epoxidation of olefins.

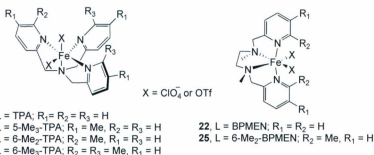
Stack and co-workers reported a  $\mu$ -oxo diiron complex for the epoxidation of terminal alkenes.<sup>128</sup> The catalyst was  $[[(\text{phen})_2(\text{H}_2\text{O})\text{Fe}^{\text{III}}]_2(\mu\text{-O})](\text{ClO}_4)_4$  or  $[[(\text{phen})_2(\text{H}_2\text{O})\text{Fe}^{\text{III}}]_2(\mu\text{-O})](\text{NO}_3)_4$  formed by the combination of an iron(III) precursor (ferric perchlorate or ferric nitrate) with 2 equiv. of phenanthroline in MeCN/H<sub>2</sub>O. A 0.25 mol% *in-situ*, or isolated, catalyst was used for a variety of substrates including electron-poor and electron-rich alkenes, styrene and allyl derivatives at 0 °C in the presence of 32% peracetic acid (Figure 1.18, Scheme 1). Good to excellent yields (up to 100%) of epoxide products were obtained within 5 min. The catalyst (**19**) consists of two phenanthroline ligands (phen) bonded to each iron center in a *cis*-fashion and therefore, bridging oxide and water ligands coordinated to the adjacent *cis* sites of iron (Figure 1.18). The active oxidant species was proposed to be a complex which might form through water displacement at one or both iron centers by a monodentate or bridging peracetic

acid. Evidence for that hypothesis was the inactivity of  $[((\text{phen})_2(\text{Cl})\text{Fe}^{\text{III}})_2(\mu\text{-O})](\text{Cl})_2$  complex towards the epoxidation of alkenes due to the stronger Fe-ligand bond strength of chloride versus water.



**Figure 1.18** Stack's Fe(phen) catalyst (**19**) and its activity towards epoxidation of olefins.

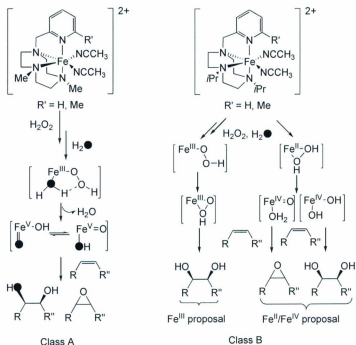
Que and co-workers<sup>68,86,129</sup> reported a series of iron complexes (Figure 1.19) containing TPA (*tris*(2-methylpyridyl)amine) or BPMEN (*N,N'*-dimethyl-*N,N'*-bis(2-pyridylmethyl)-1,2-diaminoethane) ligands and detailed mechanistic studies of epoxidation and *cis*-hydroxylation of alkenes using the complexes as catalysts. The substituent pattern on the TPA and BPMEN ligands and the two labile *cis*-coordination sites on iron were crucially important to achieving high catalyst activity. Iron complexes containing both TPA and BPMEN ligands were able to generate high-valent HO-Fe=O species, which contained both oxo and hydroxy functional groups.<sup>68,69</sup> From isotope labeling studies, it was found that when the oxo group transferred to the alkene, it produced epoxide whereas hydroxy group transfer produced *cis*-diol.



**Figure 1.19** Iron TPA and BPMEN complexes with different substituents on pyridine rings.

Recently, Costas and co-workers reported iron complexes containing <sup>RR</sup>PyTACN (pyridine derivatized triazacyclonane) (R = Me, <sup>t</sup>Pr and R' = H, Me) ligands which produced epoxide and diol from olefins.<sup>51</sup> The selectivity of products (epoxide/diol ratio) was controlled by the substituent groups on the pyridine ring. From their isotope labeling studies, it was observed that the less sterically-bulky groups such as methyl enhanced epoxide formation whereas the more bulky <sup>t</sup>Pr group favoured diol formation (Scheme 1.6). The investigated complexes were classified into two categories: class A and class B. Class A catalysts formed HO-Fe<sup>V</sup>=O intermediates *via* inserting one oxygen atom from water and another one from peroxide and favoured epoxide product formation. Class B catalysts formed intermediate Fe<sup>III</sup>-OOH or HO-Fe<sup>IV</sup>-OH *via* inserting both oxygen atoms from peroxide and favoured *cis*-hydroxylation. These complexes had earlier shown excellent efficiencies for the stereospecific hydroxylation of alkanes.<sup>51</sup>

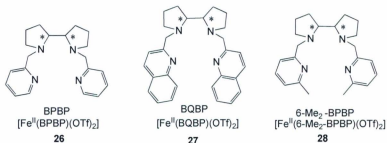




**Scheme 1.6** Mechanism of iron<sup>RR'</sup>PyTACN complexes for epoxidation/hydroxylation of olefins. ● indicates an an isotopically labeled <sup>18</sup>O.

Que *et al.* reported iron complexes bearing (BPBP), (BQBP) and 6-Me<sub>2</sub>-BPBP ligands for the oxidation of olefins with high enantiomeric excess (Figure 1.20).<sup>130</sup> In all of these complexes, two *cis*-labile ligands were coordinated *trans* to the pyrrolidine backbone and Fe-N<sub>pyrrolidine</sub> bond lengths were similar. The Fe-N<sub>pyridine/quinoline</sub> bond lengths of Fe complexes **26**, **27** and **28** were 2.192 Å, 2.272 Å and 2.264 Å indicating high-spin Fe(II) centers. Using these complexes for the oxidation of olefins with H<sub>2</sub>O<sub>2</sub>, selectivity of epoxide formation was favoured for complexes containing a less

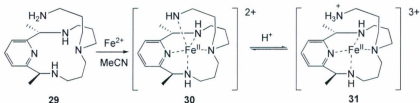
sterically bulky  $\alpha$ -position substituted pyridine such as **26**. Catalyst **26** gave a 1:4.6 ratio of *cis*-diol/epoxide product from *trans*-2-heptene using 10 equiv. of  $\text{H}_2\text{O}_2$  at ambient temperature in 20 min. Increasing the steric bulkiness of these complexes, catalyst selectivity moved towards diol formation. The complex  $[\text{Fe}^{\text{II}}(\text{BPBP})(\text{OTf})_2]$  (**28**) showed the best hydroxylation efficiency for *trans*-2-heptene, with 97% *ee* which is comparable with Sharpless asymmetric dihydroxylation.<sup>131</sup>



**Figure 1.20** Optically active ligands and their corresponding iron complexes.

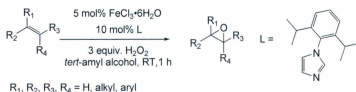
Rybak-Akimova and co-workers reported a pyridine-containing macrocyclic iron(II) complex (**30**) bearing an aminopropyl pendant arm which was an excellent catalyst for the epoxidation of cyclooctene (Figure 1.21).<sup>132</sup> The complex exhibited a distorted square-pyramidal coordination geometry where the aminopropyl pendant arm occupied the axial position. **30** only acted as an active catalyst in the presence of trifluoromethanesulfonic acid (HOTf). The pendant amino group was protonated by HOTf which opened a coordination site within the complex, which became available for the oxidizing agent or a substrate to coordinate. Using 5 mol% of complex **31**, oxidation of cyclooctene gave 89% epoxide, with 98% selectivity within 5 min. No 1,2-diol or

allylic by-products were observed. However, terminal olefins such as 1-octene gave relatively low yields (32-76%) of the corresponding epoxide.



**Figure 1.21** Biomimetic iron complex containing a pyridine macrocycle ligand bearing a pendant arm.

Beller and co-workers reported an elegant and simple method for the epoxidation of olefins using a combination of  $\text{FeCl}_3 \cdot 6\text{H}_2\text{O}$  and 2,6-pyridinedicarboxylic acid ( $\text{H}_2\text{pydic}$ ) in the presence of an organic base.<sup>133-136</sup> 30%  $\text{H}_2\text{O}_2$  was used as the terminal oxidant and good yields of epoxides were obtained. They developed another catalytic system using  $\text{FeCl}_3 \cdot 6\text{H}_2\text{O}$  and imidazole and its derivatives.<sup>137-139</sup> Through these studies, it was found that 5-chloro-1-methylimidazole as an additive increased epoxide yields for aromatic olefins, but was unsuccessful in the epoxidation of aliphatic olefins.<sup>139</sup> However, bulky imidazole additives were found to facilitate for epoxidation of a broader range of substrates including aliphatic olefins (Scheme 1.7).<sup>138</sup> Recently, Beller and Costas reported a biomimetic iron catalyst for the epoxidation of olefins using molecular oxygen at room temperature.<sup>140</sup> The catalyst was a combination of  $\text{FeCl}_3 \cdot 6\text{H}_2\text{O}$ , imidazole and  $\beta$ -ketoester (ethyl-2-oxocyclopentanecarboxylate).



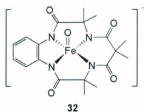
**Scheme 1.7** Olefin epoxidation by Beller and co-workers.

### 1.5.3 Fe-TAML complexes in green oxidation reactions

An adequate supply of clean drinking water is very important for healthy living,<sup>141</sup> yet pure drinking water is getting scarce in some parts of the world due to its increased contamination by potentially toxic synthetic chemicals.<sup>142</sup> For example, hazardous and bioaccumulative chemicals such as chlorophenols, nitrophenols, azo dyes and sulfur are water pollutants produced from the textile, pulp and paper, pesticides and oil refinery industries.<sup>143</sup> Degradation of these pollutants is essential for purification of water and healthy aquatic life.

Collins and co-workers have designed green oxidation catalysts for the degradation of pollutants. Their targets were attaining practical, efficient and selective catalysts for the activation of hydrogen peroxide for greening global chemical technologies.<sup>144</sup> Tetradentate ligands were chosen for iron complexes where one or two coordination sites are available for the activation of oxidizing agents such as hydrogen peroxide.<sup>145</sup> Among the ligands studied, tetraamido macrocyclic ligands (TAMLs) provided appropriate ligand fields through their strong  $\sigma$ -donor ability and avoided

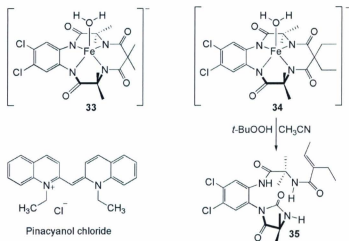
Fenton-type chemistry. Moreover, complexes of macrocyclic tetraamido-*N*-containing ligands are resistant to oxidative degradation and hydrolysis.<sup>146</sup> A high-valent iron-oxo intermediate was proposed as a key intermediate in the Fe-TAML catalytic system. The first example of a high-valent Fe-TAML complex (**32**) showed an Fe<sup>V</sup> oxo intermediate, which was characterized by UV-vis, Mössbauer, EPR and X-ray absorption spectroscopy (Figure 1.22).<sup>71</sup>



**Figure 1.22** High-valent Fe<sup>V</sup> oxo intermediate of Fe-TAML complex.

In 1998, the Collins group reported robust oxidation catalysts for the degradation of pinacyanol chloride (PC) because most commercially available dyes are comprised of 40-50% of PC (Figure 1.23).<sup>147</sup> Therefore, PC is a major aquatic pollutant in textile dyeing regions. The activation of H<sub>2</sub>O<sub>2</sub> for bleaching PC was carried out using 0.4 μmol of complex **33** at pH 7.4 (phosphate buffer). 100% PC was degraded in less than a min, as confirmed by UV-analysis. This catalyst was also applicable for the degradation of other dyes such as Chicago sky blue 6b, Evans blue, Acid blue 25, Acid red 97, Acid orange 8 and Direct violet 51. The lifetime of these catalysts were studied by varying the six-membered chelate rings. For example, complex **33** contains geminal dimethyl groups and complex **34** contains geminal diethyl groups. Comparative studies of these two catalysts

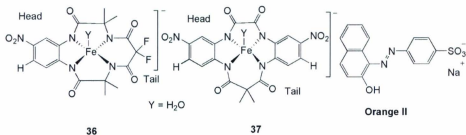
showed after seven bleaching cycles that catalyst **33** remained highly efficient whereas catalyst **34** was less active. In the presence of *tert*-butyl hydroperoxide (*t*-BuOOH) in CH<sub>3</sub>CN, 10% of the catalyst **34** was decomposed to form compound **35** via H-atom abstraction from one of the methylene C-H bonds of an ethyl group (Figure 1.23).<sup>148</sup>



**Figure 1.23** Fe-TAML activators for degradation of PC.

In 2004, Fe-TAML complex **33** was investigated for the treatment of paper and pulp mill effluent for the degradation of colour and adsorbable organic halides (AOX) (Figure 1.23). Using 0.5  $\mu\text{M}$  of Fe-TAML and 6.5 mM hydrogen peroxide at pH 11, 56% of the colour was removed from the effluent of a Kraft mill within four hours. The removal of colour varied a little when temperature was changed from 16 to 70  $^{\circ}\text{C}$ .<sup>149</sup> Therefore, the temperature was fixed at 40  $^{\circ}\text{C}$  for the effluent treatment in the laboratory as well as on a pilot plant scale.

In 2008, the Collins group designed a Fe-TAML activator based on four regulating parameters: hydrolytic stability, operational stability, speeds of peroxide activation and pHs.<sup>150</sup> Fe-TAML (**36**) attained a huge hydrolytic stability by replacing the CH<sub>3</sub> group with F on the “tail” and incorporating an NO<sub>2</sub> group instead of Cl on the “head” of TAML (Figure 1.24). Generally, Fe-TAML substituents with electron-withdrawing groups showed more oxidative reactivity and stability compared to similar catalysts with electron-donating substituents.<sup>151</sup> Also a shift of pH from ca. 10.5 to ca. 12 increased the rate of peroxide activation and catalyst efficiency for the bleaching of dyes. However, the Fe-TAML catalysts used for the large scale water treatment plant might produce fluorinated degradation fragments which are biochemically unfamiliar.



**Figure 1.24** Generation 1 (**36**) and Generation 2 (**37**) Fe-TAML activators.

In the continuing development of green oxidation catalysts, the Collins group discovered the second generation Fe-TAML activator (**37**) in 2009 (Figure 1.24).<sup>152</sup> The Generation 2 catalyst was designed in such a way that it would achieve high activity and be fluorine and chlorine free. The structure of the Generation 2 catalyst is different from Generation 1 *via* new hydrogen bond formation between the axial aqua ligand (Y) and the

amide oxygens.<sup>153</sup> Catalyst **37** was investigated for the degradation of Orange II dye ([4-[(2-hydroxynaphthyl)azo]-benzenesulfonic] Na<sup>+</sup> salt) at pH 7 to 11.<sup>152,153</sup> More than 90% of the Orange II was degraded within less than 8 min. At pH 7, it is the most active Fe-TAML activator to date.

#### 1.5.4 Iron-catalyzed C-C cross-coupling reactions

Transition metal-catalyzed carbon-carbon bond forming reactions are an important class of reactions in organic synthesis.<sup>154</sup> Palladium- and nickel-based catalysts have become central to carbon-carbon bond forming reactions for the synthesis of complex organic molecules. The price of these metals is very important in any synthesis since they might be used on an industrial scale. For example, according to Sigma-Aldrich, the current price (in Canadian dollar) of PdCl<sub>2</sub> (99.999%) is approximately \$138 g<sup>-1</sup> whereas FeCl<sub>2</sub> (99.9%) is \$31 g<sup>-1</sup>. Nickel has been shown to be toxic, which is a threat for consumer goods and health care products.<sup>155,156</sup> Furthermore, both Pd and Ni catalyst systems need the support of rationally designed ligands, which can be costly and have high molecular weights. Therefore, alternatives that are similarly effective, yet cheaper and non-toxic, are desirable.



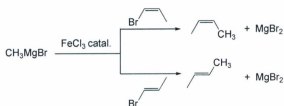
Recently, iron catalysts have been shown to address to some extent these socio-economical and environmental challenges.<sup>1,157-160</sup> The typical reaction partners for iron-catalyzed cross-coupling reactions are organometallic nucleophiles, specifically, Grignard reagents and electrophiles such as alkyl, alkenyl, aryl, or acyl halides. However, in certain cases, organomanganese, copper, and zinc derivatives are used as organometallic nucleophiles. A common protocol for iron-catalyzed cross-coupling reactions employs an Fe(II) or Fe(III) precursor which is reduced *in-situ* by the organometallic nucleophiles.<sup>161</sup>

Kochi and co-workers first introduced iron-catalyzed cross-coupling reactions of alkenyl halides with Grignard reagents.<sup>162</sup> They described the coupling between vinyl halides and alkylmagnesium bromides using FeCl<sub>3</sub> (Scheme 1.8). The solvent employed was THF and reaction conditions were optimized by varying the temperature (0-25 °C) and catalyst loadings (0.01-0.05 mol%). They obtained a maximum yield of 83% 1-octene from *n*-C<sub>6</sub>H<sub>13</sub>MgBr (40 mmol) and CH<sub>2</sub>=CHBr (204 mmol).



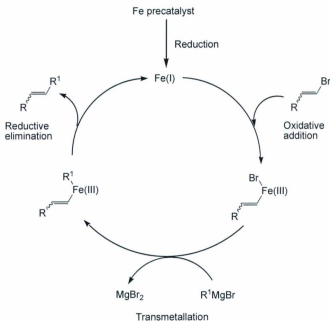
**Scheme 1.8** Cross-coupling reaction between Grignard reagents and vinyl halides.

The process proceeded in a highly stereospecific manner with a retention of the vinyl halide configuration. *Trans*-propenyl bromide reacted 15 times faster than the *cis*-isomer with methylmagnesium bromide (Scheme 1.9). In the case of ethylmagnesium bromide, a significant amount of ethane side-product was produced via  $\beta$ -hydride elimination reaction.<sup>163</sup>



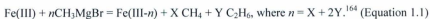
**Scheme 1.9** Stereospecific nature of cross-coupling reaction reported by Kochi *et al.*

Kochi reported the cross-coupling of alkenyl halides with Grignard reagents using different Fe(III) catalyst precursors.<sup>164</sup> Using a sterically-bulky iron source, such as Fe(dbm)<sub>3</sub>(tris(dibenzoylmethido)), the catalyst stability increased but a large excess of vinyl halides was still required. This proposed catalytic cycle is shown in Scheme 1.10.<sup>164-166</sup> The catalytically active Fe(I) species was formed *in-situ* by the reduction of the Fe(III) precursor with 2 equiv. of a Grignard reagent (RMgX). The resulting Fe(I) species undergoes oxidative addition of vinyl halide to re-form the Fe(III) species.

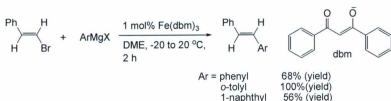


**Scheme 1.10** Kochi's proposed mechanism.

Transmetallation of alkyl groups from the Grignard reagent followed by reductive elimination of the cross-coupled product regenerates the Fe(I) species. The presence of an Fe(I) species was proposed due to the production of methane and ethane gas according to Equation 1.1. The value of  $n$  was found to be close to 2, which supports the theory of the reduction of Fe(III) to Fe(I). However, the proposed catalytic cycle has limitations as the intermediate organometallic species were not detected or isolated.



In 1983, Molander *et al.* further developed cross-coupling of alkenyl halides with Grignard reagents by introducing the solvent DME and lowering the reaction temperature to  $-20\text{ }^{\circ}\text{C}$ .<sup>167</sup> Product yield was improved to 100% and no excess alkenyl halides were required (Scheme 1.11).



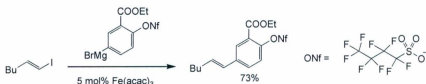
**Scheme 1.11** Cross-coupling of vinyl halides with Grignard reagents by Molander *et al.*

Cahiez *et al.* showed the beneficial effect of the co-solvent NMP (*N*-methylpyrrolidine) for these coupling reactions. Only 5% cross-coupled product was obtained using THF as the solvent whereas adding 9 equiv. of NMP increased the product yield to 85%. They assumed that NMP stabilized the intermediate iron species. Stereo- and chemoselectivity of the cross-coupled products was obtained from the substrates which possessed functional groups such as amides, esters, ketones and alkyl chlorides (Scheme 1.12).<sup>168,169</sup>



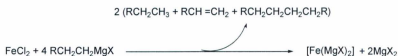
**Scheme 1.12** Effect of NMP in the cross-coupling reactions.

Further flexibility of these reactions was obtained by using functionalized Grignard reagents such as aryl nonaflate (ArONf) (ONf = perfluorobutane sulfonate) shown in Scheme 1.13.<sup>170</sup>



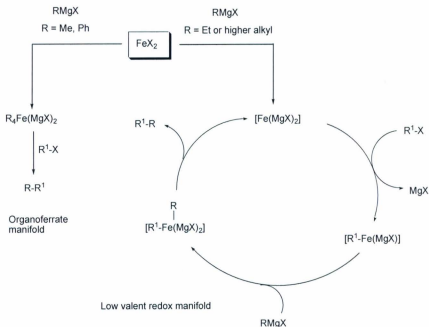
**Scheme 1.13** Cross-coupling reaction between functional Grignard reagents with alkenyl halide.

Around 30 years after Kochi's proposed mechanism, the precise iron-catalyzed cross-coupling reaction mechanism remains unknown. However, during this period, it has been speculated that Fe(0) or Fe(I) species act as catalyst intermediates but no structural evidence has been obtained.<sup>163,171</sup> It was also suggested that Fe(II) complexes acted as the catalytically active species.<sup>172</sup> In 2002, Fürstner and co-workers described cross-coupling reactions between alkyl Grignard reagents and aryl chlorides, tosylates and triflates, which had previously been reported to be unreactive.<sup>161,173,174</sup> A modified iron-catalyzed cross-coupling reaction mechanism was proposed that could undergo two different pathways. One involved "inorganic Grignard reagents," which had previously been proposed by Bogdanović<sup>175</sup> and the other proceeds by the formation of an organoferrate species.<sup>176</sup> FeCl<sub>2</sub> reacts with 4 equiv. of RMgX to give a highly reduced species [Fe(MgX)<sub>2</sub>] where iron is formally in a -2 oxidation state (Scheme 1.14).



**Scheme 1.14** Formation of Bogdanović's inorganic Grignard reagent.

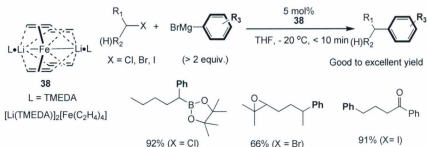
Füerstner proposed that the reduction process does not stop once a zero-valent iron species is formed, but instead leads to the formation of a negatively charged iron species through a  $\beta$ -hydride elimination. The oxidative addition of aryl halides to the reduced species forms  $\text{Fe}(0)$ , which is again attacked by the excess Grignard reagent. Reductive elimination of the desired product regenerates the active iron (-2) species (Scheme 1.15).



**Scheme 1.15** Füstner's proposed mechanism *via* low-valent intermediates vs. organoferrate manifold.

The Fe(-2) complex  $[\text{Li}(\text{tmeda})_2][\text{Fe}(\text{C}_2\text{H}_4)_4]$  (**38**), originally synthesized by Jonas *et al.* was shown to be an active catalyst for cross-coupling reactions (Scheme 1.16).<sup>177,178</sup> The complex showed good to excellent catalytic activity for the cross-coupling of aryl Grignard reagents and alkyl halides with different functional groups such as ketones, esters, enoates, nitriles, isocyanates, ethers, acetals, pinacol boronates, trialkylsilyl groups, and even terminal and internal epoxides (Scheme 1.16). The alkyl halides mainly used are comprised of primary and secondary halides but not tertiary halides due to their

involvement in the formation of radical intermediates in certain iron-catalyzed processes.<sup>179</sup> Notably, nickel-based catalysts also do not show any cross-coupling activity of sterically hindered tertiary alkyl halides with Grignard reagents.

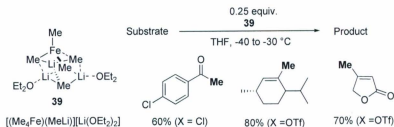


**Scheme 1.16** Fe(-2) complex for the cross-coupling of alkyl halides with different functional groups.

MeMgBr does not form Bogdanović's "inorganic Grignard reagent" due to its inability to undergo  $\beta$ -hydride elimination. It has been found that non-stabilized alkyl-iron species or organoferrate complexes were formed by reacting  $\text{FeX}_n$  ( $n = 2, 3$ ) with various organolithium or organomagnesium halide reagents (Scheme 1.15).<sup>172,180-183</sup> Fürstner and co-workers were able to isolate the organoferrate  $[(\text{Me}_2\text{Fe})(\text{MeLi})][\text{Li}(\text{OEt}_2)_2]$  (**39**) from the reaction of an ether solution of  $\text{FeCl}_3$  with an excess of MeLi at low temperature (Scheme 1.17). Crystals suitable for X-ray analysis were obtained from recrystallization in diethyl ether at  $-40^\circ\text{C}$  to  $-78^\circ\text{C}$ .<sup>184</sup> It reacted with more activated electrophiles such as acid chlorides and triflates to give the corresponding

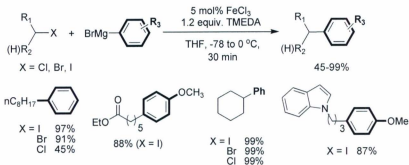


products in good yields but was unreactive towards chlorobenzoate and even iodobenzoate (Scheme 1.17).<sup>179</sup>



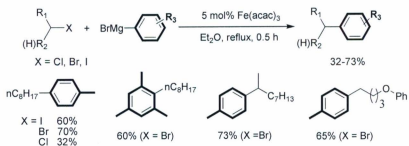
**Scheme 1.17** Organoferrate complex for the cross-coupling of acid chloride and triflates.

In 2004, Nakamura and co-workers reported iron-catalyzed cross-coupling reactions of alkyl halides with aryl Grignard reagents. Amines were shown to have a beneficial effect on their reactions. For example, TMEDA (tetramethylethylenediamine) used with  $\text{FeCl}_3$  suppressed the formation of undesirable products such as olefins.<sup>185</sup> The reaction conditions were optimized by the slow addition of 1.2 equiv. of Grignard reagent and TMEDA using a syringe pump to the 5 mol%  $\text{FeCl}_3$  solution in THF at low temperature (-78 to 0 °C). A wide variety of substrates such as cyclic, acyclic, primary and secondary alkyl halides gave good to excellent yields in the range of 45-99% of cross-coupled products (Scheme 1.18). High stereo- and chemoselectivity were observed from functionalized alkyl halides such as those bearing polar ester groups. Tertiary halides did not give any cross-coupled products, instead they gave reduction and elimination products.



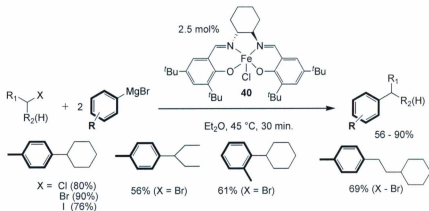
**Scheme 1.18** Cross-coupling of alkyl halides with aryl Grignard reagents reported by Nakamura *et al.*

At the same time, Nagano and Hayashi reported the cross-coupling of alkyl halides with aryl Grignard reagents using  $\text{Fe}(\text{acac})_3$  in diethyl ether.<sup>186</sup> Use of an amine additive and slow addition of the Grignard reagents were not required conditions, but refluxing the reaction mixture gave yields in the range of 32-73% for primary and secondary alkyl halides (Scheme 1.19).



**Scheme 1.19** Cross-coupling of alkyl halides with aryl Grignard reagents reported by Hayashi *et al.*

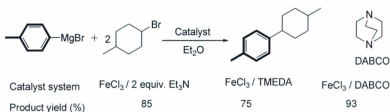
Encouraged by the results of Fürstner<sup>173,174</sup> had shown previously, Bedford and co-workers reported analogous Fe(III) salen complexes for the cross-coupling of alkyl halides with aryl Grignard reagents.<sup>187</sup> Catalyst efficiency of these complexes were studied by increasing the diamino linker length or replacing the ethylene linker with an aromatic spacer resulted in decreased catalytic activities. However, 2.5 mol% Fe(III) complex (**40**) containing a cyclohexyl linker gave 90% yield of cross-coupled product using 2 equiv. of Grignard reagent in Et<sub>2</sub>O at 45 °C (Scheme 1.20). A slight decrease in yield was observed when iodo or chloro cyclohexanes were used instead of bromocyclohexane. No activity was observed when using a bulky Grignard such as 2,6-dimethylphenylmagnesium bromide.



**Scheme 1.20** Fe(III) salen catalyzed cross-coupling by Bedford *et al.*

Bedford *et al.* have reported useful catalysts through combining  $FeCl_3$  and amines such as triethylamine, TMEDA or DABCO (diazabicyclooctane) (Scheme 1.21).<sup>188</sup> High

yields (40 to 100%) of cross-coupled products were obtained and notably the slow addition of Grignard reagent was not a required. Regarding amine use, the best activities were obtained with either mono- or bidentate tertiary amines, while chelating primary and secondary bis-amine ligands afforded catalysts with lower activity. No excess of amine was required and Fe:N mole ratio was always kept at 1:2.

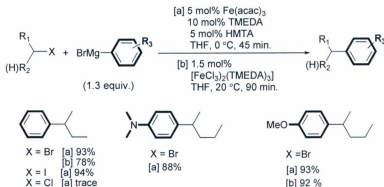


**Scheme 1.21**  $\text{FeCl}_3$ /amine catalyzed cross-coupling by Bedford *et al.*

Bedford *et al.* have used PEG (polyethylene glycol) stabilized iron nanoparticle catalysts for cross-coupling reactions. The nanoparticles were formed *in-situ* by the reduction of  $\text{FeCl}_3$  by Grignard reagents.<sup>189</sup> An ether solution of  $\text{FeCl}_3$  and PEG with 5 equiv. of *o*-tolylmagnesium bromide turned black and formed iron nanoparticles between 7-13 nm in size. Employing 5 mol% of these iron nanoparticles, 30 to 91% yields of cross-coupled products were obtained from primary and secondary alkyl halides by heating the reactions to 45 °C in  $\text{Et}_2\text{O}$ . However, using sterically-bulky Grignard reagents such as 2,6-dimethylphenyl magnesium bromide did not give any cross-coupled products.

Cahiez *et al.* reported a catalyst system using hexamethylenetetramine (HMTA) and TMEDA with  $\text{Fe}(\text{acac})_3$  for the cross-coupling of primary and secondary alkyl

halides with aryl Grignard reagents.<sup>190</sup> Good to excellent yields (39 to 94%) of cross-coupled products were obtained from primary and secondary alkyl bromides and iodides but no cross-coupled products were obtained from alkyl chlorides (Scheme 1.22). Grignard reagents (1.3 equiv.) were added slowly using a syringe pump over 45 min. This contrasts with the work of Bedford *et al.* where TMEDA and FeCl<sub>3</sub> were used for the cross-coupling and slow addition was not required. Primary alkyl bromides and iodides gave lower yields than their secondary counterparts. They also developed a more convenient method of using FeCl<sub>3</sub> as a catalyst precursor. FeCl<sub>3</sub> is hygroscopic and corrosive. Therefore, they converted FeCl<sub>3</sub> to [(FeCl<sub>3</sub>)<sub>2</sub>(TMEDA)<sub>3</sub>] complex with the support of TMEDA which was easily isolated by filtration, and was easily handled as a catalyst precursor.



**Scheme 1.22** Novel iron based catalyst systems by Cahiez *et al.*

Kozak and co-workers are interested in the exploration of single-component iron catalysts for carbon-carbon cross-coupling reactions of alkyl halides and aryl Grignard reagents. Recently, iron halide complexes bearing tetradentate and tridentate amine-bis(phenolate) ligands have been reported for C-C cross-coupling reactions.<sup>191-193</sup> At present, the Kozak group is interested in the investigation of iron acetylacetonate complexes bearing tetradentate amine-bis(phenolate) ligands, which would be single component catalysts for the cross-coupling of alkyl halides (mainly chlorides) with aryl Grignard reagents. This approach will be presented in Chapter 4 of this thesis.

Following Kochi,<sup>162</sup> Kumada<sup>194</sup> and Corriu's<sup>195</sup> innovative discoveries, impressive progress has been made for cross-coupling reactions of Grignard reagents. Generally nickel- and palladium-catalyzed cross-coupling processes are frequently used in academia and industry. However, in recent years, non-toxic and inexpensive metal-based iron catalysts have been discovered for this C-C cross-coupling reaction. Mechanisms of iron-catalyzed cross-coupling reactions are not well-established yet, and detailed studies continue to be needed so further progress can be made.

### **1.6 History and prospects of amine-bis(phenol) ligands**

Phenol-containing ligands generate phenoxy radicals which are similar to the tyrosine containing metalloproteins involved in oxygen dependant enzymatic catalysts.<sup>196-199</sup> This property inspired chemists to design transition metal complexes of different phenol-containing ligands for the development of homogeneous catalysts and mimicking structural and functional model complexes of metalloenzymes. Amine-

bis(phenol) ligand containing transition metal complexes have been used as effective catalysts for polymerization reactions. For example, Kol *et al.* reported a series of early transition metal complexes (Group IV and V) supported by amine-bis(phenolate) ligands as active catalysts for the polymerization of 1-hexene.<sup>200-204</sup> Aluminum complexes of amine-bis(phenolate) ligands and their catalytic reactivity toward ring-opening polymerization of  $\epsilon$ -caprolactone has been reported by Chen *et al.*<sup>205</sup> Lanthanide complexes of amine-bis(phenolate) ligands have also shown catalytic activity in polymerization of lactide monomers.<sup>206, 207</sup> Thus, amine-bis(phenol) ligands are extensively used for main group metals, early transition metals and lanthanides but their late transition metal chemistry is underdeveloped.

The objective of this thesis is the synthesis and characterization of iron complexes containing amine-bis(phenolate) ligands and the study of these complexes as homogeneous catalysts. One of the advantages of using amine-bis(phenol) ligands is the possibility of fine-tuning their structure. One way of achieving this goal is by changing the ligand's backbone, for example, an *N,N'*-dimethylethylenediamine backbone; or an *N,N*-dimethylethylenediamine backbone. The pendant arm can also be modified by using different donor atoms such as an oxygen-containing cyclic (tetrahydrofurfuryl), or a linear ether (ethylmethyl ether), or a nitrogen-containing pyridine. This leads to the variation of coordination environment on the metal center *via* different donor ability and geometries. Also, substituents on ligands influence the metal center of the complexes electronically and/or sterically. These coordination parameters play an important role for metal complexes and their catalytic properties.

## 1.7 References

1. B. Plietker, *Iron Catalysis in Organic Chemistry: Reactions and Applications*, Wiley-VCH, Weinheim, 2008.
2. J. C. Bailar and A. F. Trotman-Dickenson, *Comprehensive Inorganic Chemistry, Iron, Vol 3*, Pergamon Press, Oxford, 1973.
3. J. A. Mcleverty and T. J. Meyer, *Comprehensive Coordination Chemistry II, Iron, Vol 5*, Elsevier Ltd., New York, 2004.
4. T. J. Collins, K. L. Kostka, E. Münck and E. S. Uffelman, *J. Am. Chem. Soc.*, 1990, **112**, 5637-5639.
5. A. Nanthakumar and H. M. Goff, *J. Am. Chem. Soc.*, 1990, **112**, 4047-4049.
6. J. F. Berry, E. Bill, E. Bothe, S. D. George, B. Mienert, F. Neese and K. Wieghardt, *Science*, 2006, **312**, 1937-1941.
7. B. Plietker, *Iron Catalysis: Fundamentals and Applications*, Springer, New York, 2011.
8. S. J. Lippard and J. M. Berg, *Principles of Bioinorganic Chemistry*, University Science Books, Mill Valley, CA, 1994.
9. C.-L. Sun, B.-J. Li and Z.-J. Shi, *Chem. Rev.*, 2011, **111**, 1293-1314.
10. J. Ribas Gispert, *Coordination Chemistry*, Wiley-VCH, Weinheim, 2008.
11. E.-i. Ochiai, *Bioinorganic Chemistry: A Survey*, Academic Press, New York, 2008.
12. M. W. Vetting, D. A. D'Argenio, L. N. Ornston and D. H. Ohlendorf, *Biochemistry*, 2000, **39**, 7943-7955.



13. A. M. Orville, N. Elango, J. D. Lipscomb and D. H. Ohlendorf, *Biochemistry*, 1997, **36**, 10039-10051.
14. M. Costas, K. Chen and L. Que, *Coord. Chem. Rev.*, 2000, **200**, 517-544.
15. A. L. Feig and S. J. Lippard, *Chem. Rev.*, 1994, **94**, 759-805.
16. D. D. Cox, S. J. Benkovic, L. M. Bloom, F. C. Bradley, M. J. Nelson, L. Que and D. E. Wallick, *J. Am. Chem. Soc.*, 1988, **110**, 2026-2032.
17. D. D. Cox and L. Que, *J. Am. Chem. Soc.*, 1988, **110**, 8085-8092.
18. L. Que, R. C. Kolanczyk and L. S. White, *J. Am. Chem. Soc.*, 1987, **109**, 5373-5380.
19. H. G. Jang, D. D. Cox and L. Que, *J. Am. Chem. Soc.*, 1991, **113**, 9200-9204.
20. M. Pascaly, M. Duda, F. Schweppe, K. Zurlinden, F. K. Müller and B. Krebs, *J. Chem. Soc., Dalton Trans.*, 2001, 828-837.
21. M. Pascaly, C. Nazikkol, F. Schweppe, A. Wiedemann, K. Zurlinden and B. Krebs, *Anorg. Allg. Chem.*, 2000, **626**, 50-55.
22. M. Pascaly, M. Duda, A. Rompel, B. H. Sift, W. Meyer-Klaucke and B. Krebs, *Inorg. Chim. Acta*, 1999, **291**, 289-299.
23. M. Merkel, F. K. Müller and B. Krebs, *Inorg. Chim. Acta*, 2002, **337**, 308-316.
24. P. Mialane, E. Anxolabéhère-Mallart, G. Blondin, A. Nivorojkine, J. Guilhem, L. Tchertanova, M. Cesario, N. Ravi, E. Bominaar, J. J. Girerd and E. Münck, *Inorg. Chim. Acta*, 1997, **263**, 367-378.
25. M. Velusamy, M. Palaniandavar, R. S. Gopalan and G. U. Kulkarni, *Inorg. Chem.*, 2003, **42**, 8283-8293.

26. M. Velusamy, R. Mayilmurugan and M. Palaniandavar, *Inorg. Chem.*, 2004, **43**, 6284-6293.
27. E. Safaei, T. Weyhermüller, E. Bothe, K. Wiegardt and P. Chaudhuri, *Eur. J. Inorg. Chem.*, 2007, 2334-2344.
28. R. Van Gorkum, J. Berding, A. M. Mills, H. Kooijman, D. M. Tooke, A. L. Spek, I. Mutikainen, U. Turpeinen, J. Reedijk and E. Bouwman, *Eur. J. Inorg. Chem.*, 2008, 1487-1496.
29. A. C. Rosenzweig, P. Nordlund, P. M. Takahara, C. A. Frederick and S. J. Lippard, *Chem. Biol.*, 1995, **2**, 409-418.
30. M. H. Baik, M. Newcomb, R. A. Friesner and S. J. Lippard, *Chem. Rev.*, 2003, **103**, 2385-2419.
31. T. Glaser, R. H. Pawelke and M. Heidemeier, *Anorg. Allge. Chem.*, 2003, **629**, 2274-2281.
32. R. Mayilmurugan, H. Stoeckli-Evans, E. Suresh and M. Palaniandavar, *Dalton Trans.*, 2009, 5101-5114.
33. C. J. Whiteoak, R. T. M. de Rosales, A. J. P. White and G. J. P. Britovsek, *Inorg. Chem.*, 2010, **49**, 11106-11117.
34. B. Meunier, *Biomimetic Oxidations Catalyzed by Transition Metal Complexes*, Imperial College Press, London, 2000.
35. I. Bertini, *Biological Inorganic Chemistry: Structure and Reactivity*, University Science Books, Sausalito, CA, 2007.

36. J. T. Groves, R. C. Haushalter, M. Nakamura, T. E. Nemo and B. J. Evans, *J. Am. Chem. Soc.*, 1981, **103**, 2884-2886.
37. P. A. MacFaul, K. U. Ingold, D. D. M. Wayner and L. Que, *J. Am. Chem. Soc.*, 1997, **119**, 10594-10598.
38. Y. H. Dong, H. Fujii, M. P. Hendrich, R. A. Leising, G. F. Pan, C. R. Randall, E. C. Wilkinson, Y. Zang, L. Que, B. G. Fox, K. Kauffmann and E. Münck, *J. Am. Chem. Soc.*, 1995, **117**, 2778-2792.
39. H. F. Hsu, Y. H. Dong, L. J. Shu, V. G. Young and L. Que, *J. Am. Chem. Soc.*, 1999, **121**, 5230-5237.
40. C. A. Grapperhaus, B. Mienert, E. Bill, T. Weyhermüller and K. Wieghardt, *Inorg. Chem.*, 2000, **39**, 5306-5317.
41. C. Kim, K. Chen, J. H. Kim and L. Que, *J. Am. Chem. Soc.*, 1997, **119**, 5964-5965.
42. K. B. Jensen, C. J. McKenzie, L. P. Nielsen, J. Z. Pedersen and H. M. Svendsen, *Chem. Commun.*, 1999, 1313-1314.
43. V. Balland, F. Banse, E. Anxolabéhère-Mallart, M. Ghiladi, T. A. Mattioli, C. Philouze, G. Blondin and J. J. Girerd, *Inorg. Chem.*, 2003, **42**, 2470-2477.
44. A. J. Simaan, S. Dopner, F. Banse, S. Bourcier, G. Bouchoux, A. Boussac, P. Hildebrandt and J. J. Girerd, *Eur. J. Inorg. Chem.*, 2000, 1627-1633.
45. J. U. Rohde, J. H. In, M. H. Lim, W. W. Brennessel, M. R. Bukowski, A. Stubna, E. Münck, W. Nam and L. Que, *Science*, 2003, **299**, 1037-1039.

46. J. E. Penner-Hahn, E. K. Smith, T. J. McMurry, M. Renner, A. L. Balch, J. T. Groves, J. H. Dawson and K. O. Hodgson, *J. Am. Chem. Soc.*, 1986, **108**, 7819-7825.
47. T. Wolter, W. Meyer-Klaucke, M. Muther, D. Mandon, H. Winkler, A. X. Trautwein and R. Weiss, *J. Inorg. Biochem.*, 2000, **78**, 117-122.
48. C. E. MacBeth, A. P. Golombek, V. G. Young, Jr., C. Yang, K. Kuczera, M. P. Hendrich and A. S. Borovik, *Science*, 2000, **289**, 938-941.
49. M. Costas, J.-U. Rohde, A. Stubna, R. Y. N. Ho, L. Quaroni, E. Münck and L. Que, Jr., *J. Am. Chem. Soc.*, 2001, **123**, 12931-12932.
50. M. H. Lim, J. U. Rohde, A. Stubna, M. R. Bukowski, M. Costas, R. Y. N. Ho, E. Münck, W. Nam and L. Que, *PANS*, 2003, **100**, 3665-3670.
51. A. Company, L. Gomez, X. Fontrodona, X. Ribas and M. Costas, *Chem. Eur. J.*, 2008, **14**, 5727-5731.
52. J. Kaizer, E. J. Klinker, N. Y. Oh, J. U. Rohde, W. J. Song, A. Stubna, J. Kim, E. Münck, W. Nam and L. Que, *J. Am. Chem. Soc.*, 2004, **126**, 472-473.
53. V. Bolland, M. F. Charlot, F. Banse, J. J. Girerd, T. A. Mattioli, E. Bill, J. F. Bartoli, P. Battioni and D. Mansuy, *Eur. J. Inorg. Chem.*, 2004, 301-308.
54. M. P. Jensen, M. Costas, R. Y. N. Ho, J. Kaizer, A. M. I. Payeras, E. Münck, L. Que, J. U. Rohde and A. Stubna, *J. Am. Chem. Soc.*, 2005, **127**, 10512-10525.
55. M. R. Bukowski, K. D. Koehntop, A. Stubna, E. L. Bominaar, J. A. Halfen, E. Münck, W. Nam and L. Que, *Science*, 2005, **310**, 1000-1002.

56. M. Martinho, F. Banse, J. F. Bartoli, T. A. Mattioli, P. Battioni, O. Horner, S. Bourcier and J. J. Girerd, *Inorg. Chem.*, 2005, **44**, 9592-9596.
57. T. K. Paine, M. Costas, J. Kaizer and L. Que, *J. Bio. Inorg. Chem.*, 2006, **11**, 1098-1099.
58. J. Bautz, M. R. Bukowski, M. Kerscher, A. Stubna, P. Comba, A. Lienke, E. Münck and L. Que, *Angew. Chem. Int. Ed.*, 2006, **45**, 5681-5684.
59. C. R. Goldsmith and T. D. P. Stack, *Inorg. Chem.*, 2006, **45**, 6048-6055.
60. J. Bautz, P. Comba, C. L. de Laorden, M. Menzel and G. Rajaraman, *Angew. Chem. Int. Ed.*, 2007, **46**, 8067-8070.
61. R. Mas-Balleste, M. Fujita and L. Que, *Dalton Trans.*, 2008, 1828-1830.
62. J. Kaizer, M. Costas and L. Que, *Angew. Chem. Int. Ed.*, 2003, **42**, 3671-3673.
63. T. J. Groves, Han, Y-Z, *In Cytochrome P450: Structure, Mechanism, and Biochemistry, 2nd ed.*, Ortiz de Montellano, Paul R., Ed., Plenum Press, New York, 1995.
64. K. Chen and L. Que, *J. Am. Chem. Soc.*, 2001, **123**, 6327-6337.
65. D. L. Harris and G. H. Loew, *J. Am. Chem. Soc.*, 1998, **120**, 8941-8948.
66. R. Y. N. Ho, G. Roelfes, B. L. Feringa and L. Que, *J. Am. Chem. Soc.*, 1999, **121**, 264-265.
67. K. Chen, M. Costas and L. Que, *J. Chem. Soc. Dalton Trans.*, 2002, 672-679.
68. K. Chen, M. Costas, J. H. Kim, A. K. Tipton and L. Que, *J. Am. Chem. Soc.*, 2002, **124**, 3026-3035.

69. A. Bassan, M. R. A. Blomberg, P. E. M. Siegbahn and L. Que, *Angew. Chem. Int. Ed.*, 2005, **44**, 2939-2941.
70. A. Company, Y. Feng, M. Guell, X. Ribas, J. M. Luis, L. Que and M. Costas, *Chem. Eur. J.*, 2009, **15**, 3359-3362.
71. F. T. de Oliveira, A. Chanda, D. Banerjee, X. P. Shan, S. Mondal, L. Que, E. L. Bominaar, E. Münck and T. J. Collins, *Science*, 2007, **315**, 835-838.
72. P. Das and L. Que, *Inorg. Chem.*, 2010, **49**, 9479-9485.
73. R. L. Carlin, *Magnetochemistry*, Springer-Verlag, New York, 1986.
74. C. J. O'Connor, *Research Frontiers in Magnetochemistry*, World Scientific, N.J., 1993.
75. A. Earnshaw, *Introduction to Magnetochemistry*, Academic Press., New York, 1968.
76. K. Itoh and M. Kinoshita, *Molecular Magnetism: New Magnetic Materials*, Kodansha, Tokyo, 2000.
77. D. H. R. Barton, M. J. Gastiger and W. B. Motherwell, *J. Chem. Soc., Chem. Commun.*, 1983, 41-43.
78. D. H. R. Barton, M. J. Gastiger and W. B. Motherwell, *J. Chem. Soc., Chem. Commun.*, 1983, 731-733.
79. D. H. R. Barton, R. S. Haymotherwell and W. B. Motherwell, *Tetrahedron Lett.*, 1983, **24**, 1979-1982.
80. S. S. Kim, S. K. Sar and P. Tamrakar, *Bull. Korean Chem. Soc.*, 2002, **23**, 937-938.

81. M. Nakanishi and C. Bolm, *Adv. Synth. Catal.*, 2007, **349**, 861-864.
82. M. Lenze and E. B. Bauer, *J. Mol. Catal. A: Chem.*, 2009, **309**, 117-123.
83. T. Newhouse and P. S. Baran, *Angew. Chem., Int. Ed.*, **50**, 3362-3374.
84. S. Tanase and E. Bouwman, *Adv. Inorg. Chem.*, 2006, vol. 58, pp. 29-75.
85. J. Kim, R. G. Harrison, C. Kim and L. Que, *J. Am. Chem. Soc.*, 1996, **118**, 4373-4379.
86. K. Chen and L. Que, *Chem. Commun.*, 1999, 1375-1376.
87. J. England, G. J. P. Britovsek, N. Rabadia and A. J. P. White, *Inorg. Chem.*, 2007, **46**, 3752-3767.
88. O. Y. Lyakin, K. P. Bryliakov, G. J. P. Britovsek and E. P. Talsi, *J. Am. Chem. Soc.*, 2009, **131**, 10798-10799.
89. J. England, C. R. Davies, M. Banaru, A. J. P. White and G. J. P. Britovsek, *Adv. Synth. Catal.*, 2008, **350**, 883-897.
90. J. England, R. Gondhia, L. Bigorra-Lopez, A. R. Petersen, A. J. P. White and G. J. P. Britovsek, *Dalton Trans.*, 2009, 5319-5334.
91. C. Kim, K. Chen, J. H. Kim and L. Que, *J. Am. Chem. Soc.*, 1997, **119**, 5964-5965.
92. T. Okuno, S. Ito, S. Ohba and Y. Nishida, *J. Chem. Soc., Dalton Trans.*, 1997, 3547-3551.
93. M. S. Chen and M. C. White, *Science*, 2007, **318**, 783-787.
94. M. S. Chen and M. C. White, *Science*, 2010, **327**, 566-571.

95. N. A. Vermeulen, M. S. Chen and M. C. White, *Tetrahedron*, 2009, **65**, 3078-3084.
96. L. Gomez, I. Garcia-Bosch, A. Company, J. Benet-Buchholz, A. Polo, X. Sala, X. Ribas and M. Costas, *Angew. Chem. Int. Ed.*, 2009, **48**, 5720-5723.
97. B. Bornils, W. A. Herrmann, *Applied Homogeneous Catalysis with Organometallic Compounds, Vol.1, 2nd Ed.*, Wiley-VCH, Weinheim, 2002.
98. K. A. Jorgensen, *Chem. Rev.*, 1989, **89**, 431-458.
99. M. Beller, C. Bolm, *Transition Metals for Organic Synthesis: Building Blocks and Fine Chemicals, 2<sup>nd</sup> Ed., Vol. 2*, Wiley-VCH, Weinheim, 2004.
100. J.-E. Bäckvall, *Modern Oxidation Methods*, Wiley-VCH, Weinheim, 2004.
101. R. Ugo, *Aspects of Homogeneous Catalysis, Vol. 4*, D. Reidel, Dordrecht, 1981.
102. J. R. Monnier, *Appl. Catal. A: General*, 2001, **221**, 73-91.
103. B. S. Lane and K. Burgess, *Chem. Rev.*, 2003, **103**, 2457-2473.
104. M. Bosing, A. Noh, I. Loose and B. Krebs, *J. Am. Chem. Soc.*, 1998, **120**, 7252-7259.
105. M. K. Tse, C. Dobler, S. Bhor, M. Klawonn, W. Magerlein, H. Hugl and M. Beller, *Angew. Chem. Int. Ed.*, 2004, **43**, 5255-5260.
106. M. K. Tse, M. Klawonn, S. Bhor, C. Dobler, G. Anilkumar, H. Hugl, W. Magerlein and M. Beller, *Org. Lett.*, 2005, **7**, 987-990.
107. S. Bhor, G. Anilkumar, M. K. Tse, M. Klawonn, C. Dobler, B. Bitterlich, A. Grotevendt and M. Beller, *Org. Lett.*, 2005, **7**, 3393-3396.
108. F. Shi, M. K. Tse and M. Beller, *J. Mol. Catal.*, 2007, **270**, 68-75.



109. F. Shi, M. K. Tse and M. Beller, *Adv. Synth. Catal.*, 2007, **349**, 303-308.
110. W. A. Herrmann, R. W. Fischer and D. W. Marz, *Angew. Chem. Int. Ed.*, 1991, **30**, 1638-1641.
111. M. Colladon, A. Scarso, P. Sgarbossa, R. A. Michelin and G. Strukul, *J. Am. Chem. Soc.*, 2006, **128**, 14006-14007.
112. Y. Sawada, K. Matsumoto, S. Kondo, H. Watanabe, T. Ozawa, K. Suzuki, B. Saito and T. Katsuki, *Angew. Chem. Int. Ed.*, 2006, **45**, 3478-3480.
113. K. Matsumoto, Y. Sawada, B. Saito, K. Sakai and T. Katsuki, *Angew. Chem. Int. Ed.*, 2005, **44**, 4935-4939.
114. A. Mahammed and Z. Gross, *J. Am. Chem. Soc.*, 2005, **127**, 2883-2887.
115. K. Kamata, K. Yamaguchi, S. Hikichi and N. Mizuno, *Adv. Synth. Catal.*, 2003, **345**, 1193-1196.
116. W. Adam, P. L. Alsters, R. Neumann, C. R. Saha-Moller, D. Sloboda-Rozner and R. Zhang, *J. Org. Chem.*, 2003, **68**, 1721-1728.
117. B. S. Lane, M. Vogt, V. J. DeRose and K. Burgess, *J. Am. Chem. Soc.*, 2002, **124**, 11946-11954.
118. B. S. Lane and K. Burgess, *J. Am. Chem. Soc.*, 2001, **123**, 2933-2934.
119. J. P. Renaud, P. Battioni, J. F. Bartoli and D. Mansuy, *J. Chem. Soc., Chem. Commun.*, 1985, 888-889.
120. W. Zhang, J. L. Loebach, S. R. Wilson and E. N. Jacobsen, *J. Am. Chem. Soc.*, 1990, **112**, 2801-2803.

Chapter 1: Introduction and overview

121. E. N. Jacobsen, A. Pfaltz, and H. Yamamoto, *Comprehensive Asymmetric Catalysis I-III, Vol. 2*, Springer-Verlag, New York, 1999.
122. R. Irie, K. Noda, Y. Ito, N. Matsumoto and T. Katsuki, *Tetrahedron Lett.*, 1990, **31**, 7345-7348.
123. T. G. Traylor, S. Tsuchiya, Y. S. Byun and C. Kim, *J. Am. Chem. Soc.*, 1993, **115**, 2775-2781.
124. W. Nam, H. J. Lee, S. Y. Oh, C. Kim and H. G. Jang, *J. Inorg. Biochem.*, 2000, **80**, 219-225.
125. M. C. White, A. G. Doyle and E. N. Jacobsen, *J. Am. Chem. Soc.*, 2001, **123**, 7194-7195.
126. W. W. Nam, R. Ho and J. S. Valentine, *J. Am. Chem. Soc.*, 1991, **113**, 7052-7054.
127. R. J. Guajardo, S. E. Hudson, S. J. Brown and P. K. Mascharak, *J. Am. Chem. Soc.*, 1993, **115**, 7971-7977.
128. G. Dubois, A. Murphy and T. D. P. Stack, *Org. Lett.*, 2003, **5**, 2469-2472.
129. M. Costas, A. K. Tipton, K. Chen, D. H. Jo and L. Que, *J. Am. Chem. Soc.*, 2001, **123**, 6722-6723.
130. K. Suzuki, P. D. Oldenburg and L. Que, *Angew. Chem. Int. Ed.*, 2008, **47**, 1887-1889.
131. H. C. Kolb, M. S. Vannieuwenhze and K. B. Sharpless, *Chem. Rev.*, 1994, **94**, 2483-2547.
132. S. Taktak, W. H. Ye, A. M. Herrera and E. V. Rybak-Akimova, *Inorg. Chem.*, 2007, **46**, 2929-2942.

133. G. Anilkumar, B. Bitterlich, F. G. Gelalcha, M. K. Tse and M. Beller, *Chem. Commun.*, 2007, 289-291.
134. B. Bitterlich, G. Anilkumar, F. G. Gelalcha, B. Spilker, A. Grotevendt, R. Jackstell, M. K. Tse and M. Beller, *Chem. Asian J.*, 2007, **2**, 521-529.
135. B. Bitterlich, K. Schröder, M. K. Tse and M. Beller, *Eur. J. Org. Chem.*, 2008, 4867-4870.
136. K. Schröder, K. Junge, A. Spannenberg and M. Beller, *Catal. Today*, 2010, **157**, 364-370.
137. K. Schröder, S. Enthaler, B. Join, K. Junge and M. Beller, *Adv. Synth. Catal.*, 2010, **352**, 1771-1778.
138. K. Schröder, S. Enthaler, B. Bitterlich, T. Schulz, A. Spannenberg, M. K. Tse, K. Junge and M. Beller, *Chem. Eur. J.*, 2009, **15**, 5471-5481.
139. K. Schröder, X. Tong, B. Bitterlich, M. K. Tse, F. G. Gelalcha, A. Bruckner and M. Beller, *Tetrahedron Lett.*, 2007, **48**, 6339-6342.
140. K. Schröder, B. Join, A. J. Amali, K. Junge, X. Ribas, M. Costas and M. Beller, *Angew. Chem. Int. Ed.*, 2011, **50**, 1425-1429.
141. *Guidelines for Drinking Water Quality, 3rd Ed., World Health Organization: Geneva*, 2008.
142. C. G. Daughton, *Compr. Anal. Chem.*, 2007, **50**, 1-58.
143. T. J. Collins, *Acc. Chem. Res.*, 2002, **35**, 782-790.
144. T. J. Collins, *Acc. Chem. Res.*, 1994, **27**, 279-285.

145. F. C. Anson, J. A. Christie, T. J. Collins, R. J. Coots, T. T. Furutani, S. L. Gipson, J. T. Keech, T. E. Krafft, B. D. Santarsiero and G. H. Spies, *J. Am. Chem. Soc.*, 1984, **106**, 4460-4472.
146. A. Ghosh, A. D. Ryabov, S. M. Mayer, D. C. Horner, D. E. Prasuhn, Jr., G. S. Sen, L. Vuocolo, C. Culver, M. P. Hendrich, C. E. F. Rickard, R. E. Norman, C. P. Horwitz and T. J. Collins, *J. Am. Chem. Soc.*, 2003, **125**, 12378-12379.
147. C. P. Horwitz, D. R. Fooksman, L. D. Vuocolo, S. W. Gordon-Wylie, N. J. Cox and T. J. Collins, *J. Am. Chem. Soc.*, 1998, **120**, 4867-4868.
148. M. J. Bartos, S. W. Gordon-Wylie, B. G. Fox, L. J. Wright, S. T. Weintraub, K. E. Kauffmann, E. Münck, K. L. Kostka, E. S. Uffelman, C. E. F. Rickard, K. R. Noon and T. J. Collins, *Coord. Chem. Rev.*, 1998, **174**, 361-390.
149. K. G. Wingate, T. R. Stuthridge, L. J. Wright, C. P. Horwitz and T. J. Collins, *Water Sci. and Technol.*, 2004, **49**, 255-260.
150. D. L. Popescu, A. Chanda, M. J. Stadler, S. Mondal, J. Tehranchi, A. D. Ryabov and T. J. Collins, *J. Am. Chem. Soc.*, 2008, **130**, 12260-12261.
151. A. D. Ryabov and T. J. Collins, *Adv. Inorg. Chem.*, 2009, vol. 61, pp. 471-521.
152. W. C. Ellis, C. T. Tran, M. A. Denardo, A. Fischer, A. D. Ryabov and T. J. Collins, *J. Am. Chem. Soc.*, 2009, **131**, 18052-18053.
153. W. C. Ellis, C. T. Tran, R. Roy, M. Rusten, A. Fischer, A. D. Ryabov, B. Blumberg and T. J. Collins, *J. Am. Chem. Soc.*, 2010, **132**, 9774-9781.
154. A. d. Meijere and F. Diederich, *Metal-Catalyzed Cross-Coupling Reactions*, Wiley-VCH, Weinheim, 2004.

155. L. Friberg, G. Nordberg and V. B. Vouk, *Handbook on the Toxicology of Metals*, North-Holland Biomedical Press, Amsterdam, 1979.
156. J. J. Hostýnek and H. I. Maibach, *Nickel and the Skin: Absorption, Immunology, Epidemiology, and Metallurgy*, CRC Press, Boca Raton, 2002.
157. E. B. Bauer, *Curr. Org. Chem.*, 2008, **12**, 1341-1369.
158. C. Bolm, J. Legros, J. Le Paih and L. Zani, *Chem. Rev.*, 2004, **104**, 6217-6254.
159. S. Enthaler, K. Junge and M. Beller, *Angew. Chem. Int. Ed.*, 2008, **47**, 3317-3321.
160. W. M. Czaplik, M. Mayer, J. Cvengros and A. Jacobi von Wangelin, *ChemSusChem*, 2009, **2**, 396-417.
161. B. D. Sherry and A. Fürstner, *Acc. Chem. Res.*, 2008, **41**, 1500-1511.
162. M. Tamura and J. Kochi, *Synthesis*, 1971, 303-305.
163. R. S. Smith and J. K. Kochi, *J. Org. Chem.*, 1976, **41**, 502-509.
164. S. M. Neumann and J. K. Kochi, *J. Org. Chem.*, 1975, **40**, 599-606.
165. J. K. Kochi, *Acc. Chem. Res.*, 1974, **7**, 351-360.
166. J. K. Kochi, *J. Organomet. Chem.*, 2002, **653**, 11-19.
167. G. A. Molander, B. J. Rahn, D. C. Shubert and S. E. Bonde, *Tetrahedron Lett.*, 1983, **24**, 5449-5452.
168. G. Cahiez and H. Avedissian, *Synthesis*, 1998, 1199-1205.
169. G. Cahiez and S. Marquis, *Pure Appl. Chem.*, 1996, **68**, 53-60.
170. W. Dohle, F. Kopp, G. Cahiez and P. Knochel, *Synlett.*, 2001, 1901-1904.
171. G. F. Lehr and R. G. Lawler, *J. Am. Chem. Soc.*, 1984, **106**, 4048-4049.
172. T. Kauffmann, *Angew. Chem. Int. Ed.*, 1996, **35**, 386-403.

173. A. Fürstner, A. Leitner, M. Mendez and H. Krause, *J. Am. Chem. Soc.*, 2002, **124**, 13856-13863.
174. A. Fürstner and A. Leitner, *Angew. Chem. Int. Ed.*, 2002, **41**, 609-612.
175. B. Bogdanović and M. Schwickardi, *Angew. Chem. Int. Ed.*, 2000, **39**, 4610-4612.
176. A. Fürstner and R. Martin, *Chemistry Lett.*, 2005, **34**, 624-629.
177. R. Martin and A. Fürstner, *Angew. Chem. Int. Ed.*, 2004, **43**, 3955-3957.
178. K. Jonas, L. Schieferstein, C. Kruger and Y. H. Tsay, *Angew. Chem. Int. Ed.*, 1979, **18**, 550-551.
179. A. Fürstner, R. Martin, H. Krause, G. Seidel, R. Goddard and C. W. Lehmann, *J. Am. Chem. Soc.*, 2008, **130**, 8773-8787.
180. E. J. Corey, H. Yamamoto, D. K. Herron and K. Achiwa, *J. Am. Chem. Soc.*, 1970, **92**, 6635-6636.
181. E. J. Corey and G. H. Posner, *Tetrahedron Lett.*, 1970, 315-318.
182. T. Kauffmann, K. U. Voss and G. Neiteler, *Chem. Ber.*, 1993, **126**, 1453-1459.
183. T. Kauffmann, B. Laarmann, D. Menges and G. Neiteler, *Chem. Ber.*, 1992, **125**, 163-169.
184. A. Fürstner, H. Krause and C. W. Lehmann, *Angew. Chem. Int. Ed.*, 2006, **45**, 440-444.
185. M. Nakamura, K. Matsuo, S. Ito and E. Nakamura, *J. Am. Chem. Soc.*, 2004, **126**, 3686-3687.
186. T. Nagano and T. Hayashi, *Org. Lett.*, 2004, **6**, 1297-1299.

187. R. B. Bedford, D. W. Bruce, R. M. Frost, J. W. Goodby and M. Hird, *Chem. Commun.*, 2004, 2822-2823.
188. R. B. Bedford, D. W. Bruce, R. M. Frost and M. Hird, *Chem. Commun.*, 2005, 4161-4163.
189. R. B. Bedford, M. Betham, D. W. Bruce, S. A. Davis, R. M. Frost and M. Hird, *Chem. Commun.*, 2006, 1398-1400.
190. G. Cahiez, V. Habiak, C. Duplais and A. Moyeux, *Angew. Chem. Int. Ed.*, 2007, **46**, 4364-4366.
191. A. M. Reckling, D. Martin, L. N. Dawe, A. Decken and C. M. Kozak, *J. Organomet. Chem.*, 2011, **696**, 787-794.
192. X. Qian, L. N. Dawe and C. M. Kozak, *Dalton Trans.*, 2011, **40**, 933-943.
193. R. R. Chowdhury, A. K. Crane, C. Fowler, P. Kwong and C. M. Kozak, *Chem. Commun.*, 2008, 94-96.
194. K. Tamao, K. Sumitani and M. Kumada, *J. Am. Chem. Soc.*, 1972, **94**, 4374-4376.
195. R. J. P. Corriu and J. P. Masse, *J. Chem. Soc., Chem. Commun.*, 1972, 144.
196. J. A. Halfen, B. A. Jazdzewski, S. Mahapatra, L. M. Berreau, E. C. Wilkinson, L. Que and W. B. Tolman, *J. Am. Chem. Soc.*, 1997, **119**, 8217-8227.
197. Y. D. Wang and T. D. P. Stack, *J. Am. Chem. Soc.*, 1996, **118**, 13097-13098.
198. E. Bill, J. Müller, T. Weyhermüller and K. Wieghardt, *Inorg. Chem.*, 1999, **38**, 5795-5802.
199. Y. Shimazaki, S. Huth, A. Odani and O. Yamauchi, *Angew. Chem. Int. Ed.*, 2000, **39**, 1666-1669.

200. S. Gendler, S. Segal, I. Goldberg, Z. Goldschmidt and M. Kol, *Inorg. Chem.*, 2006, **45**, 4783-4790.
201. S. Segal, I. Goldberg and M. Kol, *Organometallics*, 2005, **24**, 200-202.
202. S. Groysman, E. Y. Tshuva, I. Goldberg, M. Kol, Z. Goldschmidt and M. Shuster, *Organometallics*, 2004, **23**, 5291-5299.
203. S. Groysman, I. Goldberg, M. Kol, E. Genizi and Z. Goldschmidt, *Organometallics*, 2003, **22**, 3013-3015.
204. S. Groysman, I. Goldberg, M. Kol, E. Genizi and Z. Goldschmidt, *Inorg. Chim. Acta*, 2003, **345**, 137-144.
205. C. T. Chen, C. A. Huang and B. H. Huang, *Dalton Trans.*, 2003, 3799-3803.
206. F. M. Kerton, A. C. Whitwood and C. E. Willans, *Dalton Trans.*, 2004, 2237-2244.
207. A. Amgoune, C. M. Thomas, T. Roisnel and J. F. Carpentier, *Chem. Eur. J.*, 2006, **12**, 169-179.



## Co-Authorship Statement

This PhD thesis consists of joint research that has been published in part in three peer reviewed journals.

### **Chapter 2:** Synthesis and structure of amine-bis(phenolate)Fe(III) halide complexes

This chapter contains some of the results published in the article "**Synthesis and structure of iron(III) diamine-bis(phenolate) complexes**", *Dalton Transactions*, 2008, 2991-2998 and additional results.

**Authors:** Kamrul Hasan, Candace Fowler, Philip Kwong, Angela K. Crane, Julie L. Collins and Christopher M. Kozak

*The first author (Kamrul Hasan)* contributed 50% of the content of the article as a main researcher including: designing and performing experiments, analyzing and collecting data, and writing the corresponding experimental section. The PhD candidate re-wrote material from this paper that is included in Chapter 2. He contributed to all aspects of the research reported in Chapter 2 including conducting the literature review, designing and performing experiments, analyzing and collecting data, presenting and discussing results with the principal investigator (C.M. Kozak).

*The co-authors (Candace Fowler, Philip Kwong and Angela K. Crane)* were undergraduate researchers who collectively performed 50% of the experiments and data analysis but this data is not included in this thesis.

The co-author (*Julie L. Collins*) was the crystallographer in the Centre for Chemical Analysis, Research and Training (C-CART) who collected X-ray diffraction data and solved the structures.

*The corresponding author (Christopher M. Kozak)* is the principal investigator and came up with original ideas for this research. He oversaw data analysis, design of new experiments, writing and submission of the manuscript, responding to the questions and comments of peer reviewers, and supervision of the student co-authors.

### **Chapter 3:** Iron-catalyzed epoxidation of olefins using hydrogen peroxide

This chapter was published in its entirety under the above title in the journal *Green Chemistry*, 2011, **13**, 1230-1237.

**Authors:** Kamrul Hasan, Nicole Brown and Christopher M. Kozak

*The first author (Kamrul Hasan)* contributed to all aspects of the project including: literature review, designing and performing experiments, analyzing and collecting data, presenting and discussing results with the corresponding author, mentoring Nicole Brown, writing the early drafts of the manuscript and addressing the questions and comments of peer reviewers.

*The co-author (Nicole Brown)* was an undergraduate summer research student who performed 10% of the experiments and data analysis.

*The corresponding author (Christopher M. Kozak)* is the principal investigator and provided the initial ideas for experiments performed. He oversaw data analysis, design of

new experiments, revision and submission of the manuscript. He responded to questions and comments from peer reviewers, and supervised the student co-authors.

**Chapter 4:** Synthesis, structure and C-C cross-coupling activity of amine-bis(phenolate)iron(acac) complexes

This chapter was published in its entirety under the above title in the journal *European Journal of Inorganic Chemistry*, 2011, 4610-4621.

**Authors:** Kamrul Hasan, Louise N. Dawe and Christopher M. Kozak

*The first author (Kamrul Hasan)* contributed to all aspects of the project including: literature review, designing and performing experiments, analyzing and collecting data, presenting and discussing results with corresponding author, and writing the early drafts of the manuscript.

*The co-author (Louise N. Dawe)* was the crystallographer in the Centre for Chemical Analysis, Research and Training (C-CART) who collected X-ray diffraction data and solved the structures.

*The corresponding author (Christopher M. Kozak)* is the principal investigator and suggested initial experiments in this study. He oversaw data analysis, design of new experiments, revision and submission of the manuscript. He responded to questions and comments from peer reviewers, and supervised the first co-author.

## **Chapter 2. Synthesis and structure of amine-bis(phenolate)Fe(III) halide complexes**

A part of this chapter has been published: Kamrul Hasan, Candace Fowler, Philip Kwong, Angela K. Crane, Julie L. Collins and Christopher M. Kozak,\* *Dalton Trans*, 2008, 2991-2998.

Some modifications of this published paper have been made to expand the discussion and for the sake of consistency with the remainder of the thesis.

### **2.1 Introduction**

Transition metal catalyst design is an important field of research both in industry and academia.<sup>1</sup> An approach towards catalyst discovery is the rational design and preparation of ligands which can impart novel chemistry when incorporated into a metal's coordination sphere. For example, amine-bis(phenol) molecules form a class of ligand precursors, which contain both  $\sigma$  donor nitrogen and  $\pi$  donor oxygen atoms. These molecules act as dianionic chelating ligands. Also, synthesis of these ligand precursors is straightforward and water is used as solvent which gives high yields of the desired products.<sup>2,3</sup> Amine-bis(phenolate) ligands can strongly coordinate with highly oxophilic early transition metals and form well-defined structural complexes displaying a wide

range of reactivity.<sup>4</sup> In the early 1990s, there was a demand for the synthesis of non-metallocene-based ligands because of extensively patented cyclopentadienyl-based polymerization catalysts. Kol *et al.* employed tridentate amine-bis(phenolate) ligands as alternatives to cyclopentadienyl groups for the early transition metal (Ti and Zr) polymerization catalysts.<sup>5,6</sup> However, later they improved the catalyst's activity by modifying the ligands through introducing a pendant donor arm, such as dimethylethylamine, ethylmethylether or pyridine and different substituent groups on the phenolate rings. Also, in combination with Group 4 and 5 metals, these catalysts display high activities towards olefin and cyclic ester polymerizations.<sup>7-21</sup> Group 3 and lanthanide metal complexes of these ligands have been used as catalysts or initiators for ring-opening polymerization of lactide and  $\epsilon$ -caprolactone.<sup>22-32</sup> By comparison, there has been much less use of amine-bis(phenolate) ligands with the first row late transition metals,<sup>33-43</sup> whereas the chemistry of monoanionic phenoxytriamine ligands with these metals is far more developed.<sup>44-57</sup> A number of Fe(III) complexes of this class of ligand has been reported and studied as a result of their close relationship to phenol-containing ligands found in non-heme iron-containing metalloenzymes.<sup>33,34,58-65</sup> Particularly interesting is their similarity to catechol dioxygenases, iron proteins that catalyze the oxidative cleavage of catechol or its derivatives to the incorporation of molecular oxygen. Also, phenol-containing ligands have a similarity to the tyrosine radicals found in many metalloproteins.<sup>66-69</sup> Indeed, the principal focus of amine-bis(phenolate) iron chemistry to-date has been with respect to its use in mimicking the structural and functional features of redox-active bioinorganic systems.<sup>70-72</sup> However, exploration of amine-bis(phenolate)

iron complexes as catalysts for organic synthesis is still underdeveloped, therefore, it might be a fruitful area of research to explore new inexpensive iron-based catalysts for organic synthesis.

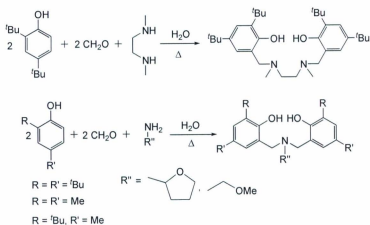
The Kozak group has recently begun exploring the catalytic potential of iron complexes supported by various amine-bis(phenolate) ligands bearing an additional pendant arm, such as an ether or amine group. For example, they have reported Fe(III) compounds supported by tetradentate and tridentate amine-bis(phenolate) ligands, which are effective catalysts for cross-coupling of aryl Grignard reagents with alkyl halides, including secondary alkyl halides and benzyl halides.<sup>73</sup> Inspired by these results, the further development of iron complexes of amine-bis(phenolate) ligands seemed appropriate. This chapter describes the synthesis, structure and spectroscopic properties of a related class of iron(III) complexes supported by amine-bis(phenolate) ligands.

## **2.2 Results and Discussion**

### **2.2.1 Ligand synthesis**

Amine-bis(phenol) ligand precursors were synthesized by modified literature procedures employing Mannich condensation reactions (Scheme 2.1). A one-pot reaction using the corresponding phenol, primary or secondary amine and formaldehyde was performed. The use of water as a reaction medium proves much more effective for generating desired products and allows shorter reaction times.<sup>2,3</sup> The amine and formaldehyde were added to the aqueous suspension of the substituted phenol and were heated at reflux overnight. The resulting solids were separated using filtration and

removal of solvent under vacuum gave the desired products as colourless solids. The ligands were purified by recrystallization from hot ethanol. Following this procedure, five ligands were prepared (Scheme 2.1). Substituents in the 2 and 4-position of the phenols were either both *tert*-butyl or methyl or a combination of *tert*-butyl and methyl groups, and the amines were *N,N'*-dimethylethylenediamine, tetrahydrofurfurylamine or methoxyethylamine. Figure 2.1 shows the small library of amine-bis(phenol) ligands studied in this chapter.



**Scheme 2.1** Synthesis of amine-bis(phenol) ligands.

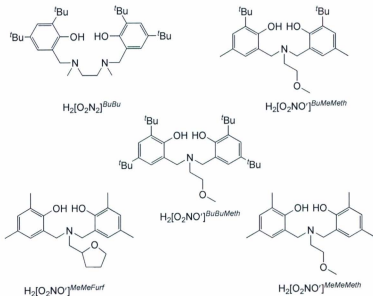


Figure 2.1 Library of amine-bis(phenol) ligands studied in this chapter.

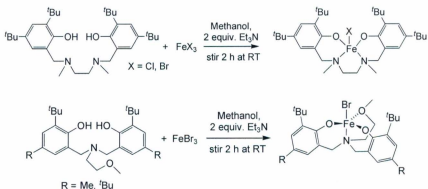
### 2.2.2 Synthesis of Fe(III) complexes

Amine-bis(phenol) ligands contain -OH groups that can potentially react with metal centers. Metallation with alkali metal reagents can be accomplished using *n*-BuLi, NaH or KH to generate  $M_2[L]$ . For example, several structurally-characterized amine-bis(phenolate) lithium salts have been reported in the literature.<sup>74-78</sup> These can be used in metallation reactions to produce transition metal complexes. Another route to such species is the direct reaction of a protonated ligand with suitable metal precursors such as  $Zn(CH_2Ph)_4$ ,  $Zr(NMe_2)_4$ ,  $La[N(SiHMe_2)_2]_3(THF)_2$ , and  $Y(CH_2SiMe_3)_3(THF)_2$  by the elimination of alkane or amine. Also, these protonated ligands can react with late



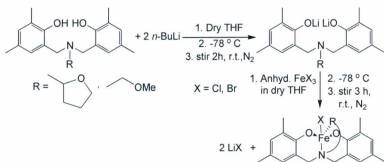
transition metal halide salts, such as anhydrous  $\text{FeCl}_3$  or  $\text{FeBr}_3$  by the replacement of kinetically-labile halide anions.

Amine-bis(phenolate)Fe(III) halide complexes were prepared by a protonolysis reaction between the ligand precursors and the anhydrous Fe(III) halide salts (Scheme 2.2). A methanolic solution of anhydrous  $\text{FeCl}_3$  was added dropwise to a methanolic slurry of the ligand at room temperature. 2.0 equiv. of  $\text{NEt}_3$  solution was added to the resulting dark blue solution. After 2 h stirring, the reaction mixture was evaporated to dryness and extracted either toluene or acetone or dichloromethane. Filtration, followed by removal of solvent gave the analytically pure paramagnetic complexes in good yield (89%). A similar procedure was followed for preparing other amine-bis(phenolate)Fe(III) complexes using anhydrous  $\text{FeBr}_3$  salt (Scheme 2.2)

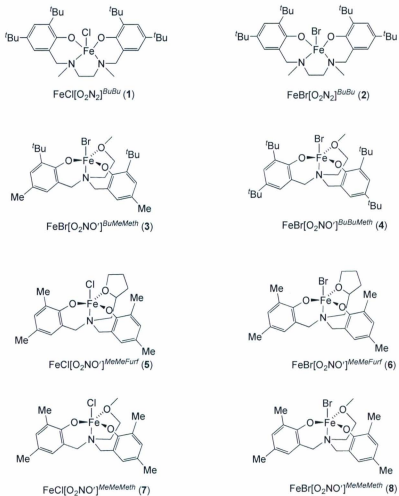


**Scheme 2.2** Synthesis of amine-bis(phenolate)Fe(III) halide complexes.

There is an alternative way of preparing amine-bis(phenolate)Fe(III) halide complexes, where the ligand is first lithiated, followed by transmetalation. A ligand and anhydrous  $\text{FeCl}_3$  were added under nitrogen atmosphere into two different Schlenk tubes and dry THF was added to produce a colourless ligand solution and very pale green metal salt solution. To the ligand solution, 2.0 equiv. of *n*-BuLi was added at  $-78^\circ\text{C}$  and the mixture was warmed to room temperature then stirred for 2 h (Scheme 2.3). The lithiated ligand solution was then transferred to the metal salt solution at  $-78^\circ\text{C}$  *via* cannula, warmed to room temperature and stirred for 3 h. The resulting reaction mixture became intense violet coloured. Solvent was removed and the residue was extracted with dichloromethane and filtered through Celite. Removal of solvent *in vacuo* gave pure paramagnetic dark-violet products. A similar procedure was followed for other amine-bis(phenolate)Fe(III) halide complexes using anhydrous  $\text{FeBr}_3$ . The eight amine-bis(phenolate)Fe(III) halide complexes synthesized in this study are shown in Figure 2.2.



**Scheme 2.3** Synthesis of amine-bis(phenolate)Fe(III) halide complexes *via* salt metathesis.

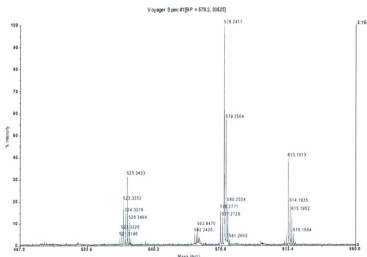


**Figure 2.2** Library of synthesized amine-bis(phenolate)Fe(III) halide complexes.

### 2.2.3 Characterization of Fe(III) complexes

#### 2.2.3.1 MALDI-TOF mass spectrometry

All the synthesized amine-bis(phenolate)Fe(III) halide complexes contained  $d^5$  metal centers and were paramagnetic at room temperature. Therefore,  $^1\text{H}$  NMR was not suitable for their characterization as the paramagnetic metal center gives rise to line broadening as  $T_2$ , the longitudinal relaxation time is decreased. MALDI-TOF mass spectrometry was employed as a primary characterization technique and anthracene was used as the matrix. The spectra of these complexes showed either the relevant molecular ion peaks or fragment ions resulting from loss of halides. For example, the MALDI-TOF mass spectrum of complex  $\text{FeCl}[\text{O}_2\text{N}_2]^{\text{BuBu}}$  (**1**) shows the molecular ion peak at  $m/z$  613.2 amu which is close to the calculated exact mass 613.3 amu for that complex (Figure 2.3).

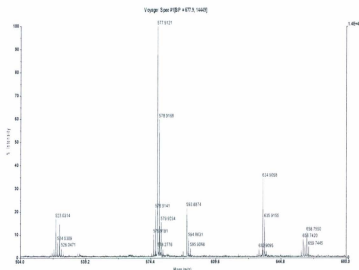


**Figure 2.3** MALDI-TOF mass spectrum of  $\text{FeCl}[\text{O}_2\text{N}_2]^{\text{BuBu}}$  (**1**).

References begin on page 120

The molecular ion peak was assigned based on its isotopic distribution pattern, which is almost similar to the calculated pattern. The most intense peak of this spectrum observed at  $m/z$  of 578.2 amu corresponds to the loss of Cl<sup>-</sup> ion to give  $[\text{Fe}[\text{O}_2\text{N}_2]^{\text{BuBu}}]^+$ , which has a calculated mass of 578.4 amu.

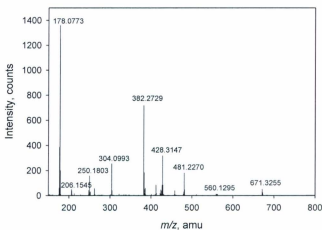
The molecular ion peak of complex  $\text{FeBr}[\text{O}_2\text{N}_2]^{\text{BuBu}}$  (**2**) occurs at  $m/z$  658.8 amu which is close to the calculated molecular weight 658.6 amu (Figure 2.4). The isotopic distribution pattern of the molecular ion peak has a close resemblance to its calculated molecular ion peak. The most intense peak of the spectrum observed at  $m/z$  577.9 amu corresponds to the  $[\text{Fe}[\text{O}_2\text{N}_2]^{\text{BuBu}}]^+$  ion, which was generated by the loss of bromide from its molecular ion.



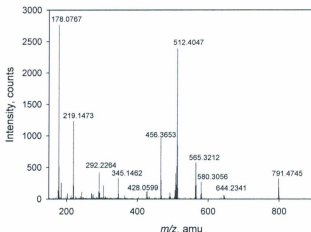
**Figure 2.4** MALDI-TOF mass spectrum of  $\text{FeBr}[\text{O}_2\text{N}_2]^{\text{BuBu}}$  (**2**).

References begin on page 120

The molecular ion peaks of complexes,  $\text{FeBr}[\text{O}_2\text{NO}]^{\text{BuMeMeth}}$  (**3**) and  $\text{FeBr}[\text{O}_2\text{NO}]^{\text{BuMeMeth}}$  (**4**) were observed at  $m/z$  560.1 and 644.2 amu respectively, which are close to their calculated values  $m/z$  560.1 and 644.2 amu. Also, both complexes exhibited another characteristic peak for the loss of bromide ion corresponding to the  $[\text{Fe}[\text{O}_2\text{NO}]^{\text{BuMeMeth}}]^+$  and  $[\text{Fe}[\text{O}_2\text{NO}]^{\text{BuMeMeth}}]^+$  ion, respectively. Figure 2.5 and Figure 2.6 show the MALDI-TOF mass spectra of these two complexes. In both cases, peaks with masses higher than the molecular ions were obtained but these remain unidentified.



**Figure 2.5** MALDI-TOF mass spectrum of  $\text{FeBr}[\text{O}_2\text{NO}]^{\text{BuMeMeth}}$  (**3**).



**Figure 2.6** MALDI-TOF mass spectrum of  $\text{FeBr}[\text{O}_2\text{NO}]^{\text{BaBuMeth}}$  (**4**).

MALDI-TOF mass spectra of complexes **5-8** were also obtained using anthracene as the matrix. In all cases, mass peaks greater than molecular ion peaks were observed but these remain unidentified. In the case of complexes **6-8**, molecular ion peaks were not observed. However, the peaks corresponding to the loss of halides were observed in all four cases. MALDI-TOF mass spectra of these complexes are given in the Appendix of this thesis.

### 2.2.3.2 Molecular structure determination

Attempts were made to grow suitable crystals for X-ray crystallographic analysis of all the synthesized amine-bis(phenolate)Fe(III) halide complexes. Different crystallization techniques were employed using different solvents, but only the slow evaporation method gave suitable crystals for three of the complexes **1, 2 and 3**. Crystals

*References begin on page 120*

of the complexes,  $\text{FeCl}[\text{O}_2\text{N}_2]^{\text{BuBu}}$  (**1**) and  $\text{FeBr}[\text{O}_2\text{N}_2]^{\text{BuBu}}$  (**2**) were isolated from acetone/hexane (1:1) solutions and were analyzed by single crystal X-ray diffraction. These two molecules were nearly isostructural, except for the halide ligand. The asymmetric units of both complexes contained one chiral molecule but both enantiomers were observed in the unit cells. Figure 2.7 and Figure 2.8 show the ORTEP diagrams and atom labeling schemes for complexes  $\text{FeCl}[\text{O}_2\text{N}_2]^{\text{BuBu}}$  (**1**) and  $\text{FeBr}[\text{O}_2\text{N}_2]^{\text{BuBu}}$  (**2**), respectively. Selected bond lengths and bond angles of these two molecules are presented in Table 2.1.

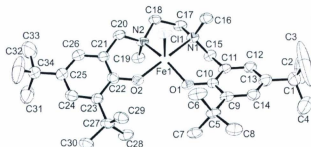
The Fe(III) centers in both complexes were coordinated by a dianionic tetradentate ligand composed of an  $\text{O}_2\text{N}_2$  donor set. The Fe(III) ions were bonded to two phenolate oxygen atoms and two nitrogen donor atoms of the ligand backbone which defined the basal plane of the square pyramid. The apical site was occupied by a chloride ion in complex **1** and a bromide ion in complex **2**. Methyl groups of the ethylenediamine fragment were *trans*-oriented. No *cis*-methyl-containing complex was present in these structures, however, a related structure reported by Girerd, Münck and co-workers contains both the *trans* and *cis* isomers.<sup>61</sup>

The phenolate oxygen and iron (Fe-O) bond distances were 1.849(3) and 1.862(3) Å for Fe(1)-O(1) and Fe(1)-O(2) in molecule **1** and were 1.835(4) and 1.837(3) Å for Fe(1)-O(1) and Fe(1)-O(2) in molecule **2**, respectively. The Fe-O distances of complex **1** were slightly longer than those of the complex **2**. However, the overall Fe-O bond distances of these complexes were shorter than the average octahedral Fe-O bond

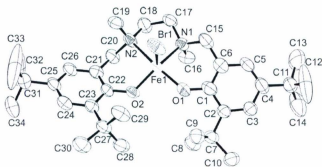


distance of 1.92 Å observed in complexes possessing phenolate donor ligands.<sup>33,34,41,42,58,</sup>

60,62-65,79-81



**Figure 2.7** ORTEP diagram and atom labeling scheme for  $\text{FeCl}[\text{O}_2\text{N}_2]^{\text{BuBu}}$  (**1**) (thermal ellipsoids shown at 50% probability). Hydrogen atoms removed for clarity.



**Figure 2.8** ORTEP diagram and atom labeling scheme for  $\text{FeBr}[\text{O}_2\text{N}_2]^{\text{BuBu}}$  (**2**) (thermal ellipsoids shown at 50% probability). Hydrogen atoms removed for clarity.

Specifically, the Fe-O distances in these complexes were shorter than the Fe(1)-O(1) and Fe(1)-O(2) distances of 1.900(2) Å and 1.880(2) Å in an octahedral complex  $\text{Fe}(\text{acac})[\text{O}_2\text{N}_2]^{\text{BuBu}}$ , employing the same amine-bis(phenolate) ligand and an acetylacetonate co-ligand.<sup>82</sup> This indicates a stronger oxygen-iron overlap in lower

*References begin on page 120*

coordination number complexes possessing square pyramidal and trigonal bipyramidal geometries compared to those with an octahedral geometry. Therefore, the observed Fe-O bond distances in molecules **1** and **2** were close to those found in iron(III) complexes with distorted trigonal bipyramidal geometries supported by tripodal tetradentate amine-bis(phenolate) ligands.<sup>43,63,83</sup> Also, the Fe-O bond distances of complexes **1** and **2** were similar to square pyramidal Fe(III) complexes containing bis(phenolate) ligands.<sup>40,61,84</sup> The Fe(1)-Cl(1) distance of 2.2393(12) Å in **1** was shorter than the distance of 2.291 Å in the trigonal bipyramidal Fe(III)-bis(phenolate) complex, reported by Palaniandavar *et al.*,<sup>63</sup> but similar to the Fe-Cl lengths observed in other square pyramidal iron(III) complexes possessing salen or diamine-bis(phenolate) ligands.<sup>59,61</sup> The Fe(1)-Br(1) distance of 2.3679(12) Å in **2** was longer than the Fe(1)-Cl(1) distance of **1**, but shorter than that reported in other five-coordinate iron(III) bromide complexes.<sup>85,86</sup> The Fe-N distances were 2.274(3) and 2.161(3) Å for Fe(1)-N(1) and Fe(1)-N(2) in complex **1** and were 2.151(4) and 2.265(4) Å for Fe(1)-N(1) and Fe(1)-N(2) in complex **2**, respectively. The asymmetry in these bond distances could be steric in nature, since the longer Fe-N interactions in each molecule corresponded to the nitrogen donor where the *N*-methyl group is orientated *cis* to the halide ligand. Recently, Palaniandavar *et al.* reported a related square pyramidal bis(phenolate)Fe(III) complex supported by a 1,4-diazepane ligand backbone where the two Fe-N bonds were symmetric having lengths of 2.202(4) Å.<sup>84</sup> The Fe-N bond distances in complex **1** and **2** were close to the Fe-N distances in the related square pyramidal,<sup>61</sup> trigonal bipyramidal<sup>63</sup> and octahedral complexes.<sup>81,87</sup>

Typical Fe<sup>III</sup>-N distances in octahedral systems are  $\sim 2.15$ - $2.20$  Å.<sup>33,34,36-39,58,60, 63,64,88,89</sup> The O-C<sub>ipso</sub> bond lengths were 1.357(5) and 1.337(5) Å for O(1)-C(10) and O(2)-C(22), in complex **1** and are 1.350(8) and 1.352(6) Å for O(1)-C(1) and O(2)-C(22) in complex **2**, respectively. Typically, O-C<sub>ipso</sub> bond lengths are about  $\sim 1.33$  Å for metal complexes containing amine-bis(phenolate) ligands.<sup>33-35, 42, 43, 63, 81, 83</sup>

The geometries of the Fe(III) centers were distorted square pyramidal. The O(1)-Fe(1)-O(2), O(1)-Fe(1)-N(1), N(1)-Fe(1)-N(2) and O(2)-Fe(1)-N(2) angles were 94.13(13)°, 87.71(13)°, 78.75(13)° and 85.87(14)° in **1** and are 94.37(17)°, 86.07(18)°, 78.87(17)° and 88.16(15)° in **2**, respectively. In both of the complexes, only the O(1)-Fe(1)-O(2) angle was more than 90° and the other three angles were less than 90°, since the two amine nitrogens of the ligand backbone form a five-membered chelating ring between them at the Fe(III) center. The Fe-O-C bond angles in **1** were 129.6(2)° for Fe(1)-O(1)-C(10) and 135.9(2)° for Fe(1)-O(2)-C(22) while **2** gave an Fe(1)-O(1)-C(1) angle of 136.5(4)° and Fe(1)-O(2)-C(22) of 129.1(3)°. The geometric parameter  $\tau = (\beta - \alpha)/60$  is applicable to five-coordinate structures as an index for the degree of trigonality between trigonal bipyramidal (where  $\tau = 1$ ) and square pyramidal geometries (where  $\tau = 0$ ).<sup>90</sup> The coordination geometries around iron(III) in both **1** and **2** were biased toward square pyramidal with a trigonality index,  $\tau$ , of 0.31 in **1** [ $\beta$  is given by O(2)-Fe(1)-N(1) and  $\alpha$  by O(1)-Fe(1)-N(2)] and 0.25 in **2** [ $\beta$  is given by O(1)-Fe(1)-N(2) and  $\alpha$  by O(2)-Fe(1)-N(1)].

**Table 2.1** Selected bond lengths (Å) and angles (°) for the complex 1, 2 and 3.

<b>Bond lengths (Å) / Bond angles (°)</b>	<b>FeCl[O<sub>2</sub>N<sub>2</sub>]<sup>BuBu</sup> (1)</b>	<b>FeBr[O<sub>2</sub>N<sub>2</sub>]<sup>BuBu</sup> (2)</b>	<b>FeBr[O<sub>2</sub>NO']<sup>BuMeMeth</sup> (3)</b>
Fe(1)-O(1)	1.849(3)	1.835(4)	1.866(2)
Fe(1)-O(2)	1.862(3)	1.837(3)	1.850(2)
Fe(1)-O(3)			2.098(2)
Fe(1)-N(1)	2.274(3)	2.151(4)	2.231(3)
Fe(1)-N(2)	2.161(4)	2.265(4)	
Fe(1)-Cl(1)	2.2393(12)		
Fe(1)-Br(1)		2.3679(12)	2.4242(6)
O(1)-C(1)		1.350(8)	
O(1)-C(10) <sub>psa</sub>	1.357(5)		
O(1)-C(5) <sub>psa</sub>			1.346(4)
O(2)-C(22)	1.337(5)	1.352(6)	
O(2)-C(15) <sub>psa</sub>			1.349(4)
O(1)-Fe(1)-O(2)	94.13(13)	94.37(17)	113.45(10)
O(1)-Fe(1)-N(1)	87.71(13)	86.07(18)	87.92(9)
N(1)-Fe(1)-N(2)	78.75(13)	78.87(17)	
O(2)-Fe(1)-N(2)	85.87(14)	88.16(15)	
O(2)-Fe(1)-O(3)			115.97(10)
O(1)-Fe(1)-O(3)			127.29(10)
O(1)-Fe(1)-N(2)	139.37(13)	157.9(2)	
O(2)-Fe(1)-N(1)	158.15(14)	142.81(17)	88.69(9)
O(3)-Fe(1)-N(1)			76.16(10)
O(1)-Fe(1)- Cl(1)/Br(1)	112.29(10)	101.79(19)	94.53(7)
O(2)-Fe(1)- Cl(1)/Br(1)	102.36(11)	110.46(12)	103.63(7)
O(3)-Fe(1)-Br(1)			90.85(7)

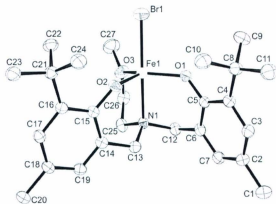
References begin on page 120

N(1)-Fe(1)- Cl(1)/Br(1)	97.02(10)	105.78(13)	165.18(7)
N(2)-Fe(1)- Cl(1)/Br(1)	107.32(10)	97.80(14)	
Fe(1)-O(1)-C(10) <sub>psso</sub>	129.6(3)		
Fe(1)-O(1)-C(1)		136.5(4)	
Fe(1)-O(1)-C(5) <sub>psso</sub>			131.00(19)
Fe(1)-O(2)-C(22)	135.9(3)	129.2(3)	
Fe(1)-O(2)-C(15) <sub>psso</sub>			133.69(18)

Single crystals suitable for X-ray diffraction of  $\text{FeBr}[\text{O}_2\text{NO}]^{\text{BaMeMeb}}$  (**3**) were obtained in a acetone/hexane (1:1) solution as with the previously reported two complexes. Figure 2.9 shows the ORTEP diagram and atom labeling scheme of complex **3**. Selected bond lengths and angles are given in the Table 2.1 for comparison with the other two complexes reported earlier. The coordination geometry of the Fe(III) center was distorted trigonal bipyramidal. The iron atom was bonded to the two phenolate oxygen atoms and the methoxy oxygen atom of the pendant arm, which defined the trigonal plane of the pyramid. The central nitrogen atom of the ligand backbone and the bromide ion occupied the apical sites.

The iron-to-phenolate Fe-O bond distances of complex **3** were 1.866(2) and 1.850(2) Å for Fe(1)-O(1) and Fe(1)-O(2), respectively. These bond distances were similar to the Fe-O distances in other five coordinated trigonal bipyramidal and square pyramidal iron complexes using bis(phenolate) ligands previously reported by the Kozak group<sup>91</sup> and the Palaniandavar group.<sup>63</sup> However, they were shorter than the average Fe-

O bond length of 1.92 Å observed in octahedral Fe(III) complexes.<sup>33,34,41,42,58,60,62-65,79,80</sup> Fe(1)-O(3) bond length of the complex was 2.098(2) Å which was longer than the other two Fe-O<sub>phen</sub> bond lengths. This was not surprising, since the methoxy oxygen was a mildly weak donor compared to phenolate oxygen donor ligands.



**Figure 2.9** ORTEP diagram and atom labeling scheme for  $\text{FeBr}[\text{O}_2\text{NO}]^{\text{BuMeMeth}}$  (**3**) (thermal ellipsoids shown at 50% probability). Hydrogen atoms removed for clarity.

The Fe-N bond length of complex **3** was 2.231(3) Å which was slightly longer than average Fe-N bond distances of ~ 2.15-2.20 Å in related octahedral complexes.<sup>33,34,36-39,58,60,63,64,88,89</sup> Also, this distance was shorter than Fe-N distances in related trigonal bipyramidal Fe(III) amine-bis(phenolate) complexes.<sup>63,91</sup> The Fe-Br bond length of the complex was 2.4242(6) Å which was longer than the Fe-Br bond length of the previously reported square pyramidal complex but similar to the other five coordinated Fe(III) complexes.<sup>85,86</sup> The O-C<sub>pho</sub> bond lengths of the complex were 1.346(4) and 1.349(4) Å for O(1)-C(5) and O(2)-C(15). The bond angles in the equatorial

*References begin on page 120*

plane were  $113.45(10)^\circ$ ,  $115.97(10)^\circ$  and  $127.29(10)^\circ$  for O(1)-Fe(1)-O(2), O(2)-Fe(1)-O(3) and O(1)-Fe(1)-O(3), respectively. The deviation from the ideal  $120^\circ$  angles makes the complex geometry distorted trigonal bipyramidal. Also, the angle N(1)-Fe(1)-Br(1) was  $165.18(7)^\circ$ , which deviated from the linear  $180^\circ$ . The Fe-O-C<sub>ipso</sub> bond angles of the complex were  $131.00(19)^\circ$  and  $133.69(18)^\circ$  for Fe(1)-O(1)-C(5) and Fe(1)-O(2)-C(15), respectively. These bent angles indicate that the phenolate oxygens hybridization is in between  $sp^2$  and  $sp$ . The coordination geometry around Fe(III) was biased toward trigonal bipyramidal with a trigonality index  $\tau$  of 0.86 [ $\beta$  is given for N(1)-Fe(1)-Br(1)  $165.18(7)^\circ$  and  $\alpha$  is given for O(1)-Fe(1)-O(2)  $113.45(10)^\circ$ ]. Crystallographic data of three of these molecules are given in Table 2.4.

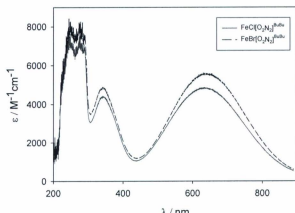
### 2.2.3.3 UV-vis spectroscopy

Electronic absorption spectra of all the synthesized amine-bis(phenolate)Fe(III) halide complexes were carried out in different solvents of varying polarity. The employed solvents were methanol, THF, toluene and acetonitrile. Spectra of all the complexes show multiple intense bands in the UV and visible regions. The variations of absorption bands in the spectra were due to structural changes at the metal center, such as the different coordination geometries or coordination of solvent molecules. In general, the electronic absorption spectra of these amine-bis(phenolate) complexes were not significantly affected by the nature of the tetradentate ligand's environment. This was not unexpected because the electron-donating ability of these ligands was relatively similar. However, a small effect could occur *via* the change of ligand backbone from linear ethylenediamine to an amine containing a pendant arm because they give different geometries.

Also, the pendant arm, for example, the tetrahydrofurfuryl group would only be a mildly better donor than the methyl ether group and therefore, result in similar spectra. Variation of substituents on the phenolate ring systems such as methyl or *tert*-butyl groups primarily led to changes that are steric rather than electronic in nature. Changing the halide from chloride to bromide did, however, affect the intensity of the transitions.

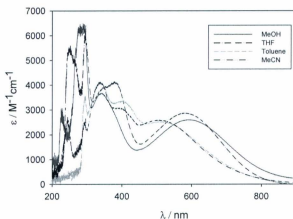
UV-vis spectra of the two structurally-characterized complexes such as  $\text{FeCl}[\text{O}_2\text{N}_2]^{\text{BuBu}}$  (**1**) and  $\text{FeBr}[\text{O}_2\text{N}_2]^{\text{BuBu}}$  (**2**) are shown in Figure 2.10. Both of these complexes were dissolved in methanol at a concentration of  $3.10 \times 10^{-4} \text{ mol L}^{-1}$  and generated blue-violet colour solutions. UV-vis spectra of these complexes show four absorption bands in the UV and visible regions. The absorption maxima observed in the near UV region (below 300 nm) were caused by  $\pi$  to  $\pi^*$  transitions involving phenolate units. Intense, high energy bands were also observed around 340 nm for the ligand to metal charge-transfer (LMCT) transition from HOMO (highest occupied molecular orbital) of the phenolate oxygen to the half-filled  $d_{x^2-d_y^2}/d_{z^2}$  orbitals of the Fe(III) center. The lowest energy bands were observed around the 640 nm region for the LMCT from the phenolate oxygen to the  $d\pi^*$  orbital of the Fe(III) center. Both of these complexes have identical structures, except for the halide anion. For this reason, the lowest energy band of the bromide complex  $\text{FeBr}[\text{O}_2\text{N}_2]^{\text{BuBu}}$  (**2**) was observed at slightly longer wavelength (643 nm) than for the chloride complex  $\text{FeCl}[\text{O}_2\text{N}_2]^{\text{BuBu}}$  (**1**) of 632 nm. In both of these complexes, no d-d transition was observed.





**Figure 2.10** Electronic absorption spectra of  $\text{FeCl}[\text{O}_2\text{N}_2]^{\text{BuBu}}$  (1) and  $\text{FeBr}[\text{O}_2\text{N}_2]^{\text{BuBu}}$  (2) in methanol.

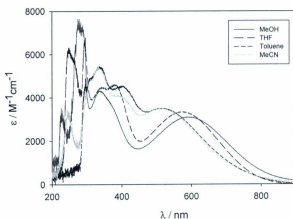
The polarity of solvents had some effect on the electronic absorption spectra of the coordination complexes. Figure 2.11 shows the UV-vis spectra of the  $\text{FeBr}[\text{O}_2\text{NO}]^{\text{BuMeMeth}}$  (3) complex which were carried out in each of the four different solvents: methanol, THF, toluene and acetonitrile, respectively. A noticeable solvent-dependent shift of these LMCT bands was observed. The lowest energy LMCT bands of the complex were found to follow: methanol < THF < toluene < acetonitrile, where the absorption spectrum in acetonitrile contained this band at the lowest wavelength (510 nm), down from 595 nm in methanol. The absorption spectra in toluene and THF displayed this LMCT band at 518 and 578 nm, respectively.



**Figure 2.11** Electronic absorption spectra of  $\text{FeBr}[\text{O}_2\text{NO}]^{\text{BuMeMeth}}$  (**3**) in methanol, THF, toluene and acetonitrile solutions.

The effect of solvent on the UV-vis spectra was also studied for complex  $\text{FeBr}[\text{O}_2\text{NO}]^{\text{BuBuMeth}}$  (**4**) using four different solvents namely methanol, THF, toluene and acetonitrile, respectively (Figure 2.12). Like the previous complex, noticeable solvent dependent shifts of the LMCT bands were observed. The lowest energy bands of complex  $\text{FeBr}[\text{O}_2\text{NO}]^{\text{BuBuMeth}}$  (**4**) followed the trend: methanol (586 nm) < THF (574 nm) < toluene (516 nm) < acetonitrile (507 nm). The nature of the solvent dependent shifts of the lowest energy bands of  $\text{FeBr}[\text{O}_2\text{NO}]^{\text{BuBuMeth}}$  (**4**) were similar to those of complex **3** because both of these complexes are structurally identical except for one substituent, namely a *tert*-butyl instead of methyl group on the phenolate rings.

For comparison, molar absorption coefficients and wavelengths of the two LMCT bands of complexes  $\text{FeBr}[\text{O}_2\text{NO}]^{\text{BuMeMeth}}$  (3) and  $\text{FeBr}[\text{O}_2\text{NO}]^{\text{BuBuMeth}}$  (4) are shown in Table 2.2.



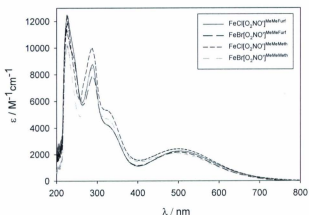
**Figure 2.12** Electronic absorption spectra of  $\text{FeBr}[\text{O}_2\text{NO}]^{\text{BuBuMeth}}$  (4) in methanol, THF, toluene and acetonitrile solutions.

**Table 2.2** Comparison of molar absorption coefficients of the two LMCT bands of  $\text{FeBr}[\text{O}_2\text{NO}]^{\text{BuMeMeth}}$  (3) and  $\text{FeBr}[\text{O}_2\text{NO}]^{\text{BuBuMeth}}$  (4) complexes.

Solvent	$\text{FeBr}[\text{O}_2\text{NO}]^{\text{BuMeMeth}}$	$\text{FeBr}[\text{O}_2\text{NO}]^{\text{BuBuMeth}}$
	$\lambda$ (nm), $\epsilon$ ( $\text{L mol}^{-1} \text{cm}^{-1}$ )	$\lambda$ (nm), $\epsilon$ ( $\text{L mol}^{-1} \text{cm}^{-1}$ )
Methanol	340, 3685	337, 4334
	595, 2608	586, 3097
THF	380, 4119	397, 4619
	578, 2874	574, 3338
Toluene	342, 4105	337, 5461
	518, 2508	516, 3496
Acetonitrile	340, 4109	334, 5393
	510, 2586	507, 3488

Again, UV-vis spectroscopy was employed for the characterization of amine-bis(phenolate)Fe(III) halide complexes (5-8) containing the relatively less sterically-bulky methyl substituents. Figure 2.13 shows the UV-vis spectra of  $\text{FeCl}[\text{O}_2\text{NO}]^{\text{MeMeFurf}}$  (5),  $\text{FeBr}[\text{O}_2\text{NO}]^{\text{MeMeFurf}}$  (6),  $\text{FeCl}[\text{O}_2\text{NO}]^{\text{MeMeMeth}}$  (7) and  $\text{FeBr}[\text{O}_2\text{NO}]^{\text{MeMeMeth}}$  (8) in methanol. All of these complexes showed multiple absorption bands like the previously reported complexes. Two LMCT absorption bands were observed around 330 nm and 500 nm respectively. These complexes showed similar absorption bands since all of these complexes possess the same geometry. However, two of these complexes contained chloride and ethyl methyl ether pendant arm and the other two complexes contained bromide and tetrahydrofurfuryl pendant arm.

References begin on page 120



**Figure 2.13** Electronic absorption spectra of  $\text{FeCl}[\text{O}_2\text{NO}]^{\text{MeMeFarf}}$  (5),  $\text{FeBr}[\text{O}_2\text{NO}]^{\text{MeMeFarf}}$  (6),  $\text{FeCl}[\text{O}_2\text{NO}]^{\text{MeMeMeth}}$  (7) and  $\text{FeBr}[\text{O}_2\text{NO}]^{\text{MeMeMeth}}$  (8) in methanol.

#### 2.2.3.4 Magnetic studies

Magnetic susceptibility data for all the amine-bis(phenolate)Fe(III) halide complexes were collected at room temperature using either a Faraday balance or a Johnson-Matthey magnetic susceptibility balance. The magnetic moments of these complexes were between 4.6 to 6.2  $\mu_B$  (Table 2.3), which is expected for a high-spin  $d^5$  Fe(III) center. However,  $\text{FeBr}[\text{O}_2\text{N}_2]^{\text{BuBu}}$  (2), exhibited a slightly elevated magnetic moment of 6.2  $\mu_B$  at room temperature, compared to 5.9  $\mu_B$  observed for the related chloride complex,  $\text{FeCl}[\text{O}_2\text{N}_2]^{\text{BuBu}}$  (1). This elevated magnetic moment might not arise from spin-orbit coupling, since spin-orbit coupling is very unlikely for the first row

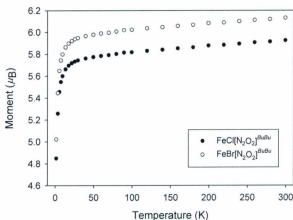
transition complexes.<sup>92</sup> Also, a few of these complexes exhibited slightly lower magnetic moments than expected due to the presence of impurities such as unreacted ligands or lithium halides. Some of these analyzed complexes consistently showed low % carbon values.

**Table 2.3** Room temperature magnetic moments determined by Faraday balance or Johnson-Matthey magnetic susceptibility balance.

Complex	Magnetic moment ( $\mu_B$ )
FeCl[O <sub>2</sub> N <sub>2</sub> ] <sup>BuBu</sup> (1)	5.9
FeBr[O <sub>2</sub> N <sub>2</sub> ] <sup>BuBu</sup> (2)	6.2
FeBr[O <sub>2</sub> NO] <sup>BuMeMeth</sup> (3)	5.0
FeBr[O <sub>2</sub> NO] <sup>BuBuMeth</sup> (4)	4.7
FeCl[O <sub>2</sub> NO] <sup>MeMeFurf</sup> (5)	5.5
FeBr[O <sub>2</sub> NO] <sup>MeMeFurf</sup> (6)	5.9
FeCl[O <sub>2</sub> NO] <sup>MeMeMeth</sup> (7)	4.6

Variable temperature magnetic susceptibility data of FeCl[O<sub>2</sub>N<sub>2</sub>]<sup>BuBu</sup> (1) and FeBr[O<sub>2</sub>N<sub>2</sub>]<sup>BuBu</sup> (2) were acquired for 2 to 300 K in an applied magnetic field of 0.1 T. Figure 2.14 shows magnetic moment ( $\mu_B$ ) vs. temperature (T) plots for both of the complexes. As mentioned earlier, the magnetic moments of FeCl[O<sub>2</sub>N<sub>2</sub>]<sup>BuBu</sup> (1) and FeBr[O<sub>2</sub>N<sub>2</sub>]<sup>BuBu</sup> (2) at 300 K were 5.9 and 6.2  $\mu_B$  respectively. Magnetic moments of these complexes showed slow, smooth reductions in their moments as the temperature

was lowered down to 20 K. In this temperature range, neither displayed any sharp spin-crossover behavior.



**Figure 2.14** Magnetic moment vs. Temperature plots of  $\text{FeCl}[\text{O}_2\text{N}_2]^{\text{BuBu}}$  (1) and  $\text{FeBr}[\text{O}_2\text{N}_2]^{\text{BuBu}}$  (2).

The magnetic behaviour of  $\text{FeCl}[\text{O}_2\text{N}_2]^{\text{BuBu}}$  (1) and  $\text{FeBr}[\text{O}_2\text{N}_2]^{\text{BuBu}}$  (2) showed normal Curie-Weiss paramagnetism [ $\chi_m = C/(T-\theta)$ ]. The Weiss constants for both of the complexes were identical ( $\theta = -0.9$  K) and indicate antiferromagnetic alignment of independent iron(III) centers. Below 20 K, the moments dropped more sharply; at 2 K the observed magnetic moments were 4.83 and 5.15  $\mu_B$  for  $\text{FeCl}[\text{O}_2\text{N}_2]^{\text{BuBu}}$  (1) and  $\text{FeBr}[\text{O}_2\text{N}_2]^{\text{BuBu}}$  (2), respectively.

Similarly, room temperature and variable temperature magnetic moments data for  $\text{FeBr}[\text{O}_2\text{NO}]^{\text{BuMeMeth}}$  (3) were collected over the temperature range 2 to 300 K in an

applied magnetic field of 0.1 T. Figure 2.15 shows the magnetic moment ( $\mu_B$ ) vs. temperature (T) plots of the complex. The magnetic moment at 300 K was  $4.7 \mu_B$  which was less than the expected  $5.9 \mu_B$  for five unpaired electrons of the Fe(III) center. Although the material was crystalline, however, some unreacted ligand impurity may have remained in the sample. Elemental analysis of that complex showed a slightly higher percentage value of carbon and hydrogen compared with the values expected. This complex also showed the slow and smooth reduction of its magnetic moment between 20 and 300 K. Also, below 20 K, the magnetic moment decreases rapidly down to  $4.06 \mu_B$  at 2K.

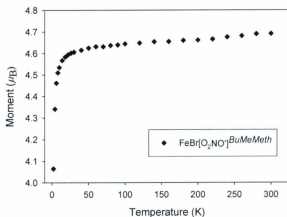


Figure 2.15 Magnetic moment vs. temperature plots of  $\text{FeBr}[\text{O}_2\text{NO}]^{\text{BuMeMeth}}$  (3).



## 2.3 Conclusion

A small library of amine-bis(phenol) ligands has been synthesized by modified literature procedures employing Mannich condensation reactions of the selected phenol, primary or secondary amine and formaldehyde. Using these tetradentate ligands, a series of Fe(III) complexes was prepared by reacting the ligands with anhydrous  $\text{FeX}_3$  salts ( $X = \text{Cl}, \text{Br}$ ). The synthetic procedures were quite simple and the yields of the desired products were excellent (Section 2.4.5). All of the eight complexes reported were five-coordinate and exhibit either square-pyramidal or trigonal bipyramidal geometry depending on the ligand employed. Among them, three of these complexes were structurally characterized by single crystal X-ray diffraction. Also, analytically pure paramagnetic complexes were verified by elemental analysis and MALDI-TOF mass spectrometry. MALDI-TOF mass spectra showed the relative molecular ion peaks or fragments by the loss of halides. Room temperature magnetic moment measurements demonstrated the presence of high-spin  $d^5$  Fe(III) centers. Furthermore, electronic absorption spectra in the UV-vis range exhibited intense charge transfer bands, which were strongly solvent-dependent.

## 2.4 Experimental Section

### 2.4.1 Materials and methods

Chemical reagents were purchased from Aldrich and Alfa Aesar. Commercially available solvents were used without further purification except for THF, which was dried by distillation under an atmosphere of nitrogen from Na/benzophenone.

Reactions for synthesizing ligands and some iron complexes were performed in air. Some other iron complexes (**5-8**) were synthesized under an atmosphere of dry, oxygen-free nitrogen by means of Schlenk line techniques.

#### 2.4.2 Instrumentation

$^1\text{H}$  and  $^{13}\text{C}$  NMR spectra were recorded in  $\text{CDCl}_3$  on a Bruker AVANCE III 300 MHz instrument with a BBFO probe and semi-automated sample handling. Data are reported as follows: chemical shift, multiplicity (s = singlet, d = doublet, dd = doublet of doublets, t = triplet, b = broad, m = multiplet), coupling constant ( $J$ , Hz). Spectra were processed using MestReNova software.

The MALDI-TOF mass spectra of  $\text{FeCl}[\text{O}_2\text{N}_2]^{\text{BuBu}}(\mathbf{1})$  and  $\text{FeBr}[\text{O}_2\text{N}_2]^{\text{BuBu}}(\mathbf{2})$  were recorded on an Applied Biosystems Voyager DE-PRO equipped with a reflectron, delayed ion extraction and high performance nitrogen laser (337 nm). Samples were prepared at a concentration of  $0.03 \text{ mg mL}^{-1}$  in methanol. Matrix (anthracene) was mixed at a concentration of  $0.03 \text{ mg mL}^{-1}$  to promote desorption and ionization. Separate vials were used to mix  $20 \mu\text{L}$  of the sample solution with  $20 \mu\text{L}$  of the matrix solution.  $1 \mu\text{L}$  of the sample and matrix mixture were spotted on a MALDI plate. MALDI-TOF mass spectra of complexes **3-8** were performed using an ABI QSTAR XL Applied Biosystems/MDS hybrid quadrupole TOF MS/MS system equipped with an MALDI-2 ion source. Samples were prepared at a concentration of  $10.0 \text{ mg mL}^{-1}$  in toluene. Anthracene was used as the matrix, which was mixed at a concentration of  $10.0 \text{ mg mL}^{-1}$ .

UV-vis spectra were recorded on an Ocean Optics USB4000+ fiber optic spectrophotometer. CHN analyses were carried out by Guelph Chemical Laboratories, Guelph, ON, Canada or Canadian Microanalytical Services, Delta, BC, Canada.

The room temperature magnetic measurements were done using either a Faraday or a Johnson-Matthey magnetic susceptibility balance. The data were corrected for the diamagnetism of all atoms and the balance was calibrated using  $\text{Hg}[\text{Co}(\text{NCS})_4]$ . The variable temperature magnetic measurements were run on a Quantum Designs MPMS5 SQUID magnetometer.

### 2.4.3 X-ray crystallography

Crystallographic data for compounds **1**, **2** and **3** are summarized in Table 2.4. All data collections were performed on a Rigaku AFC8-Saturn 70 diffractometer equipped with a CCD area detector, using graphite monochromated Mo-K $\alpha$  radiation ( $\lambda = 0.71073$  Å). Suitable crystals were selected and mounted on glass fibers using Paratone-N oil and freezing to either -120 or -160 °C. In each case the data were processed<sup>93,94</sup> and corrected for Lorentz and polarization effects and absorption.<sup>95</sup> Neutral atom scattering factors for all non-hydrogen atoms were taken from the International Tables for X-ray Crystallography.<sup>96</sup> All structures were solved by direct methods using SIR92<sup>97</sup> and expanded using Fourier techniques (DIRDIF99).<sup>98</sup> All non-hydrogen atoms were refined anisotropically. Hydrogen atoms were refined using the riding model.

Anomalous dispersion effects were included in  $F_{\text{calc}}$ ;<sup>99</sup> the values for  $\Delta f'$  and  $\Delta f''$  were those of Creagh and McAuley.<sup>100</sup> The values for the mass attenuation coefficients

are those of Creagh and Hubbell.<sup>101</sup> All calculations were performed using the Crystal Structure<sup>102,103</sup> crystallographic software package except for refinement, which was performed using SHELXL-97.<sup>104</sup> In the structures of **1** and **2**, no suitable point model could be found for a region of diffuse electron density in the asymmetric unit that corresponded to a partial occupancy *n*-hexane molecule. The Platon<sup>105</sup> Squeeze<sup>106</sup> procedure was applied in the solution of **1** to recover 142 electrons per unit cell in two voids (total volume 1946 Å<sup>3</sup>); this represents 17.75 electrons per asymmetric unit. In **2**, it was applied to recover 342 electrons per unit cell in two voids (total volume 2032 Å<sup>3</sup>); this represents 42.75 electrons per asymmetric unit. Structural illustrations were created using ORTEP-III for Windows.<sup>107</sup>

**Table 2.4** Crystallographic and structural refinement data for compounds **1**, **2** and **3**

Compound	<b>1</b>	<b>2</b>	<b>3</b>
Chemical formula	C <sub>34</sub> H <sub>54</sub> ClFeN <sub>2</sub> O <sub>2</sub> · C <sub>6</sub> H <sub>14</sub>	C <sub>34</sub> H <sub>54</sub> BrFeN <sub>2</sub> O <sub>2</sub> · C <sub>6</sub> H <sub>14</sub>	C <sub>27</sub> H <sub>39</sub> BrFeNO <sub>3</sub>
Formula weight	700.26	744.72	561.35
T/K	113	113	138(2)
Colour, habit	Blue, prism	Blue, platelet	Black, platelet
Crystal dimensions/ mm	0.40 × 0.40 × 0.20	0.55 × 0.27 × 0.08	0.47 X 0.24 X 0.12
Crystal system	Monoclinic	Monoclinic	Monoclinic
Space group	C2/c (#15)	C2/c (#15)	P2 <sub>1</sub> /c (#14)
a/ Å	33.575(12)	32.711(14)	12.2762(19)
b/ Å	13.954(5)	14.027(6)	11.1411(15)
c/ Å	17.830(6)	18.074(8)	19.870(3)
α/ °	90	90	90.00
β/ °	102.144(8)	101.330(8)	103.834(2)
γ/ °	90	90	90.00
V/ Å <sup>3</sup>	8166(5)	8166(5)	2638.8(7)
Z	8	8	4
D <sub>c</sub> /g cm <sup>-3</sup>	1.139	1.217	1.431
μ(Mo-Kα)/ cm <sup>-1</sup>	4.672	13.894	2.113
F(000)	3048.00	3192.00	1172.00
θ range for collection <sup>o</sup>	1.9 to 30.9	1.9 to 31.0	2.38 to 26.50
Reflections collected	41294	20292	19730
Independent reflections	8439	8344	5406
R(int)	0.053	0.040	0.0282
R, wR2 (all)	0.1095, 0.2831	0.1205, 0.3028	0.0545, 0.1325
R, wR2 [I > 2σ(I)]	0.0996, 0.2727	0.0972, 0.2732	0.0502, 0.1295
GOF on F <sup>2</sup>	1.061	1.043	1.100

### 2.4.4 Synthesis of ligands

A small library of amine-bis(phenol) ligands was synthesized following the literature procedure.<sup>2,3</sup> Representative syntheses and spectroscopic characterization of these ligands such as <sup>1</sup>H and <sup>13</sup>C NMR are presented here. Original spectroscopic characterization data of the ligand H<sub>2</sub>[O<sub>2</sub>N<sub>2</sub>]<sup>BuBu</sup> was obtained by Kol and co-workers<sup>13</sup> and H<sub>2</sub>[O<sub>2</sub>NO]<sup>BuMeMeth</sup> and H<sub>2</sub>[O<sub>2</sub>NO]<sup>MeMeMeth</sup> were obtained by Kerton and co-workers.<sup>3</sup>

**H<sub>2</sub>[O<sub>2</sub>N<sub>2</sub>]<sup>BuBu</sup>:** *N,N'*-dimethylethane-1,2-diamine (5.43 g, 0.0616 mol) was added to a vigorously stirred mixture of 2,4-di-*tert*-butylphenol (25.419 g, 0.1232 mol) and 37% aqueous formaldehyde (9.17 mL, 0.1232 mol) in water (50 mL). The mixture was heated to reflux for 12 h. Upon cooling, a large quantity of beige solid formed. The solvents were decanted and the remaining solid residue was washed with cold methanol to give a white powder (30.00 g, 93% yield). Crystalline product was obtained by slow cooling of a hot ethanol solution. <sup>1</sup>H NMR (300 MHz, 295 K, δ): 10.67 (br, 2H, OH); 7.20 (d, <sup>4</sup>J<sub>HH</sub> = 2.5 Hz, 2H, ArH); 6.80 (d, <sup>4</sup>J<sub>HH</sub> = 2.5 Hz, 2H, ArH); 3.66 (s, 4H, Ar-CH<sub>2</sub>); 2.63 (s, 4H, N-CH<sub>2</sub>); 2.26 (s, 6H, N-CH<sub>3</sub>); 1.39 (s, 18H, C(CH<sub>3</sub>)<sub>3</sub>); 1.27 (s, 18H, C(CH<sub>3</sub>)<sub>3</sub>). <sup>13</sup>C {<sup>1</sup>H} (75 MHz, 295 K, δ): 154.19 (Ar-C-OH); 140.51 (Ar-C-C(CH<sub>3</sub>)<sub>3</sub>); 135.62 (Ar-C-C(CH<sub>3</sub>)<sub>3</sub>); 123.32 (Ar-CH); 122.98 (Ar-CH); 121.00 (Ar-C-CH<sub>2</sub>); 62.73 (N-CH<sub>3</sub>); 53.78 (N-CH<sub>2</sub>); 41.62 (Ar-CH<sub>2</sub>); 34.88 (C(CH<sub>3</sub>)<sub>3</sub>); 34.16 (C(CH<sub>3</sub>)<sub>3</sub>); 31.72 (C(CH<sub>3</sub>)<sub>3</sub>); 29.63 (C(CH<sub>3</sub>)<sub>3</sub>).

**H<sub>2</sub>[O<sub>2</sub>NO]<sup>BuMeMeth</sup>:** <sup>1</sup>H NMR (300 MHz, 295 K, δ): 8.40 (s, 2H, OH); 7.0 (d, <sup>4</sup>J<sub>HH</sub> = 1.5 Hz, 2H, ArH); 6.72 (d, <sup>4</sup>J<sub>HH</sub> = 1.5 Hz, 2H, ArH); 3.71 (s, 4H, ArCH<sub>2</sub>); 3.52 (t, <sup>3</sup>J<sub>HH</sub> = 5.1 Hz, 2H, CH<sub>2</sub>O); 3.46 (s, 3H, OCH<sub>3</sub>); 2.73 (t, <sup>3</sup>J<sub>HH</sub> = 5.1 Hz, 2H, NCH<sub>2</sub>); 2.24 (s, 6H,

ArCH<sub>3</sub>); 1.41 (s, 18H, ArC(CH<sub>3</sub>)<sub>3</sub>). <sup>13</sup>C{<sup>1</sup>H} (75 MHz, 295 K, δ): 153.04 (Ar-C-OH); 136.83 (Ar-C-C(CH<sub>3</sub>)<sub>3</sub>); 128.79 (Ar-C-CH<sub>3</sub>); 127.36 (Ar-CH); 127.24 (Ar-CH); 122.44 (Ar-C-CH<sub>2</sub>-N); 71.51 (Ar-CH<sub>2</sub>); 58.86 (OCH<sub>3</sub>); 51.37 (N-CH<sub>2</sub>-CH<sub>2</sub>-O); 57.62(N-CH<sub>2</sub>-CH<sub>2</sub>-O); 34.71 (C(CH<sub>3</sub>)<sub>3</sub>); 29.57 (C(CH<sub>3</sub>)<sub>3</sub>); 20.78 (Ar-CH<sub>3</sub>).

**H<sub>2</sub>[O<sub>2</sub>NO<sup>-</sup>]<sup>BuBuMeth</sup>**: <sup>1</sup>H NMR (300 MHz, 295 K, δ): 8.48 (br, 2H, OH); 7.20 (d, <sup>4</sup>J<sub>HH</sub> = 2.6 Hz, 2H, ArH); 6.88 (d, <sup>4</sup>J<sub>HH</sub> = 2.6 Hz, 2H, ArH); 3.73 (s, 4H, Ar-CH<sub>2</sub>); 3.55 (t, <sup>3</sup>J<sub>HH</sub> = 5.0 Hz, 2H, N-CH<sub>2</sub>); 3.45 (s, 3H, O-CH<sub>3</sub>); 2.74 (t, <sup>3</sup>J<sub>HH</sub> = 5.0 Hz, 2H, O-CH<sub>2</sub>); 1.40 (s, 18H, C(CH<sub>3</sub>)<sub>3</sub>); 1.26 (s, 18H, C(CH<sub>3</sub>)<sub>3</sub>). <sup>13</sup>C{<sup>1</sup>H} (75 MHz, 298K, δ): 152.91 (Ar-C-OH); 140.79 (Ar-C-C(CH<sub>3</sub>)<sub>3</sub>); 135.08 (Ar-C-C(CH<sub>3</sub>)<sub>3</sub>); 124.91 (Ar-CH); 123.48 (Ar-CH); 121.64 (Ar-C-CH<sub>2</sub>); 71.49 (Ar-CH<sub>2</sub>); 58.90 (O-CH<sub>3</sub>); 58.10 (N-CH<sub>2</sub>-CH<sub>2</sub>); 51.40 (O-CH<sub>2</sub>); 35.01 (C(CH<sub>3</sub>)<sub>3</sub>); 34.14 (C(CH<sub>3</sub>)<sub>3</sub>); 31.71 (C(CH<sub>3</sub>)<sub>3</sub>); 29.62 (C(CH<sub>3</sub>)<sub>3</sub>).

**H<sub>2</sub>[O<sub>2</sub>NO<sup>-</sup>]<sup>MeMeFurf</sup>**: <sup>1</sup>H NMR (300 MHz, 295 K, δ): 8.77 (br, 2H, OH); 6.84 (d, <sup>4</sup>J<sub>HH</sub> = 2.1 Hz, 2H, ArH); 6.65 (d, <sup>4</sup>J<sub>HH</sub> = 2.1 Hz, 2H, ArH); 4.19 (m, 1H, CHO); 4.00 (m, 2H, CH<sub>2</sub>O); 3.85 (d, <sup>2</sup>J<sub>HH</sub> = 2.1 Hz, 2H, Ar-CH<sub>2</sub>); 3.62 (d, <sup>2</sup>J<sub>HH</sub> = 2.1 Hz, 2H, Ar-CH<sub>2</sub>); 2.54 (m, 2H, N-CH<sub>2</sub>Furf); 2.22 (s, 6H, Ar-CH<sub>3</sub>); 2.21 (s, 6H, Ar-CH<sub>3</sub>); 1.91 (m, 4H, CH<sub>2</sub>-CH<sub>2</sub>). <sup>13</sup>C{<sup>1</sup>H} (75 MHz, 295 K, δ): 152.51 (Ar-C-OH); 131.19 (Ar-C-CH<sub>3</sub>); 128.79 (Ar-C-CH<sub>3</sub>); 127.72 (Ar-CH); 125.22 (Ar-CH); 121.16 (Ar-C-CH<sub>2</sub>-N); 68.40 (CH); 57.11 (CH<sub>2</sub>); 56.22 (CH<sub>2</sub>); 29.57(CH<sub>2</sub>); 25.26 (CH<sub>2</sub>); 20.42 (Ar-CH<sub>3</sub>); 16.12 (Ar-CH<sub>3</sub>).

**H<sub>2</sub>[O<sub>2</sub>NO<sup>-</sup>]<sup>MeMeMeth</sup>**: <sup>1</sup>H NMR (300 MHz, 295 K, δ): 8.43 (br, 2H, OH); 6.85 (d, <sup>4</sup>J<sub>HH</sub> = 1.6 Hz, 2H, ArH); 6.67 (d, <sup>4</sup>J<sub>HH</sub> = 1.6 Hz, 2H, ArH); 3.73(s, 4H, Ar-CH<sub>2</sub>); 3.58 (t, <sup>3</sup>J<sub>HH</sub> = 5.1 Hz, 2H, O-CH<sub>2</sub>); 3.47 (s, 3H, O-CH<sub>3</sub>); 2.70 (t, <sup>3</sup>J<sub>HH</sub> = 5.1 Hz, 2H, N-CH<sub>2</sub>); 2.21 (s, 6H, Ar-CH<sub>3</sub>), 2.20 (s, 6H, Ar-CH<sub>3</sub>). <sup>13</sup>C{<sup>1</sup>H} (75 MHz, 295 K, δ): 152.31 (Ar-C-OH);

131.22 (Ar-C-CH<sub>3</sub>); 128.44 (Ar-C-CH<sub>3</sub>); 127.94 (Ar-CH); 125.15 (Ar-CH); 121.15 (Ar-C-CH<sub>2</sub>-N); 71.56 (Ar-CH<sub>2</sub>); 59.06 (O-CH<sub>3</sub>); 57.05(O-CH<sub>2</sub>); 50.87 (N-CH<sub>2</sub>CH<sub>2</sub>); 20.40 (Ar-CH<sub>3</sub>); 16.05 (Ar-CH<sub>3</sub>).

#### 2.4.5 Synthesis of metal complexes

**FeCl[O<sub>2</sub>N<sub>2</sub>]<sup>BuBu</sup> (1):** To a methanolic slurry of recrystallized H<sub>2</sub>[N<sub>2</sub>O<sub>2</sub>]<sup>BuBu</sup>, (2.00 g, 3.81 mmol) was added a solution of anhydrous FeCl<sub>3</sub> (0.62 g, 3.81 mmol) in methanol resulting in an intense blue solution. To this solution was added triethylamine (771 mg, 7.62 mmol) and the resulting mixture was stirred for 2 h. Solvent was removed under vacuum; the residue was extracted with methanol and filtered through Celite. Removal of solvent under vacuum yielded 2.07 g of a dark-blue, analytically pure product (89%). Crystals suitable for X-ray diffraction were obtained by slow evaporation of a solution of 1 in a 1:1 mixture of hexane and acetone. Anal. calcd for C<sub>34</sub>H<sub>54</sub>ClFeN<sub>2</sub>O<sub>2</sub>: C, 66.50; H, 8.86; N, 4.56%. Found C, 66.57; H, 9.05; N, 4.13%. MS (MALDI-TOF) *m/z* (% ion): 613.20 (40, [M]<sup>+</sup>), 578.24 (100, [M-Cl]<sup>+</sup>), 525.34 (32, [L]<sup>+</sup>). UV-vis (CH<sub>3</sub>OH) λ<sub>max</sub>, nm (ε): 638 (4834), 343 (4828). μ<sub>eff</sub> (solid, 25 °C): 5.9 μ<sub>B</sub>.

**FeBr[O<sub>2</sub>N<sub>2</sub>]<sup>BuBu</sup> (2):** To a methanolic slurry of recrystallized H<sub>2</sub>[N<sub>2</sub>O<sub>2</sub>]<sup>BuBu</sup>, (2.00 g, 3.81 mmol) was added a solution of anhydrous FeBr<sub>3</sub> (1.13 g, 3.81 mmol) in methanol resulting in an intense blue solution. To this solution was added triethylamine (771 mg, 7.62 mmol) and the resulting mixture was stirred for 2 h. Solvent was removed under vacuum; the residue was extracted with methanol and filtered through Celite. Removal of solvent under vacuum yielded 2.47 g of a dark-blue, analytically pure product (98%).



Crystals suitable for X-ray diffraction were obtained by slow evaporation of a solution of **2** in a 1:1 mixture of hexanes and acetone. Anal. calcd for  $C_{34}H_{54}BrFeN_2O_2$ : C, 62.01; H, 8.26; N, 4.25%. Found C, 62.34; H, 8.45; N 4.22%. MS (MALDI-TOF)  $m/z$  (% ion): 656.89 (25,  $[M]^+$ ), 578.04 (100,  $[M-Br]^+$ ), 525.16 (18,  $[L]^+$ ). UV-vis ( $CH_3OH$ )  $\lambda_{max}$ , nm ( $\epsilon$ ): 634 (5602), 343 (4888).  $\mu_{eff}$  (solid, 25 °C): 6.2  $\mu_B$ .

**FeBr[O<sub>2</sub>NO<sup>-</sup>]<sup>BuMeMeth</sup> (3)**: To a slurry of recrystallized  $H_2[O_2NO]^{BuMeMeth}$ , (2.47 g, 5.78 mmol) in methanol was added a solution of anhydrous  $FeBr_3$  (1.70 g, 5.78 mmol) in methanol resulting in an intense blue solution. To this solution was added triethylamine (1.15 g, 11.56 mmol) and the resulting mixture was stirred for 2 h. Solvent was removed under vacuum; the residue was extracted with acetone and filtered through Celite. Removal of solvent under vacuum yielded 3.21 g of a dark-purple, analytically pure product (55%). Crystals suitable for X-ray diffraction were obtained by slow evaporation of a solution of **3** in a 1:1 mixture of hexanes and acetone. Anal. Calcd for  $C_{27}H_{39}BrFeNO_3$ : C, 57.77; H, 7.00; N, 2.50. Found C, 58.08; H, 7.29; N, 2.48. MS (MALDI-TOF)  $m/z$  (% ion): 560.13 (10,  $[M]^+$ ), 481.23 (30,  $[M-Br]^+$ ). UV-vis (solvent)  $\lambda_{max}$ , nm ( $\epsilon$ ): (methanol) 592 (3680), 331 (5000); (acetonitrile) 515 (4200), 400 (5000); (THF) 566 (4000), 339 (5800); (toluene) 517 (4500), 406 (5900).  $\mu_{eff}$  (solid, 25 °C) 5.0  $\mu_B$ .

**FeBr[O<sub>2</sub>NO<sup>-</sup>]<sup>BuBuMeth</sup> (4)**: To a slurry of recrystallized  $H_2[O_2NO]^{BuBuMeth}$ , (4.34 g, 8.49 mmol) in methanol was added a solution of anhydrous  $FeBr_3$  (2.51 g, 8.49 mmol) in methanol resulting in an intense blue solution. To this solution was added triethylamine (1.71 g, 16.98 mmol) and the resulting mixture was stirred for 2 h. Solvent was removed

under vacuum; the residue was extracted with toluene and filtered through Celite. Removal of solvent under vacuum yielded 4.38 g of a dark-purple product (80%). Anal. Calcd for  $C_{33}H_{51}BrFeNO_3$ : C, 61.40; H, 7.96; N, 2.17. Found C, 62.00; H, 8.20; N, 2.28. MS (MALDI-TOF)  $m/z$  (% ion): 644.26 (10,  $[M]^+$ ), 565.32 (30,  $[M-Br]^+$ ). UV-vis (solvent)  $\lambda_{max}$ , nm ( $\epsilon$ ): (methanol) 562 (2530), 335 (4000); (acetonitrile) 489 (3200), 400 (3800); (THF) 538 (2730), 381 (4210); (toluene) 498 (3180), 402 (4120).  $\mu_{eff}$  (solid, 25 °C) 4.9  $\mu_B$ .

**FeCl[O<sub>2</sub>NO]<sup>MeMeFurf</sup> (5):** Ligand  $H_2[O_2NO]^{\text{MeMeFurf}}$  (4.01 g, 10.85 mmol) and anhydrous FeCl<sub>3</sub> (1.76 g, 10.85 mmol) were added under nitrogen to two different Schlenk tubes. Dry THF was added to make a colourless ligand solution and a very pale green metal salt solution. To the ligand solution, *n*-BuLi (13.5 ml, 21.70 mmol) was added at -78 °C and allowed to reach room temperature and stir for 2 h. Then the lithiated ligand solution was transferred to the metal salt solution *via* cannula at -78 °C, allowed to warm to room temperature and stirred for 3 h. The resulting reaction mixture became intense violet colour. The solvent was removed and the residue was extracted with dichloromethane and filtered through Celite. Removal of solvent under vacuum yielded 3.89 g (78%) of a dark-violet product. Anal. Calcd for  $C_{23}H_{29}ClFeNO_3$ : C, 60.21; H, 6.37; N, 3.05%. Found C, 59.39; H, 6.34; N, 3.23%. MALDI-TOF MS (positive mode, anthracene);  $m/z$  (% of ion): 458.12 (10,  $[M]^+$ ), 423.15 (50,  $[M-Cl]^+$ ). UV-vis (CH<sub>3</sub>OH)  $\lambda_{max}$ , nm ( $\epsilon$ ): 226 (12485), 289 (8764), 330 (4124), 502 (2274).  $\mu_{eff}$  (solid, 18 °C): 5.5  $\mu_B$ .

**FeBr[O<sub>2</sub>NO]<sup>MeMeFurf</sup> (6):** Ligand H<sub>2</sub>[O<sub>2</sub>NO]<sup>MeMeFurf</sup> (4.01 g, 10.85 mmol) and anhydrous FeBr<sub>3</sub> (3.20 g, 10.84 mmol) were added under nitrogen to two different Schlenk tubes. Dry THF was added to make a colourless ligand solution and a pale green metal salt solution. To the ligand solution, *n*-BuLi (13.5 ml, 21.70 mmol) was added at -78 °C, allowed to reach room temperature and stirred for 2 h. Then the lithiated ligand solution was transferred to the metal salt solution via cannula at -78 °C, allowed to warm to room temperature and stirred for 3 h. The resulting reaction mixture became intense violet in colour. Solvent was removed and the residue was extracted with dichloromethane and filtered through Celite. Removal of solvent under vacuum yielded 4.83 g (89%) of a dark-violet product. Anal. Calcd for C<sub>23</sub>H<sub>29</sub>BrFeNO<sub>3</sub>; C, 54.89; H, 5.81; N, 2.78%. Calcd for 6·0.50 LiBr: C, 50.49; H, 5.34; N, 2.56%. Found C, 50.50; H, 5.54; N, 2.69%. MALDI-TOF MS (positive mode, anthracene); *m/z* (% of ion): 846.31 (Dimer of C<sub>23</sub>H<sub>29</sub>FeNO<sub>3</sub>), 423.15 (100, [M-Br]<sup>+</sup>), 366.21 (10, [M-Br-C<sub>3</sub>H<sub>6</sub>O]<sup>+</sup>). UV-vis (CH<sub>3</sub>OH) λ<sub>max</sub>, nm (ε): 224 (11436), 288(7883), 333 (4039), 500 (2190). μ<sub>eff</sub> (solid, 18 °C): 5.9 μ<sub>B</sub>.

**FeCl[O<sub>2</sub>NO]<sup>MeMeMeth</sup> (7):** Ligand H<sub>2</sub>[O<sub>2</sub>NO]<sup>MeMeMeth</sup> (3.70 g, 10.77 mmol) and anhydrous FeCl<sub>3</sub> (1.75 g, 10.77 mmol) were added under nitrogen to two different Schlenk tubes. Dry THF was added to make a colourless ligand solution and a very pale green metal salt solution. To the ligand solution, *n*-BuLi (13.47 ml, 21.55 mmol) was added at -78 °C, allowed to reach room temperature and stirred for 2 h. Then the lithiated ligand solution was transferred to the metal salt solution *via* cannula at -78 °C, allowed to warm to room temperature and stirred for 3 h yielding a dark mixture. The solvent was

*References begin on page 120*

removed and the residue extracted with dichloromethane and filtered through Celite. Removal of the solvent under vacuum yielded 4.46 g (96%) of a dark blue powder. Anal. Calcd for  $C_{21}H_{27}ClFeNO_3$ ; C, 58.29; H, 6.29; N, 3.24%. Calcd for 7·0.26 LiCl: C, 56.84; H, 6.13; N, 3.16%. Found C, 56.83; H, 6.56; N, 3.35%. MALDI-TOF MS (positive mode, anthracene);  $m/z$  (% of ion): 397.14 (70,  $[M-Cl]^+$ ). UV-vis ( $CH_3OH$ )  $\lambda_{max}$ , nm ( $\epsilon$ ): 237 (16600), 279 (17325), 327 (7009), 540 (4614).  $\mu_{eff}$  (solid, 18 °C): 4.6  $\mu_B$ .

**FeBr[O<sub>2</sub>NO]<sup>MeMeMeth</sup> (8)**: Ligand  $H_2[O_2NO]^{\text{MeMeMeth}}$  (3.70 g, 10.77 mmol) and anhydrous FeBr<sub>3</sub> (3.07 g, 10.40 mmol) were added under nitrogen to two different Schlenk tubes. Dry THF was added to make a colourless ligand solution and a very pale green metal salt solution. To the ligand solution, *n*-BuLi (13.47 ml, 21.55 mmol) was added at -78 °C, allowed to reach room temperature and stirred for 2 h. Then the lithiated ligand solution was transferred to the metal salt solution *via* cannula at -78 °C, allowed to warm to room temperature and stirred for 3 h. The resulting reaction mixture became very dark. The solvent was removed, and the residue was extracted with dichloromethane and filtered through Celite. Removal of the solvent under vacuum yielded 4.53 g (91%) of a dark powder. Elemental analysis showed lower % carbon value than expected indicated that the product was impure. MALDI-TOF MS (positive mode, anthracene);  $m/z$  (% of ion): 397.14 (100,  $[M-Br]^+$ ). UV-vis ( $CH_3OH$ )  $\lambda_{max}$ , nm ( $\epsilon$ ): 237 (16600), 279 (17325), 327 (7009), 540 (4614).

## 2.5 References

1. L. Brandsma, S. F. Vasilevsky and H. D. Verkrujisse, *Application of Transition Metal Catalysts in Organic Synthesis*, Springer-Verlag, New York, 1999.
2. K. L. Collins, L. J. Corbett, S. M. Butt, G. Madhurambal and F. M. Kerton, *Green Chem. Lett. Rev.*, 2007, **1**, 31-35.
3. F. M. Kerton, S. Holloway, A. Power, R. G. Soper, K. Sheridan, J. M. Lynam, A. C. Whitwood and C. E. Willans, *Can. J. Chem.*, 2008, **86**, 435-443.
4. S. Groysman, E. Sergeeva, I. Goldberg and M. Kol, *Inorg. Chem.*, 2005, **44**, 8188-8190.
5. E. Y. Tshuva, M. Versano, I. Goldberg, M. Kol, H. Weitman and Z. Goldschmidt, *Inorg. Chem. Commun.*, 1999, **2**, 371-373.
6. E. Y. Tshuva, I. Goldberg, M. Kol, H. Weitman and Z. Goldschmidt, *Chem. Commun.*, 2000, 379-380.
7. A. Yeori, I. Goldberg and M. Kol, *Macromolecules*, 2007, **40**, 8521-8523.
8. A. Yeori, I. Goldberg, M. Shuster and M. Kol, *J. Am. Chem. Soc.*, 2006, **128**, 13062-13063.
9. S. Gendler, S. Segal, I. Goldberg, Z. Goldschmidt and M. Kol, *Inorg. Chem.*, 2006, **45**, 4783-4790.
10. S. Segal, I. Goldberg and M. Kol, *Organometallics*, 2005, **24**, 200-202.
11. S. Groysman, E. Y. Tshuva, I. Goldberg, M. Kol, Z. Goldschmidt and M. Shuster, *Organometallics*, 2004, **23**, 5291-5299.

12. S. Groysman, I. Goldberg, M. Kol, E. Genizi and Z. Goldschmidt, *Inorg. Chim. Acta*, 2003, **345**, 137-144.
13. E. Y. Tshuva, I. Goldberg and M. Kol, *J. Am. Chem. Soc.*, 2000, **122**, 10706-10707.
14. C. Lorber, F. Wolff, R. Choukroun and L. Vendier, *Eur. J. Inorg. Chem.*, 2005, 2850-2859.
15. A. J. Chmura, M. G. Davidson, M. D. Jones, M. D. Lunn, M. F. Mahon, A. F. Johnson, P. Khunkamchoo, S. L. Roberts and S. S. F. Wong, *Macromolecules*, 2006, **39**, 7250-7257.
16. Y. Sarazin, R. H. Howard, D. L. Hughes, S. M. Humphrey and M. Bochmann, *Dalton Trans.*, 2006, 340-350.
17. M. Hu, M. Wang, H. Zhu, L. Zhang, H. Zhang and L. Sun, *Dalton Trans.*, 2010, **39**, 4440-4446.
18. M. D. Jones, M. G. Davidson and G. Kociok-Kohn, *Polyhedron*, 2010, **29**, 697-700.
19. A. Cohen, J. Kopilov, I. Goldberg and M. Kol, *Organometallics*, 2009, **28**, 1391-1405.
20. A. Cohen, A. Yeori, J. Kopilov, I. Goldberg and M. Kol, *Chem. Commun.*, 2008, 2149-2151.
21. S. Gendler, A. L. Zelikoff, J. Kopilov, I. Goldberg and M. Kol, *J. Am. Chem. Soc.*, 2008, **130**, 2144-2145.

22. F. M. Kerton, A. C. Whitwood and C. E. Willans, *Dalton Trans.*, 2004, 2237-2244.
23. H. E. Dyer, S. Huijser, A. D. Schwarz, C. Wang, R. Duchateau and P. Mountford, *Dalton Trans.*, 2008, 32-35.
24. F. Bonnet, A. R. Cowley and P. Mountford, *Inorg. Chem.*, 2005, **44**, 9046-9055.
25. A. Amgoune, C. M. Thomas and J. F. Carpentier, *Pure Appl. Chem.*, 2007, **79**, 2013-2030.
26. A. Amgoune, C. M. Thomas, T. Roisnel and J. F. Carpentier, *Chem. Eur. J.*, 2006, **12**, 169-179.
27. Y. M. Yao, M. T. Ma, X. P. Xu, Y. Zhang, Q. Shen and W. T. Wong, *Organometallics*, 2005, **24**, 4014-4020.
28. M. A. Sinenkov, G. K. Fukin, A. V. Cherkasov, N. Ajellal, T. Roisnel, F. M. Kerton, J.-F. Carpentier and A. A. Trifonov, *New J. Chem.*, 2011, **35**, 204-212.
29. H. E. Dyer, S. Huijser, N. Susperregui, F. Bonnet, A. D. Schwarz, R. Duchateau, L. Maron and P. Mountford, *Organometallics*, 2010, **29**, 3602-3621.
30. D. T. Dugah, B. W. Skelton and E. E. Delbridge, *Dalton Trans.*, 2009, 1436-1445.
31. C. E. Willans, M. A. Sinenkov, G. K. Fukin, K. Sheridan, J. M. Lynam, A. A. Trifonov and F. M. Kerton, *Dalton Trans.*, 2008, 3592-3598.
32. H. E. Dyer, S. Huijser, A. D. Schwarz, C. Wang, R. Duchateau and P. Mountford, *Dalton Trans.*, 2008, 32-35.

33. E. Safaei, T. Weyhermüller, E. Bothe, K. Wieghardt and P. Chaudhuri, *Eur. J. Inorg. Chem.*, 2007, 2334-2344.
34. T. Weyhermüller, T. K. Paine, E. Bothe, E. Bill and P. Chaudhuri, *Inorg. Chim. Acta*, 2002, **337**, 344-356.
35. U. K. Das, J. Bobak, C. Fowler, S. E. Hann, C. F. Petten, L. N. Dawe, A. Decken, F. M. Kerton and C. M. Kozak, *Dalton Trans.*, 2010, **39**, 5462-5477.
36. T. Nagataki and S. Itoh, *Chem. Lett.*, 2007, **36**, 748-749.
37. L. Rodríguez, E. Labisbal, A. Sousa-Pedrares, J. A. Garcia-Vazquez, J. Romero, M. L. Duran, J. A. Real and A. Sousa, *Inorg. Chem.*, 2006, **45**, 7903-7914.
38. A. Philibert, F. Thomas, C. Philouze, S. Hamman, E. Saint-Aman and J. L. Pierre, *Chem. Eur. J.*, 2003, **9**, 3803-3812.
39. O. Rotthaus, F. Thomas, O. Jarjayes, C. Philouze, E. Saint-Aman and J. L. Pierre, *Chem. Eur. J.*, 2006, **12**, 6953-6962.
40. J. B. H. Strautmann, S. DeBeer George, E. Bothe, E. Bill, T. Weyhermüller, A. Stammmler, H. Bögge and T. Glaser, *Inorg. Chem.*, 2008, **47**, 6804-6824.
41. G. R. van, J. Berding, A. M. Mills, H. Kooijman, D. M. Tooke, A. L. Spek, I. Mutikainen, U. Turpeinen, J. Reedijk and E. Bouwman, *Eur. J. Inorg. Chem.*, 2008, 1487-1496.
42. T. Weyhermüller, R. Wagner and P. Chaudhuri, *Eur. J. Inorg. Chem.*, 2011, 2547-2557.
43. X. Qian, L. N. Dawe and C. M. Kozak, *Dalton Trans.*, 2011, **40**, 933-943.



44. W. A. Chomitz, S. G. Minasian, A. D. Sutton and J. Arnold, *Inorg. Chem.*, 2007, **46**, 7199-7209.
45. H. Adams, N. A. Bailey, I. K. Campbell, D. E. Fenton and Q.-Y. He, *J. Chem. Soc., Dalton Trans.*, 1996, 2233-2237.
46. M. C. B. de Oliveira, M. Scarpellini, A. Neves, H. Terenzi, A. J. Bortoluzzi, B. Szpoganics, A. Greatti, A. S. Mangrich, E. M. de Sousa, P. M. Fernandez and M. R. Soares, *Inorg. Chem.*, 2005, **44**, 921-929.
47. S. Ito, S. Nishino, H. Itoh, S. Ohba and Y. Nishida, *Polyhedron*, 1998, **17**, 1637-1642.
48. I. A. Koval, M. Huisman, A. F. Stassen, P. Gamez, M. Lutz, A. L. Spek and J. Reedijk, *Eur. J. Inorg. Chem.*, 2004, 591-600.
49. M. M. Olmstead, T. E. Patten and C. Troeltzsch, *Inorg. Chim. Acta*, 2004, **357**, 619-624.
50. N. Reddig, D. Pursche and A. Rompel, *Dalton Trans.*, 2004, 1474-1480.
51. N. Reddig, D. Pursche, B. Krebs and A. Rompel, *Inorg. Chim. Acta*, 2004, **357**, 2703-2712.
52. N. Reddig, D. Pursche, M. Kloskowski, C. Slinn, S. M. Baldeau and A. Rompel, *Eur. J. Inorg. Chem.*, 2004, 879-887.
53. S. Sarkar, A. Mondal, J. Ribas, M. G. B. Drew, K. Pramanik and K. K. Rajak, *Eur. J. Inorg. Chem.*, 2004, 4633-4639.
54. Y. Shimazaki, S. Huth, S. Karasawa, S. Hirota, Y. Naruta and O. Yamauchi, *Inorg. Chem.*, 2004, **43**, 7816-7822.

55. X. Zhang, T. J. Emge and K. C. Hultsch, *Organometallics*, 2010, **29**, 5871-5877.
56. Y.-L. Wong, C.-Y. Mak, H. S. Kwan and H. K. Lee, *Inorg. Chim. Acta*, 2010, **363**, 1246-1253.
57. W. A. Chomitz and J. Arnold, *Chem.-Eur. J.*, 2009, **15**, 2020-2030.
58. J. Hwang, K. Govindaswamy and S. A. Koch, *Chem. Commun.*, 1998, 1667-1668.
59. T. Kurahashi, K. Oda, M. Sugimoto, T. Ogura and H. Fujii, *Inorg. Chem.*, 2006, **45**, 7709-7721.
60. M. Merkel, F. K. Müller and B. Krebs, *Inorg. Chim. Acta*, 2002, **337**, 308-316.
61. P. Mialane, E. Anxolabéhère-Mallart, G. Blondin, A. Nivorojkine, J. Guilhem, L. Tchertanova, M. Cesario, N. Ravi, E. Bominaar, J.-J. Girerd and E. Münck, *Inorg. Chim. Acta*, 1997, **263**, 367-378.
62. M. S. Shongwe, C. H. Kaschula, M. S. Adsetts, E. W. Ainscough, A. M. Brodie and M. J. Morris, *Inorg. Chem.*, 2005, **44**, 3070-3079.
63. M. Velusamy, M. Palaniandavar, R. S. Gopalan and G. U. Kulkarni, *Inorg. Chem.*, 2003, **42**, 8283-8293.
64. M. Velusamy, R. Mayilmurugan and M. Palaniandavar, *Inorg. Chem.*, 2004, **43**, 6284-6293.
65. R. Viswanathan, M. Palaniandavar, T. Balasubramanian and T. P. Muthiah, *Inorg. Chem.*, 1998, **37**, 2943-2951.
66. J. A. Halfen, B. A. Jazdzewski, S. Mahapatra, L. M. Berreau, E. C. Wilkinson, L. Que and W. B. Tolman, *J. Am. Chem. Soc.*, 1997, **119**, 8217-8227.
67. Y. D. Wang and T. D. P. Stack, *J. Am. Chem. Soc.*, 1996, **118**, 13097-13098.

68. E. Bill, J. Müller, T. Weyhermüller and K. Wieghardt, *Inorg. Chem.*, 1999, **38**, 5795-5802.
69. Y. Shimazaki, S. Huth, A. Odani and O. Yamauchi, *Angew. Chem. Int. Ed.*, 2000, **39**, 1666-1669.
70. M. Lanznaster, H. P. Hratchian, M. J. Heeg, L. M. Hryhorczuk, B. R. McGarvey, H. B. Schlegel and C. N. Verani, *Inorg Chem*, 2006, **45**, 955-957.
71. M. Lanznaster, M. J. Heeg, G. T. Yee, B. R. McGarvey and C. N. Verani, *Inorg. Chem.*, 2007, **46**, 72-78.
72. S. Yan, L. Que, Jr., L. F. Taylor and O. P. Anderson, *J. Am. Chem. Soc.*, 1988, **110**, 5222-5224.
73. R. R. Chowdhury, A. K. Crane, C. Fowler, P. Kwong and C. M. Kozak, *Chem. Commun.*, 2008, 94-96.
74. R. K. Dean, S. L. Granville, L. N. Dawe, A. Decken, K. M. Hattenhauer and C. M. Kozak, *Dalton Trans.*, 2010, **39**, 548-559.
75. C. E. Willans, M. A. Sinenkov, G. K. Fukin, K. Sheridan, J. M. Lynam, A. A. Trifonov and F. M. Kerton, *Dalton Trans*, 2008, 3592-3598.
76. F. M. Kerton, C. M. Kozak, K. Luettgen, C. E. Willans, R. J. Webster and A. C. Whitwood, *Inorg. Chim. Acta*, 2006, **359**, 2819-2825.
77. C.-A. Huang and C.-T. Chen, *Dalton Trans.*, 2007, 5561-5566.
78. W. Clegg, M. G. Davidson, D. V. Graham, G. Griffen, M. D. Jones, A. R. Kennedy, C. T. O'Hara, L. Russo and C. M. Thomson, *Dalton Trans.*, 2008, 1295-1301.

79. E. Safaei, I. Saberikia, A. Wojtczak, Z. Jagličić and A. Kozakiewicz, *Polyhedron*, 2011, **30**, 1143-1148.
80. M. S. Shongwe, B. A. Al-Rashdi, H. Adams, M. J. Morris, M. Mikuriya and G. R. Hearne, *Inorg. Chem.*, 2007, **46**, 9558-9568.
81. A. M. Reckling, D. Martin, L. N. Dawe, A. Decken and C. M. Kozak, *J. Organomet. Chem.*, 2011, **696**, 787-794.
82. K. Hasan, L. N. Dawe and C. M. Kozak, *Eur. J. Inorg. Chem.*, 2011, 4610-4621.
83. L. H. Tong, Y.-L. Wong, S. I. Pascu and J. R. Dilworth, *Inorg. Chim. Acta*, 2010, **363**, 1297-1300.
84. R. Mayilmurugan, M. Sankaralingam, E. Suresh and M. Palaniandavar, *Dalton Trans.*, 2010, **39**, 9611-9625.
85. M. D. Fryzuk, D. B. Leznoff, E. S. F. Ma, S. J. Rettig and V. G. Young, Jr., *Organometallics*, 1998, **17**, 2313-2323.
86. G. A. Abakumov, V. K. Cherkasov, M. P. Bubnov, L. G. Abakumova, V. N. Ikorskii, G. V. Romanenko and A. I. Poddel'sky, *Russ. Chem. Bull.*, 2006, **55**, 44-52.
87. C. J. Whiteoak, d. R. R. T. Martin, A. J. P. White and G. J. P. Britovsek, *Inorg. Chem.*, 2010, **49**, 11106-11117.
88. K. Sundaravel, T. Dhanalakshmi, E. Suresh and M. Palaniandavar, *Dalton Trans.*, 2008, 7012-7025.
89. R. Mayilmurugan, K. Visvaganesan, E. Suresh and M. Palaniandavar, *Inorg. Chem.*, 2009, **48**, 8771-8783.

90. A. W. Addison, T. N. Rao, J. Reedijk, R. J. Van and G. C. Verschoor, *J. Chem. Soc., Dalton Trans.*, 1984, 1349-1356.
91. K. Hasan, C. Fowler, P. Kwong, A. K. Crane, J. L. Collins and C. M. Kozak, *Dalton Trans.*, 2008, 2991-2998.
92. R. L. Carlin, *Magnetochemistry*, Springer-Verlag, New York, 1986.
93. J. W. Pflugrath, *Acta Crystallogr., Sect. D.*, 1999, **55**, 1718-1725.
94. *Crystal clear. An Integrated Program for the Collection and Processing of Area Detector Data*, Rigaku Corporation, Tokyo, **1997-2004**.
95. A. C. Larson, *Crystallographic Computing*, Munksgaard, Copenhagen, 1970.
96. D. T. Cromer and J. T. Waber, *International Tables for X-ray Crystallography*, The Kynoch Press, Birmingham, England, 1974.
97. A. Altomare, G. Cascarano, C. Giacovazzo, A. Guagliardi, M. Burla, G. Polidori and M. Camalli, *J. Appl. Cryst.*, 1994, **27**, 435.
98. P. T. Beurskens, G. Admiraal, G. Beurskens, W. P. Bosman, R. de Gelder, R. Israel and J. M. M. Smits, *DIRDIF99*, University of Nijmegen, Netherlands, 1999.
99. J. A. Ibers and W. C. Hamilton, *Acta Crystallogr.*, 1964, **17**, 781.
100. D. C. Creagh and W. J. McAuley, *International Tables for Crystallography*, Kluwer Academic Publishers, Boston, 1992.
101. D. C. Creagh and J. H. Hubbell, *International Tables for Crystallography*, Kluwer Academic Publishers, Boston, 1992.

102. D. J. Watkin, C. K. Prout, J. R. Carruthers and P. W. Betteridge, Chemical Crystallography Laboratory, Oxford, UK, 1996.
103. *CrystalStructure 3.7.0: Crystal Structure Analysis Package*, Rigaku and Rigaku/MSK, The Woodlands TX, **2000–2005**.
104. G. M. Sheldrick, University of Göttingen, Germany, 1997.
105. A. L. Spek, *J. Appl. Crystallogr.*, 2003, **36**, 7-13.
106. P. van der Sluis and A. L. Spek, *Acta Crystallogr., Sect. A: Found. Crystallogr.*, 1990, **A46**, 194-201.
107. L. J. Farrugia, *J. Appl. Cryst.*, 1997, **30**, 565.

## ***Chapter 3. Iron-catalyzed epoxidation of olefins using hydrogen peroxide***

This chapter has been published in part by, Kamrul Hasan, Nicole Brown and Christopher M. Kozak,\* *Green Chem.*, 2011, **13**, 1230-1237.

Some modifications of the published manuscript have been made to expand the discussion and for the sake of consistency with the remainder of the thesis.

### ***3.1 Introduction***

Metal-catalyzed oxygenation of organic substrates is becoming an increasingly important reaction in modern organic synthesis.<sup>1</sup> The development of catalytic epoxidation agents that are rapid, selective, scalable, and inexpensive with a wide substrate scope remains an important goal. Olefins are one of the most important starting materials for organic synthesis and their oxidation leads to various value-added products such as epoxides, alcohols, aldehydes, ketones, and carboxylic acids. These in turn are important building blocks for the production of bulk and fine chemicals.<sup>2</sup> The quest for clean, selective oxidation processes has been motivated by the need for atom-efficient

technologies adhering to the principles of green chemistry.<sup>3</sup> The use of stoichiometric oxidants that generate significant waste, especially toxic metal residues such as chromates and permanganates is being discouraged in favour of catalytic processes. For economical and ecological reasons, molecular oxygen<sup>4</sup> and hydrogen peroxide are the preferred oxidants. Hydrogen peroxide is generally easier to handle, cheap and produces water as a by-product.<sup>5</sup> Thus, hydrogen peroxide develops an ideal system by combining with a non-toxic and inexpensive metal source for epoxidation reactions, especially in liquid-phase processes in industry.<sup>6-13</sup> Therefore, the use of H<sub>2</sub>O<sub>2</sub> in combination with catalytic amounts of first row late transition metals such as Fe or Mn is desirable.

The use of H<sub>2</sub>O<sub>2</sub> in combination with simple non-heme Mn<sup>7</sup> or Fe<sup>14,15</sup> complexes is limited, due to the vigorous decomposition of H<sub>2</sub>O<sub>2</sub> in the presence of these metals.<sup>16-18</sup> However, recent development of Mn catalysts for the epoxidation of alkenes was explored through the use of heterogeneous Mn(II) exchanged zeolites in a bicarbonate solution<sup>19</sup> and a SiO<sub>2</sub>-immobilized Mn(II) complex in an ammonium acetate solution.<sup>20</sup> In the SiO<sub>2</sub>-immobilized Mn(II) acetylacetonate system, the active catalytic features of the homogeneous system were successfully embedded onto the silica surface. Furthermore, a small number of non-heme iron-catalyzed epoxidation catalysts have recently been prepared. For example, Jacobsen reported an Fe-MEP catalyst (MEP = *N,N'*-dimethyl-*N,N'*-bis(2-pyridylmethyl)ethane-1,2-diamine)<sup>21</sup> and Stack described an oxide-bridged bimetallic iron catalyst bearing phenanthroline ligands.<sup>22</sup> Both of these catalysts employ acetic acid, which in the case of Jacobsen's system is proposed to give the active iron species, whereas in Stack's system it is used to generate peracetic acid as the active

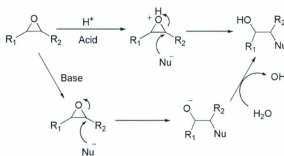


oxidant upon reaction with  $\text{H}_2\text{O}_2$ . Recently, Beller demonstrated that a combination of  $\text{FeCl}_3 \cdot 6\text{H}_2\text{O}$ , with and without pyridine-2,6-dicarboxylic acid ( $\text{H}_2\text{pydic}$ ) and an organic base catalyzed the epoxidation of olefins with  $\text{H}_2\text{O}_2$  in good yield.<sup>23-27</sup> During these studies, it was shown that 5-chloro-1-methylimidazole was capable of high yielding epoxidations of aromatic alkenes (e.g. styrenes and stilbenes) without the use of  $\text{H}_2\text{pydic}$ , but was unsuccessful for aliphatic alkenes.<sup>25</sup> A combination of  $\text{H}_2\text{pydic}$  with bulky imidazole bases was required for epoxidation of a broader range of substrates.<sup>26</sup>

The Kozak group is interested in pursuing the reactivity of iron complexes supported by amine-bis(phenolate) ligands for catalytic organic synthesis. For example, recently published results from the Kozak group are the use of iron(III) complexes of tridentate and tetradentate amine-bis(phenolate) ligands as effective catalysts for C-C cross coupling between aryl Grignard reagents and alkyl halides.<sup>28-30</sup> These Fe(III) complexes are inexpensive and possess low environmental toxicity, and are therefore interesting candidates for further study of their reactivity. This chapter describes the use of simple iron(III) chloride salts in the presence of readily available organic *N*-containing bases, as well as the influence of amine-bis(phenol) ligands, for catalytic epoxidation of internal and terminal, aromatic and aliphatic olefins using  $\text{H}_2\text{O}_2$ .

### 3.2 Results and Discussion

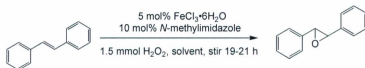
Selective epoxidation of olefins is challenging because the three-membered cyclic ether is highly strained. As a result, epoxides are quite reactive and ring-opening of the epoxide by nucleophiles leads to the formation of other products. For example, nucleophiles can attack the epoxide in the presence of acid or base to form an alcohol (Scheme 3.1).



**Scheme 3.1** Nucleophilic addition to the epoxide.

Imidazole plays a crucial role in biological systems especially in metalloenzymes.<sup>31</sup> It is also used as an additive for epoxidation catalysis with iron porphyrin complexes.<sup>32</sup> Inspired by the recent results obtained by the group of Beller, preliminary screening started with using a mixture of appropriate amounts of  $\text{FeCl}_3 \cdot 6\text{H}_2\text{O}$  and 1-methylimidazole in a number of solvents (Table 3.1). *Trans*-stilbene was chosen as the substrate for these exploratory epoxidation reactions and  $\text{H}_2\text{O}_2$  as the oxidant. A solution of  $\text{H}_2\text{O}_2$  was added over a period of 1 h at  $1 \text{ mL h}^{-1}$  using a syringe pump. In the first instance, *tert*-amyl alcohol was used as the solvent due to its use in previously

reported metal-catalyzed epoxidation reactions.<sup>33,34</sup> Using these conditions, 31% *trans*-stilbene oxide was obtained after stirring the reaction mixture at room temperature for 19 h (Table 3.1, Entry 1). Beller and co-workers observed 18% yield of *trans*-stilbene oxide in 1 h under these reaction conditions,<sup>26,35</sup> however, they went on to show that *trans*-stilbene oxide formation was improved to 80% using 5-chloro-1-methylimidazole instead of 1-methylimidazole.<sup>25</sup> The use of non-halogenated organic additives is desirable from an environmental perspective, but also in terms of cost, since 1-methylimidazole is approximately 400 times less expensive than 5-chloro-1-methylimidazole.<sup>36</sup> Therefore, it would be good to improve the yield of epoxide using the inexpensive 1-methylimidazole as an additive. It was found that only *tert*-amyl alcohol, acetonitrile and acetone gave significant conversions with excellent selectivity, with acetone giving the best result for the epoxidation of *trans*-stilbene (Entry 6) at room temperature, giving 40% yield of stilbene oxide. Heating the reaction to 62 °C for 19 h, however, increased the yield to 90% with 97% selectivity showing that modestly elevated temperatures are required to obtain a significant increase in conversion of starting material and yield of desired epoxide products. In the absence of either FeCl<sub>3</sub>·6H<sub>2</sub>O or 1-methylimidazole compounds, no conversion of alkene to epoxide was observed.

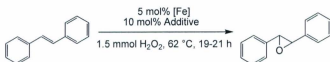
**Table 3.1** Epoxidation of *trans*-stilbene in different solvents.<sup>a</sup>

Entry	Solvent	Conv. (%)	Yield (%)
1	<i>tert</i> -Amyl alcohol	31	31
2	Isopropyl alcohol	0	0
3	Water	0	0
4	Dichloromethane	0	0
5	Acetonitrile	35	35
6	Acetone	40	40
7	Acetone	93 <sup>b</sup>	90 <sup>b</sup>

<sup>a</sup> Reaction conditions: To a 50 mL Schlenk tube, FeCl<sub>3</sub>·6H<sub>2</sub>O (0.025 mmol), 1-methylimidazole (0.05 mmol), solvent (9 mL), *trans*-stilbene (0.5 mmol), and dodecane (GC internal standard, 100 μL) were added in sequence at 25 °C in air. The mixture was stirred and a solution of 30% H<sub>2</sub>O<sub>2</sub> (170 μL, 1.5 mmol) in solvent (830 μL) was added over a period of 1 h using a syringe pump. The reaction mixture was stirred at 25 °C for 18-21 h. Conversion and yields were determined by GC analysis. <sup>b</sup> The reaction mixture was heated for 20 h at 62 °C.

Having observed such promising results when mixtures of Fe(III), 1-methylimidazole and H<sub>2</sub>O<sub>2</sub> were heated with *trans*-stilbene, the influence of the iron salt on epoxidation in acetone was examined (Table 3.2). Iron(III) chloride hexahydrate (Strem Chemicals, 97+%) afforded excellent conversion and high yield of the corresponding epoxide (Entry 1 shows the average of three runs). Similar results were obtained using anhydrous FeCl<sub>3</sub> (Sigma Aldrich, 97%), which demonstrates

reproducibility when different sources of the salt were used (Entry 2). Surprisingly, other Fe(III) salts did not show any catalytic epoxidation activity with *trans*-stilbene (Entries 3 to 5), whereas iron(II) chloride gave high conversion of *trans*-stilbene, but the yield of epoxide was much lower than for iron(III) chloride (Entry 6). The nature of the counterion appears significant, since Fe(II) salts with different anions (*i.e.* tetrafluoroborate, perchlorate and acetate) (Entries 7 to 9) gave low conversions and yields. In the case of iron(II) acetate, using acetic acid instead of 1-methylimidazole does not improve conversion, but selectivity was increased (Entry 10). Interestingly, even iron(III) oxide showed some catalytic activity toward epoxidation of *trans*-stilbene (Entry 11). What this study shows is the apparent importance of the chloride ion to epoxidation catalysis under these conditions. Therefore, other first-row transition metal chlorides (*i.e.*  $\text{MnCl}_2 \cdot 4\text{H}_2\text{O}$ ,  $\text{CoCl}_2 \cdot 6\text{H}_2\text{O}$ ,  $\text{NiCl}_2 \cdot 6\text{H}_2\text{O}$  and  $\text{CuCl}_2$ ) were examined using these reaction conditions. Slow addition of  $\text{H}_2\text{O}_2$  solutions to acetone solutions containing 1-methylimidazole, *trans*-stilbene and 5 mol% metal chloride followed by heating showed no conversion of the alkene to oxidized products.

**Table 3.2** Epoxidation of *trans*-stilbene in the presence of different iron sources.<sup>a</sup>

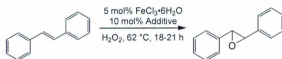
Entry	Iron source	Additive	Conv.(%)	Yield (%)	Select. (%)
1	FeCl <sub>3</sub> ·6H <sub>2</sub> O	1-Methylimidazole	93	90	97
2	FeCl <sub>3</sub>	1-Methylimidazole	100	90	90
3	FeBr <sub>3</sub>	1-Methylimidazole	0	0	0
4	Fe(NO <sub>3</sub> ) <sub>3</sub> ·9H <sub>2</sub> O	1-Methylimidazole	0	0	0
5	Fe(acac) <sub>3</sub>	1-Methylimidazole	0	0	0
6	FeCl <sub>2</sub>	1-Methylimidazole	88	49	55
7	Fe(BF <sub>4</sub> ) <sub>2</sub> ·6H <sub>2</sub> O	1-Methylimidazole	19	9	44
8	Fe(ClO <sub>4</sub> ) <sub>2</sub> ·H <sub>2</sub> O	1-Methylimidazole	16	16	100
9	Fe(CH <sub>3</sub> COO) <sub>2</sub>	1-Methylimidazole	19	10	54
10	Fe(CH <sub>3</sub> COO) <sub>2</sub>	Acetic acid	20	18	94
11	Fe <sub>2</sub> O <sub>3</sub> (powder)	1-Methylimidazole	12	9	76

<sup>a</sup> Reaction conditions: To a 45 mL reaction tube of a Radleys Carousel Reactor<sup>TM</sup>, Fe salt (0.025 mmol), additive (0.05 mmol), acetone (9 mL), *trans*-stilbene (0.5 mmol), and dodecane (GC internal standard, 50  $\mu$ L) were added in sequence at r.t. in air. The mixture was stirred and a solution of 30% H<sub>2</sub>O<sub>2</sub> (170  $\mu$ L, 1.5 mmol) in acetone (830  $\mu$ L) was added over a period of 1 h by a syringe pump. The reaction mixture was heated to 62  $^\circ$ C for 18-21 h. Conversion and yields were determined by GC-MS and NMR analysis. Selectivity refers to the ratio of yield to conversion in percentage.

Next, the effect of different additives in combination with  $\text{FeCl}_3 \cdot 6\text{H}_2\text{O}$  was studied for the epoxidation of *trans*-stilbene. The additives were selected to include either acidic or basic functionality that can easily coordinate with Fe(III). Among the additives, carboxylates can bridge metal centers and activated carbonyl groups can easily react with peroxide to enhance the epoxidation process.<sup>5</sup> However, a relatively low yield of epoxide was obtained using acetic acid under the experimental conditions used (Table 3.3, Entry 1), and a number of unidentified by-products, which will be mentioned below, were observed by GC-MS. In the presence of diphenylamine (Entry 2), no significant conversion of *trans*-stilbene was observed. This might be due to the bulkiness of the phenyl groups, which hinder its ability to coordinate with the iron center. However, in the case of *N*-phenylpyrrole conversion was 53% and yield for the epoxide product was 37% (Entry 3). In these cases (Entries 1-3), the main by-products were benzaldehyde and 1,2-diphenylethane-1,2-diol. These by-products were observed in reactions where low yields of *trans*-stilbene oxide were obtained. Employing 3,5-dimethylpyrazole (Entry 4) showed relatively low yield and conversion toward *trans*-stilbene epoxidation. As mentioned above, using 1-methylimidazole with  $\text{FeCl}_3 \cdot 6\text{H}_2\text{O}$  gave an excellent yield (90%) and selectivity (97%) for epoxidation of *trans*-stilbene, but heating was required to achieve optimum results (Entry 5). Therefore, other N- and C- substituted imidazoles were investigated to see their effect on catalytic activity, but none proved as effective as 1-methylimidazole. Using the 2-position substituted 1,2-dimethylimidazole, a 52% yield with 67% conversion was obtained for *trans*-stilbene epoxidation (Entry 6).

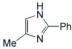
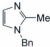
Increasing the amount of  $\text{H}_2\text{O}_2$  to 3.0 mmol (a six-fold excess versus olefin substrate), but maintaining the Fe(III) loading at 5 mol% with respect to *trans*-stilbene, increased conversion to 100%, but the yield increased only slightly to 66%. This was a vast improvement compared to a previous report where iron-catalyzed epoxidation in the presence of 1,2-dimethylimidazole showed very poor conversion (7%) and yield (4%) of epoxide.<sup>26</sup> Using C-substituted 2-ethyl-4-methyl imidazole gave a relatively low yield (40%) and conversion (56%) (Entry 7). Increasing the amount of  $\text{H}_2\text{O}_2$  to 3.0 mmol from 1.5 mmol improved the conversion to 100% with a 65% yield. The bulkier 2-phenyl-4-methylimidazole produced 33% *trans*-stilbene oxide (Entry 8) when oxidized using 1.5 mmol of  $\text{H}_2\text{O}_2$ .



**Table 3.3** Epoxidation of *trans*-stilbene in the presence of different additives.<sup>a</sup>

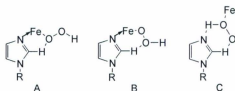
Entry	Additive	Conv. (%)	Yield (%)	Selectivity (%)
1	CH <sub>3</sub> CO <sub>2</sub> H	51	16	30
2		44	0	0
3		53	37	70
4		50	30	60
5		93	90	97
		19 <sup>b</sup>	18 <sup>b</sup>	91 <sup>b</sup>
6		67	52	78
		7 <sup>b</sup>	4 <sup>b</sup>	61 <sup>b</sup>
		100 <sup>c</sup>	66 <sup>c</sup>	66 <sup>c</sup>
7		56	40	71
		100 <sup>c</sup>	65 <sup>c</sup>	65 <sup>c</sup>

Chapter 3. Iron-catalyzed epoxidation of olefins using hydrogen peroxide

8		36 <sup>c</sup>	33 <sup>c</sup>	92 <sup>c</sup>
9		5 <sup>b</sup>	5 <sup>b</sup>	87 <sup>b</sup>

<sup>a</sup> Reaction conditions: To a 45 mL reaction tube of a Radleys Carousel Reactor™, FeCl<sub>3</sub>·6H<sub>2</sub>O (0.025 mmol), additive (0.05 mmol), acetone (9 mL), *trans*-stilbene (0.5 mmol), and dodecane (GC internal standard, 50 μL) were added in sequence at 25 °C in air. The mixture was stirred and a solution of 30% H<sub>2</sub>O<sub>2</sub> (170 μL, 1.5 mmol) in acetone (830 μL) was added over a period of 1 h using a syringe pump. The reaction mixture was heated to 62 °C for 18-21 h. Conversion and yields were determined by GC-MS and NMR analysis. Selectivity refers to the ratio of yield to conversion in percentage. <sup>b</sup> Previously reported conditions:<sup>26</sup> 0.5 mmol *trans*-stilbene, 5 mol% FeCl<sub>3</sub>·6H<sub>2</sub>O and 10 mol% imidazole derivative, *tert*-amyl alcohol (9 mL), 0.44 mmol dodecane as internal standard were added in sequence at room temperature in air. To this mixture a solution of 30% H<sub>2</sub>O<sub>2</sub> (170 mL, 1.5 mmol) in *tert*-amyl alcohol (830 mL) was added over 1 h at room temperature by syringe pump. Conversion and yield were determined by GC analysis. Selectivity refers to the chemoselectivity of epoxide from olefin. <sup>c</sup> 30% H<sub>2</sub>O<sub>2</sub> (340 μL, 3.0 mmol) in acetone (1660 μL) was added over a period of 2 h using a syringe pump.

Results obtained using 2-substituted imidazoles show considerably higher activity than in previous reports where it was found that the substitution pattern of the imidazole was critically important for obtaining significant catalytic activity towards the epoxidation of olefins. Specifically, the presence of alkyl groups in the 2-position of the imidazole was previously found to be detrimental to the epoxidation of *trans*-stilbene compared to those having H-functionalized 2-positions (Entries 6 and 9).<sup>26</sup> The decreased reactivity of the 2-substituted imidazoles was proposed to result from the involvement of a carbene-type ligand in the catalytic cycle<sup>37</sup> or hydrogen bonding between the proton in the 2-position of a coordinated imidazole and an iron hydroperoxo species (Scheme 3.2).



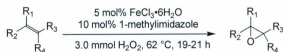
Scheme 3.2 Intra (A and B) and intermolecular (C) hydrogen bonding between H-2 in imidazole and ferric hydroperoxo (FeOOH) species.

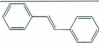


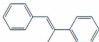
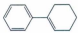
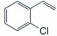



It was found that using imidazoles bearing alkyl groups in the 2-position does not necessarily result in poor yields of epoxide under our conditions (Entries 6, 7 and 8). This does not necessarily invalidate the involvement of a carbene-type interaction of the imidazole since “abnormal” carbenes (*i.e.* bonded to the metal *via* the 5-position) are still possible.<sup>38</sup> Also, while intramolecular hydrogen bonding may not be likely due to the position of the hydrogen-bond donor relative to the basic nitrogen atom of the imidazole ring, intermolecular hydrogen bonding may still be achieved. Regardless, by obtaining a moderate yield of epoxide using 2-position substituted imidazoles suggests other mechanistic pathways are conceivable using these reaction conditions.

Various other substrates were studied for epoxidation catalyzed by  $\text{FeCl}_3 \cdot 6\text{H}_2\text{O}$  (5 mol%) and 1-methylimidazole (10 mol%) and the results are given in Table 3.4. As observed in Table 3.3, Entries 6 and 7, use of six-fold excess of  $\text{H}_2\text{O}_2$  led to improved yields, therefore these conditions were employed for further reactions. Thus, the conversion of *trans*-stilbene could be improved to 100% with a 100% yield of epoxide product upon heating the reaction to 62 °C for 21 h (Table 3.4, Entry 1). This catalytic


system was applicable for both aliphatic and aromatic systems and mono-, di- and tri-substituted olefins could be epoxidized in good-to-excellent yields and selectivity. Iron-catalyzed epoxidation of *cis*-stilbene is typically low yielding and the best result reported in the literature to date is 34% conversion with 24% yield of epoxide.<sup>25</sup> Using the  $\text{FeCl}_3 \cdot 6\text{H}_2\text{O}/1$ -methylimidazole system in acetone gave better conversion (66%) and yield (64%), however, *cis*-stilbene was converted to *trans*-stilbene oxide (Entry 2) as determined by  $^1\text{H}$  NMR spectroscopy. Heating the reaction for 48 rather than 20 h improved the conversion to 87% with 76% yield. The conversion of *trans*- $\beta$ -methyl styrene was quantitative; however, the yield of the epoxide product was moderate (Entry 3). Under the same conditions, trisubstituted acyclic (Entry 4) and cyclic alkenes (Entry 5) could also be converted to epoxides in excellent yields. Terminal olefins (Entries 6 to 8) are a particularly challenging class of substrate for epoxidation due to their relatively electron deficient nature.<sup>5,39,40</sup> Halo-substituted styrenes (Entries 6 to 8) showed moderate conversion and selectivity for epoxidation, even for the *ortho*-substituted 2-chlorostyrene. The main by-product in these cases was halogen-substituted acetophenone. It appears that both steric and electronic effects limit olefin conversion. For example, *trans*-stilbene conversion was 100% (Entry 1) whereas *cis*-stilbene conversion was 66% (Entry 2) under the same conditions, likely because of steric constraints caused by *cis*-oriented phenyl groups. Also the moderately sterically-encumbered *trans*- $\alpha$ -methyl stilbene gave a conversion of 91% (Entry 4) which was between that observed for the *trans* and *cis*-stilbene conversions. Regarding electronic effects, for halo-substituted electron-deficient olefins (Entries 6-8) conversions of 80-86% could be achieved, which were lower than

unsubstituted terminal olefins like *trans*- $\beta$ -methyl styrene (100%) (Entry 3). Cyclic aliphatic alkenes could be converted to epoxides with varying yields (Entries 9 to 11). Limonene oxide has been employed as a feedstock for polycarbonate synthesis<sup>41</sup> and since it can be obtained from renewable sources (*e.g.* citrus fruit peels), a catalytic, green method of epoxidation is desirable. Catalytic limonene epoxidation has been previously achieved by using dioxomolybdenum complexes with *t*-BuOOH heated to 55 °C for 24 h obtaining 95% epoxide product with 100% selectivity.<sup>42</sup> Iron has also showed catalytic limonene epoxidation with H<sub>2</sub>O<sub>2</sub> as the oxidant but the yields are typically much lower. For example, iron polynitroporphyrin complexes produced a 24% yield of limonene oxide in a 1:1 mixture of CH<sub>2</sub>Cl<sub>2</sub> and MeCN.<sup>43</sup> Also, Fe<sup>II</sup>(bpy)<sub>2</sub><sup>2+</sup> gave 46% limonene oxide in MeCN after 24 h, but side-products such as carvone and carveol were also produced.<sup>44</sup> Our catalyst system was investigated for epoxidation of both (+) and (-) limonene (Entries 12 and 13) and high conversions (~ 90%) with good yields (~ 69%) were obtained. To date, these are the highest yields of limonene oxide obtained by Fe-catalyzed epoxidation. Unfortunately, no stereocontrol was observed as both isomers of limonene were converted to mixtures of the *cis* and *trans* epoxide products.

**Table 3.4** Olefinic substrates screened for epoxidation.<sup>a</sup>

Entry	Substrate	Conv. (%)	Yield (%)	Select. (%)
1		100	100	100
2		66	64	97
		87 <sup>b</sup>	76 <sup>b</sup>	87 <sup>b</sup>
3		100	64	64
4		91	91	100
5		100	95	95
6		84	58	69
			8 <sup>c</sup>	
7		86	69	80
			15 <sup>c</sup>	
8		80	65	81
			15 <sup>c</sup>	
9		95	65	68

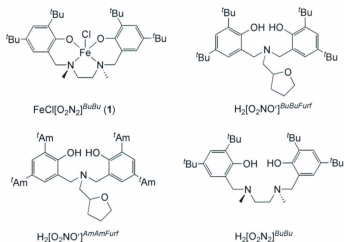
Chapter 3. Iron-catalyzed epoxidation of olefins using hydrogen peroxide

10		79	69	87
11		100	95	95
12		96	66	63
13		87	72	83

<sup>a</sup> Reaction conditions: To a 45 mL reaction tube of a Radleys Carousel Reactor™, FeCl<sub>3</sub>·6H<sub>2</sub>O (0.025 mmol), 1-methylimidazole (0.05 mmol), acetone (9 mL), olefin (0.5 mmol), and dodecane (GC internal standard, 50 μL) were added in sequence at 25 °C in air. The mixture was stirred and a solution of 30% H<sub>2</sub>O<sub>2</sub> (340 μL, 3.0 mmol) in acetone (1660 μL) was added over a period of 2 h using a syringe pump and heated at 62 °C for 19-21 h. Conversion and yields were determined by GC-MS and NMR analysis. Selectivity refers to the ratio of yield to conversion in percentage. <sup>b</sup> Heated to 62 °C for 48 h. <sup>c</sup> Yield of ketone by-product.

The use of 2,6-pyridinedicarboxylic acid as an ancillary ligand in combination with simple amines for Fe-catalyzed epoxidation of olefins by H<sub>2</sub>O<sub>2</sub> has been reported.<sup>23,45,46</sup> Use of this ligand was thought to be crucial for obtaining high yield of epoxide products, but it was later shown that by using sterically demanding imidazole ligands the need for 2,6-pyridinedicarboxylic acid was alleviated.<sup>26</sup> The Kozak group has reported the catalytic activity of Fe(III) complexes bearing tetradentate and tridentate amine-bis(phenolate) ligands towards C-C cross-coupling reactions.<sup>28-30</sup> There is a structural similarity between 2,6-pyridinedicarboxylic acid and amine-bis(phenol) ligands (Figure 3.1), namely they both possess acidic -OH sites and neutral N-donors. Therefore, Fe(III) amine-bis(phenolate) complexes were investigated for catalytic epoxidation of

olefins to see whether any enhancement of reactivity could be obtained. However, using a combination of pre-made Fe(III) amine-bis(phenolate) complex **1** (the iron chloride complex of  $[\text{O}_2\text{N}_2]^{\text{BuBu}}$ , shown in Figure 3.1) and 1-methylimidazole only gave 36% yield of *trans*-stilbene oxide in acetone (Table 3.5, Entry 1).



**Figure 3.1** Iron complex **1** and tetradentate amine-bis(phenol) proligands used in this study.

Next, the effect of *in-situ* iron complexation by amine-bis(phenol) ligands,  $\text{H}_2[\text{O}_2\text{NO}]^{\text{BuBuFurf}}$ ,  $\text{H}_2[\text{O}_2\text{NO}]^{\text{AmAmFurf}}$  and  $\text{H}_2[\text{O}_2\text{N}_2]^{\text{BuBu}}$  was studied. Screening of ligand effects was conducted by adding the appropriate amount of  $\text{FeCl}_3 \cdot 6\text{H}_2\text{O}$  to solutions of tetradentate amine-bis(phenol) proligands,  $\text{H}_2[\text{O}_2\text{NO}]^{\text{BuBuFurf}}$ ,  $\text{H}_2[\text{O}_2\text{NO}]^{\text{AmAmFurf}}$  or  $\text{H}_2[\text{O}_2\text{N}_2]^{\text{BuBu}}$  in *tert*-amyl alcohol at 25 °C. To these mixtures were added the basic or acidic co-catalysts.<sup>47</sup> These conditions were generally found to give at least modest yields



in other iron-catalyzed epoxidations.<sup>24</sup> However, only the use of imidazole bases gave any epoxide product (yields ~30%) (Entries 2-4) and no significant influence was observed by varying the ligand. No yields of epoxide products were obtained in the presence of triethylamine, pyrrolidine or acetic acid with  $\text{H}_2[\text{O}_2\text{N}_2]^{BuBu}$  and  $\text{FeCl}_3 \cdot 6\text{H}_2\text{O}$ , even after prolonged stirring at 25 °C (Entries 5-7).

**Table 3.5** Screening of Fe(III) complexes with tetradentate amine-bis(phenol) ligands.<sup>a</sup>

Entry	Complex/Proligand	Additive	Conv. (%)	Yield (%)
1	$\text{FeCl}[\text{O}_2\text{N}_2]^{BuBu}$ ( <b>1</b> )	1-Methylimidazole	36 <sup>b</sup>	36 <sup>b</sup>
2	$\text{H}_2[\text{O}_2\text{NO}]^{BuBuFurf}$	1-Methylimidazole	30	26
3	$\text{H}_2[\text{O}_2\text{NO}]^{BuBuFurf}$	Imidazole	27	24
4	$\text{H}_2[\text{O}_2\text{NO}]^{AmAmFurf}$	1-Methylimidazole	33	29
5	$\text{H}_2[\text{O}_2\text{N}_2]^{BuBu}$	Triethylamine	0	0
6	$\text{H}_2[\text{O}_2\text{N}_2]^{BuBu}$	Pyrrolidine	0	0
7	$\text{H}_2[\text{O}_2\text{N}_2]^{BuBu}$	Acetic acid	0	0

<sup>a</sup> Reaction conditions: To a 25 mL Schlenk tube,  $\text{FeCl}_3 \cdot 6\text{H}_2\text{O}$  (0.025 mmol), ligand (0.025 mmol, if used), additive (0.05 mmol), *tert*-amyl alcohol (9 mL), *trans*-stilbene (0.5 mmol), and dodecane (GC internal standard, 100  $\mu\text{L}$ ) were added in sequence at 25 °C in air. The mixture was stirred and a solution of 30%  $\text{H}_2\text{O}_2$  (170  $\mu\text{L}$ , 1.5 mmol) in *tert*-amyl alcohol (830  $\mu\text{L}$ ) was added over a period of 1 h using a syringe pump and stirred at 25 °C for 19 h. Conversion and yields were determined by GC-MS analysis. <sup>b</sup> Acetone was used as solvent.

Since these tetradentate ligands did not show promise as ancillary ligands in Fe-catalyzed epoxidation of *trans*-stilbene, the less-coordinatively demanding tridentate amine-bis(phenol) ligands (abbreviated  $H_2[O_2N]$ ) were studied (Figure 3.2) using 1-methylimidazole as co-catalyst. An aqueous solution of  $H_2O_2$  was diluted in acetone and added to a mixture of  $FeCl_3 \cdot 6H_2O$ ,  $H_2[O_2N]$ , 1-methylimidazole and *trans*-stilbene in acetone. Also, since the reactions in Table 3.5 gave unimpressive yields of epoxide at room temperature, the reactions given in Table 3.6 were heated to 62 °C for 20 h. Under these conditions, all the systems studied exhibited catalytic activity toward the epoxidation of *trans*-stilbene, but unlike the tetradentate ligands, a slight ligand effect was observed.

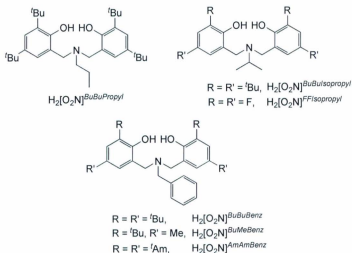


Figure 3.2 Tridentate amine-bis(phenol) ligands used in this study.

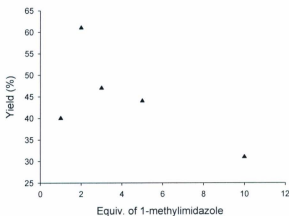
In the presence of ligands with electron-donating and sterically bulky *tert*-butyl groups in the *ortho*- and *para*- positions relative to the phenol oxygen atom (Table 3.6, Entries 1, 2 and 4), *trans*-stilbene oxide formed in 51–64% yield with 69–85% selectivity. The lowest yield was obtained using proligand  $\text{H}_2[\text{O}_2\text{N}]^{\text{FFIsopropyl}}$ , which possesses electron-withdrawing fluoro groups (Entry 3). Highest selectivity (90%) was achieved using the more bulky *tert*-amyl-substituted ligand  $\text{H}_2[\text{O}_2\text{N}]^{\text{AmAmBenz}}$  (Entry 6) with a 56% overall yield of *trans*-stilbene oxide. Nonetheless, what is apparent is that the presence of these ligands in the catalytic system actually lowers the epoxidation activity compared to the use of only  $\text{FeCl}_3 \cdot 6\text{H}_2\text{O}$  and 1-methylimidazole in acetone under heating conditions.

**Table 3.6** Epoxidation of *trans*-stilbene using tridentate amine-bis(phenol) ligands with  $\text{FeCl}_3 \cdot 6\text{H}_2\text{O}$ .<sup>a</sup>

Entry	Ligand	Conv. (%)	Yield (%)	Select. (%)
1	$\text{H}_2[\text{O}_2\text{N}]^{\text{tBuBuPropyl}}$	75	64	85
2	$\text{H}_2[\text{O}_2\text{N}]^{\text{tBuBuIsopropyl}}$	67	51	76
3	$\text{H}_2[\text{O}_2\text{N}]^{\text{FFIsopropyl}}$	57	34	60
4	$\text{H}_2[\text{O}_2\text{N}]^{\text{tBuBuBenz}}$	88	61	69
5	$\text{H}_2[\text{O}_2\text{N}]^{\text{tBuMeBenz}}$	59	49	83
6	$\text{H}_2[\text{O}_2\text{N}]^{\text{AmAmBenz}}$	62	56	90

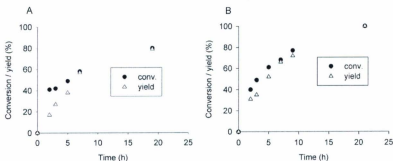
<sup>a</sup> Reaction conditions: To a 45 mL reaction tube of a Radleys Carousel Reactor<sup>TM</sup>,  $\text{FeCl}_3 \cdot 6\text{H}_2\text{O}$  (0.025 mmol), ligand (0.025 mmol), 1-methylimidazole (0.05 mmol), acetone (9 mL), *trans*-stilbene (0.5 mmol), and dodecane (GC internal standard, 50  $\mu\text{L}$ ) were added in sequence at 25 °C. in air. The mixture was stirred and a solution of 30%  $\text{H}_2\text{O}_2$  (170  $\mu\text{L}$ , 1.5 mmol) in acetone (830  $\mu\text{L}$ ) was added over a period of 1 h using a syringe pump and heated at 62 °C for 19–21 h. Conversion and yields were determined by GC-MS and NMR analysis. Selectivity refers to the ratio of yields to conversion in percentage.

The optimized conditions for these epoxidation reactions were using 2.0 equiv. of 1-methylimidazole to 1.0 equiv.  $\text{FeCl}_3 \cdot 6\text{H}_2\text{O}$ . The additive's role was examined by varying the amount of 1-methylimidazole used in the epoxidation process. Epoxidation of *trans*-stilbene was carried out using different equivalents of 1-methylimidazole in combination with  $\text{FeCl}_3 \cdot 6\text{H}_2\text{O}$  and the  $\text{H}_2[\text{O}_2\text{N}]^{\text{BuBuBenz}}$  ligand in acetone, and heating the reaction mixture to 62 °C for 19-21 h (Figure 3.3). From this observation it was found that either lower or higher loadings of 1-methylimidazole decreased the formation of *trans*-stilbene oxide. Only 2.0 equiv. of 1-methylimidazole gave the maximum yield of epoxide product under the conditions investigated.



**Figure 3.3** Yield of *trans*-stilbene oxide obtained by epoxidation of *trans*-stilbene vs. equivalents of 1-methylimidazole added.

During these studies,  $\text{FeCl}_3 \cdot 6\text{H}_2\text{O}$  and 1-methylimidazole in acetone were found to be the best catalytic system for olefin epoxidation by dilute  $\text{H}_2\text{O}_2$ . However, the reactions proceeded slowly and required heating for several hours to achieve high yields of epoxide product. Preliminary kinetic studies of the catalyst system were performed by monitoring two epoxidation reactions in the presence and absence of amine-bis(phenol) proligand,  $\text{H}_2[\text{O}_2\text{N}]^{\text{BuBuBenz}}$ . Plots of conversion and yield versus time are given in Figure 3.4. From these observations, it was found that the rate of epoxide formation decreases over time, but the epoxidation continues to proceed over the duration of the experiments. As shown in Figure 3.4 A, the presence of  $\text{H}_2[\text{O}_2\text{N}]^{\text{BuBuBenz}}$  actually slows the rate of the epoxidation of *trans*-stilbene and only 79% conversion and yield were obtained after 20 h, whereas the reaction was complete (100% conversion and yield) within 21 h when no amine-bis(phenolate) ligand was present (Figure 3.4 B).



**Figure 3.4** Monitoring the progress of epoxidation of *trans*-stilbene in presence of (A) and absence of amine-bis(phenol) ligand  $\text{H}_2[\text{O}_2\text{N}]^{\text{BuBuBenz}}$  (B).

Because of the lengths of time involved in these epoxidation reactions, it was reasonable to query whether any  $\text{H}_2\text{O}_2$  was present in the reaction after this time period. In other words, was all the peroxide consumed early in the reaction or perhaps converted to another oxidant? Titrations were performed of several reaction mixtures after 21 h to quantify any unreacted  $\text{H}_2\text{O}_2$  that may remain. Under the conditions employed in Table 3.4, Entry 1, titration of the mixture after 21 h revealed that 5.8% of the added  $\text{H}_2\text{O}_2$  remains. Using 170  $\mu\text{L}$  of  $\text{H}_2\text{O}_2$ , as performed in Table 3.2, Entry 1, 2.8% of the added  $\text{H}_2\text{O}_2$  remained. The consumption of  $\text{H}_2\text{O}_2$  has some limiting effect on the olefin conversion. Namely, as shown in Table 3.2, entry 1, 93% conversion of *trans*-stilbene was obtained when using 170  $\mu\text{L}$  of  $\text{H}_2\text{O}_2$  whereas 100% conversion of *trans*-stilbene was obtained when using 340  $\mu\text{L}$  of  $\text{H}_2\text{O}_2$  (Table 3.4, Entry 1). When 170  $\mu\text{L}$  of  $\text{H}_2\text{O}_2$  was added to  $\text{Fe}(\text{acac})_3$  as the iron source instead of  $\text{FeCl}_3 \cdot 6\text{H}_2\text{O}$  (Table 3.2, Entry 5), the remaining  $\text{H}_2\text{O}_2$  was 2.5%, but no epoxidation was observed. Therefore, it appears the iron catalyst precursors do not influence the rate of consumption of  $\text{H}_2\text{O}_2$ , but they are vital to the epoxidation process itself. The solvent used also shows some effect on the consumption of  $\text{H}_2\text{O}_2$  because 9.9% of the  $\text{H}_2\text{O}_2$  remains when acetonitrile was used as solvent (Table 3.1, Entry 5). During the reaction,  $\text{H}_2\text{O}_2$  may have been converted to another oxidant, such as  $\text{HOCl}$ , and another researcher in the Kozak group will undertake these investigations. Also, a very recent report by Beller and co-workers showed that  $\text{FeCl}_3 \cdot 6\text{H}_2\text{O}$  in the presence of a  $\beta$ -ketoester (ethyl-2-oxocyclopentanecarboxylate) epoxidizes olefins using air as the oxidant and no  $\text{H}_2\text{O}_2$  was required.<sup>48</sup> Because the reactions presented in this thesis were also conducted under aerobic conditions, it was

questioned whether it was the presence of air rather than peroxide that led to epoxidation. Performing the reaction in air as described in Table 3.2, Entry 1 or Table 3.4, Entry 1, without the addition of  $\text{H}_2\text{O}_2$  showed no formation of epoxide product.

The exact nature of the catalytic species remains unknown at this time, however, crystalline material was obtained from a solution of  $\text{FeCl}_3 \cdot 6\text{H}_2\text{O}$  and 2 equiv. of 1-methylimidazole in acetone and X-ray diffraction studies of this product unsurprisingly revealed it to be the octahedral complex, trichlorotrakis(1-methylimidazole)iron(III).<sup>49</sup> Generally, high-valent iron-oxo compounds act as the catalytic species for oxygen-activating non-heme iron enzymes.<sup>50</sup> The reaction of iron porphyrin complexes with  $\text{H}_2\text{O}_2$  forms high-valent iron(IV)oxo porphyrin cation radical intermediates,  $[(\text{Porp})\text{Fe}^{\text{IV}}=\text{O}]^{+\bullet}$ , which are generated *via* O-O bond heterolysis.<sup>32</sup> In the catalyst system presented here, a high-valent iron-oxo species could also be the active catalyst. A proposed catalytic cycle is shown in Figure 3.5. Of course it cannot be ignored that the combination of acetone and  $\text{H}_2\text{O}_2$  under acidic conditions can result in the formation of explosive cyclic peroxides,<sup>51</sup> and therefore this solvent may not be suitable for industrial applications involving  $\text{H}_2\text{O}_2$ . Nonetheless, no accumulation of alkylperoxides was observed when performed on a laboratory scale. Indeed, the formation of 2-hydroperoxy-2-hydroxypropane (hphp) has been proposed as a reason for decreased decomposition of the oxidant in the presence of a metal catalyst.<sup>1</sup> Thus, due to the dilution of the  $\text{H}_2\text{O}_2$  solution in acetone, the epoxidation reaction was favoured over oxidant decomposition. Therefore, hphp could be considered either an "oxidant reservoir" which gradually

released  $\text{H}_2\text{O}_2$  maintaining a low oxidant concentration or it might be directly involved in the epoxidation pathway itself. Further mechanistic studies are required.

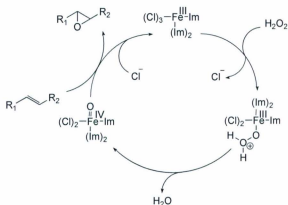


Figure 3.5 Proposed catalytic cycle via an iron-oxo intermediate.

### 3.3 Conclusions

A simple epoxidation of both terminal and substituted (both endo- and exocyclic) olefins was achieved using low concentrations of  $\text{FeCl}_3 \cdot 6\text{H}_2\text{O}$  and 1-methylimidazole in acetone. The use of acetone as a solvent presents a potential advantage over other solvents typically employed, namely toxic acetonitrile, dichloromethane (a suspected carcinogen), and costly *tert*-butyl or *tert*-amyl alcohols. Also, this catalytic system employed a simple and readily available additive/co-catalyst 1-methylimidazole, which is considerably less expensive than other imidazole-containing co-catalysts reported to date.



### 3.4 Experimental

#### 3.4.1 General experimental conditions

Unless otherwise stated, all manipulations were performed in air by using a Radleys Carousel Reactor. Organic reagents, solvents and alkene substrates were purchased from either Sigma-Aldrich or Alfa Aesar and used without further purification.  $\text{FeCl}_3 \cdot 6\text{H}_2\text{O}$  was purchased from Strem Chemicals, 1-methylimidazole from ACROS, and 30%  $\text{H}_2\text{O}_2$  from ACP Chemicals. Complex **1** was prepared using the published procedure.<sup>52</sup> All the ligands were prepared by Mannich condensation in water<sup>29,53</sup>, which were modifications of the originally reported syntheses.<sup>54-56</sup>

#### 3.4.2 Instrumentation

NMR spectra were recorded in  $\text{CDCl}_3$  on a Bruker Avance-500 and referenced to TMS. Gas chromatography mass spectrometry (GC-MS) analyses were performed using an Agilent Technologies 7890A GC system coupled to an Agilent Technologies 5975C mass selective detector. The chromatograph is equipped with electronic pressure control, split/splitless and on-column injectors, and an HP5-MS column.

#### 3.4.3 General method for epoxidation catalysis reactions

Acetone (9 mL) was added to  $\text{FeCl}_3 \cdot 6\text{H}_2\text{O}$  (0.025 mmol, 5.0 mol%) in a 45 mL reaction tube of the Carousel Reactor and the solution was stirred. The pale yellow solution darkened to intense yellow following the addition of 1-methylimidazole (0.05 mmol, 10 mol%). The alkene substrate (0.5 mmol) and dodecane (100 or 50  $\mu\text{L}$  as

internal standard) were added to the solution at room temperature in air. 30% aqueous  $\text{H}_2\text{O}_2$  (170  $\mu\text{L}$ , 1.5 mmol or 340  $\mu\text{L}$ , 3.0 mmol) was dissolved in acetone (870  $\mu\text{L}$  or 1660  $\mu\text{L}$ , respectively) and was added to the reaction mixture over a period of 1 or 2 h by a syringe pump. The reaction mixture was then stirred and heated to 62  $^\circ\text{C}$  for 19–21 h. The reaction was quenched and the products were obtained by passing through a plug of silica. Water was removed by the addition of anhydrous  $\text{Na}_2\text{SO}_4$ . The mixture was analyzed by GC-MS and quantified using  $^1\text{H}$  NMR. NMR samples were prepared by careful removal of solvent and dissolving the residue in  $\text{CDCl}_3$ .

#### 3.4.4 Method for determination of $\text{H}_2\text{O}_2$ concentration

Determination of remaining  $\text{H}_2\text{O}_2$  was performed by cooling the epoxidation reactions to room temperature and removing any precipitated material by filtration through glass-fiber filter paper. The filtered solution was acidified using 3 M  $\text{H}_2\text{SO}_4$  (0.8 mL for reactions using 170  $\mu\text{L}$  30%  $\text{H}_2\text{O}_2$  or 1.2 mL for reactions using 340  $\mu\text{L}$  30%  $\text{H}_2\text{O}_2$ ). The acidic solution was titrated with standardized 0.10 M  $\text{KMnO}_4$  solution.

### 3.5 Notes and references

1. J.-E. Bäckvall, *Modern Oxidation Methods*, Wiley-VCH, Weinheim, 2004.
2. M. Beller and C. Bolm, *Transition Metals for Organic Synthesis*, Wiley-VCH, Weinheim, 2004.
3. P. T. Anastas and J. C. Warner, *Green Chemistry: Theory and Practice*, Oxford University Press, New York, 2000.
4. T. Punniyamurthy, S. Velusamy and J. Iqbal, *Chem. Rev.*, 2005, **105**, 2329–2363.

5. B. S. Lane and K. Burgess, *Chem. Rev.*, 2003, **103**, 2457-2473.
6. B. S. Lane, M. Vogt, V. J. DeRose and K. Burgess, *J. Am. Chem. Soc.*, 2002, **124**, 11946-11954.
7. B. S. Lane and K. Burgess, *J. Am. Chem. Soc.*, 2001, **123**, 2933-2934.
8. M. Colladon, A. Scarso, P. Sgarbossa, R. A. Michelin and G. Strukul, *J. Am. Chem. Soc.*, 2006, **128**, 14006-14007.
9. Y. Sawada, K. Matsumoto, S. Kondo, H. Watanabe, T. Ozawa, K. Suzuki, B. Saito and T. Katsuki, *Angew. Chem. Int. Ed.*, 2006, **45**, 3478-3480.
10. K. Matsumoto, Y. Sawada, B. Saito, K. Sakai and T. Katsuki, *Angew. Chem. Int. Ed.*, 2005, **44**, 4935-4939.
11. A. Mahammed and Z. Gross, *J. Am. Chem. Soc.*, 2005, **127**, 2883-2887.
12. K. Kamata, K. Yamaguchi, S. Hikichi and N. Mizuno, *Adv. Synth. Catal.*, 2003, **345**, 1193-1196.
13. W. Adam, P. L. Alsters, R. Neumann, C. R. Saha-Moller, D. Sloboda-Rozner and R. Zhang, *J. Org. Chem.*, 2003, **68**, 1721-1728.
14. G. B. Shul'pin, C. C. Golfeto, G. Suess-Fink, L. S. Shul'pina and D. Mandelli, *Tetrahedron Lett.*, 2005, **46**, 4563-4567.
15. D. H. R. Barton and D. K. Taylor, *Pure Appl. Chem.*, 1996, **68**, 497-504.
16. W. Nam, R. Ho and J. S. Valentine, *J. Am. Chem. Soc.*, 1991, **113**, 7052-7054.
17. T. G. Traylor, S. Tsuchiya, Y. S. Byun and C. Kim, *J. Am. Chem. Soc.*, 1993, **115**, 2775-2781.
18. D. Dolphin, T. G. Traylor and L. Y. Xie, *Acc. Chem. Res.*, 1997, **30**, 251-259.

19. B. Qi, X. H. Lu, D. Zhou, Q. H. Xia, Z. R. Tang, S. Y. Fang, T. Pang and Y. L. Dong, *J. Mol. Catal. A: Chem.*, 2010, **322**, 73-79.
20. A. Stamatidis, D. Giasafaki, K. C. Christoforidis, Y. Deligiannakis and M. Louloudi, *J. Mol. Catal. A: Chem.*, 2010, **319**, 58-65.
21. M. C. White, A. G. Doyle and E. N. Jacobsen, *J. Am. Chem. Soc.*, 2001, **123**, 7194-7195.
22. G. Dubois, A. Murphy and T. D. P. Stack, *Org. Lett.*, 2003, **5**, 2469-2472.
23. G. Anilkumar, B. Bitterlich, F. G. Gelalcha, M. K. Tse and M. Beller, *Chem. Commun.*, 2007, 289-291.
24. B. Bitterlich, G. Anilkumar, F. G. Gelalcha, B. Spilker, A. Grotevendt, R. Jackstell, M. K. Tse and M. Beller, *Chem. Asian J.*, 2007, **2**, 521-529.
25. K. Schröder, X. Tong, B. Bitterlich, M. K. Tse, F. G. Gelalcha, A. Bruckner and M. Beller, *Tetrahedron Lett.*, 2007, **48**, 6339-6342.
26. K. Schröder, S. Enthaler, B. Bitterlich, T. Schulz, A. Spannenberg, M. K. Tse, K. Junge and M. Beller, *Chem. Eur. J.*, 2009, **15**, 5471-5481.
27. K. Schröder, S. Enthaler, B. Join, K. Junge and M. Beller, *Adv. Synth. Catal.*, 2010, **352**, 1771-1778.
28. R. R. Chowdhury, A. K. Crane, C. Fowler, P. Kwong and C. M. Kozak, *Chem. Commun.*, 2008, 94-96.
29. X. Qian, L. N. Dawe and C. M. Kozak, *Dalton Trans.*, 2011, **40**, 933-943.
30. A. M. Reckling, D. Martin, L. N. Dawe, A. Decken and C. M. Kozak, *J. Organomet. Chem.*, 2011, **696**, 787-794.

31. M. Costas, M. P. Mehn, M. P. Jensen and L. Que, *Chem. Rev.*, 2004, **104**, 939-986.
32. W. Nam, H. J. Lee, S. Y. Oh, C. Kim and H. G. Jang, *J. Inorg. Biochem.*, 2000, **80**, 219-225.
33. M. K. Tse, S. Bhor, M. Klawonn, G. Anilkumar, H. J. Jiao, C. Dobler, A. Spannenberg, W. Magerlein, H. Hugl and M. Beller, *Chem. Eur. J.*, 2006, **12**, 1855-1874.
34. M. K. Tse, S. Bhor, M. Klawonn, G. Anilkumar, H. J. Jiao, A. Spannenberg, C. Dobler, W. Magerlein, H. Hugl and M. Beller, *Chem. Eur. J.*, 2006, **12**, 1875-1888.
35. K. Schröder, K. Junge, A. Spannenberg and M. Beller, *Catal. Today*, 2010, **157**, 364-370.
36. According to Alfa Aesar, pricing in US dollars for 1-methylimidazole was approximately \$20/100 g, whereas 5-chloro-1-methylimidazole was \$87/g.
37. W. A. Herrmann, *Angew. Chem. Int. Ed.*, 2002, **41**, 1290-1309.
38. S. Grundemann, A. Kovacevic, M. Albrecht, J. W. Faller and R. H. Crabtree, *Chem. Commun.*, 2001, 2274-2275.
39. G. Grigoropoulou, J. H. Clark and J. A. Elings, *Green Chem.*, 2003, **5**, 1-7.
40. I. Arends and R. A. Sheldon, *Top. Catal.*, 2002, **19**, 133-141.
41. C. M. Byrne, S. D. Allen, E. B. Lobkovsky and G. W. Coates, *J. Am. Chem. Soc.*, 2004, **126**, 11404-11405.

42. S. M. Bruno, C. C. L. Pereira, M. S. Balula, M. Nolasco, A. A. Valente, A. Hazell, M. Pillinger, P. Ribeiro-Claro and I. S. Goncalves, *J. Mol. Catal. A: Chem.*, 2007, **261**, 79-87.
43. J. F. O. Bartoli, K. Le Barch, M. Palacio, P. Battioni and D. Mansuy, *Chem. Commun.*, 2001, 1718-1719.
44. D. Narog, A. Szczepanik and A. Sobkowiak, *Catal. Lett.*, 2008, **120**, 320-325.
45. F. G. Gelalcha, G. Anilkumar, M. K. Tse, A. Brueckner and M. Beller, *Chem. Eur. J.*, 2008, **14**, 7687-7698.
46. B. Bitterlich, K. Schröder, M. K. Tse and M. Beller, *Eur. J. Org. Chem.*, 2008, **2008**, 4867-4870.
47. The reaction of the protic ligands with  $\text{FeCl}_3$  generates 2 equiv. of HCl: therefore any basic additives, such as imidazoles, would become ionized (e.g. from imidazolium chloride). Excess base is therefore required to neutralize the acid and allow for sufficient Lewis basic sites to be present in solution.
48. K. Schröder, B. Join, A. J. Amali, K. Junge, X. Ribas, M. Costas and M. Beller, *Angew. Chem. Int. Ed.*, 2011, **50**, 1425-1429, S1425/1421-S1425/1429.
49. S. A. Cotton, V. Franckevicius and J. Fawcett, *Polyhedron*, 2002, **21**, 2055-2061.
50. X. P. Shan and L. Que, *J. Inorg. Biochem.*, 2006, **100**, 421-433.
51. R. Wolffenstein, *Chemische Berichte*, 1895, **28**, 2265.
52. K. Hasan, C. Fowler, P. Kwong, A. K. Crane, J. L. Collins and C. M. Kozak, *Dalton Trans.*, 2008, 2991-2998.

53. F. M. Kerton, S. Holloway, A. Power, R. G. Soper, K. Sheridan, J. M. Lynam, A. C. Whitwood and C. E. Willans, *Can. J. Chem.*, 2008, **86**, 435-443.
54. S. Groysman, I. Goldberg, M. Kol, E. Genizi and Z. Goldschmidt, *Inorg. Chim. Acta*, 2003, **345**, 137-144.
55. E. Y. Tshuva, I. Goldberg and M. Kol, *J. Am. Chem. Soc.*, 2000, **122**, 10706-10707.
56. E. Y. Tshuva, I. Goldberg, M. Kol and Z. Goldschmidt, *Organometallics*, 2001, **20**, 3017-3028.

## **Chapter 4. Synthesis, structure, and C-C cross-coupling activity of amine-bis(phenolate)iron(acac) complexes**

This chapter has been published as an article: Kamrul Hasan, Louise N. Dawe and Christopher M. Kozak,\* *Eur. J. Inorg. Chem.*, 2011, 4610-4621.

Some modification of the published manuscript was done, including addition of several MALDI-TOF mass and IR spectra,  $^1\text{H}$  and  $^{13}\text{C}$  NMR data of cross-coupled products and ligands, changing the abbreviation of ligands and numbering of the complexes.

### **4.1 Introduction**

The use of chelating tetradentate amine-bis(phenolate) ligands has recently played an increasingly important role in transition metal catalyst design. They have been predominantly used with high oxidation-state early transition metals where they were employed as alternative auxiliary ligands to cyclopentadienyl-based systems. In combination with Group 4 and 5 metals they display high activities towards olefin and cyclic ester polymerization.<sup>1-10</sup> Also, Group 3 and lanthanide metal complexes of these ligands have been effective as catalysts or initiators for ring-opening polymerization of



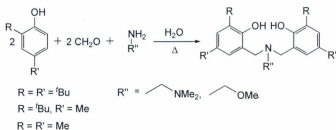
lactide and  $\epsilon$ -caprolactone.<sup>11-16</sup> By comparison, there has been limited use of amine-bis(phenolate) ligands with first row late transition metals,<sup>17-24</sup> whereas the chemistry of monoanionic phenoxytriimine ligands with these metals is far more developed.<sup>25-35</sup> The Kozak group is interested in the development of new inexpensive, non-toxic and environmentally friendly iron-based catalysts for organic synthesis. Following the pioneering work of Kochi,<sup>36</sup> iron catalysts have been found that are complementary to Ni or Pd systems for the coupling of Grignard reagents with organohalides.<sup>37-40</sup> The groups of Fürstner,<sup>41-48</sup> Cahiez,<sup>49-55</sup> Nakamura<sup>56-59</sup> and others<sup>60-64</sup> have reported various iron catalysts for cross-coupling reactions of organomagnesium halides and organohalides. Also, Bedford and co-workers showed that Fe(salen) complexes can be used as catalysts for the cross-coupling of aryl Grignard reagents with alkyl halides.<sup>65</sup> The use of Fe(acac)<sub>3</sub> as a source of Fe(III) has been investigated by numerous groups because of its superior ease of handling compared to highly hygroscopic FeCl<sub>3</sub>.<sup>38,50,51,54,60,66,67</sup> Generally, it has been found that using additives such as TMEDA, NMP or hexamethylenetetramine (HMTA) with Fe(acac)<sub>3</sub> improved selectivity for cross-coupling over homo-coupling of the Grignard reagent. Recently, the Kozak group reported Fe(III) compounds supported by tetradentate and tridentate amine-bis(phenolate) ligands, which were effective catalysts for cross-coupling of aryl Grignard reagents with alkyl halides, including secondary alkyl halides and benzyl halides.<sup>68-70</sup> It was postulated whether amine-bis(phenolate)iron(acac) complexes would be active single-component catalysts for C-C cross-coupling of aryl Grignard reagents with alkyl halides.

This chapter describes the synthesis and structural, spectroscopic and electrochemical characterization of a series of these complexes and preliminary studies of their C-C cross coupling activity.

## 4.2 Results and Discussion

### 4.2.1 Ligand synthesis

The substituted amine-bis(phenol) compounds shown in Scheme 4.1 were prepared by modified literature procedures employing Mannich condensation of the corresponding phenol, amine and formaldehyde. Previously, these compounds have been prepared in refluxing methanol.<sup>7,10,71-74</sup> The use of water as a reaction medium proves much more effective at generating the desired compounds in higher yield and requires shorter heating time.<sup>75,76</sup> Following the same procedure, five amine-bis(phenol) ligands were synthesized (Figure 4.1). The synthesis and characterization of the linear tetradentate  $H_2[O_2N_2]^{BuBu}$  ligand was discussed in Chapter 2 of this thesis.



**Scheme 4.1** Synthesis of amine-bis(phenol) ligands.

Chapter 4. Synthesis, structure and C-C cross-coupling activity of amine-bis(phenolate)iron(acac) complexes

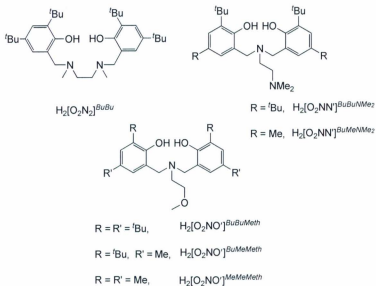
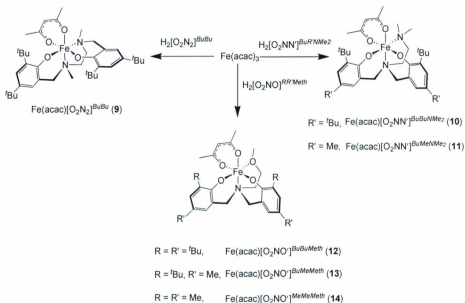


Figure 4.1 Library of amine-bis(phenol) ligands.

#### 4.2.2 Synthesis of Fe(III)(acac) complexes

Amine-bis(phenolate)Fe(acac) complexes were prepared by the method reported by Bouwman,<sup>77</sup> who examined pyridyl-substituted amine-bis(phenolate) complexes as catalytic driers of alkyd paints, and Chaudhuri, who performed electrochemical and magnetic studies on iron complexes of tetrahydrofurfuryl-substituted ligands.<sup>22</sup> Slow addition of a methanol solution of Fe(acac)<sub>3</sub> to a methanolic slurry of ligand under constant stirring, followed by addition of triethylamine gave the desired complexes (Scheme 4.2), which were precipitated from acetone solutions by the addition of water. The products thus obtained were generally found to be analytically pure, but in some

cases contamination with unreacted proligand was observed. A detailed analysis is given below.



**Scheme 4.2** Synthesis of amine-bis(phenolate)iron(III)acac complexes.

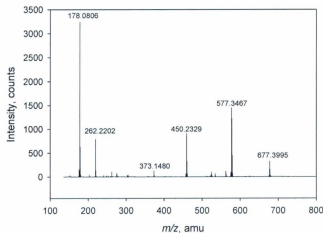
MALDI-TOF mass spectrometry was carried out on complexes **9-14** using anthracene as the matrix. The mass spectra of the complexes showed molecular ion peaks and characteristic fragment ions, namely the acetylacetonate ligand which was lost from the parent ion in all of these complexes, and  $[\text{M}-(\text{acac})]^+$  peaks were observed in all spectra. IR spectra of these compounds were recorded using a diamond crystal ATR module. Most of these complexes (**9**, **10**, **11**, **12** and **13**) showed two characteristic bands

at 1584 and 1520  $\text{cm}^{-1}$  corresponding to the  $\nu_{\text{CO}}$  of the acetylacetonate ligand. Complex **14** showed a band at 1571  $\text{cm}^{-1}$  instead of 1584  $\text{cm}^{-1}$ , possibly due to changes in the electron density at the metal caused by varying the substituents on the phenolate groups of the ligand.

### 4.2.3 Structural characterization

#### 4.2.3.1 MALDI-TOF Mass spectrometry

All the synthesized amine-bis(phenolate)iron(acac) complexes were paramagnetic in nature as they contained high-spin  $d^5$  iron centers. Therefore,  $^1\text{H}$  NMR was not suitable for the characterization of these paramagnetic complexes. However, MALDI-TOF mass spectrometry was employed as a primary characterization technique and anthracene was used as the matrix. The MALDI-TOF mass spectra of all these complexes showed the relevant molecular ion peaks and characteristic fragment ions after loss of the acetylacetonate co-ligand. For example, the MALDI-TOF mass spectrum of complex  $\text{Fe}(\text{acac})[\text{O}_2\text{N}_2]^{\text{BuBu}}$  (**9**) is shown in Figure 4.2. The molecular ion peak was observed at  $m/z$  677.4 amu, which is identical to the calculated molecular ion mass of  $m/z$  677.4 amu. A prominent fragment ion peak in the spectrum appeared at  $m/z$  577.3 amu corresponding to the  $[\text{M}-(\text{acac})-1]^+$  ion, which was generated by the loss of acetylacetonate co-ligand from the molecular ion. This peak has an excellent agreement with its calculated value of  $m/z$  577.3 amu.

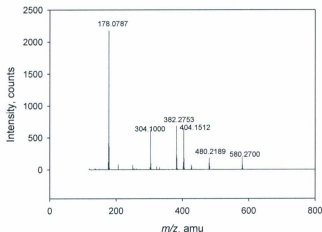


**Figure 4.2** MALDI-TOF mass spectrum of the complex  $\text{Fe}(\text{acac})[\text{O}_2\text{N}_2]^{\text{BuBu}}$  (**9**).

Similar to complex **9**, complex **13** was characterized by its MALDI-TOF mass spectrum. Figure 4.3 shows the mass spectrum of the complex **13**. The molecular ion peak of that complex was observed at  $m/z$  580.3 amu which is close to the calculated molecular ion mass of  $m/z$  580.3 amu. Another characteristic fragment ion peak in the spectrum was observed at  $m/z$  480.2 amu corresponding to the  $[\text{M}(\text{acac})-\text{I}]^+$  ion, which was generated by the loss of acetylacetonate co-ligand from the molecular ion. The mass of that peak is also close to its calculated value of  $m/z$  480.2 amu.

Similar to these two complexes, complexes **10**, **11**, **12** and **14** also showed molecular ion peaks and the fragment ion peaks formed by the loss of the acetylacetonate

co-ligand. The MALDI-TOF mass spectra of these four complexes are given in the Appendix of this thesis.



**Figure 4.3** MALDI-TOF mass spectrum of the complex  $\text{Fe}(\text{acac})[\text{O}_2\text{NO}^-]^{\text{BuMeMeth}}$  (**13**).

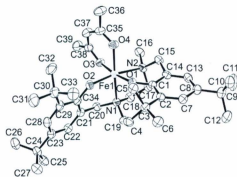
#### 4.2.3.2 Single crystal X-ray structure

Single crystals of complexes **9**, **10**, **11**, and **13** suitable for X-ray diffraction were obtained by slow evaporation of methanol/diethyl ether (1:1) solutions. Selected bond lengths and angles are given in Table 4.1 and crystallographic data are given in Table 4.6. In all complexes the iron ion was bonded to two phenolate oxygen atoms and two neutral donor atoms of the ligand. In all four complexes, the  $\beta$ -diketonate co-ligand was coordinated in the typical *cis*-fashion. The molecular structure of the complex **9** is shown in Figure 4.4. The asymmetric unit of complex **9** contained one chiral molecule but both

enantiomers were found in the unit cell. Methyl groups of the ethylenediamine fragment were *trans*-oriented. No *cis*-methyl-containing complex was present in the structure. Previously reported Fe(III)amine-bis(phenolate) halide complexes from the Kozak group using the same ligand also contained only *trans*-oriented *N,N'*-dimethylethylenediamine fragments.<sup>78</sup> However, a related structure reported by Girerd, Münck and co-workers contained both the *trans* and *cis* isomers.<sup>79</sup> The geometry of the iron(III) center was distorted octahedral. The O(2)-Fe(1)-N(2), O(4)-Fe(1)-N(1) and O(1)-Fe(1)-O(3) angles were 165.20(11)°, 167.26(11)° and 171.06(10)° respectively, which are less than the ideal linear geometry. The two phenolate oxygen atoms were *cis*-oriented, with O(2) lying *trans* to a backbone amine donor, N(2), and O(1) *trans* to an oxygen, O(3), of the acac ligand. The Fe(1)-O(1) and Fe(1)-O(2) distances were 1.900(2) Å and 1.880(2) Å, respectively. These bond lengths were similar to the Fe-O<sub>phenolate</sub> lengths observed in related distorted octahedral iron(III) complexes possessing phenolate ligands.<sup>22,77,80,81</sup> They were, however, longer than the average Fe-O bond distance in trigonal bipyramidal or square pyramidal complexes, as expected due to the higher coordination number.<sup>23,24,78,82,83</sup> Specifically, the Fe-O distances of this complex were longer than the Fe(1)-O(1) and Fe(1)-O(2) distances of 1.848(2) Å and 1.862(3) Å in FeCl[O<sub>2</sub>N<sub>2</sub>]<sup>84</sup> and 1.836(5) Å and 1.837(3) Å in FeBr[O<sub>2</sub>N<sub>2</sub>]<sup>85</sup>, which contain the same amine-bis(phenolate) ligand.<sup>78</sup> In complex **9**, the Fe(1)-N(1) and Fe(1)-N(2) bond lengths were 2.234(3) Å and 2.274(3) Å, respectively. The Fe(1)-N(2) length was slightly longer than Fe(1)-N(1) because it was *trans* to a strong phenolate oxygen donor. Typical Fe<sup>III</sup>-N distances in octahedral systems were ~ 2.15-2.20 Å.<sup>17-20,22,24,82-84</sup> The two Fe-O bonds of



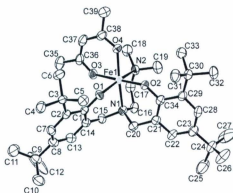
the acac ligand were not identical. The Fe(1)-O(4) bond, which was *trans* to an amine nitrogen donor, is 2.008(3) Å whereas the Fe(1)-O(3) *trans* to a phenolate oxygen donor was 2.064(3) Å. The lengths of O(1)-C(1) and O(2)-C(34) were around the average of ~1.33 Å found in metal complexes of amine-bis(phenolate) ligands.<sup>22,24,82</sup> The Fe-O-C bond angles of complex **9** were 138.4(2)° for Fe(1)-O(1)-C(1) and 137.8(2)° for Fe(1)-O(1)-C(34). These bond angles were larger than those observed in previously reported amine-bis(phenolate)Fe(acac) complexes<sup>22,77</sup> and suggest the O(1) and O(2) atoms possess a hybridization in between  $sp^2$  and  $sp$ .



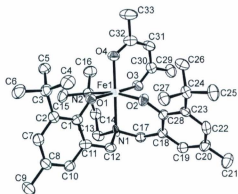
**Figure 4.4** ORTEP diagram and atom labeling scheme for the complex **9** (thermal ellipsoids shown at 50% probability). Hydrogen atoms removed for clarity.

The molecular structures of complexes **10** and **11** are shown in Figure 4.5 and Figure 4.6, respectively. Both of these complexes contained two independent molecules in each asymmetric unit. Although some bond lengths and angles varied between these

two molecules, metric parameters for only one of these independent molecules are presented in Table 4.1 for each of complexes **10** and **11**.



**Figure 4.5** ORTEP and atom labeling scheme for complex **10** (thermal ellipsoids shown at 50% probability). Hydrogen atoms removed for clarity.



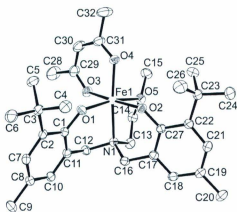
**Figure 4.6** ORTEP diagram and atom labeling scheme for complex **11** (thermal ellipsoids shown at 50% probability). Hydrogen atoms removed for clarity.

The geometries of the Fe(III) centers in both complexes were distorted octahedral. In complex **10**, the O(1)-Fe(1)-N(2), O(4)-Fe(1)-N(1) and O(2)-Fe(1)-O(3) angles were 160.43(16)°, 168.40(16)° and 177.32(15)°, respectively, which are less than the ideal linear geometry. Similarly in complex **11**, the O(2)-Fe(1)-N(2), O(4)-Fe(1)-N(1) and O(1)-Fe(1)-O(3) angles were 175.77(18)°, 173.26(79)° and 162.07(19)°, respectively. In complex **10**, the Fe(1)-O(1) distance was 1.907(3) Å and Fe(1)-O(2) was 1.899(3) Å. Whereas in complex **11**, the Fe(1)-O(1) distance was 1.882(4) Å and Fe(1)-O(2) was 1.881(4) Å. In both of these complexes, the Fe-O distances were similar to the Fe-O<sub>phenolate</sub> lengths observed in related distorted octahedral iron(III) complexes possessing phenolate ligands,<sup>22,77,80,81</sup> as well as in complex **10**. The two nitrogen donor atoms in the ligand showed bond lengths of 2.192(4) Å and 2.290(4) Å for Fe(1)-N(1) and Fe(1)-N(2), respectively, in **10**, and lengths of 2.120(6) Å and 2.263(5) Å for Fe(1)-N(1) and Fe(1)-

N(2), respectively, in **11**. In both complexes, the Fe(1)-N(2) distances were longer than the Fe(1)-N(1) distances because of the *trans*-positioned strong electron donating phenolate oxygen. In complex **10**, the Fe(1)-N(1) distance was similar to the previously reported Fe-N distance of amine-bis(phenolate)Fe(acac) complexes.<sup>22,77</sup> However, the Fe(1)-N(2) distance was longer than the relative Fe-N distance of the octahedral complexes.<sup>22,77,80,81</sup> In complex **11**, the Fe(1)-N(1) distance was shorter than the corresponding Fe-N distance of 2.181(3) Å in the related trigonal bipyramidal complex, FeCl[O<sub>2</sub>NO]<sup>BuMeNMe<sub>2</sub></sup> employing the same ligand.<sup>78</sup> In complexes **10** and **11**, the Fe(1)-O(3) distances were 2.072(4) Å and 2.066(4) Å, respectively which were slightly longer than the Fe(1)-O(4) distances of 1.987(4) Å and 1.983(4) Å because of their location *trans* to phenolate oxygens. The Fe-O-C bond angles Fe(1)-O(1)-C(1) of 131.3(3) Å and Fe(1)-O(2)-C(34) of 133.9(3) Å in **10** and Fe(1)-O(1)-C(1) of 133.7(4) Å and Fe(1)-O(2)-C(28) of 133.6(4) Å in **11** were similar to the previously reported amine-bis(phenolate)Fe(III)acac complexes.<sup>22,77</sup>

**Table 4.1** Selected bond lengths [ $\text{\AA}$ ] and angles [ $^\circ$ ] for the complex **9**, **10**, **11** and **13**.

	<b>9</b>	<b>10</b>	<b>11</b>	<b>13</b>
Fe(1)-O(1)	1.900(2)	1.907(3)	1.882(4)	1.8785(11)
Fe(1)-O(2)	1.880(2)	1.899(3)	1.881(4)	1.8979(11)
Fe(1)-O(3)	2.064(3)	2.072(4)	2.066(4)	2.0722(11)
Fe(1)-O(4)	2.008(3)	1.987(4)	1.983(4)	1.9897(11)
Fe(1)-O(5)				2.2174(11)
Fe(1)-N(1)	2.234(3)	2.192(4)	2.120(6)	2.2024(13)
Fe(1)-N(2)	2.274(3)	2.290(4)	2.263(5)	
O(1)-C( <i>ipso</i> )	1.334(4) "C1"	1.335(6) "C1"	1.331(7) "C1"	1.3333(18) "C1"
O(2)-C( <i>ipso</i> )	1.336(4) "C34"	1.330(6) "C34"	1.327(7) "C28"	1.3380(17) "C27"
O(1)-Fe(1)-O(2)	97.63(11)	97.13(15)	96.00(19)	101.55(5)
O(1)-Fe(1)-O(3)	171.06(10)	85.48(15)	175.77(18)	88.75(5)
O(1)-Fe(1)-O(4)	101.53(11)	103.83(15)	93.44(18)	101.73(5)
O(2)-Fe(1)-O(3)	91.38(11)	177.32(15)	88.22(19)	169.41(5)
O(2)-Fe(1)-O(4)	91.12(11)	93.43(15)	99.38(19)	94.26(5)
O(1)-Fe(1)-N(1)	97.52(11)	86.60(15)	90.67(18)	89.20(5)
O(2)-Fe(1)-N(1)	86.36(10)	90.24(15)	84.80(18)	89.90(5)
O(3)-Fe(1)-N(1)	84.76(10)	89.31(15)	89.37(19)	87.77(5)
O(4)-Fe(1)-N(1)	167.26(11)	168.40(16)	173.79(19)	167.25(5)
N(1)-Fe(1)-N(2)	79.08(11)	78.70(17)	80.62(18)	
O(1)-Fe(1)-N(2)	87.00(10)	160.43(16)	94.57(19)	
O(2)-Fe(1)-N(2)	165.20(11)	95.79(15)	162.07(19)	
O(3)-Fe(1)-N(2)	84.94(10)	81.53(15)	81.26(19)	
O(4)-Fe(1)-N(2)	92.36(11)	89.97(16)	94.40(19)	
O(1)-Fe(1)-O(5)				161.41(5)
O(2)-Fe(1)-O(5)				89.35(4)
O(3)-Fe(1)-O(5)				80.07(5)
O(4)-Fe(1)-O(5)				92.31(5)
Fe(1)-O(1)-C( <i>ipso</i> )	138.4(2) "C1"	131.3(3) "C1"	133.7(4) "C1"	135.42(10) "C1"
Fe(1)-O(2)-C( <i>ipso</i> )	137.8(2) "C34"	133.9(3) "C34"	133.6(4) "C28"	132.63(10) "C27"

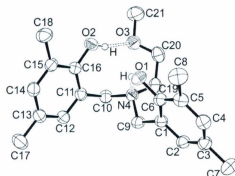


**Figure 4.7** ORTEP diagram and atom labeling scheme for complex **13** (thermal ellipsoids shown at 50% probability). Hydrogen atoms are removed for clarity.

The molecular structure of complex **13** is shown in Figure 4.7. Unlike **10** and **11**, the asymmetric unit of complex **13** contained one molecule. The iron ion was bonded to two phenolate oxygen atoms, one neutral nitrogen donor and the oxygen of the ether pendant arm. The  $\beta$ -diketonate co-ligand was coordinated in the typical *cis*-fashion. The geometry of the iron(III) center was distorted octahedral. The two phenolate-oxygens were *cis*-oriented with one lying *trans* to the ether oxygen and the other *trans* to an oxygen of the acac ligand. The angles O(1)-Fe(1)-O(5), O(4)-Fe(1)-N(1) and O(2)-Fe(1)-O(3) were 161.41(5)°, 167.25(5)°, 169.41(5)°, respectively, which are less than true linear geometry. The Fe(1)-O(1) and Fe(1)-O(2) distances were 1.8785(11) Å and 1.8979(11) Å which are similar to those in complexes **9**, **10** and **11**. The Fe(1)-N(1) distance was 2.2024(13) Å, which is consistent with the other three complexes discussed earlier. As with complexes **9**, **10** and **11**, the Fe(1)-O(3) distance of 2.0722(11) Å was

slightly longer than the Fe(1)-O(4) distance of 1.9897(11) Å because of the *trans*-positioned phenolate oxygen donor. The Fe(1)-O(1)-C(1) bond angle was 135.42(10)° and Fe(1)-O(2)-C(27) was 132.63(10)°. The Fe(1)-O(1)-C(1) angle was slightly larger than that of complexes **10** and **11** but smaller than that of complex **9**. However the Fe(1)-O(2)-C(27) angle was smaller than that of the other three complexes, **9**, **10** and **11**.

Reaction of  $\text{H}_2[\text{O}_2\text{NO}]^{\text{MeMeMeth}}$  with  $\text{Fe}(\text{acac})_3$  and triethylamine afforded complex **14** as confirmed by MALDI-TOF-MS and FTIR. However, contamination with  $\text{H}_2[\text{O}_2\text{NO}]^{\text{MeMeMeth}}$  was evident. Recrystallization from methanol/diethyl ether solution gave bright red-coloured crystals; however, X-ray diffraction showed these crystals to be  $\text{H}_2[\text{O}_2\text{NO}]^{\text{MeMeMeth}}$ . Because of the similar solubilities of **14** and  $\text{H}_2[\text{O}_2\text{NO}]^{\text{MeMeMeth}}$ , it was not possible to obtain pure **14** or to remove  $\text{H}_2[\text{O}_2\text{NO}]^{\text{MeMeMeth}}$  from the product. Multiple recrystallization steps still showed contamination by  $\text{H}_2[\text{O}_2\text{NO}]^{\text{MeMeMeth}}$ . The structure of  $\text{H}_2[\text{O}_2\text{NO}]^{\text{MeMeMeth}}$  is shown in Figure 4.8. Selected bond lengths and angles are given in Table 4.2 and crystallographic data are given in Table 4.6.



**Figure 4.8** ORTEP diagram and atom labeling scheme for the  $\text{H}_2[\text{O}_2\text{NO}]^{\text{MeMeMe}}$  ligand (thermal ellipsoids shown at 50% probability). Only O-H bonded hydrogens atoms are shown.

**Table 4.2** Selected bond lengths [ $\text{\AA}$ ] and angles [ $^\circ$ ] for  $\text{H}_2[\text{O}_2\text{NO}]^{\text{MeMeMe}}$ .

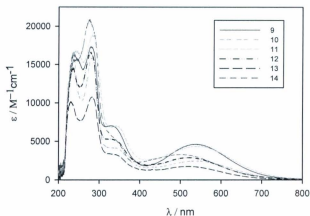
O(1)-C(6)	1.3704(17)	O(1)-C(6)-C(1)	121.25(13)
O(2)-C(16)	1.3752(16)	O(1)-C(6)-C(5)	118.14(12)
O(3)-C(20)	1.427(2)	O(2)-C(16)-C(15)	116.57(12)
O(3)-C(21)	1.414(2)	O(2)-C(16)-C(11)	122.47(12)
N(4)-C(9)	1.4684(19)	C(21)-O(3)-C(20)	112.50(15)
N(4)-C(10)	1.4864(18)	C(10)-N(4)-C(9)	109.39(11)
N(4)-C(19)	1.4730(18)	C(19)-N(4)-C(9)	111.76(12)

#### 4.2.3.3 Electronic absorption data

Electronic absorption spectra of all the amine-bis(phenolate)Fe(acac) complexes were recorded in methanol solution (Figure 4.9). Spectra of all the complexes showed multiple intense bands in the UV and visible regions. In complexes **9-14**, intense absorptions were observed in the near-UV regions (below 300 nm). These were caused



by  $\pi \rightarrow \pi^*$  transitions involving the phenolate units and possibly the  $\pi_3 \rightarrow \pi_4$  transition of the acetylacetonate (acac) ligands. Absorptions around 240 nm were observed in the spectra of unmetallated ligand precursors but the absorptions around 280 nm are also observed in amine-bis(phenolate) complexes not containing acac ligands.<sup>21,78,85</sup> Two absorptions between 340-550 nm were assigned as charge-transfer transitions from ligand-to-metal (LMCT). The high energy bands around 340 nm arose from the transitions between the  $p_\pi$  orbital of the phenolate oxygen and the half filled  $d_{x^2-y^2}/d_{z^2}$  orbital of high-spin-Fe(III). The lowest energy bands around 550 nm were proposed to arise from charge-transfer transitions from the  $p_\pi$  orbital of the phenolate to the half-filled  $d_{\pi^*}$  orbital of high-spin, Fe(III). Another band around 355 nm was assigned to the metal-to-ligand transition of the metal  $d_{xz}$  or  $d_{yz}$  orbital to the  $\beta$ -diketonate  $\pi_4$  orbital, in agreement with the assignment of bands in the spectrum observed for  $\text{Fe}(\text{acac})_3$ .<sup>86,87</sup> However, this band also overlapped with the bands arising from phenolate oxygen-to-metal transitions in complexes **9-14**.



**Figure 4.9** Electronic absorption spectra of complexes **9-14** in methanol.

Previously, LMCT bands of amine-bis(phenolate)Fe(III) halide complexes have been reported and these exhibited a noticeable solvent-dependant shift to higher frequency according to the following trend: methanol < THF < toluene < acetonitrile, where the absorption spectrum in acetonitrile showed this band at lowest wavelength (496 nm) down from 607 nm in methanol.<sup>78</sup> The influence of solvent polarity on the charge transfer transitions of amine-bis(phenolate)Fe(III)(acac) complexes was studied. Complexes **9** and **11** were investigated in four different solvents: methanol, THF, toluene and acetonitrile (Figure 4.10 and Figure 4.11). The two lower energy bands of complex **9** in four different solvents were found not to vary significantly and were observed around 340 and 550 nm. Specifically, the lowest energy LMCT bands were observed in different solvents at the following wavelengths: Toluene (550 nm), THF (547 nm), MeOH (545

nm) and MeCN (535 nm). It appears that only a minor solvent-dependant shift was observed because of the multidentate nature of the acac and  $[O_2N_2]$  ligands, which prohibits ligand dissociation or structural distortion in solution. This might also be due to the rigidity of the ligand backbone of complex **9**. For complex **11**, the lowest energy bands were found to have a small but more noticeable solvent-dependant shift: Toluene (565 nm), MeCN (545 nm), MeOH (543 nm) and THF (534 nm) (Figure 4.11). The slightly stronger shift might be attributed to the presence of a potentially more labile pendant neutral donor, which could undergo dissociation in good donor solvents such as THF. The stronger solvent dependence observed in the halide containing compounds was possibly a result of the highly labile halide ligands, which have been shown to dissociate in solution.<sup>78</sup> Hence donor solvents were very likely to coordinate to the metal and influence the ligand field.

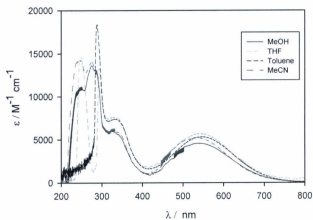


Figure 4.10 Electronic absorption spectra of **9** in methanol, THF, toluene and acetonitrile solutions.

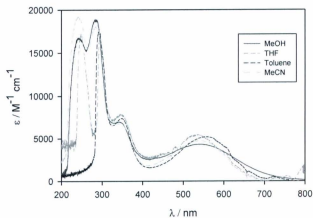


Figure 4.11 Electronic absorption spectra of **11** in methanol, THF, toluene and acetonitrile solutions.

#### 4.2.3.4 FT-IR Spectroscopy

FT-IR spectra of all the synthesized amine-bis(phenolate)Fe(III)(acac) complexes were recorded using a diamond crystal ATR module. All of the spectra showed multiple peaks in the fingerprint region and between 1200 and 1600  $\text{cm}^{-1}$ . Also, around 3000  $\text{cm}^{-1}$ , two peaks were observed for aromatic C=C and aliphatic C-H stretching of the ligand backbone. Most importantly, all of these complexes showed two characteristic peaks around 1520 and 1571  $\text{cm}^{-1}$  corresponding to the  $\nu_{\text{CO}}$  of the acetylacetonate co-ligand while bonded to the metal center. Figure 4.12 shows a representative IR spectrum of complex  $\text{Fe}(\text{acac})[\text{O}_2\text{NN}^{\text{BuMeNM}_2}]$  (**11**) where two characteristic peaks were observed at 1585 and 1519  $\text{cm}^{-1}$  respectively. The IR spectrum of amine-bis(phenol) ligands did not contain these two peaks (Figure 4.13). However, in the IR spectrum of  $\text{Fe}(\text{acac})[\text{O}_2\text{NO}^{\text{MeMeMeth}}]$  (**14**) one of the characteristic peaks shifted from 1584  $\text{cm}^{-1}$  to 1571  $\text{cm}^{-1}$  (Figure 4.14). This might be due to a different electronic environment at the metal center resulting from the substituent groups on the phenolate rings of the ligands.

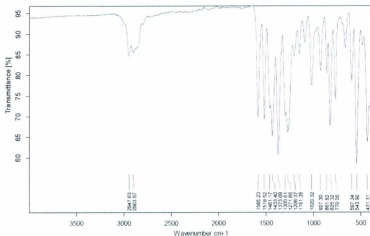


Figure 4.12 IR spectrum of  $\text{Fe}(\text{acac})[\text{O}_2\text{NN}']^{\text{BuMeNMe}_2}$  (11).

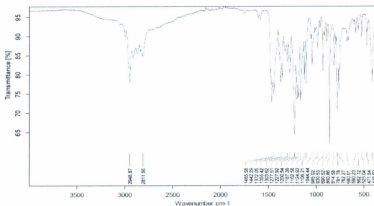


Figure 4.13 IR spectrum of ligand  $\text{H}_2[\text{O}_2\text{NN}']^{\text{BuMeNMe}_2}$ .

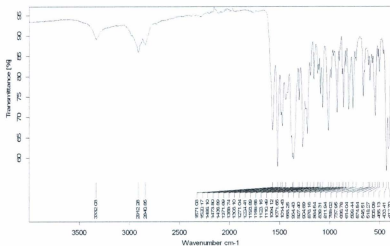


Figure 4.14 IR spectrum of the complex  $\text{Fe}(\text{acac})[\text{O}_2\text{NO}]^{\text{MeMeMeth}}$  (14).

#### 4.2.3.5 Magnetic Properties

Magnetic susceptibility data for crystalline samples of complexes **9-13** were collected at room temperature using a Johnson-Matthey magnetic susceptibility balance. Average magnetic moments in the solid state were adjusted for diamagnetic corrections using Pascal's constants. The magnetic moments [ $\mu_{\text{eff}} = (8\chi_{\text{m}}T)^{1/2}$ ] of complexes **9-13** are given in Table 4.3. The magnetic moments of these complexes were in the range of 5.4 to 6.1  $\mu_{\text{B}}$ . For complex **12**, the magnetic moment was measured to be 5.4  $\mu_{\text{B}}$ , which was slightly lower than expected for a high-spin  $d^5$  ion. As mentioned above, this might be due to the presence of unreacted ligand, which was difficult to separate from the iron complexes. The elemental analysis of the sample used for measurement supported the presence of 6%  $\text{H}_2[\text{O}_2\text{NO}]^{\text{BuBuMeth}}$  impurity. Complexes **9**, **10**, **11** and **13** showed

References begin on page 208

magnetic moments between 5.8 and 6.1  $\mu_B$ , which were within the expected range for high-spin octahedral Fe(III) complexes.

**Table 4.3** Effective magnetic moments for complexes **9-13** in the solid state.

Complex	$\mu_{\text{eff}} / \mu_B$	Complex	$\mu_{\text{eff}} / \mu_B$
<b>9</b>	6.1	<b>12</b>	5.4
<b>10</b>	6.0	<b>13</b>	6.0
<b>11</b>	5.8		

#### 4.2.3.6 Cyclic voltammetry

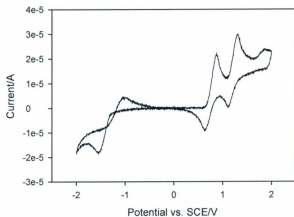
Electrochemistry experiments were carried out using a three-compartment electrochemical cell, consisting of a platinum counter electrode, saturated-calomel reference electrode (SCE) and a glassy-carbon working electrode. Complexes **9-14** were investigated by cyclic voltammetry (CV) in  $\text{CH}_2\text{Cl}_2$  solutions containing 0.1 M [*n*-Bu)<sub>4</sub>N]PF<sub>6</sub> as electrolyte. The results are summarized in Table 4.4 and representative cyclic voltammograms of **9** and **12** are shown in Figure 4.15 and Figure 4.16, respectively. Voltammograms of **10**, **11**, **13**, and **14** are given in the Appendix. All experiments were performed at a scan rate of 100 mV s<sup>-1</sup>. The CVs of complexes **9** and **12** were similar and displayed two reversible oxidation peaks and one quasi-reversible (or irreversible) reduction peak, and were consistent with electrochemical studies for a related Fe(acac) complex bearing an amine-bis(phenolate) ligand with a tetrahydrofurfuryl pendant arm.<sup>22</sup> Complexes **10**, **11**, **13** and **14** exhibited reversible oxidation responses.



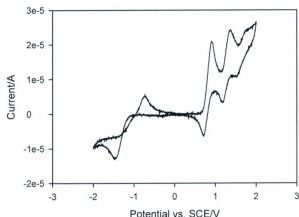
**Table 4.4** Electrode peak potentials for oxidation and reduction of complexes **9** to **14**.

Compound	$E^2 / V$	$E^1 / V$	$E^3 / V$
<b>9</b>	$E^2_{1/2} = +1.22^a$	$E^1_{1/2} = +0.77^a$	$E^3_{p,red} = -1.55,$ $E^3_{p,ox} = -1.02$
<b>10</b>	$E^2_{p,ox} = +1.38,$ $E^2_{p,red} = +1.20$	$E^1_{p,ox} = +0.78,$ $E^1_{p,red} = +0.31$	$E^3_{p,red} = -1.55,$ $E^3_{p,ox} = -0.76$
<b>11</b>	$E^2_{p,ox} = +1.34,$ $E^2_{p,red} = +1.11$	$E^1_{p,ox} = +0.79,$ $E^1_{p,red} = +0.54$	$E^3_{p,red} = -1.55,$ $E^3_{p,ox} = -0.79$
<b>12</b>	$E^2_{1/2} = +1.27^a$	$E^1_{1/2} = +0.81^a$	$E^3_{p,red} = -1.47,$ $E^3_{p,ox} = -0.72$
<b>13</b>	$E^2_{p,ox} = +1.51,$ $E^2_{p,red} = +1.51$	$E^1_{p,ox} = +0.90,$ $E^1_{p,red} = +0.65$	$E^3_{p,red} = -1.33,$ $E^3_{p,ox} = -0.78$
<b>14</b>	$E^2_{p,ox} = +1.21,$ $E^2_{p,red} = +1.13$	$E^1_{p,ox} = +0.83,$ $E^1_{p,red} = +0.67$	$E^3_{p,red} = -1.10,$ $E^3_{p,ox} = -0.82$

<sup>a</sup> Reversible reaction,  $E_{1/2}$  is given.



**Figure 4.15** Cyclic voltammogram of **9** in  $CH_2Cl_2$  (0.1M  $[(n-Bu)_4N]PF_6$ ) at 25 °C and a scan rate of 100  $mV s^{-1}$ .



**Figure 4.16** Cyclic voltammogram of **12** in  $\text{CH}_2\text{Cl}_2$  (0.1M  $[(n\text{-Bu})_4\text{N}]\text{PF}_6$ ) at 25 °C and a scan rate of  $100 \text{ mV s}^{-1}$ .

These events might be ligand centered redox couples, *i.e.* phenolate/phenoxy radical, or a metal centered Fe(III)/Fe(IV) redox process, which has been proposed for a related Fe(acac)amine-bis(phenolate) complex bearing a pyridyl pendant arm.<sup>77</sup> However, metal-centered oxidations are unlikely in these complexes because of difficulties in attaining the less stable Fe(IV) oxidation state. Complexes **9-14** showed quasi-reversible or irreversible redox events at negative potentials. These might be attributed to one-electron metal-centered  $\text{Fe}^{\text{II}}/\text{Fe}^{\text{III}}$  redox couples.

#### 4.2.4 Cross-coupling catalysis studies

The Kozak group has reported that Fe(III) complexes supported by amine-bis(phenolate) ligands are suitable catalysts for C-C cross-coupling of aryl Grignard reagents with alkyl halides including alkyl chlorides bearing  $\beta$ -hydrogens. Iron(III) halide compounds based on tetradentate amine-bis(phenolate) ligands showed good activity as catalysts for the cross-coupling of aryl Grignards with primary and secondary alkyl halides,<sup>70</sup> but the presence of halide groups on the phenolate groups led to decreased activity.<sup>68</sup> With these systems, diethyl ether was superior as a solvent to THF for cross-coupling reactions. Also, it was found that reactions performed at room temperature or higher gave superior results to those conducted at lower temperatures.<sup>69</sup> Recent results showed that Fe(III) compounds based on tridentate amine-bis(phenolate) ligands showed better catalytic activity towards selected cross-coupling reactions than their tetradentate counterparts.<sup>69</sup> In some cases, the use of microwave-assisted heating of the reaction mixture improved the yields. Here, the halide anion in the tetradentate amine-bis(phenolate)iron complexes has been replaced with an acac co-ligand, and the effect on catalytic activity was examined. The present study employed amine-bis(phenolate)Fe(III)(acac) complexes as catalysts for cross-coupling of *o*-tolylmagnesium bromide with 2° alkyl halides in diethyl ether at room temperature or at 100 °C using microwave-assisted heating. The results of this study are summarized in Table 4.5. An initial reaction of cyclohexyl bromide with *o*-tolylmagnesium bromide in the presence of complex **9** gave an excellent yield of cross-coupled product after 30 minutes at room temperature. Cyclohexyl chloride could also be used as the electrophilic

References begin on page 208

partner, but yields of product varied depending on the catalyst used. Catalysts employing a ligand with an amine pendent arm gave relatively lower yields of cross-coupled products (Table 4.5, Entries 2 and 3). However, ligands with ether pendent arms gave excellent yields (up to 96%) of cross-coupled products (Entries 4-6). There have been only a few reports of Kumada type cross-coupling using cyclohexyl chloride. Bedford and co-workers showed good to modest yields (70-80%) of cross-coupled products between cyclohexyl chloride and *p*-tolylmagnesium bromide using different Fe-based catalysts such as Fe(salen) complexes, FeCl<sub>3</sub>/amine and Fe nanoparticles.<sup>65,88,89</sup> Nakamura and co-workers obtained 99% yield of cross-coupled product from cyclohexyl chloride and phenylmagnesium bromide while using FeCl<sub>3</sub>/TMEDA (TMEDA = tetramethylethylenediamine) as catalyst.<sup>58</sup> Their procedure required the slow addition of Grignard reagent to the reaction mixture. Also, they noticed that TMEDA suppressed the formation of undesirable side products *via* the loss of hydrogen halide from the alkyl halides.


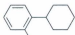








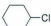

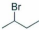
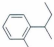
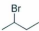

Complexes 9-14 were investigated for cross-coupling of the acyclic secondary alkyl halide, 2-bromobutane with *o*-tolylmagnesium bromide. In these reactions, poor yields (12-17%) of cross-coupled products were observed (Entries 7 to 12). This was in stark contrast to the promising results observed by Nakamura and co-workers for the cross-coupling of 2-bromobutane with phenylmagnesium bromide, where 94% yield of cross-coupled product was obtained using FeCl<sub>3</sub>/TMEDA.<sup>58</sup> Recently, Cahiez and co-workers reported using the combination of Fe(acac)<sub>3</sub> and TMEDA/HMTA (HMTA = hexamethylenetetramine) (10% TMEDA:5% HMTA vs. alkyl halide).<sup>51</sup> In both cases,

Grignard reagents were added slowly to the reaction mixture. Whereas 2-bromobutane and 2-iodobutane gave excellent yields, only a trace amount of cross-coupled product was obtained using 2-chlorobutane as the alkyl halide. Using our system, 12% of cross-coupled product using 2-chlorobutane and *o*-tolylmagnesium bromide was obtained (Entry 13), although our catalysts did not give good results for 2-bromobutane. Fe(acac)<sub>3</sub> showed excellent catalytic activity for the cross-coupled of secondary alkyl halide and aryl Grignard reagents in the presence of additives TMEDA and HMTA.<sup>51</sup> Also, Fe(acac)<sub>3</sub> without any additives has been reported as an efficient catalyst for the cross-coupling of aryl Grignard reagents and alkyl halides possessing β-hydrogens.<sup>60</sup> However, Fe(acac)<sub>3</sub> under the conditions studied here gave only 17% yield of cross-coupled products using 2-bromobutane.

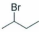
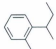
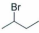

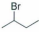

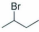
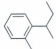
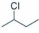
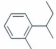
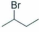

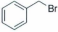
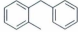
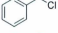
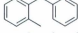
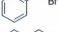
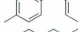


Recently Bedford and co-workers reported iron catalyzed Negishi coupling of benzyl halides with diaryl zinc and Fe-Zn co-catalyzed Suzuki coupling of benzyl halides with tetraarylborate.<sup>90,91</sup> The cross-coupling of benzyl halides (Br and Cl) with *o*-tolylmagnesium bromide and *p*-tolylmagnesium bromide was studied in the presence of complex **12**. Reaction of benzyl bromide with *o*-tolyl Grignard gave 60% yield of cross-coupled product after 30 min at room temperature (Entry 15). Benzyl chloride gave a similarly moderate yield (Entry 16). Using *p*-tolylmagnesium bromide, however, gave slightly lower yields than *o*-tolylmagnesium bromide with the respective benzyl halide (Entries 17 and 18). All the GC-MS spectra and <sup>1</sup>H and <sup>13</sup>C NMR spectra of particular cross-coupling products are given in the appendix. These preliminary studies show amine-bis(phenolate)Fe(III)(acac) complexes have some catalytic activity towards cross-

coupling of aryl Grignard reagents with alkyl halides. However, for the substrates studied thus far, they were generally inferior to simple  $\text{Fe}(\text{acac})_3$ -containing systems<sup>38,50,51,54,60,66,67</sup> or amine-bis(phenolate)iron halide complexes previously reported by the Kozak group.<sup>70,92</sup>

**Table 4.5** Cross coupling of aryl Grignard reagents with alkyl halides catalyzed by amine-bis(phenolate)Fe(acac) complexes.<sup>a</sup>

Entry	Complex	Alkyl halide	Product	Yield (%)
1	<b>9</b>			97 <sup>b</sup>
2	<b>10</b>			33
3	<b>11</b>			55
4	<b>12</b>			96
5	<b>13</b>			80
6	<b>14</b>			79
7	<b>9</b>			17
8	<b>10</b>			12

Chapter 4. Synthesis, structure and C-C cross-coupling activity of amine-bis(phenolate)iron(acac) complexes

9	11			16
10	12			13
11	13			16
12	14			14
13	13			12
14	Fe(acac) <sub>3</sub>			17
15	12			60 <sup>b</sup>
16	12			52 <sup>b</sup>
17	12			49 <sup>b</sup>
18	12			37 <sup>b</sup>

**Reaction conditions:** Catalyst (0.05 mmol), alkyl halide (1.00 mmol), Et<sub>2</sub>O (1.50 mL), Grignard reagent (2.00 mmol), dodecane as internal standard (1.0 mmol), MW heating 100 °C for 10 min. The reaction was quenched by addition of 2.50 mL of 1.00 M HCl (aq). The product yields were quantified by GC-MS and confirmed by NMR. <sup>b</sup> Stirred at 25 °C for 30 min.

### **4.3 Conclusion**

A series of Fe(III)(acac) complexes supported by amine-bis(phenolate) ligands has been synthesized and characterized. Representative complexes **9**, **10**, **11** and **13** have been structurally characterized by single crystal X-ray diffraction and all complexes reported contained six-coordinate Fe(III) centers and exhibited distorted octahedral geometries. Moreover, all of these paramagnetic complexes were analytically verified by elemental analysis and MALDI-TOF mass spectrometry. Magnetic moment measurements indicated high-spin  $d^5$  iron centers. Electronic absorption spectra in the UV-vis range exhibited strong charge-transfer bands, which were slightly solvent dependent. Cyclic voltammograms of these complexes showed reversible ligand-centered redox processes. Preliminary studies of all the complexes for the catalytic cross-coupling of aryl Grignard reagents with alkyl halides were performed and showed the coupling of *o*-tolylmagnesium bromide with cyclohexyl chloride was influenced by the amine-bis(phenolate) ligand employed. Generally, the yield of arylcyclohexane was high. However, acyclic 2-halobutane showed poor yields of product whereas benzylhalides showed moderate activity for cross-coupling. Investigations for other substrates are currently in progress.

### **4.4 Experimental Section**

#### **4.4.1 General considerations**

Unless otherwise stated, all manipulations were performed in air. Reagents were purchased either from Aldrich or Alfa Aesar and used without further purification. The



syntheses of  $\text{H}_2[\text{O}_2\text{N}_2]^{BuBu}$  to  $\text{H}_2[\text{O}_2\text{NO}]^{MeMeMeth}$  were conducted by modified literature procedure in water,<sup>75,76</sup> and a representative synthesis of  $\text{H}_2[\text{O}_2\text{NO}]^{BuMeMeth}$  and other ligands characterization data are given below.  $\text{Fe}(\text{acac})_3$  (99%) was purchased from Strem Chemicals. Anhydrous diethyl ether was purified using an MBraun Solvent Purification System.

#### **4.4.2 Instrumentation**

NMR spectra were recorded in  $\text{CDCl}_3$  on a Bruker Avance III 300 MHz instrument with a 5 mm multinuclear broadband observe (BBFO) probe. MALDI-TOF MS spectra were performed using an ABI QSTAR XL Applied Biosystems/MDS hybrid quadrupole TOF MS/MS system equipped with an oMALDI-2 ion source. Samples were prepared at a concentration of  $10.0 \text{ mg mL}^{-1}$  in toluene. Anthracene was used as the matrix, which was mixed at a concentration of  $10.0 \text{ mg mL}^{-1}$ . UV-vis spectra were recorded on an Ocean Optics USB4000+ fiber optic spectrophotometer. IR spectra were recorded on a Bruker Alpha IR spectrometer equipped with a diamond crystal ATR module. Room temperature magnetic moments were determined using a Johnson-Matthey magnetic susceptibility balance. The data were corrected for the diamagnetism of all atoms and the balance was calibrated using  $\text{Hg}[\text{Co}(\text{NCS})_4]$ . Cyclic voltammetry measurements were performed on a Model HA 301 Hokuto Deuko Potentiostat/Galvanostat. Elemental analyses were carried out by Canadian Microanalytical Services Ltd. Delta, BC, Canada. Gas chromatography mass spectrometry (GC-MS) analyses were performed using an Agilent Technologies 7890GC

system coupled to an Agilent Technologies 5975C mass selective detector (MSD). The chromatograph is equipped with electronic pressure control, split/splitless and on-column injectors, and an HP5 MS column. Microwave-heated reactions were performed using a Biotage Initiator™ Eight microwave synthesizer.

#### 4.4.3 X-Ray crystallography

Crystallographic data for compounds **9**, **10**, **11**, **13** and  $\text{H}_2[\text{O}_2\text{NO}]^{\text{MeMeMeth}}$  are summarized in Table 4.6. All data collections were performed on a Rigaku AFC8-Saturn 70 diffractometer equipped with a CCD area detector, using graphite monochromated Mo-K $\alpha$  radiation ( $\lambda = 0.71073 \text{ \AA}$ ). Suitable crystals were selected and mounted on glass fibers using Paratone-N oil and freezing to  $-120 \text{ }^\circ\text{C}$ , or  $-100 \text{ }^\circ\text{C}$  in the case of  $\text{H}_2[\text{O}_2\text{NO}]^{\text{MeMeMeth}}$ . The data were processed<sup>93,94</sup> and corrected for Lorentz and polarization effects and absorption.<sup>95</sup> Neutral atom scattering factors for all non-hydrogen atoms were taken from the International Tables for X-ray Crystallography.<sup>96</sup> All structures were solved by direct methods using SIR92<sup>97</sup> and expanded using Fourier techniques (DIRDIF99).<sup>98</sup> All non-hydrogen atoms were refined anisotropically. Hydrogen atoms were refined using the riding model.

Anomalous dispersion effects were included in  $F_{\text{calc}}$ .<sup>99</sup> The values for  $\Delta f'$  and  $\Delta f''$  were those of Creagh and McAuley.<sup>100</sup> The values for the mass attenuation coefficients are those of Creagh and Hubbell.<sup>101</sup> All calculations were performed using the CrystalStructure<sup>102,103</sup> crystallographic software package except for refinement, which was performed using SHELXL-97.<sup>104</sup> In complexes **10** and **11**, two chemical formula unit

*Chapter 4. Synthesis, structure and C-C cross-coupling activity of amine-bis(phenolate)iron(acac) complexes*

moieties are present in the asymmetric unit, and therefore Z was set to 8 in order to reflect the formula per one moiety. In complex **10**, one *tert*-butyl group is disordered over two sites. This was refined in two parts; PART 1 (C(64), C(65), C(66) and corresponding H-atoms) are present at 0.8-occupancy, while PART 2 (C(67), C(68), C(69) and corresponding H-atoms) are present at 0.2-occupancy. ISOR restraints were introduced in order to prevent C(67) and C(69) from becoming non-definite positive. Structural illustrations were created using ORTEP-III for Windows.<sup>105</sup>

**Table 4.6** Crystallographic and structural refinement data for compounds **9**, **10**, **11**, **13** and  $\text{H}_2[\text{O}_2\text{NO}]^{\text{Mo/MoMth}}$

Compound reference	<b>9</b>	<b>10</b>	<b>11</b>
Chemical formula	$\text{C}_{39}\text{H}_{61}\text{FeN}_2\text{O}_4$	$\text{C}_{39}\text{H}_{61}\text{FeN}_2\text{O}_4$	$\text{C}_{33}\text{H}_{49}\text{FeN}_2\text{O}_4$
Formula Mass	677.77	677.77	593.61
Crystal system	Orthorhombic	Monoclinic	Monoclinic
$a/\text{\AA}$	13.9905(15)	13.7115(19)	10.158(3)
$b/\text{\AA}$	20.485(3)	23.240(3)	23.434(7)
$c/\text{\AA}$	27.491(3)	27.809(4)	27.388(8)
$\alpha/^\circ$	90.00	90.00	90.00
$\beta/^\circ$	90.00	115.343(3)	90.045(8)
$\gamma/^\circ$	90.00	90.00	90.00
Unit cell volume/ $\text{\AA}^3$	7878.9(16)	8008.7(19)	6520(3)
Temperature/K	153(2)	153(2)	153(2)
Space group	<i>Pbca</i>	<i>P2<sub>1</sub>/c</i>	<i>P2<sub>1</sub>/c</i>
No. of formula units per unit cell, <i>Z</i>	8	8	8
Radiation type	MoK $\alpha$	MoK $\alpha$	MoK $\alpha$
Absorption coefficient, $\mu/\text{mm}^{-1}$	0.421	0.414	0.499
No. of reflections measured	80834	106542	49036
No. of independent reflections	8155	14074	11284
$R_{\text{int}}$	0.0929	0.1091	0.0796
Final $R_I$ values ( $I > 2\sigma(I)$ )	0.0923	0.1093	0.1100
Final $wR(F^2)$ values ( $I > 2\sigma(I)$ )	0.1549	0.1999	0.2564
Final $R_I$ values (all data)	0.0961	0.1193	0.1183
Final $wR(F^2)$ values (all data)	0.1563	0.2045	0.2619
Goodness of fit on $F^2$	1.455	1.342	1.176

Chapter 4. Synthesis, structure and C-C cross-coupling activity of amine-bis(phenolate)iron(acac) complexes

Compound reference	<b>13</b>	<b>H<sub>2</sub>[O<sub>2</sub>NO<sup>-</sup>]<sup>MeMeMeth</sup></b>
Chemical formula	C <sub>32</sub> H <sub>46</sub> FeNO <sub>5</sub>	C <sub>21</sub> H <sub>29</sub> NO <sub>3</sub>
Formula Mass	580.57	343.45
Crystal system	Monoclinic	Orthorhombic
<i>a</i> /Å	9.5103(12)	8.7923(5)
<i>b</i> /Å	23.403(3)	13.8917(9)
<i>c</i> /Å	14.5291(19)	16.3005(10)
$\alpha$ /°	90.00	90.00
$\beta$ /°	104.444(2)	90.00
$\gamma$ /°	90.00	90.00
Unit cell volume/Å <sup>3</sup>	3131.5(7)	1990.9(2)
Temperature/K	153(2)	173(2)
Space group	<i>P</i> 2 <sub>1</sub> / <i>c</i>	<i>P</i> 2 <sub>1</sub> 2 <sub>1</sub>
No. of formula units per unit cell, <i>Z</i>	4	4
Radiation type	MoK $\alpha$	MoK $\alpha$
Absorption coefficient, $\mu$ /mm <sup>-1</sup>	0.519	0.076
No. of reflections measured	41710	21544
No. of independent reflections	7144	5472
<i>R</i> <sub>int</sub>	0.0318	0.0263
Final <i>R</i> <sub>i</sub> values ( <i>I</i> > 2 $\sigma$ ( <i>I</i> ))	0.0396	0.0473
Final <i>wR</i> ( <i>F</i> <sup>2</sup> ) values ( <i>I</i> > 2 $\sigma$ ( <i>I</i> ))	0.1049	0.1417
Final <i>R</i> <sub>i</sub> values (all data)	0.0413	0.0487
Final <i>wR</i> ( <i>F</i> <sup>2</sup> ) values (all data)	0.1068	0.1444
Goodness of fit on <i>F</i> <sup>2</sup>	1.086	1.076

#### 4.4.4 Synthesis of ligands

A small library of amine-bis(phenol) ligands was synthesized following the literature procedure.<sup>75</sup> <sup>1</sup>H and <sup>13</sup>C NMR data of the ligands H<sub>2</sub>[O<sub>2</sub>N<sub>2</sub>]<sup>BuBu</sup>, H<sub>2</sub>[O<sub>2</sub>NO<sup>-</sup>]<sup>BuBuMeth</sup> and H<sub>2</sub>[O<sub>2</sub>NO<sup>-</sup>]<sup>MeMeMeth</sup> are presented in Chapter 2 of this thesis. However, a representative synthesis of H<sub>2</sub>[O<sub>2</sub>NO<sup>-</sup>]<sup>BuMeMeth</sup> and <sup>1</sup>H and <sup>13</sup>C NMR data of

Chapter 4. Synthesis, structure and C-C cross-coupling activity of amine-bis(phenolate)iron(acac) complexes

the other ligands are presented here. Original characterization data of the ligands  $\text{H}_2[\text{O}_2\text{NN}']^{\text{BuBuNMe}_2}$ ,  $\text{H}_2[\text{O}_2\text{NN}']^{\text{BuMeNMe}_2}$  were obtained by Kol and co-workers.<sup>10,72</sup>

**$\text{H}_2[\text{O}_2\text{NO}']^{\text{BuMeMeth}}$** : 2-Methoxyethylamine (4.63 g, 0.0616 mol) was added to a vigorously stirred mixture of 2-*tert*-butyl-4-methylphenol (20.236 g, 0.1232 mol) and 37% aqueous formaldehyde (9.17 mL, 0.1232 mol) in water (50 mL). The mixture was heated to reflux for 12 h. Upon cooling, a large quantity of beige solid formed. The solvents were decanted and the remaining solid residue was washed with cold methanol to give a white powder (25.00 g, 95% yield). Crystalline product was obtained by slow cooling of a hot diethyl ether solution. <sup>1</sup>H NMR (300 MHz, 295 K,  $\delta$ ): 8.40 (s, 2H, OH); 7.0 (d, <sup>4</sup> $J_{\text{HH}} = 1.5$  Hz, 2H, ArH); 6.72 (d, <sup>4</sup> $J_{\text{HH}} = 1.5$  Hz, 2H, ArH); 3.71 (s, 4H, ArCH<sub>2</sub>); 3.52 (t, <sup>3</sup> $J_{\text{HH}} = 5.1$  Hz, 2H, CH<sub>2</sub>O); 3.46 (s, 3H, OCH<sub>3</sub>); 2.73 (t, <sup>3</sup> $J_{\text{HH}} = 5.1$  Hz, 2H, NCH<sub>2</sub>); 2.24 (s, 6H, ArCH<sub>3</sub>); 1.41 (s, 18H, ArC(CH<sub>3</sub>)<sub>3</sub>). <sup>13</sup>C{<sup>1</sup>H} (75 MHz, 295K,  $\delta$ ): 153.04 (Ar-C-OH); 136.83 (Ar-CH); 128.79 (Ar-CH); 127.36 (Ar-CH); 127.24 (Ar-CH); 122.44 (Ar-C-CH<sub>2</sub>-N); 71.51 (Ar-CH<sub>2</sub>); 58.86 (OCH<sub>3</sub>); 51.37 (N-CH<sub>2</sub>-CH<sub>2</sub>-O); 57.62 (N-CH<sub>2</sub>-CH<sub>2</sub>-O); 34.71 (C(CH<sub>3</sub>)<sub>3</sub>); 29.57 (C(CH<sub>3</sub>)<sub>3</sub>); 20.78 (Ar-CH<sub>3</sub>).

**$\text{H}_2[\text{O}_2\text{NN}']^{\text{BuBuNMe}_2}$** : <sup>1</sup>H NMR (300 MHz, 295 K,  $\delta$ ): 9.78 (s, 2H, OH); 7.19 (d, <sup>4</sup> $J_{\text{HH}} = 2.5$  Hz, 2H, ArH); 6.87 (d, <sup>4</sup> $J_{\text{HH}} = 2.5$  Hz, 2H, ArH); 3.60 (s, 4H, ArCH<sub>2</sub>); 2.58 (t, <sup>3</sup> $J_{\text{HH}} = 4.0$  Hz, 4H, NCH<sub>2</sub>CH<sub>2</sub>NMe<sub>2</sub>); 2.30 (s, 6H, NMe<sub>2</sub>); 1.38 (s, 18H, ArC(CH<sub>3</sub>)<sub>3</sub>); 1.26 (s, 18H, ArC(CH<sub>3</sub>)<sub>3</sub>). <sup>13</sup>C{<sup>1</sup>H} (75 MHz, 295K,  $\delta$ ): 153.30 (Ar-C-OH); 140.17 (Ar-CH); 136.09 (Ar-CH); 124.83 (Ar-CH); 123.35 (Ar-CH); 121.63 (Ar-CH); 56.60 (Ar-CH<sub>2</sub>); 55.95

(N(CH<sub>3</sub>)<sub>2</sub>); 49.07 (N-CH<sub>2</sub>-CH<sub>2</sub>-NMe<sub>2</sub>); 44.90(N-CH<sub>2</sub>-CH<sub>2</sub>-NMe<sub>2</sub>); 35.04 (C(CH<sub>3</sub>)<sub>3</sub>);  
34.10 (C(CH<sub>3</sub>)<sub>3</sub>); 31.75 (C(CH<sub>3</sub>)<sub>3</sub>); 29.58(C(CH<sub>3</sub>)<sub>3</sub>).

**H<sub>2</sub>[O<sub>2</sub>N<sub>2</sub>]<sup>BuMeNMe<sub>2</sub></sup>**: <sup>1</sup>H NMR (300 MHz, 295 K, δ): 9.64 (s, 2H, OH); 6.97 (d, <sup>4</sup>J<sub>HH</sub> = 2.2 Hz, 2H, ArH); 6.69 (d, <sup>4</sup>J<sub>HH</sub> = 2.2 Hz, 2H, ArH); 3.54 (s, 4H, ArCH<sub>2</sub>); 2.54 (t, <sup>3</sup>J<sub>HH</sub> = 3.7 Hz, 4H, NCH<sub>2</sub>CH<sub>2</sub>NMe<sub>2</sub>); 2.27 (s, 6H, NMe<sub>2</sub>); 2.16 (s, 6H, Ar-CH<sub>3</sub>); 1.36 (s, 18H, ArC(CH<sub>3</sub>)<sub>3</sub>). <sup>13</sup>C {<sup>1</sup>H} (75 MHz, 295K, δ): 153.40 (Ar-C-OH); 136.85 (Ar-CH); 128.75 (Ar-CH); 127.10 (Ar-CH); 126.71 (Ar-CH); 122.51 (Ar-CH); 56.03 (Ar-CH<sub>2</sub>); 55.80 (N(CH<sub>3</sub>)<sub>2</sub>); 49.03 (N-CH<sub>2</sub>-CH<sub>2</sub>-NMe<sub>2</sub>); 44.77 (N-CH<sub>2</sub>-CH<sub>2</sub>-NMe<sub>2</sub>); 34.74 (C(CH<sub>3</sub>)<sub>3</sub>); 29.55 (C(CH<sub>3</sub>)<sub>3</sub>); 20.79 (Ar-CH<sub>3</sub>).

#### 4.4.5 Synthesis of metal complexes

**Fe(acac)[O<sub>2</sub>N<sub>2</sub>]<sup>BuBu</sup> (9)**: To a methanolic slurry of recrystallized H<sub>2</sub>[O<sub>2</sub>N<sub>2</sub>]<sup>BuBu</sup>, (1.53 g, 2.92 mmol) was added a solution of Fe(acac)<sub>3</sub> (1.03 g, 2.92 mmol) in methanol with stirring resulting in a brown-red solution. To this solution was added triethylamine (590 mg, 5.84 mmol) followed by heating to 64 °C for 0.5 h. The solution's colour changed to dark-purple. The solvent was evaporated and the residue dissolved in acetone (50 mL). Addition of an equal volume of H<sub>2</sub>O precipitates the complex, which was collected on a frit and dried *in vacuo* to obtain 1.20 g (61%) of dark-purple powder. Crystals suitable for X-ray diffraction were obtained by slow evaporation of a solution of **9** in a 1:1 mixture of methanol and diethyl ether. Anal. Calcd for C<sub>39</sub>H<sub>61</sub>FeN<sub>2</sub>O<sub>4</sub>: C, 69.11; H, 9.07; N, 4.13%. Found C, 68.51; H, 9.11; N, 4.29%. MALDI-TOF MS (positive mode, anthracene); *m/z* (% of ion): 677.40 (25, [M]<sup>+</sup>), 577.35 (100, [M-acac-  
References begin on page 208

1]⁺). UV-vis (CH<sub>3</sub>OH) λ<sub>max</sub>, nm (ε): 237 (16600), 279 (17325), 327 (7009), 540 (4614). IR (neat): ν (cm<sup>-1</sup>) = 2954, 2902, 2865, 1584, 1521, 1465, 1441, 1375, 1360, 1307, 1274, 1250, 1237, 1203, 1167, 1129, 1017, 967, 929, 914, 875, 840, 808, 791, 780, 766, 748, 612, 545, 469, 450, 431. μ<sub>eff</sub> (solid, 21.8 °C): 6.1 μ<sub>B</sub>.

**Fe(acac)[O<sub>2</sub>NN']<sup>BuBuNMe<sub>2</sub></sup> (10):** To a methanolic slurry of recrystallized H<sub>2</sub>[O<sub>2</sub>NN']<sup>BuBuNMe<sub>2</sub></sup> (3.51 g, 6.68 mmol) was added a solution of Fe(acac)<sub>3</sub> (2.36 g, 6.68 mmol) in methanol with stirring resulting in a brown-red solution. To this solution was added triethylamine (1.35 g, 13.37 mmol) followed by heating to 64 °C for 0.5 h. The solution's colour changed to dark-purple. The solvent was evaporated and the residue dissolved in acetone (50 mL). Addition of an equal volume of H<sub>2</sub>O precipitates the complex, which was collected on a frit and dried *in vacuo* to obtain 3.02 g (67%) of dark-purple powder. Crystals suitable for X-ray diffraction were obtained by slow evaporation of a solution of **10** in a 1:1 mixture of methanol and diethyl ether. Anal. Calcd for C<sub>39</sub>H<sub>61</sub>FeN<sub>2</sub>O<sub>4</sub>: C, 69.11; H, 9.07; N, 4.13%. Found C, 69.44; H, 9.13; N, 4.18%. MALDI-TOF MS (positive mode, anthracene); *m/z* (% of ion): 677.40 (9, [M]<sup>+</sup>), 577.35 (9, [M-acac-1]<sup>+</sup>), 466.35 (100, [M-acac-Fe-C<sub>3</sub>H<sub>9</sub>N+2H]<sup>+</sup>). UV-vis (CH<sub>3</sub>OH) λ<sub>max</sub>, nm (ε): 236 (16626), 279 (15865), 316 (4306), 535 (2441). IR (neat): ν (cm<sup>-1</sup>) = 2951, 2903, 2866, 1587, 1520, 1479, 1465, 1442, 1415, 1376, 1360, 1303, 1284, 1268, 1256, 1228, 1201, 1165, 1125, 1107, 1023, 925, 876, 840, 824, 809, 775, 748, 666, 544, 472, 429, 406. μ<sub>eff</sub> (solid, 21.8 °C): 6.0 μ<sub>B</sub>.

**Fe(acac)[O<sub>2</sub>NN']<sup>BuMeNMe<sub>2</sub></sup> (11):** To a methanolic slurry of recrystallized H<sub>2</sub>[O<sub>2</sub>NN']<sup>BuMeNMe<sub>2</sub></sup> (3.01 g, 6.81 mmol) was added a solution of Fe(acac)<sub>3</sub> (2.41 g, 6.81



mmol) in methanol with stirring resulting in a brown-red solution. To this solution was added triethylamine (1.37 g, 13.56 mmol) followed by heating to 64 °C for 0.5 h. The solution's colour changed to dark-purple. The solvent was evaporated and the residue was dissolved in acetone (50 mL). Addition of an equal volume of H<sub>2</sub>O precipitates the complex, which was collected on a frit and dried *in vacuo* to obtain 2.85 g (71%) of dark-purple powder. Crystals suitable for X-ray diffraction were obtained by slow evaporation of a solution of **11** in a 1:1 mixture of methanol and diethyl ether. Anal. Calcd for C<sub>33</sub>H<sub>49</sub>FeN<sub>2</sub>O<sub>4</sub>: C, 66.77; H, 8.32; N, 4.72%. Found C, 66.91; H, 8.24; N, 4.76%. MALDI-TOF MS (positive mode, anthracene); *m/z* (% of ion): 593.30 (8, [M]<sup>+</sup>), 496.26 (16, [M-acac]<sup>+</sup>). UV-vis (CH<sub>3</sub>OH) λ<sub>max</sub>, nm (ε): 243 (16747), 284 (18893), 343 (6952), 522 (4326). IR (neat): ν (cm<sup>-1</sup>) = 2949, 2905, 1585, 1519, 1462, 1434, 1374, 1301, 1274, 1207, 1151, 1019, 927, 862, 825, 770, 665, 597, 545, 431, 403. μ<sub>eff</sub> (solid, 21.8 °C): 5.8 μ<sub>B</sub>.

**Fe(acac)[O<sub>2</sub>NO]<sup>BuBuMeth</sup> (12)**: To a methanolic slurry of recrystallized H<sub>2</sub>[O<sub>2</sub>NO]<sup>BuBuMeth</sup> (3.30 g, 6.46 mmol) was added a solution of Fe(acac)<sub>3</sub> (2.28 g, 6.46 mmol) in methanol with stirring resulting in a brown-red solution. To this solution was added triethylamine (1.31 g, 12.92 mmol) followed by heating to 64 °C for 0.5 h. The solution's colour changed to dark-purple. The solvent was evaporated and the residue was dissolved in acetone (50 mL). Addition of an equal volume of H<sub>2</sub>O precipitates the complex, which was collected on a frit and dried *in vacuo* to obtain 2.52 g (59%) of dark-purple powder. Crystals suitable for X-ray diffraction were obtained by slow evaporation of a solution of **12** in a 1:1 mixture of methanol and diethyl ether. Anal. Calcd for

References begin on page 208

$C_{38}H_{58}FeNO_5$ : C, 68.66; H, 8.79; N, 2.11%. Calcd for  $12 \cdot 0.06 H_2[O_2NO]^{BuMeMeth}$ : C, 69.05; H, 8.87; N, 2.13. Found C, 69.09; H, 8.85; N, 2.19%. MALDI-TOF MS (positive mode, anthracene);  $m/z$  (% of ion): 664.37 (36,  $[M]^+$ ), 564.32 (7,  $[M-acac-1]^+$ ), 511.41 (57,  $[L_3]^+$ ), 466.37 (100,  $[M-acac-Fe-C_2H_5O+2H]^+$ ). UV-vis ( $CH_3OH$ )  $\lambda_{max}$  nm ( $\epsilon$ ): 235 (14575), 277 (16612), 340 (5142), 522 (2887). IR (neat):  $\nu$  ( $cm^{-1}$ ) = 2954, 2904, 2868, 1585, 1521, 1474, 1442, 1381, 1363, 1299, 1273, 1233, 1202, 1165, 1123, 1096, 1018, 932, 878, 840, 771, 657, 549, 481, 437, 407.  $\mu_{eff}$  (solid, 18.2 °C): 5.4  $\mu_B$ .

**Fe(acac)[O<sub>2</sub>NO]<sup>BuMeMeth</sup> (13)**: To a methanolic slurry of recrystallized  $H_2[O_2NO]^{BuMeMeth}$ , (3.11 g, 7.27 mmol) was added a solution of  $Fe(acac)_3$  (2.57 g, 7.27 mmol) in methanol with stirring resulting in a brown-red solution. To this solution was added triethylamine (1.56 g, 14.54 mmol) followed by heating to 64 °C for 0.5 h. The solution's colour changed to dark-purple. The solvent was evaporated and the residue was dissolved in acetone (50 mL). Addition of an equal volume of  $H_2O$  precipitates the complex, which was collected on a frit and dried *in vacuo* to obtain 2.98 g (71%) of obtain dark-purple powder. Crystals suitable for X-ray diffraction were obtained by slow evaporation of a solution of **13** in a 1:1 mixture of methanol and diethyl ether. Anal. Calcd for  $C_{32}H_{46}FeNO_5$ : C, 66.20; H, 7.99; N, 2.41%. Found C, 66.10; H, 8.08; N, 2.42%. MALDI-TOF MS (positive mode, anthracene);  $m/z$  (% of ion): 580.27 (29,  $[M]^+$ ), 480.22 (26,  $[M-acac-1]^+$ ) 382.28 (100,  $[M-acac-Fe-C_2H_5O + 2H]^+$ ). UV-vis ( $CH_3OH$ )  $\lambda_{max}$ , nm ( $\epsilon$ ): 232 (10275), 282 (10771), 342 (3263), 522 (1742). IR (neat):  $\nu$  ( $cm^{-1}$ ) = 2953, 2910, 1581, 1521, 1469, 1437, 1365, 1298, 1270, 1232, 1204, 1150, 1094, 1059, 1016, 927, 861, 826, 770, 663, 595, 549, 434, 406.  $\mu_{eff}$  (solid, 18.8 °C): 6.0  $\mu_B$ .

**Fe(acac)[O<sub>2</sub>NO]<sup>MeMeMeth</sup> (14):** To a methanolic slurry of recrystallized H<sub>2</sub>[O<sub>2</sub>NO]<sup>MeMeMeth</sup>, (2.61 g, 7.60 mmol) was added a solution of Fe(acac)<sub>3</sub> (2.68 g, 7.60 mmol) in methanol with stirring resulting in a brown-red solution. To this solution was added triethylamine (1.54 g, 15.21 mmol) followed by heating to 64 °C for 0.5 h. The solution's colour changed to dark-purple. The solvent was evaporated and the residue was dissolved in acetone (50 mL). Addition of an equal volume of H<sub>2</sub>O precipitates the complex, which was collected on a frit and dried *in vacuo* to obtain 2.89 g (77%) of dark-purple powder. The product contained a consistently high degree of contamination with proligand H<sub>2</sub>[O<sub>2</sub>NO]<sup>MeMeMeth</sup>. Therefore, satisfactory combustion analyses could not be obtained and crystals of proligand always contaminated crystals of the complex. MALDI-TOF MS (positive mode, anthracene); *m/z* (% of ion): 496.18 (20, [M]<sup>+</sup>), 397.13 (50, [M-acac]<sup>+</sup>). UV-vis (CH<sub>3</sub>OH) λ<sub>max</sub>, nm (ε): 240 (14684), 277 (19617), 344 (4705), 544 (3088). IR (neat): ν (cm<sup>-1</sup>) = 2912, 2845, 1570, 1520, 1478, 1438, 1364, 1306, 1267, 1226, 1158, 1117, 1073, 1016, 929, 866, 809, 768, 663, 600, 549, 507, 434, 411.

#### 4.4.6 General method for cross-coupling catalysis

*Method A.* Procedure for cross-coupling at room temperature: The selected iron complex (0.10 mmol) in CH<sub>2</sub>Cl<sub>2</sub> (3 mL) was added to a 45 mL Schlenk tube and the solvent removed *in vacuo*. To the catalyst were added Et<sub>2</sub>O (5 mL) and alkyl halide (2.0 mmol). To this vigorously stirred solution was added a solution of aryl Grignard reagent (4.0 mmol) dropwise. The resulting mixture was stirred for 30 min, then dodecane (2.0 mmol as internal standard) was added and the reaction quenched with 5 mL 1.0 M

HCl(aq). The organic phase was extracted with Et<sub>2</sub>O (5 mL) and dried over MgSO<sub>4</sub>. The mixture was analyzed by GC-MS and NMR.

*Method B.* Procedure for cross-coupling under microwave-heating: The selected iron complex (0.05 mmol) and a magnetic stir bar were added to a Biotage™ microwave vial, which was sealed with a septum cap. A solution of alkyl halide (1.0 mmol) in Et<sub>2</sub>O (2.5 mL) was injected into the vial, followed by 2.00 mmol of Grignard reagent solution. The mixture was heated in a Biotage Initiator™ Eight Microwave Synthesizer using the following parameters: time = 10 min; *T* = 100 °C; pre-stirring = off; absorption level = normal; fixed hold time = on. Upon completion, 1.00 mmol of dodecane (internal standard) was added to the mixture followed by 2.5 mL of 1.0M HCl(aq) to quench. The product yields were quantified by GC-MS and NMR.

#### 4.4.7 <sup>1</sup>H and <sup>13</sup>C{<sup>1</sup>H} NMR spectral data of cross-coupled products

**1-Cyclohexyl-2-methylbenzene:** <sup>1</sup>H NMR (300 MHz, 295 K, CDCl<sub>3</sub>): δ = 7.04-7.24 (m, 4H); 2.71 (m, 1H), 2.32 (s, 3H); 1.83 (m, 5H); 1.37 (m, 5H). <sup>13</sup>C{<sup>1</sup>H} NMR (75 MHz, 295 K, CDCl<sub>3</sub>): δ = 19.41, 26.43, 26.99, 33.74, 40.18, 125.38, 125.43, 126.16, 130.26, 135.16, 145.97.

**1-Sec-butyl-2-methylbenzene:** <sup>1</sup>H NMR (300 MHz, 295 K, CDCl<sub>3</sub>): δ = 7.04-7.21 (m, 4H); 2.89 (sextet, *J*<sub>HH</sub> = 7.0, 1H); 2.32 (s, 3H); 1.59 (m, 2H); 1.20 (d, <sup>3</sup>*J*<sub>HH</sub> = 7.0, 3H); 0.86 (t, <sup>3</sup>*J*<sub>HH</sub> = 7.4, 3H). <sup>13</sup>C{<sup>1</sup>H} NMR (75 MHz, 295 K, CDCl<sub>3</sub>): δ = 12.33, 19.63, 21.20, 30.58, 36.21, 125.35, 126.14, 130.15, 135.45, 145.89.

**1-benzyl-2-methylbenzene:**  $^1\text{H}$  NMR (300 MHz, 295 K,  $\text{CDCl}_3$ ):  $\delta$  = 7.09-7.28 (m, 9H); 3.98 (s, 2H); 2.24 (s, 3H).  $^{13}\text{C}\{^1\text{H}\}$  NMR (75 MHz, 295 K,  $\text{CDCl}_3$ ):  $\delta$  = 19.80, 39.60, 126.05, 126.13, 128.52, 128.87, 130.09, 130.42, 135.91, 136.74, 139.05, 140.52.

**1-benzyl-4-methylbenzene:**  $^1\text{H}$  NMR (300 MHz, 295 K,  $\text{CDCl}_3$ ):  $\delta$  = 7.04-7.48 (m, 9H); 3.93 (s, 2H); 2.30 (s, 3H).  $^{13}\text{C}\{^1\text{H}\}$  NMR (75 MHz, 295 K,  $\text{CDCl}_3$ ):  $\delta$  = 21.16, 41.60, 126.06, 126.89, 128.42, 128.89, 128.95, 129.23, 129.52, 136.76, 138.37, 141.86.

#### 4.5 References

1. A. Yeori, I. Goldberg and M. Kol, *Macromolecules*, 2007, **40**, 8521-8523.
2. A. Yeori, I. Goldberg, M. Shuster and M. Kol, *J. Am. Chem. Soc.*, 2006, **128**, 13062-13063.
3. S. Gendler, S. Segal, I. Goldberg, Z. Goldschmidt and M. Kol, *Inorg. Chem.*, 2006, **45**, 4783-4790.
4. S. Segal, I. Goldberg and M. Kol, *Organometallics*, 2005, **24**, 200-202.
5. S. Groysman, E. Y. Tshuva, I. Goldberg, M. Kol, Z. Goldschmidt and M. Shuster, *Organometallics*, 2004, **23**, 5291-5299.
6. S. Groysman, I. Goldberg, M. Kol, E. Genizi and Z. Goldschmidt, *Inorg. Chim. Acta*, 2003, **345**, 137-144.
7. E. Y. Tshuva, I. Goldberg and M. Kol, *J. Am. Chem. Soc.*, 2000, **122**, 10706-10707.
8. C. Lorber, F. Wolff, R. Choukroun and L. Vendier, *Eur. J. Inorg. Chem.*, 2005, 2850-2859.

*Chapter 4. Synthesis, structure and C-C cross-coupling activity of amine-bis(phenolate)iron(acac) complexes*

9. A. J. Chmura, M. G. Davidson, M. D. Jones, M. D. Lunn, M. F. Mahon, A. F. Johnson, P. Khunkamchoo, S. L. Roberts and S. S. F. Wong, *Macromolecules*, 2006, **39**, 7250-7257.
10. Y. Sarazin, R. H. Howard, D. L. Hughes, S. M. Humphrey and M. Bochmann, *Dalton Trans.*, 2006, 340-350.
11. F. M. Kerton, A. C. Whitwood and C. E. Willans, *Dalton Trans.*, 2004, 2237-2244.
12. H. E. Dyer, S. Huijser, A. D. Schwarz, C. Wang, R. Duchateau and P. Mountford, *Dalton Trans.*, 2008, 32-35.
13. F. Bonnet, A. R. Cowley and P. Mountford, *Inorg. Chem.*, 2005, **44**, 9046-9055.
14. A. Amgoune, C. M. Thomas and J. F. Carpentier, *Pure Appl. Chem.*, 2007, **79**, 2013-2030.
15. A. Amgoune, C. M. Thomas, T. Roisnel and J. F. Carpentier, *Chem. Eur. J.*, 2006, **12**, 169-179.
16. Y. M. Yao, M. T. Ma, X. P. Xu, Y. Zhang, Q. Shen and W. T. Wong, *Organometallics*, 2005, **24**, 4014-4020.
17. T. Nagataki and S. Itoh, *Chem. Lett.*, 2007, **36**, 748-749.
18. L. Rodriguez, E. Labisbal, A. Sousa-Pedrares, J. A. Garcia-Vazquez, J. Romero, M. L. Duran, J. A. Real and A. Sousa, *Inorg. Chem.*, 2006, **45**, 7903-7914.
19. A. Philibert, F. Thomas, C. Philouze, S. Hamman, E. Saint-Aman and J. L. Pierre, *Chem. Eur. J.*, 2003, **9**, 3803-3812.

*Chapter 4. Synthesis, structure and C-C cross-coupling activity of amine-bis(phenolate)iron(acac) complexes*

20. O. Rotthaus, F. Thomas, O. Jarjayes, C. Philouze, E. Saint-Aman and J. L. Pierre, *Chem. Eur. J.*, 2006, **12**, 6953-6962.
21. U. K. Das, J. Bobak, C. Fowler, S. E. Hann, C. F. Petten, L. N. Dawe, A. Decken, F. M. Kerton and C. M. Kozak, *Dalton Trans.*, 2010, **39**, 5462-5477.
22. E. Safaei, T. Weyhermüller, E. Bothe, K. Wieghardt and P. Chaudhuri, *Eur. J. Inorg. Chem.*, 2007, 2334-2344.
23. J. B. H. Strautmänn, S. DeBeer, George, E. Bothe, E. Bill, T. Weyhermüller, A. Stämmler, H. Bögge and T. Glaser, *Inorg. Chem.*, 2008, **47**, 6804-6824.
24. T. Weyhermüller, T. K. Paine, E. Bothe, E. Bill and P. Chaudhuri, *Inorg. Chim. Acta*, 2002, **337**, 344-356.
25. W. A. Chomitz, S. G. Minasian, A. D. Sutton and J. Arnold, *Inorg. Chem.*, 2007, **46**, 7199-7209.
26. H. Adams, N. A. Bailey, I. K. Campbell, D. E. Fenton and Q.-Y. He, *J. Chem. Soc., Dalton Trans.*, 1996, 2233-2237.
27. M. C. B. de Oliveira, M. Scarpellini, A. Neves, H. Terenzi, A. J. Bortoluzzi, B. Szpoganics, A. Greatti, A. S. Mangrich, E. M. de Sousa, P. M. Fernandez and M. R. Soares, *Inorg. Chem.*, 2005, **44**, 921-929.
28. S. Ito, S. Nishino, H. Itoh, S. Ohba and Y. Nishida, *Polyhedron*, 1998, **17**, 1637-1642.
29. I. A. Koval, M. Huisman, A. F. Stassen, P. Gamez, M. Lutz, A. L. Spek and J. Reedijk, *Eur. J. Inorg. Chem.*, 2004, 591-600.

30. M. M. Olmstead, T. E. Patten and C. Troeltzsch, *Inorg. Chim. Acta*, 2004, **357**, 619-624.
31. N. Reddig, D. Pursche and A. Rompel, *Dalton Trans.*, 2004, 1474-1480.
32. N. Reddig, D. Pursche, B. Krebs and A. Rompel, *Inorg. Chim. Acta*, 2004, **357**, 2703-2712.
33. N. Reddig, D. Pursche, M. Kloskowski, C. Slinn, S. M. Baldeau and A. Rompel, *Eur. J. Inorg. Chem.*, 2004, 879-887.
34. S. Sarkar, A. Mondal, J. Ribas, M. G. B. Drew, K. Pramanik and K. K. Rajak, *Eur. J. Inorg. Chem.*, 2004, 4633-4639.
35. Y. Shimazaki, S. Huth, S. Karasawa, S. Hirota, Y. Naruta and O. Yamauchi, *Inorg. Chem.*, 2004, **43**, 7816-7822.
36. J. K. Kochi, *Acc. Chem. Res.*, 1974, **7**, 351-360.
37. A. C. Frisch and M. Beller, *Angew. Chem. Int. Ed.*, 2005, **44**, 674-688.
38. A. Fürstner and R. Martin, *Chem. Lett.*, 2005, **34**, 624-629.
39. W. M. Czaplik, M. Mayer, J. Cvengros and A. Jacobi von Wangelin, *ChemSusChem*, 2009, **2**, 396-417.
40. A. Rudolph and M. Lautens, *Angew. Chem. Int. Ed.*, 2009, **48**, 2656-2670.
41. A. Fürstner, *Angew. Chem. Int. Ed.*, 2009, **48**, 1364-1367.
42. B. D. Sherry and A. Fürstner, *Acc. Chem. Res.*, 2008, **41**, 1500-1511.
43. A. Fürstner, H. Krause and C. W. Lehmann, *Angew. Chem. Int. Ed.*, 2006, **45**, 440-444.
44. R. Martin and A. Fürstner, *Angew. Chem. Int. Ed.*, 2004, **43**, 3955-3957.



*Chapter 4. Synthesis, structure and C-C cross-coupling activity of amine-bis(phenolate)iron(acac) complexes*

45. A. Fürstner and A. Leitner, *Angew. Chem. Int. Ed.* 2003, **42**, 308-311.
46. A. Fürstner, D. De Souza, L. Parra-Rapado and J. T. Jensen, *Angew. Chem. Int. Ed.*, 2003, **42**, 5358-5360.
47. A. Fürstner and A. Leitner, *Angew. Chem. Int. Ed.*, 2002, **41**, 609-612.
48. A. Fürstner, A. Leitner, M. Mendez and H. Krause, *J. Am. Chem. Soc.*, 2002, **124**, 13856-13863.
49. G. Cahiez, A. Moyeux, J. Buendia and C. Duplais, *J. Am. Chem. Soc.*, 2007, **129**, 13788-13789.
50. G. Cahiez, C. Duplais and A. Moyeux, *Org. Lett.*, 2007, **9**, 3253-3254.
51. G. Cahiez, V. Habiak, C. Duplais and A. Moyeux, *Angew. Chem. Int. Ed.*, 2007, **46**, 4364-4366.
52. G. Cahiez, C. Chaboche, F. Mahuteau-Betzer and M. Ahr, *Org. Lett.*, 2005, **7**, 1943-1946.
53. W. Dohle, F. Kopp, G. Cahiez and P. Knochel, *Synlett*, 2001, 1901-1904.
54. G. Cahiez and H. Avedissian, *Synthesis*, 1998, 1199-1205.
55. C. Duplais, F. Bures, I. Sapountzis, T. J. Korn, G. Cahiez and P. Knochel, *Angew. Chem., Int. Ed.*, 2004, **43**, 2968-2970.
56. T. Hatakeyama, S. Hashimoto, K. Ishizuka and M. Nakamura, *J. Am. Chem. Soc.*, 2009, **131**, 11949-11963.
57. T. Hatakeyama and M. Nakamura, *J. Am. Chem. Soc.*, 2007, **129**, 9844-9845.
58. M. Nakamura, K. Matsuo, S. Ito and E. Nakamura, *J. Am. Chem. Soc.*, 2004, **126**, 3686-3687.

*Chapter 4. Synthesis, structure and C-C cross-coupling activity of amine-bis(phenolate)iron(acac) complexes*

59. T. Hatakeyama, Y. Yoshimoto, T. Gabriel and M. Nakamura, *Org. Lett.*, 2008, **10**, 5341-5344.
60. T. Nagano and T. Hayashi, *Org. Lett.*, 2004, **6**, 1297-1299.
61. K. G. Dongol, H. Koh, M. Sau and C. L. L. Chai, *Adv. Synth. Catal.*, 2007, **349**, 1015-1018.
62. C. C. Kofink, B. Blank, S. Pagano, N. Goetz and P. Knochel, *Chem. Commun.*, 2007, 1954-1956.
63. J. Norinder, A. Matsumoto, N. Yoshikai and E. Nakamura, *J. Am. Chem. Soc.*, 2008, **130**, 5858-5859.
64. M. Carril, A. Correa and C. Bolm, *Angew. Chem. Int. Ed.*, 2008, **47**, 4862-4865.
65. R. B. Bedford, D. W. Bruce, R. M. Frost, J. W. Goodby and M. Hird, *Chem. Commun.*, 2004, 2822-2823.
66. G. A. Molander, B. J. Rahn, D. C. Shubert and S. E. Bonde, *Tetrahedron Lett.*, 1983, **24**, 5449-5452.
67. N. Ostergaard, B. T. Pedersen, N. Skjaerbaek, P. Vedso and M. Begtrup, *Synlett*, 2002, 1889-1891.
68. A. M. Reckling, D. Martin, L. N. Dawe, A. Decken and C. M. Kozak, *J. Organomet. Chem.*, 2011, **696**, 787-794.
69. X. Qian, L. N. Dawe and C. M. Kozak, *Dalton Trans.*, 2011, **40**, 933-943.
70. R. R. Chowdhury, A. K. Crane, C. Fowler, P. Kwong and C. M. Kozak, *Chem. Commun.*, 2008, 94-96.

Chapter 4. Synthesis, structure and C-C cross-coupling activity of amine-  
bis(phenolate)iron(acac) complexes

71. E. Y. Tshuva, S. Groysman, I. Goldberg, M. Kol and Z. Goldschmidt, *Organometallics*, 2002, **21**, 662-670.
72. E. Y. Tshuva, I. Goldberg, M. Kol and Z. Goldschmidt, *Organometallics*, 2001, **20**, 3017-3028.
73. S. Groysman, I. Goldberg, M. Kol, E. Genizi and Z. Goldschmidt, *Organometallics*, 2004, **23**, 1880-1890.
74. T. Toupance, S. R. Dubberley, N. H. Rees, B. R. Tyrrell and P. Mountford, *Organometallics*, 2002, **21**, 1367-1382.
75. F. M. Kerton, S. Holloway, A. Power, R. G. Soper, K. Sheridan, J. M. Lynam, A. C. Whitwood and C. E. Willans, *Can. J. Chem.*, 2008, **86**, 435-443.
76. K. L. Collins, L. J. Corbett, S. M. Butt, G. Madhurambal and F. M. Kerton, *Green Chem. Lett. Rev.*, 2007, **1**, 31-35.
77. R. Van Gorkum, J. Berding, A. M. Mills, H. Kooijman, D. M. Tooke, A. L. Spek, I. Mutikainen, U. Turpeinen, J. Reedijk and E. Bouwman, *Eur. J. Inorg. Chem.*, 2008, 1487-1496.
78. K. Hasan, C. Fowler, P. Kwong, A. K. Crane, J. L. Collins and C. M. Kozak, *Dalton Trans.*, 2008, 2991-2998.
79. P. Mialane, E. AnxolabéhèreMallart, G. Blondin, A. Nivorojkine, J. Guilhem, L. Tchertanova, M. Cesario, N. Ravi, E. Bominaar, J. J. Girerd and E. Münck, *Inorg. Chim. Acta*, 1997, **263**, 367-378.
80. R. Viswanathan, M. Palaniandavar, T. Balasubramanian and T. P. Muthiah, *Inorg. Chem.*, 1998, **37**, 2943-2951.

*Chapter 4. Synthesis, structure and C-C cross-coupling activity of amine-bis(phenolate)iron(acac) complexes*

81. M. Merkel, F. K. Müller and B. Krebs, *Inorg. Chim. Acta*, 2002, **337**, 308-316.
82. M. Velusamy, M. Palaniandavar, R. S. Gopalan and G. U. Kulkarni, *Inorg. Chem.*, 2003, **42**, 8283-8293.
83. J. Hwang, K. Govindaswamy and S. A. Koch, *Chem. Commun.*, 1998, 1667-1668.
84. M. Velusamy, R. Mayilmurugan and M. Palaniandavar, *Inorg. Chem.*, 2004, **43**, 6284-6293.
85. R. K. Dean, S. L. Granville, L. N. Dawe, A. Decken, K. M. Hattenhauer and C. M. Kozak, *Dalton Trans.*, 2010, 548-559.
86. D. W. Barnum, *J. Inorg. Nucl. Chem.*, 1961, **22**, 183-191.
87. D. W. Barnum, *J. Inorg. Nucl. Chem.*, 1961, **21**, 221-237.
88. R. B. Bedford, D. W. Bruce, R. M. Frost and M. Hird, *Chem. Commun.*, 2005, 4161-4163.
89. R. B. Bedford, M. Betham, D. W. Bruce, S. A. Davis, R. M. Frost and M. Hird, *Chem. Commun.*, 2006, 1398-1400.
90. R. B. Bedford, M. A. Hall, G. R. Hodges, M. Huwe and M. C. Wilkinson, *Chem. Commun.*, 2009, 6430-6432.
91. R. B. Bedford, M. Huwe and M. C. Wilkinson, *Chem. Commun.*, 2009, 600-602.
92. X. Qian and C. M. Kozak, *Synlett*, 852-856.
93. J. W. Pflugrath, *Acta Crystallogr., Sect. D.*, 1999, **55**, 1718-1725.
94. *Crystal clear. An Integrated Program for the Collection and Processing of Area Detector Data*, Rigaku Corporation, Tokyo, **1997-2004**.
95. A. C. Larson, *Crystallographic Computing*, Munksgaard, Copenhagen, 1970.

*Chapter 4. Synthesis, structure and C-C cross-coupling activity of amine-bis(phenolate)iron(acac) complexes*

96. D. T. Cromer and J. T. Waber, *International Tables for X-ray Crystallography*, The Kynoch Press, Birmingham, England, 1974.
97. A. Altomare, G. Cascarano, C. Giacovazzo, A. Guagliardi, M. Burla, G. Polidori and M. Camalli, *J. Appl. Cryst.*, 1994, **27**, 435.
98. P. T. Beurskens, G. Admiraal, G. Beurskens, W. P. Bosman, R. de Gelder, R. Israel and J. M. M. Smits, *DIRDIF99*, University of Nijmegen, Netherlands, 1999.
99. J. A. Ibers and W. C. Hamilton, *Acta Crystallogr.*, 1964, **17**, 781.
100. D. C. Creagh and W. J. McAuley, *International Tables for Crystallography*, Kluwer Academic Publishers, Boston, 1992.
101. D. C. Creagh and J. H. Hubbell, *International Tables for Crystallography*, Kluwer Academic Publishers, Boston, 1992.
102. D. J. Watkin, C. K. Prout, J. R. Carruthers and P. W. Betteridge, Chemical Crystallography Laboratory, Oxford, UK, 1996.
103. *CrystalStructure 3.7.0: Crystal Structure Analysis Package*, Rigaku and Rigaku/MSC, The Woodlands TX, **2000–2005**.
104. G. M. Sheldrick, University of Göttingen, Germany, 1997.
105. L. J. Farrugia, *J. Appl. Cryst.*, 1997, **30**, 565.

*Chapter 4. Synthesis, structure and C-C cross-coupling activity of amine-bis(phenolate)iron(acac) complexes*

## ***Chapter 5. Conclusion and prospects for future studies***

### ***5.1 Conclusion***

In 1941, iron (among other metals) was found to be an effective catalyst for homo-coupling of aryl Grignard reagents<sup>1</sup> and in 1971, it was used for the cross-coupling of alkenyl halides with Grignard reagents.<sup>2</sup> Since then, this discovery has been overshadowed by the use of palladium, rhodium, ruthenium and nickel based catalysts for organic synthesis. These precious metal-based catalysts have some disadvantages, such as their price, which has been increasing in recent years because of their decreasing availability as well as widespread use not only in chemical synthesis but in manufacturing and electronics. Also, some of these metals have been shown to be toxic. In particular, the toxicity of nickel is problematic for its use in consumer goods and health care products.<sup>3,4</sup> Therefore, catalysts based on abundant, inexpensive and non-toxic metals are becoming increasingly needed, and iron chemistry is taking great steps forward to fulfill this need. The present research was inspired to design iron catalysts for organic synthesis supported by amine-bis(phenolate) ligands, and the results are summarized in this chapter.

Chapter 2 of this thesis deals with the synthesis and study of Fe(III) halide complexes supported by tetradentate amine-bis(phenolate) ligands.<sup>5</sup> First, a series of amine-bis(phenol) ligands was synthesized by following modified literature procedures using water as the solvent. Eight new amine-bis(phenolate)Fe(III) halide complexes were synthesized by the reaction of anhydrous  $\text{FeX}_3$  ( $X = \text{Cl}, \text{Br}$ ) with these tetradentate amine-bis(phenol) ligands in methanol. The synthetic procedures are quite simple and yields of desired products are excellent (up to 98%). These complexes were initially characterized using MALDI-TOF mass spectrometry and the spectra showed the relevant molecular ion peaks or fragments caused by the loss of halide ligands. UV-vis spectra of these complexes showed multiple intense bands in the UV and visible regions. The absorption maxima observed in the near UV region (below 300 nm) were caused by  $\pi$  to  $\pi^*$  transitions involving phenolate units. Intense, high energy bands were observed around 330 nm and above 500 nm for the ligand-to-metal charge-transfer (LMCT) transition from the HOMO (highest occupied molecular orbital) of the phenolate oxygen to the Fe(III) center. Three of these complexes were characterized by single crystal X-ray diffraction. The coordination environment of these complexes was distorted square pyramidal or trigonal bipyramidal depending on the ligands employed. If the ligand was linear tetradentate  $\text{H}_2[\text{O}_2\text{N}_2]$ , the geometry of the complex was square pyramidal and if the ligand was tripodal tetradentate  $\text{H}_2[\text{O}_2\text{NO}]$ , the geometry of the complex was trigonal bipyramidal. Room temperature magnetic moments of these complexes were in the range of 4.6 to 6.2  $\mu_B$ , which are common for high-spin  $d^5$  iron centers. For three of these complexes, variable temperature magnetic data were collected in the temperature



range of 2 to 300 K. Plots of magnetic moment vs. temperature of these complexes showed slow and smooth reductions in their moments as the temperature is lowered to 20 K. Below this temperature the moments dropped more rapidly.

Chapter 3 of this thesis involves the iron-catalyzed epoxidation of olefins using hydrogen peroxide. Hydrogen peroxide was chosen as terminal oxidant because it is generally easy to handle, cheap and produces water as a by-product. Previously the combination of  $\text{FeCl}_3 \cdot 6\text{H}_2\text{O}$  and 5-chloro-1-methylimidazole in *tert*-amyl alcohol was reported for the epoxidation of olefins.<sup>6</sup> The use of relatively cheap solvent and non-halogenated organic additives is desirable. Therefore, initial catalytic screening was performed using a mixture of  $\text{FeCl}_3 \cdot 6\text{H}_2\text{O}$  and 1-methylimidazole for the epoxidation of *trans*-stilbene in a number of solvents by stirring the reaction mixture at 25 °C. The best result towards epoxidation of *trans*-stilbene was obtained in acetone. From the screening of different iron sources, it has been found that chloride plays an important role in the epoxidation of olefins under our conditions. A possible reason is that the formation of HOCl occurs, which may act as an oxidant, but this requires further investigation. The effect of different additives in combination with  $\text{FeCl}_3 \cdot 6\text{H}_2\text{O}$  was studied for the epoxidation of *trans*-stilbene. Imidazoles containing alkyl groups in the 2-position showed considerably higher activity than in the previous report, where decreased yield of epoxide was obtained compared to those having H-functionalized 2-positions.<sup>7</sup> Also, it was discovered that heating the reaction mixture to 62 °C for 19-21 h improved the yield of epoxides. Finally, the epoxidation process was optimized by the combination of  $\text{FeCl}_3 \cdot 6\text{H}_2\text{O}$  and 1-methylimidazole in acetone using 6.0 equiv. of  $\text{H}_2\text{O}_2$  vs. substrate as

*References begin on page 225*

the terminal oxidant.<sup>8</sup> The optimized catalyst system is applicable for epoxidation of both aliphatic and aromatic internal and terminal olefins.

*In-situ*-generated Fe(III) complexes prepared by adding  $\text{FeCl}_3 \cdot 6\text{H}_2\text{O}$  to amine-bis(phenol) ligands in solution were investigated for the epoxidation of *trans*-stilbene to see whether any enhancement of reactivity could be obtained. The combination of tetradentate amine-bis(phenol) ligands (abbreviated  $\text{H}_2[\text{O}_2\text{N}_2]$  or  $\text{H}_2[\text{O}_2\text{NO}']$ ) and  $\text{FeCl}_3 \cdot 6\text{H}_2\text{O}$  in *tert*-amyl alcohol gave around 30% yield of epoxide. However, *in-situ*-generated Fe(III) complexes made by using tridentate amine-bis(phenol) ligands (abbreviated  $\text{H}_2[\text{O}_2\text{N}]$ ), produced epoxide yields up to 64% but this was still lower than using  $\text{FeCl}_3 \cdot 6\text{H}_2\text{O}$  with imidazole co-catalysts. Preliminary kinetic studies of the catalyst system showed that the rate of epoxide formation decreases over time, but the epoxidation continues to proceed over the duration of the experiments (19-21 h).

Chapter 4 of this thesis describes the synthesis, structure and C-C cross-coupling activity of amine-bis(phenolate)Fe(III)(acac) complexes.<sup>9</sup> Six new amine-bis(phenolate)Fe(III)(acac) complexes were synthesized by the reaction of  $\text{Fe}(\text{acac})_3$  (acac = acetylacetonate) with tetradentate amine-bis(phenol) ligands in methanol. These amine-bis(phenolate)Fe(III)(acac) complexes were paramagnetic, therefore, the complexes were characterized using MALDI-TOF mass spectrometry. The spectra showed the relevant molecular ion peaks or fragments caused by the loss of acetylacetonate co-ligand. Electronic absorption spectra of all the amine-bis(phenolate)Fe(III)(acac) complexes showed multiple intense bands in the UV and

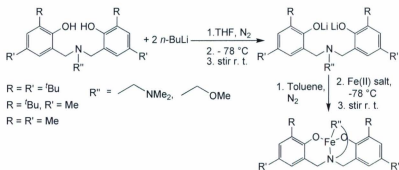
visible regions. IR spectra of these complexes showed two characteristic bands at 1571 and 1520  $\text{cm}^{-1}$  corresponding to the  $\nu_{\text{CO}}$  of the acetylacetonate co-ligand while bonded to the Fe(III) center. Four of these complexes were characterized by single crystal X-ray diffraction. The coordination environment of these complexes was distorted octahedral. Cyclic voltammograms of these complexes showed reversible ligand-centered redox processes. Room temperature magnetic moments of these complexes were between 5.4 and 6.1  $\mu_{\text{B}}$ , which were expected for high-spin  $d^5$  Fe(III) centers. Catalytic cross-coupling activity of these complexes was investigated for the coupling of alkyl halides and aryl Grignard reagents. Preliminary results showed that these complexes show good activity for the cross-coupling of *o*-tolylmagnesium bromide and cyclohexyl chloride. However, acyclic 2-halobutanes showed poor yields of product, whereas benzylhalides showed moderate activities for cross-coupling.

## 5.2 Prospects for future studies

It was found that chloride plays an important role in the epoxidation process, therefore catalysis using mixtures of chloride ions (using NaCl, for example) and non-chloride-containing iron salts (such as  $\text{Fe}_2\text{O}_3$ ) should be explored. Functional-group tolerance should also be explored by using substituted alkenes. Also, the investigation of the iron-containing species obtained from reaction with  $\text{H}_2\text{O}_2$  would provide some insight into the mechanism of the reaction.

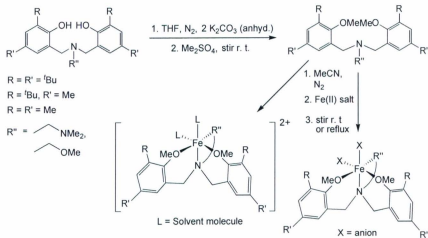
Besides epoxidation of olefins, oxidation of non-activated aliphatic C-H bonds would be a challenging field of research. Recently, Britovsek and co-workers reported

Fe(II) complexes supported by nitrogen containing linear tetradentate BPMEN (*N,N'*-dimethyl-*N,N'*-bis(2-pyridylmethyl)-1,2-diaminoethane) ligands for the oxidation of aliphatic C-H bonds.<sup>10</sup> Also, White and co-workers reported selective hydroxylation of alkanes using Fe(II) complex supported by neutral tetradentate PDP (2-((*S*)-2-[(*S*)-1-(pyridin-2-ylmethyl)pyrrolidin-2-yl]pyrrolidin-1-yl)methylpyridine)) ligands.<sup>11</sup> Inspired by these results, the synthesis of iron(II) complexes of amine-bis(phenolate) ligands and their catalytic activity for aliphatic C-H bond oxidation should be explored. A possible synthesis of Fe(II) complexes using tetradentate amine-bis(phenol) ligands is shown in Scheme 5.1. The geometry of these Fe(II) complexes would likely be distorted tetrahedral and reactive to oxidation.

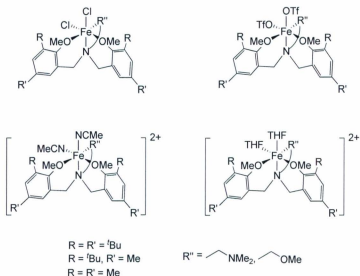


**Scheme 5.1** Synthesis of Fe(II) complexes.

Alternatively, Fe(II) complexes could be synthesized using neutral tetradentate ligands, which could be prepared by methylation of amine-bis(phenol) ligands (Scheme 5.2). The resulting complexes could be neutral six-coordinate compounds if coordinating anions were used, or cationic complexes that may be stabilized by coordinating, neutral solvento ligands and non-coordinating counter anions, such as  $\text{ClO}_4^-$  or  $\text{BF}_4^-$  (Figure 5.1). The catalytic activity of these Fe(II) complexes could be investigated towards oxidation of aliphatic and aromatic C-H bonds using  $\text{H}_2\text{O}_2$  or PhIO as a terminal oxidant.



**Scheme 5.2** Synthesis of Fe(II) complexes *via* methylation of amine-bis(phenol) ligands.



**Figure 5.1** Examples of some possible Fe(II) complexes.

Regarding the catalytic activity of the amine-bis(phenolate)Fe(III)(acac) complexes, only few of the alkyl halide substrates, such as cyclohexyl chloride and bromide, benzyl chloride and bromide, and 2-bromo- and 2-chlorobutanes were investigated for cross-coupling with *o*-tolyl and *p*-tolylmagnesium bromide. Future research of these C-C cross-coupling studies could be extended for a variety of alkyl halides especially more challenging alkyl chlorides and Grignard reagents.

### 5.3 References

1. M. S. Kharasch and E. K. Fields, *J. Am. Chem. Soc.*, 1941, **63**, 2316-2320.
2. M. Tamura and J. K. Kochi, *J. Am. Chem. Soc.*, 1971, **93**, 1487-1489.
3. L. Friberg, G. Nordberg and V. B. Vouk, *Handbook on the Toxicology of Metals*, North-Holland Biomedical Press, Amsterdam, 1979.
4. J. J. Hostýnek and H. I. Maibach, *Nickel and the Skin: Absorption, Immunology, Epidemiology, and Metallurgy*, CRC Press, Boca Raton, 2002.
5. K. Hasan, C. Fowler, P. Kwong, A. K. Crane, J. L. Collins and C. M. Kozak, *Dalton Trans.*, 2008, 2991-2998.
6. K. Schröder, X. Tong, B. Bitterlich, M. K. Tse, F. G. Gelalcha, A. Bruckner and M. Beller, *Tetrahedron Lett.*, 2007, **48**, 6339-6342.
7. K. Schröder, S. Enthaler, B. Bitterlich, T. Schulz, A. Spannberg, M. K. Tse, K. Junge and M. Beller, *Chem. Eur. J.*, 2009, **15**, 5471-5481.
8. K. Hasan, N. Brown and C. M. Kozak, *Green Chem.*, 2011, **13**, 1230-1237.
9. K. Hasan, L. N. Dawe and C. M. Kozak, *Eur. J. Inorg. Chem.*, 2011, 4610-4621.
10. J. England, R. Gondhia, L. Bigorra-Lopez, A. R. Petersen, A. J. P. White and G. J. P. Britovsek, *Dalton Trans.*, 2009, 5319-5334.
11. M. S. Chen and M. C. White, *Science*, 2007, **318**, 783-787.







